Winter 3-1-2024

Investigating the mechanisms of surface sensing using motility appendages by Pseudomonas aeruginosa PA14

Christopher James Geiger
Dartmouth College, christopher.j.geiger.gr@dartmouth.edu

Investigating the mechanisms of surface sensing using motility appendages by *Pseudomonas aeruginosa* PA14

A Thesis Submitted to the Faculty in partial fulfillment of the requirements for the degree of

Doctor of Philosophy in

Microbiology and Immunology

By Christopher J. Geiger

Guarini School of Graduate and Advanced Studies Dartmouth College
Hanover, New Hampshire
November 2023

Examining Committee:

_____
(chair) George A. O'Toole, PhD

_____
Mary Lou Guerinot, PhD

_____
Carey D. Nadell, PhD

_____
David Hershey, PhD

_____
F. Jon Kull, PhD
Dean of Guarini School of Graduate and Advanced Studies

Abstract

Biofilms are surfaced attached communities of cells encased in an extracellular matrix. The transition from free-swimming planktonic cells to a surface attached biofilm begins with cellular changes that occur after surface contact. This process is known as "surface sensing" and the opportunistic pathogen *Pseudomonas aeruginosa* PA14 uses its two motility appendages, type IV pili (T4P) and a single, polar flagellum to sense and traverse surfaces. The first cellular changes to occur within this organism upon surface contact is an increase in the second messengers cAMP and c-di-GMP. While the genes involved in surface sensing by *P. aeruginosa* are known, the mechanism by which these molecular machines sense and relay surface contact to the rest of the cell has remained a mystery. This thesis focuses on how T4P and flagellar surface contact lead to increases in cAMP and c-di-GMP, respectively. I show that the primary T4P retraction motor likely relays a surface signal to the Pil-Chp system, leading to CyaB activation and cAMP production. I also present data that supports a model whereby the stators of the flagellar motor senses surface contact and relay this information to a diguanylate cyclase leading to c-di-GMP production. These studies demonstrate how mechanical perturbations to these molecular motility machines upon surface contact can serve as cellular signals to initiate biofilm formation.

Acknowledgements

To my mentor George, I cannot thank you enough for everything that you have done for me over the past six years. Sitting with you and talking about data and potential experiments/models and trying to put all of the puzzle pieces together has been some of the most fun I've had during graduate school and will be the thing I miss most. Thank you for always being there to chat and being such a great role model as a PI. I've grown so much as a scientist and human being while in your lab and I'm extremely thankful for the safe and intellectually stimulating environment that you've created.

To my undergraduate mentor Steve, thank you so much for giving me the opportunity to join your lab and fall in love with science. There is no way I would have been accepted into graduate school without your help and I am forever thankful for your continued support and mentorship.

Thank you to the entire M2P2 community at Dartmouth especially the second and fifth floors of Remsen/Vail. Thank you to my thesis committee Mary Lou and Carey for your advice and support over the years. Thank you for all of the administrative help Karen and thank you Dave for all of the shipping help over the years! Also, thank you to JEMM for letting me crash their meetings for the past six years, I've loved getting an extra dose of microbiology with the Ross, Schultz, and Nadell labs.

Thank you to the members of the O'Toole lab both past and present. I have learned so much from everyone in the lab and my growth as a scientist and person would not have been possible without all of you. And a special thank you to the original members of team surface sensing, Sherry and Shanice for dealing with all of my dumb questions and ideas over the years and supporting me on this very difficult thesis project.

Thank you to all of my friends who have been supportive of me and understanding when I've missed important events. I would not have gotten to this point without all of your help.

A very special thank you to my parents and sister for their constant love and support. Rachel, thank you for always looking out for me over the years and being there to talk to. Mom and Dad, thank you so much for your continued love and support in my academic journey. I know I could be selling very expensive sea shells down by the seashore right now and I would have a great tan and more money but I am so much happier and fulfilled as a person and knowing that you support my decision means the world to me.

And finally thank you to my partner Amruta. You were there with me in the beginning helping me fill out applications and now seven years later here we are on the other side of the country about to wrap up my degree with our fur baby Coco-Mango! I cannot thank you enough for everything you've done and continue to do for me. Most importantly, thank you for always reminding me...

"This is water. This is water."
-David Foster Wallace

Table of Contents

A sense of touch : T4P retraction motor as a means of surface sensing by *Pseudomonas aeruginosa* PA14

Atomic Force Microscopy Measurements of Pel Polysaccharide- and Type IV pili-Mediated Adhesion of *Pseudomonas aeruginosa* PA14 to an Abiotic Surface

Appendices

List of Tables

Chapter 2

Chapter 3

List of Figures

Chapter 1

Chapter 2

Chapter 3

Chapter 1

Introduction

A sense of touch : T4P retraction motor as a means of surface sensing by *Pseudomonas aeruginosa* PA14

C.J. Geiger[1] and G.A. O'Toole[1]

[1]Department of Microbiology and Immunology, Geisel School of Medicine at Dartmouth

Author contributions:

C.J.G. wrote the chapter and performed the computational and structural analyses.

G.A.O. provided critical input and assisted in writing, organizing, and editing the chapter.

1.1 Abstract

Most microbial cells found in nature exist in matrix-covered, surface-attached communities known as biofilms. This mode of growth is initiated by the ability of the microbe to sense a surface on which to grow. The opportunistic pathogen *Pseudomonas aeruginosa* (*Pa*) PA14 utilizes a single polar flagellum and type IV pili (T4P) to sense and traverse surfaces. In *Pa,* T4P function by pulling the cell across a surface through rounds of pilus extension, surface binding and T4P retraction that is powered by hexameric ATPases. *Pa* cells that have engaged a surface and perform the T4P-dependent surface motility, known as twitching, increase production of the second messenger cAMP over multiple generations via the Pil-Chp system. This rise in cAMP allows cells and their progeny to become better adapted for surface attachment and activates virulence pathways through the cAMP-binding transcription factor Vfr. While many studies have focused on mechanisms of T4P twitching and regulation of T4P production and function by the Pil-Chp system, the mechanism by which *Pa* senses and relays a surface-engagement signal to the cell is still an open question. Here we review the current state of the surface sensing literature for *Pa.* We also propose a new model of surface sensing whereby the retraction motor PilT senses and relays the signal to the Pil-Chp system culminating in cAMP production.

"All models are wrong but some are useful"

-*George Box*

1.2 Introduction

Bacteria exist as either free swimming planktonic cells or as communities of surface attached cells encased in an extracellular matrix known as a *biofilm (1)*. Of the estimated 1.2 x 10^{30} microbial cells on planet Earth, up to 80% of them may be in a biofilm (2). The first step in transitioning from the planktonic lifestyle to the biofilm mode of growth is detecting surface engagement and transmitting this signal to the cell, which we refer to here as "surface sensing"(1, 3-5). *Pseudomonas aeruginosa* (*Pa*) is an opportunistic pathogen that is able to cause biofilm infections in persons suffering from burn wounds, cystic fibrosis, and acute leukemia(6). Like many other bacteria, *Pa* uses its two motility appendages, flagella and type IV pili (T4P), to sense and traverse surfaces (**Figure 1**)(3, 7). *Pa* possesses a single polar flagellum that rotates and propels the cell forward in both a liquid environment (swimming) and across surfaces (swarming)(8, 9). Stator proteins incorporated into the flagellum machinery utilize the cell's proton motive force (PMF) to power rotation(10-12). T4P are tiny hairlike appendages that extend from the cell's poles. Polymerization of the pilin monomer leads to extension of the pilus fiber and depolymerization leads to retraction(13, 14). In *Pa* PA14, T4P extension is powered by a single motor, PilB, and retraction is powered by a primary and accessory retraction motor, PilT and PilU, respectively. All three of these motor ATPases form hexamers and are powered by ATP hydrolysis(14-19).

The cellular parts necessary for surface sensing are present in many strains of *Pa* but the magnitude to which each of these appendages contributes to surface adaptation and biofilm formation varies widely between backgrounds (20-22). Various studies have investigated the different mechanisms of surface sensing and their impact among *Pa* strains. For example, while both *Pa* strains PA14 and PAO1 encode the Wsp and Pil-Chp systems, Pil-Chp and cAMP appears to be more critical for early surface attachment in PA14 whereas the Wsp system and c-di-GMP is more critical in the PAO1 background (20, 21). Furthermore, extracellular components that

can affect biofilm formation such as EPS vary between *Pa* backgrounds. For these reasons this review will focus on studies using *P. aeruginosa* PA14 as a model organism to study surface sensing and biofilm formation.

After surface contact by *Pa*, one of the first cellular changes to occur is the increase of the nucleotide second messenger 3'5'-cAMP (23, 24). In *Pa*, this molecule is required for further surface adaptation as well as acute virulence (25-27). Robust cAMP production by *Pa* is dependent on functional T4P and the presence of a surface (24, 28, 29). This increase in cAMP leads to a subsequent c-di-GMP response that is necessary for production of a mature biofilm (5). The biofilm can be maintained, which is an active process; or alternatively, if conditions become unfavorable, cells can disperse from the biofilm and return to the planktonic state (5, 30-34). When we say "surface sensing", we are focusing on the first few steps of biofilm initiation that lead to an increase in both nucleotide second messengers. Here we review data regarding surface sensing mediated by T4P for *Pa* PA14 and propose a new model whereby cells sense and transmit this surface engagement signal via the T4P retraction motor PilT.
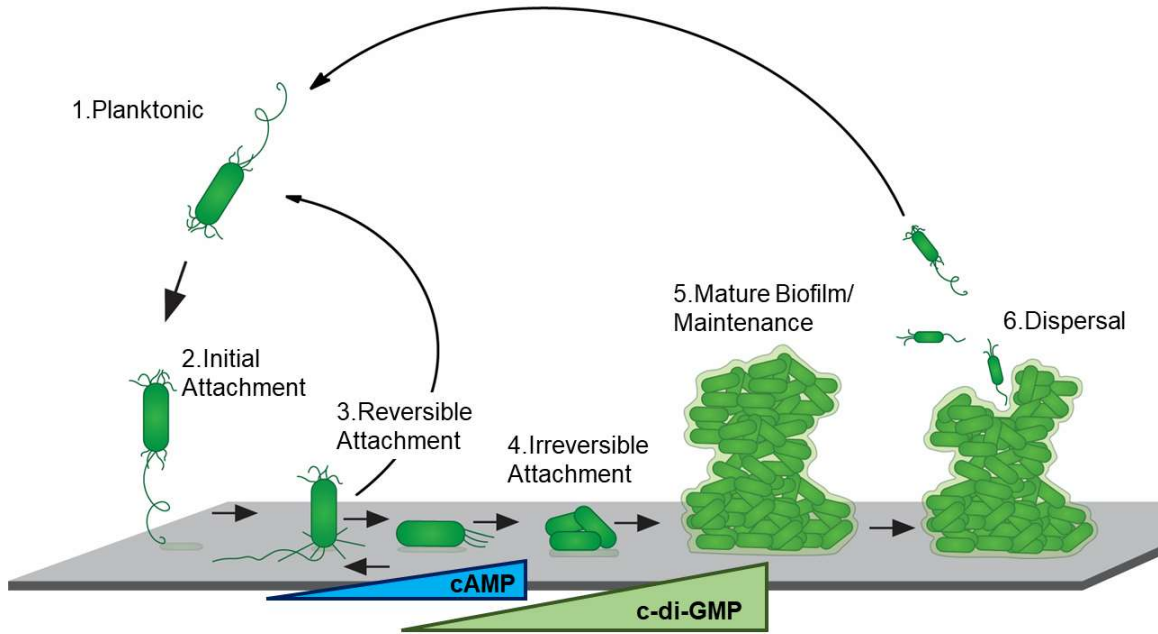
Figure 1. Diagram of the biofilm cycle of *Pseudomonas aeruginosa* PA14. Biofilm formation by *Pseudomonas aeruginosa* PA14 (green) begins with free-swimming planktonic cells (1) making initial surface attachment through its single, polar flagellum (2). After initial surface contact, bacteria can either continue to explore the surface using their motility appendages or return to the planktonic population in a process known as reversible attachment (3). As cells continue to explore the surface using T4P they become better surface adapted in a process that is mediated by cAMP level (blue triangle). Once cells are surface adapted they commit to the biofilm lifestyle and become irreversibly attached (4). As biofilm cells continue to grow on a surface they increase c-di-GMP level (green triangle) resulting in motility repression and upregulation of genes necessary for the formation of a mature biofilm (5). When conditions become unfavorable for the biofilm, cells can either passively or actively disperse into the planktonic population (6).

1.3 Surface sensing and its connection to virulence

The surface-mediated increase in cAMP to initiate biofilm formation cascade also contributes to activation of virulence genes (25, 27, 35-37). The majority of cellular changes that occur in *Pa* upon cAMP increase is due to its binding protein and virulence factor Vfr (35, 38). In terms of virulence, Vfr bound to cAMP directly activates many genes necessary for type 2 secretion systems (T2SS) and T3SS, including expression of the *exsA* gene (37). These genes are active during acute *Pa* infections. Thus, studying surface sensing will help us integrate two key aspects of bacterial biology – biofilm formation and host-microbe interactions.

1.4 Surface sensing by motility appendages

As cells near a surface, motility appendages can contact this surface leading to a dramatic change in the forces experienced by the cell envelope as well as the motors powering T4P retraction and stators powering flagellar rotation (39, 40). Here the mechanical force experienced by the cell can serve as the signal of surface engagement for the cell, a process known as mechanosensing in bacteria. This aspect of surface sensing focuses on the mechanical forces exerted on the cell due to the presence of an attachment substrate that is not encountered in a planktonic environment. For a full explanation on the difference between "surface sensing" and "mechanosensing" please see a recent review from our team (4). Below we highlight the different forces experienced by *Pa* due to motility appendages interacting with the surface and the resulting cellular changes that occur.

1.5 The forces experiences by *Pa* upon surface contact
Forces experienced by *Pa* cells upon surface contact: the flagellum

Planktonic *Pa* cells experience force due to flagellar rotation in a liquid medium. Swimming cells in a liquid with a viscosity similar to water will experience a drag force ~0.5-2 pN when swimming (39, 41). During flagellar rotation the cell body counter rotates and experiences a resistive torque ~1600 pN (39). The *Pa* flagellum motor in particular has a torque output of 2 pN*um (42). When the load on the flagellum increases either due to changes in viscosity or engagement of the cell

body or flagellum with a surface, the flagellum machinery is able to undergo remodeling to recruit more stator units (43-47). Stators only conduct protons upon incorporation into the flagellar motor. The ability to conduct protons is crucial to mechanosensitive stator recruitment, as stator mutants that no longer allow the flow of protons are not recruited to flagella (47).

Based on work in *E. coli*, under low loads, the flagellum can contain 4-6 stator units, but this number can increase to 11-16 units under high load (48-51). When the flagellum is experiencing a high load, each stator unit can contribute ~10 pN of force towards flagellar rotation (47). Stator units bind the peptidoglycan (PG) layer as well as FliG of the C ring of the flagellar base to convert the energy supplied by PMF into flagellar torque. It is thought that under high loads the stators undergo a catch-bond regime which enhances binding between stators and the flagellar machinery (52). That is, binding of the stator to the motor increases with increasing load on the flagellum.

Pa contains two sets of stators that power flagellar rotation. MotAB stators are dominant in low load environments and are produced at ~40x higher levels than the second stator set, MotCD (53). The MotCD stator is required for high load flagellar rotation like that experienced during swarming motility (8, 10, 54). Interestingly, based on signal motor measurements, both stator sets exert the same amount of torque, but flagella composed of MotCD stators are 10x more likely to be active (53).

For *Pa*, initial surface contact is mediated by the flagellum and is accompanied by a sharp increase in the flagellar load from ~5pN nm*s/revolution to >150 pN*nm s/revolution (39, 42, 55). The change in forces due to flagellar-mediated surface contact is not unique to *Pa* and many different organisms rely on their flagella to sense a surface (56-58).

Forces experienced by *Pa* cells upon surface contact - the T4P:

Under planktonic conditions T4P extend and retract freely and consequently, the force required to retract the pilus through a liquid environment is thought to be negligible (39). Although it was previously thought that surface contact by T4P stimulated retraction, it has since been shown that the rate of pilus extension and

retraction is not significantly different for surface-associated versus liquid-suspended cells (14, 59). After surface attachment by *Pa*, T4P are able to mediate two types of surface motility: upright walking and directional crawling, the latter of which is also known as twitching (3, 60-63). T4P retraction motors make up some of the strongest motors found in nature (19, 64). Some microbes are able to retract a single pilus fiber with a force upwards of 100 pN and some T4P can form bundles and cooperate during retraction to generate forces in the 1 nN range (19, 64, 65). *Pa* shows a more modest average retractive force of ~30 pN per pilus (66). A single T4P however can attain a maximal adhesive force of up to 750pN as measured by AFM and surfaces covered with the Pel exopolysaccharide have been shown to enhance T4P surface attachment (66, 67).

Twitching motility by *Pa* PA14 normally occurs through constant slow movement (~0.3 µm/s) punctuated with periods of rapid movement (1 µm/s). This increased speed occurs when multiple T4P engage the surface, and upon release of one pilus results in a "slingshot" effect, propelling the cell forward faster than pilus retraction allows (68). This increased speed is also due to the elastic, spring-like nature of T4P filaments that are able to stretch 3x their original length when under tension (69).

The retractive force of T4P in *Pa* is thought to originate from the primary and accessory retraction motors PilT and PilU, respectively (15, 19, 25, 70-73). However, it is worth noting that others have hypothesized that a large fraction of the retractive force is stored in the pilus fiber itself as there have been examples of low force retractions in the absence of any retraction motor (74, 75). PilT is able to interface with the pilus machinery directly and it is thought that when under sufficient load, PilU will bind PilT and the coordinated ATP hydrolysis of both motors are used to depolymerize the bound pilus fiber leading to pilus retraction and T4P-mediated cell movement across a surface (14, 15, 17, 70). Motor-mediated retraction of surface bound pili serve as a surface signal in *Pa* as well as other bacteria containing T4P (76-78).

Forces experienced by *Pa* cells upon surface contact: the cell body

In addition to the appendages described above, the cell body itself can bind to the surface with marked adhesive force. Note that the cell body of *Pa* PA14 without T4P and flagella can bind hydrophobic surfaces with adhesion forces up to 1000pN (67). Adhesion of the cell body to a surface can be modified by a number of factors including extracellular matrix components that are deposited on the surface or localized to the OM of the cell body itself. *Pa* produces the large adhesive protein CdrA as well as chaperone-usher pili that line the body of the cell and aids in cell-cell adhesion as well as cell-surface binding (79, 80). In addition, the CdrA adhesin can bind to the EPS Psl further enhancing surface attachment. Since many of these adhesive systems are regulated by c-di-GMP their expression varies during biofilm formation making it difficult to determine the exact level of adhesion of a given *Pa* cell contacting a surface (79, 80). How these cell surface adhesins impact surface sensing through the motility appendages is largely unexplored (66, 67, 81).

1.6 Cascade of second messenger signaling upon surface engagement

The forces experienced by the cell upon surface contact can serve as a signal to initiate cellular changes necessary for the biofilm mode of growth. One of the first cellular changes to occur is an increase in the nucleotide second messengers c-di-GMP and cAMP (24). Both *E. coli* and *Pa* have been shown to increase c-di-GMP within seconds of surface contact (82, 83).

How does surface contact by *Pa* PA14 result in an increase in second messenger production? As outlined above, for *Pa* PA14, cAMP is thought to be the first second messenger upregulated upon surface engagement, a process that requires functional T4P, the Pil-Chp system, and the adenylate cyclases CyaA and CyaB (**Figure 2**) (24, 35, 37, 84). This up-regulation of cAMP results in an increase of T4P levels after surface engagement via the increased expression of the genes required for pilus synthesis, generating a positive feedback loop for cAMP/T4P production (24). Below we will discuss the regulation of cAMP production by *Pa* PA14 and the possible mechanism whereby T4P surface engagement triggers cAMP signaling. Vfr bound to cAMP transcribes the two component system FimS-AlgR,

which directly regulates the T4P minor pilin operon (24). The minor pilins are thought to serve as an initiation complex for pilus assembly and are required for T4P function (85, 86). Among these minor pilins is PilY1, which we discuss in the next paragraph.

The activity of the diguanylate cyclase SadC has been shown to be regulated by both T4P (**Figure 2**) and flagella by *Pa* PA14 (12, 87). The data from our group and others supports a model whereby conformational changes of the protein at the tip of T4P, PilY1, due to the mechanical tension generated by pilus retraction and surface adhesion, activates a signaling pathway along the alignment complex of T4P, which modulates the activity of the diguanylate cyclase SadC (4, 12, 87, 88). The alignment complex of T4P, composed of PilMNOP, connects PilY1, buried within the PilQ porin with TsaP, to the inner membrane (IM)-localized SadC via PilN and PilO, which are also found in the IM (87, 89). The interaction between SadC and PilO has been shown to repress diguanylate cyclase activity, and furthermore, the binding strength between PilO-SadC impacts the frequency and amplitude of c-di-GMP oscillations in single *Pa* PA14 cells attaching to a surface (90).

Once released from its interaction with PilO, SadC is free to interact with other membrane components and produce c-di-GMP. When c-di-GMP increases within the cell, the protein FlgZ can bind this second messenger and the FlgZ•c-di-GMP complex will remove MotCD stator units from the flagellar machinery (12). This process not only shuts down flagellar rotation under high loads but also allows MotC to interact with SadC. This MotC-SadC interaction has been shown to have a stimulatory effect on diguanylate cyclase activity leading to a positive feedback loop of c-di-GMP production and flagellar motility repression (12). Thus, protein-protein interactions with a component of the T4P (PilO) and the flagellar machinery (MotC) can modulate the activity of SadC (12, 87). Furthermore, another surface sensing system in *Pa,* the Gac-Rsm system, has been shown to regulate SadC at the level of translation, leading to more SadC produced when the system is activated (91). These data suggest that SadC could serve as a "hub" to integrate information for the two motility machines when they engage the surface.
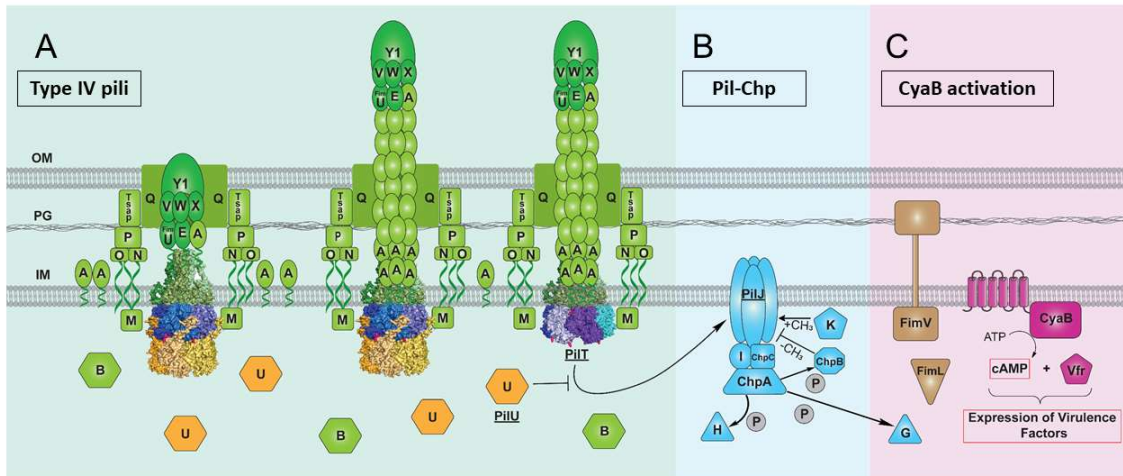
Figure 2. New proposed model for surface sensing by *P. aeruginosa*. (A) After surface binding by extended T4P, retraction of pili begins with the retraction motor PilT binding PilC. The accessory retraction motor PilU binds PilT and aids in depolymerization of the pilus fiber via conformational changes in PilC. However, if PilU is absent during retraction, we hypothesize that PilT alone is unable to exert sufficient force to power retraction and the PilT motor will stall, potentially entering a conformational state due to improper ATP binding and/or hydrolysis and/or ADP release. We believe that PilT in this stalled conformation binds PilJ of the Pil-Chp complex to transduce the surface signal from T4P to Pil-Chp (B). After PilJ activation the signal is transmitted to the kinase ChpA which leads to the phosphorylation of several response regulators including PilG. PilG along with FimV and FimL then activate the adenylate cyclase CyaB leading to an increase in cAMP (c).

1.7 cAMP regulation by *Pa*

For *Pa* PA14, compared to c-di-GMP, cAMP production and degradation uses significantly fewer proteins. There are three adenylate cyclases (AC) encoded in the *Pa* genome but only two of them, CyaA and CyaB, appear to contribute to intracellular levels of cAMP. ExoY, the third AC, is a type 3 secretion system effector toxin and is only active after being injected into another cell (92). A single phosphodiesterase, CpdA, degrades cAMP (26, 37, 92).

CyaA is a cytoplasmic adenylate cyclase but its regulation remains unknown. CyaB has been shown to contribute to the majority of cAMP under all tested conditions in *Pa (24, 36, 37, 93)*. This adenylate cyclase is a class IIIb AC which is composed of a MASE2 regulatory domain fused to a catalytic domain. The MASE2 domain attaches CyaB to the membrane in PA14 and is thought to aid in localization to the cell's poles. Like other Class IIIb ACs, CyaB has been shown to be stimulated by HCO_3^- and has an optimum pH of 7.5 when tested in vitro (94). Other chemical stimuli such as low calcium has been shown to stimulate cAMP in *Pa* by increasing the expression of the *cyaB* gene (37).

Surface dependent cAMP is produced mainly by CyaB with some contribution by CyaA (24). The cellular regulation of CyaB via its MASE2 domain has been shown to be controlled by components of the Pil-Chp system, as detailed below (24, 36, 84, 93).

All known cellular changes due to cAMP are dependent on the cAMP-binding protein Vfr that regulates genes responsible for virulence as well as surface adaptation (35, 38). The *cpdA* promoter is positively regulated by Vfr under high levels of cAMP to reduce the levels of this signal back to baseline after induction (26). A second cAMP binding protein is also found in *Pa*, CbpA, and will localize to the flagellated pole upon cAMP binding but its cellular function remains a mystery (95).

At the single cell level within *Pa,* there are out of phase oscillations between levels of cAMP and T4P activity that is able to persist over multiple generations. Surface adaptation through cAMP dependent T4P production leads to a memory of surface contact that allows cells and their progeny to remain surface adapted for several generations. This surface adaptation decreases the longer cells remain away

from a surface. Single *Pa* cells that that remain on a surface display oscillations of cAMP across several generations (23). How these oscillations of cAMP, with the recently documented oscillations of c-di-GMP, relate to each other in controlling single cell surface behavior remains an active area of study.

Regulation of CyaB activity by Pil-Chp

Several genetic screens have indicated that members of the Pil-Chp system are involved in CyaB regulation and subsequent studies have uncovered the mechanisms of signal transduction and activation.   Three proteins, FimV, PilG, and FimL, must form a complex to activate CyaB via its MASE2 domain (24, 84, 93). FimL is thought to connect FimV to PilG to form the activation complex (**Figure 2C**) (36, 93). Localization of PilG and FimL to the poles of the cell is dependent on the polar hub protein FimV (36). The FimV protein contains a peptidoglycan (PG) binding LysM motif as well as a large cytoplasmic domain with a conserved tetratricopeptide repeats (TPR) motif that is used to bind FimL (96). The LysM motif preferentially binds PG with less stem peptides, a form of PG that is only found at the poles of the cells, thus providing an explanation for the polar localization of FimV (97-100). Besides activating the AC CyaB, FimV has other roles including T4P assembly and polar localization, stopping flagellar rotation, and polar localization of other proteins like PilS (97, 101, 102). PilG, which is a response regulator (RR) of the kinase ChpA, is also required for CyaB activation. Phosphorylation of PilG is required for AC activation as well as twitching motility, but not binding to FimL or polar localization (36).

PilG is part of the larger Pil-Chp complex that is genetically and functionally similar to chemoreceptors described in other gram negative organisms (**Figure 2B**). This Che-like system contains a membrane-bound, methyl-accepting chemotaxis (MCP) protein PilJ with a periplasmic ligand binding domain (29, 103-105). The periplasmic domain has been implicated in directional twitching towards chemoattractants such as phosphatidylethanolamine, mucin, BSA, and recently phenol soluble modulins produced by *Staphylococcus aureus (105-107)*. Interestingly, addition of these chemoattractants also stimulate cAMP production via

CyaB (108). While the ligand binding domain is required for directional twitching it is not required for surface-dependent cAMP production (109).

PilJ like other MCPs is predicted to be methylated and demethylated by two proteins, PilK and ChpB, respectively, to tune sensitivity of the receptor (24). There are two predicted adaptor proteins for this system, PilI and ChpC, which likely link PilJ to ChpA (29, 103, 104). PilI is required for twitching motility but ChpC is only required for directional twitching (108). The kinase ChpA has a second response regulator in additional to PilG, PilH. Until recently the function of these two response regulators (RR)s were unknown. It has now been demonstrated that the phosphorylation state of these two proteins controls the directional twitching of *Pa* by biasing the polar localization of the T4P extension motor PilB, thereby allowing *Pa* to efficiently colonize a new surface and prevents aggregation of twitching cells (36, 110, 111). Surface-dependent activation of Pil-Chp and subsequently CyaB also require functional T4P but the mechanism by which T4P sense a surface and transmit this information to Pil-Chp is still an open question (24, 76, 84). Below we address several models proposed to explain T4P-mediated surface sensing by *Pa*, and in light of new genetic, structural and comparative genomics data, we present a new model of surface sensing by *Pa* PA14.

T4P regulation of Pil-Chp

Many studies have established the requirement for functional T4P as well as the Pil-Chp system for surface-dependent cAMP production, but the mechanism whereby T4P mediate surface sensing via Pil-Chp is still an open question. As the statistician George Box stated, "All models are wrong but some are useful". This quote nicely sums up the current state of surface sensing. Indeed, we would argue that how the T4P senses and transduces surface engagement is one of the key knowledge gaps in regard to surface sensing in *Pa*.

A previous study proposed a possible mechanism of surface sensing by T4P via the pilin monomer itself. This study demonstrated that PilA as well as its motor proteins were required for the surface-dependent cAMP response. Furthermore, a novel interaction between PilA and PilJ was described using the Bacterial Adenylate

Cyclase Two Hybrid (B2H) system. The authors speculated that the pilin monomer enters a force induced conformational change when there is sufficient tension on the pilus fiber that allows for binding with PilJ, leading to cAMP production. To test whether tension on pili alone could stimulate cAMP production, the *Pa* Δ*pilTU* mutant was subjected to increased medium flow in a flow cell resulting in a shear force of ~10pN per cell. Despite the tension on pili due to the shear force, the extent of cAMP production was identical to Δ*pilTU* strain under the no flow condition indicating that the motor-mediated retraction is necessary for surface signaling and not just tension on pili (76). Subsequent studies have demonstrated a correlation between the flux of pilins in and out of the inner membrane (IM) on surfaces of different stiffnesses and the extent of surface-dependent cAMP production. A biochemical model was developed based on the flux of PilA in the IM that accurately predicted the cAMP response of T4P motor mutants with altered extension and retraction dynamics (112). While this T4P-based model of surface sensing by *Pa* explains much of the observed data it fails to address key observations at odds with this proposed mechanism.

First, a recent study revealed a lack of correlation between the strength of binding between PilA and PilJ and levels of cAMP when grown on a surface (78). If PilA interaction with PilJ mediates the surface signal, then we would predict that stronger binding between PilA-PilJ would result in more cAMP production for surface-grown cells, but this correlation is not observed for several PilA mutants. Second, deletion of the accessory retraction motor, PilU, *increases* the cAMP response and is the only component of T4P machine that increases intracellular cAMP upon deletion (23, 24, 78, 113). As mentioned earlier, PilU can only interact with the T4P machinery to promote retraction via the primary retraction motor PilT (70, 114). The overproduction of cAMP in this background is dependent on the presence of PilT as the double Δ*pilT*Δ*pilU* mutant does not increase cAMP when grown on a surface (23, 78, 113). PilU has been shown to contribute to retraction of T4P by increasing the maximum force of retraction (70). If conformationally stretched pili were key to surface signaling we would expect a reduction in stretched pili when we eliminate one of the two motors contributing to retractive forces, resulting in less cAMP, which

again, is not what the data show. Third, expression of functionally inactive PilU, PilU-K136A, in a Δ*pilU* background phenocopies the Δ*pilU* mutant strain in terms of T4P-related phenotypes such as twitching and phage susceptibility but reduces surface-dependent, cAMP production (113). In both the Δ*pilU* mutant and a Δ*pilU* mutant over-expressing the PilU-K136A protein, T4P are only able to retract with enough force to retract pili that are bound to phage, but are unable to generate enough force to overcome the adhesion between the surface and cell body leading to twitching motility. In these two backgrounds T4P tension is below its maximum due to the lack of functional PilU, but these strains exhibit disparate cAMP responses when grown on a surface that cannot be explained by the pilin signaling model. Finally, this model necessitates interaction between a conformationally altered PilA buried in the T4P machine with PilJ in the inner membrane, a model at odds with cryoEM structures of the T4P machine (115). Alternatively, the force-induced conformational change in PilA would need to be maintained long enough for the T4P to disassemble, and pilin to diffuse into the membrane in its altered conformation to engage PilJ. Neither of these scenarios seem likely.

Due to the lack of evidence supporting a PilA-PilJ signaling model (and multiple lines of evidence arguing against this model), and growing data showing that manipulating the accessory retraction motor can affect levels of cAMP, we hypothesized that the primary retraction motor PilT may be required for sensing and relaying a surface signal to the Pil-Chp system.

1.8 A proposed model of PilT-mediated of surface sensing signal transduction

The PilT retraction motor drives depolymerization of extended T4P using the power generated by ATP hydrolysis (15, 17). Type IVa pili (T4aP), of which the T4P of *Pa* are a part of, require a homolog *pilT* to be present for the identification of a T4aP system in the genome. The other retraction motor, *pilU*, is considered an accessory gene and not all microbes with a T4aP have a *pilU* gene in their genome (116). In *Pa*, the N-terminus of the PilT monomer contains a PAS-like domain that is connected to the C-terminal NTPase domain by a flexible linker. There are several conserved

motifs in the C-terminal NTPase domain including a Walker-A motif responsible for ATP binding, a Walker-B motif responsible for ATP hydrolysis, and Asp and His boxes that coordinate the terminal phosphate group of ATP (15). The last conserved motif of PilT is the surface exposed, hydrophobic AIRNLIRE motif. Residues in the AIRNLIRE motif are required for in vivo function of PilT and mutating these residues result in cells that are unable to perform twitching motility are and are phage resistant, indicating a complete lack of any T4P retraction. Despite the lack of function, AIRNLIRE mutants are still able to oligomerize and retain ATPase activity, indicating an unexplained role of this motif in motor function (117).

T4P motors function as hexamers within bacterial cells. Oligomerization occurs by the NTD of one monomer binding to the CTD of adjacent monomers. The ATP binding occurs between monomers in the core of the hexamer (17, 19, 118, 119). The ability to bind and hydrolyze ATP leads to different stable conformations within the cytoplasm of cells. Three stable conformations have been observed for the PilT hexamer of *Pa*. A fully ATP bound C6 conformation is thought to allow binding between the PilC platform protein and the PilT hexamer. The C2 conformation of PilT where only two ATP molecules are bound is thought to be the active conformation of PilT while powering disassembly. The observed C3 conformation has no known physiological role (17).

As part of developing a model for PilT-mediated surface sensing, it is relevant to understand where PilT is localized. Localization of PilT to the poles has been shown to be dependent on the presence of functional MreB (120). However, whether PilT or PilU motors are unipolar or bipolar in their localization appears to vary with strain, expression condition, and the pressence of other proteins like FimX (15, 111, 120, 121). A mutation in the Walker-A motif of PilT (G135S) has been shown to affect polar localization while mutations in Walker-B do not (15). While many factors appear to affect T4P motor localization, one consistent observation is that all three motors are not always present at the poles of *Pa*.

Recently our group published a study with data that supports a model whereby the retraction motor PilT senses and relays the surface signal to the rest of the cell. A bacterial adenylate cyclase two-hybrid screen identified a novel interaction

between PilT and PilJ of the Pil-Chp system leading us to hypothesize that the surface signal may be transmitted through this interaction instead of the previously proposed PilA-PilJ interaction. By generating PilT mutants with differences in ATPase activity and measuring the cAMP produced when grown on a surface, as well as strength of interaction between PilT and PilJ, a linear model was developed that indicated a strong correlation between strength of interaction between PilJ and PilT-ATPase mutants and the amount of cAMP produced when cells were grown on a surface. This finding indicated to us that PilT may be "sensing" the surface through its ATPase activity and that ability to interact with PilJ was important for cAMP production. Furthermore, by manipulating levels of the accessory motor PilU, we were able to demonstrate that the surface dependent cAMP response could be modulated by the amount of PilU available to interact with PilT and that this effect of PilU on cAMP was dependent on the presence of PilT (113).

Together, these data regarding PilT and PilJ led us to propose the following model of motor-dependent surface sensing by *Pa*. In this model, PilT binds to PilC to drive retraction of extended T4P. If T4P are unbound, then retraction does not require maximal force and PilT is able to retract pili in the absence of PilU. Support for PilT functioning in the absence of PilU comes from the *pilU* mutant remaining sensitive to a phage that requires a retractile T4P for infection (73, 78). However, if T4P are bound to the surface, then PilT is unable to power disassembly in the absence of PilU, as this accessory retraction motor provides the high T4P retractive forces that are not achieved in a Δ*pilU* mutant (14, 70). If there are not enough PilU motors to aid in retraction or if the PilU motor is at the opposite pole, PilT-mediated retraction will stall in the C2 conformation (described above) potentially leading to novel hexameric conformations due to improper ATP binding or ADP diffusion out of the hexamer (17). We believe this stalled conformation then allows PilT to interact with PilJ to relay the surface signal to Pil-Chp. This model accounts for why a Δ*pilU* mutant strain would have elevated levels of cAMP. That is, in the absence of PilU, every attempt to retract surface-bound T4P would result in the "stalled conformation" of the motor.

However, one piece of data that did not fit this model was the ability of ATPase deficient PilU protein, PilU-WA, to lower cAMP in a Δ*pilU* background when PilU-WA was expressed from a plasmid. As previously mentioned, T4P in a Δ*pilU* mutant background are functionally equivalent to T4P in a Δ*pilU* background expressing *pilU*-K136A. Despite both strains being deficient in twitching motility and phage susceptibility, the strain expressing *pilU*-WA has significantly less cAMP than WT whereas the Δ*pilU* strain has elevated levels of cAMP. One possible explanation for this discrepancy is that PilU and PilJ share a binding site on PilT such that expression of a defective PilU lowers cAMP by blocking signaling to PilJ by PilT (113). Unfortunately, at the time of the publication of the PilT-PilU interaction model, we had no evidence to support this hypothesis because the residues on PilT that mediate interaction with its binding partners PilU and PilC were unknown.

1.9 Using comparative genomics to develop a model of surface sensing accounting for PilT, PilJ and the PilU accessory motor.

To predict residues that might mediate binding of PilT to its two partners we used a combination analyzing sequence conservation with structural modelling. We reasoned that conserved residues on the surface of PilT likely mediated the interactions between its binding partners. To predict which surface residues of PilT might mediate binding to PilJ versus PilU, we used the tool "alphafold multimer" (122-127).

To determine candidate residues mediating PilU binding to PilT, we first identified the residues on the surface of PilT that likely mediate interaction with PilC. We performed this analysis first for several reasons. First, we knew that PilT is able to interact with PilC in the absence of PilU given that *Pa* remains phage susceptible in a *pilU* mutant background (73). Second, we reasoned that because PilC, PilT, and PilU must all form a complex to power twitching motility, that the residues mediating PilT-PilC interaction could *not* be the residues mediating PilT-PilU interaction (7, 19, 128). Third, consistent with this supposition, cryoEM structures have shown that the PilT hexamer likely interacts with the PilC platform protein through either its N- or C-

terminal face (115). Therefore, whichever face of the PilT hexamer was mediating interaction with PilC would be unavailable for PilU binding – thus we could likely discern which face of PilT was interacting with PilC versus PilU.

Mutations that disrupt interaction between PilT and PilC would phenocopy a Δ*pilUT* mutant strain in terms of T4P retraction but would likely not affect ATPase activity or oligomerization as the residues that facilitate these functions are near the NTPase core of PilT and not on the surface of the protein. Such phenotypes occur when mutating the AIRNLIRE motif of PilT which is located on the C-terminus of the protein (117). Another piece of data supporting this hypothesis is that of the 4 PilT motors in *Geobacter sulfurreducens*, only PilT motors that contain the AIRNLIRE motif are able to complement a Δ*pilT* PAK *Pa* strain and perform twitching motility (129). This observation led us to predict that the C-terminal face of PilT mediates interaction with PilC.   In agreement with this prediction, the highest scored alphafold multimer prediction for PilT and PilC showed interaction of PilC via PilT hexamer's C-terminal face, which includes the AIRNLIRE motif (**Figure 3A/B**).

To assess the extent of conservation of residues on the C-terminal surface of the PilT hexamer, we collected the homologs of the PilT protein for all pseudomonads and then binned sequences by whether or not the genome also contained a *pilU* gene. We observed that the C-terminal surface of the PilT hexamers are highly conserved for all pseudomonads, whether or not they contain a PilU (**Figure 3C**).   This observation is in agreement with the structural predictions, as all PilTs of T4aP must bind a PilC so this PilT-PilC interaction face should be well conserved regardless of the presence or absence of PilU.
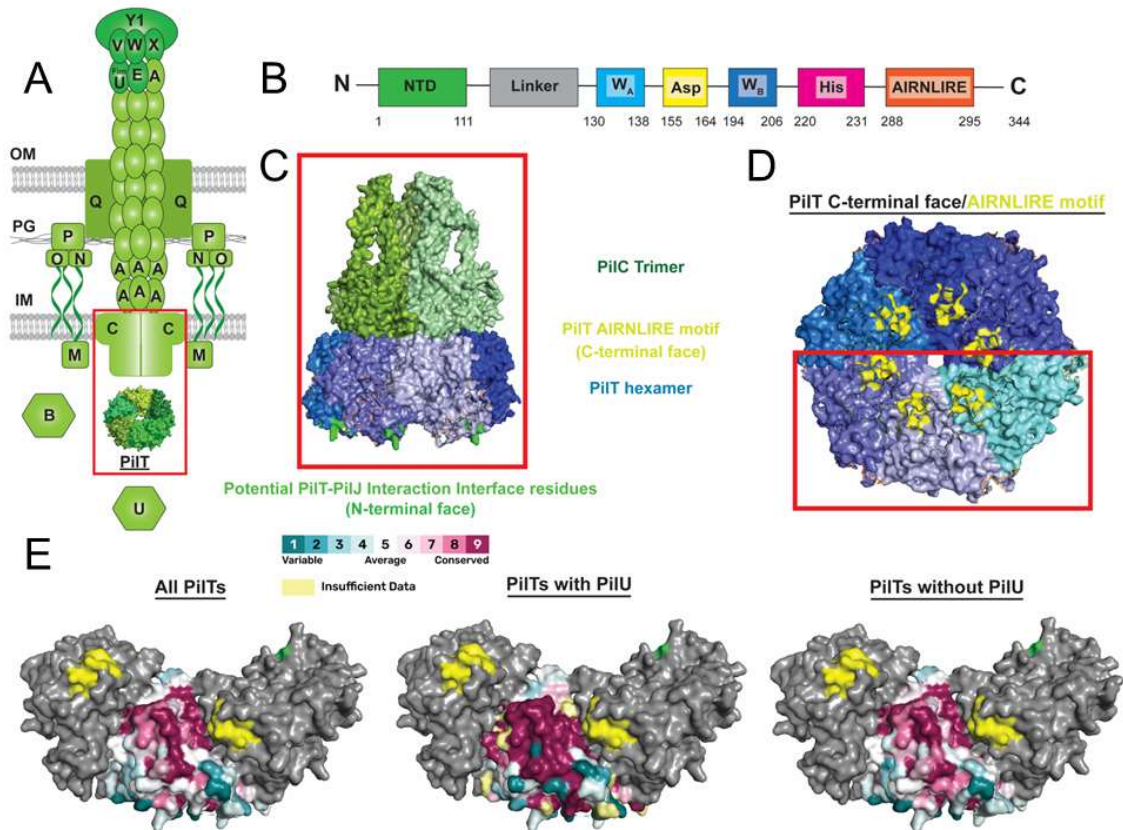
Figure 3. Predicting the interface between the C-terminal face of the PilT hexamer and the PilC hexamer. (A) An illustration of the T4P of *P. aeruginosa*. (B) A linear representation of the PilT protein with known domains labeled, and the beginning and ending aa of each domain indicated. (C) The alphafold multimer program was used to predict the structure of PilT hexamer (blue) bound to the PilC trimer (green) with the model giving the best score shown. The residues comprising the PilT-PilJ interface are highlighted in green. (D) The C-terminal face of the PilT hexamer with PilC removed. Each PilT monomer is in a different shade of blue and the conserved AIRNLIRE motif is colored in yellow. A red box encircles the monomers with conservation information mapped on the surface as shown in panel (E). (E) A BLAST search was performed on taxid: 286 for the genus *Pseudomonas* using PA14 *pilT* as a search query (left). Homologs were identified and genomes were pooled by whether a homolog of PilU could also be identified (center), or not (right). A multiple sequence alignment was then generated using Clustal Omega and the resulting multiple sequence alignment (MSA) was used with CONSURF to calculate and map conservation scores for each residue on the center monomer of the trimer shown here. PDB: 3JVV chain B was then used to map the conservation information onto each residue. The legend shows the extent of sequence identity for each residue for the central monomer. In yellow are highlighted the AIRNLIRE motif in the left and right monomers.

Given that data from the literature, structural predictions, and conservation of amino acids across PilT homologs all indicated that PilT binds PilC via the C-terminal face of the PilT hexamer, we reasoned that the N-terminal face of the PilT hexamer would be available for PilU binding. The highest scoring alphafold multimer prediction also agreed with this hypothesis and showed the N-terminal face of the PilT hexamer binding PilU (**Figure 4A/B**). When analyzing the three proteins together, we obtain a composite of the two predictions which shows the PilT hexamer's C-terminal face binding PilC and the N-terminal face of the PilT hexamer binding PilU.

Upon revisiting the conserved surface residues of PilT, we noticed that the PilT hexamer's N-terminal face (as opposed to the C-terminal face as outlined above) showed few conserved amino acids. However, when we performed this analysis with the PilT sequences from organisms which also encoded a PilU in the same genome, we find that the N-terminal face of the PilT hexamer has patches of conserved amino acids, which would make sense if these residues were under selection to maintain binding with another protein for function (i.e., PilU; **Figure 4C**).

The N-terminal face of the PilT hexamer is also the location of residues that mediate PilT-PilJ binding as determined in our previous study. In an attempt to isolate mutants of PilT that retain twitching motility but no longer bind to PilJ, a genetic screen was performed that isolated alleles of *pilT* that produced motors capable of powering twitching motility in *Pa* but are unable to bind to PilJ in the the B2H system. When mapping these mutations onto the PilT structure, 28% of the mutations mapped to a 4 residue patch on the N-terminal face of the PilT hexamer indicating to us that this was the face of PilT that interacted with PilJ. Of the four mutants making up this patch, only one of the alleles produced a stable protein when expressed in *Pa*, but surprisingly, there was no difference in the amount of cAMP observed for this H44L mutant when grown on a surface (113). However, when examining the conservation score of this residue for PilT motors that also have a PilU in the genome, this residue was the *least* conserved of the four residues identified in our screen, indicating to us that this residue was the least important for interacting

with PilJ and providing a possible explanation as to why a change in cAMP was not observed.

Together these data support the hypothesis that PilU is able to modulate PilT signaling to PilJ not only by providing force during retraction and preventing the conformational change in PilT that allows for binding to PilJ, but by also blocking the binding site for PilJ even when PilU is not actively aiding in retraction.
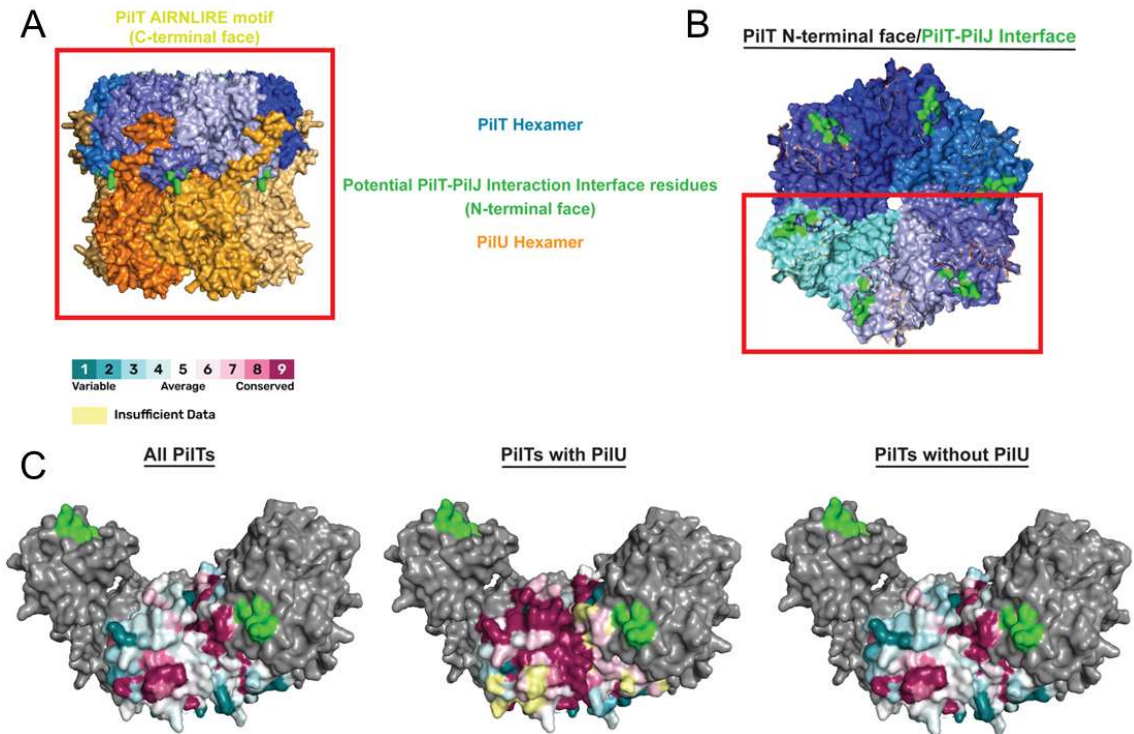
Figure 4. Predicting the interface between the N-terminal face of the PilT hexamer and the PilU or PilJ hexamers. (A) Alphafold multimer was used to predict the structure of PilT hexamer bound to the hexamer PilU with the model giving the best score shown. (B) N-terminal face of the PilT hexamer with PilU removed. Each PilT monomer is in a different shade of blue and the potential PilT-PilJ binding interface is colored in green. A red box encircles the monomers with conservation information mapped on the surface of the central monomer as shown in panel (C). (C) A BLAST search was performed on taxid: 286 for the genus *Pseudomonas* using PA14 *pilT* as a search query, homologs were identified (left), and genomes pooled by whether a homolog of PilU could also be identified (center), or not (right). A multiple sequence alignment was then generated using Clustal Omega and the resulting MSA was used with CONSURF to calculate and map conservation scores for each residue on the center monomer of the trimer shown here. PDB: 3JVV chain B was then used to map the conservation information onto each residue. The legend shows the extent of sequence identity for each residue. In green are the residues that are predicted to mediate binding with PilJ on the left and right monomers.

Consistent with our model, signaling by T4P motors has been previously reported for *Myxococcus xanthus*. In this organism, EPS production only occurs when T4P are able to interact with a surface. Mutations in the extension motor PilB were able to restore EPS production in a T4P deficient background of *Myxococcus*. A Walker-A mutation in PilB was also able to stimulate EPS production without restoring T4P motility. The PilB-WA hexamer resembles the WT PilB in the apo form, leading to the conclusion that the unbound form of PilB was the signaling conformation. Further work has demonstrated that the binding state of PilB to c-di-GMP, ATP, and ADP influences the conformation of PilB and controls whether this motor is actively polymerizing pili or performing EPS signaling (130-132). Thus, a role for T4P motors in transmitting surface signals may be a conserved mechanism. Furthermore, conformational changes in the retraction motor PilT have been implicated in *Neisseria gonorheae* when tension is applied to pili fibers. It is thought that these conformational changes may occur within the motor when the load is near or over the motor stalling limit and may serve as a signal within cells (19, 133). These data indicate that the T4P motors not only sense tension on pili but can serve as signaling proteins in other organisms as well.

1.10 Conclusions

The opportunistic pathogen *P. aeruginosa* PA14 serves as an excellent model organism to study bacterial surface sensing and adaptation, impinging on an important aspect of this bacterium's lifestyle and its ability to be a pathogen. Current data point to a model where *Pa* uses T4P to sense a surface and transmit that signal to the cell likely through its primary retraction motor PilT. This mechanism of surface sensing leads to the production of cAMP due to motor stalling.

Interestingly there are mutations in the flagellum that also stimulate the production of cAMP. Mutating the regulator of flagellar number, FleN, creates a cell with multiple polar flagella that bundle together and are unable to rotate. Researchers hypothesize that this imparts a high load on the flagellar machinery which likely also happens during initial surface attachment by the polar flagellum of

Pa. This increase in load has been shown to increase the amount of intracellular cAMP ~3-fold and is dependent on the structural hub protein FimV (102). This finding indicates to us that there are likely other mechanisms to regulate cAMP via the other surface sensing appendage in *Pa.*

Just as T4P and the flagellum regulate levels of c-di-GMP by controlling the binding partner and subsequent activity of SadC, these two appendages may be regulating levels of cAMP by controlling CyaB activity. As previously mentioned, these two second messengers oscillate at the single cell level over multiple generations (23, 90). The generation of fluorescent reporters capable of showing levels of both cAMP and c-di-GMP within the same cell will enable researchers to investigate how these oscillations relate to each other during surface sensing in *Pa*. Furthermore, these second messengers have been shown to affect different surface behaviors including twitching motility and cellular spinning when attached to a surface (23, 102). How these surface behaviors are coordinated to efficiently colonize a surface while also forming a biofilm is also an area of current research (82). As demonstrated above, the interaction of cellular appendages with a surface is critical to surface sensing and in an attempt to prevent biofilm formation, engineers have begun designing surfaces that can prevent these mechanisms of surface sensing in order to prevent the attachment and growth of microbial cells where they are not wanted (134-136).

Not only have surface topology and chemistry been shown to affect mechanisms of surface sensing in *Pa* but *Pseudomonas* phages have also been shown to interfere with T4P function. Viral proteins are able to prevent T4P function which can prevent viral superinfections but also affect surface sensing and biofilm formation (137-139). Also, while *Pa* PA14 serves as an excellent model organism on its own, this opportunistic pathogen rarely exists in nature as a monospecies biofilm. Investigating how biofilm formation and surface sensing of *Pa* is altered when in a polymicrobial community is also being investigated in the field. Other pathogens like *S. aureus* are known to produce molecules that can affect T4P surface behavior and how that change in surface behavior affects biofilm phenotypes is currently being investigated (106, 107). Finally, the environments in which *Pa* colonizes during

infection are extremely different from ideal laboratory conditions with differences in oxygen concentrations, surface stiffness, viscosity, and carbon and nitrogen sources that can affect *Pa* physiology as well as biofilm formation (140). As mentioned above, Pa is known to directionally twitch towards many different biologically relevant molecules such as mucin, BSA, and oligopeptides which also lead to an increase in intracellular cAMP (108). How all of these environmentally relevant factors affect surface sensing during infection and biofilm formation through the mechanisms outlined above will be a major area of research in the coming years.

It is still left to see how the principles learned in *Pa* surface sensing can be applied to other microbes including those that lack motility appendages altogether.

1.12 References

1. O'Toole GA, Wong GC. 2016. Sensational biofilms: surface sensing in bacteria. Current Opinion in Microbiology 30:139-146.
2. Flemming H-C, Wuertz S. 2019. Bacteria and archaea on Earth and their abundance in biofilms. Nature Reviews Microbiology 17:247-260.
3. Maier B, Wong GCL. 2015. How Bacteria Use Type IV Pili Machinery on Surfaces. Trends Microbiol 23:775-788.
4. Shanice S. Webster, Gerard C. L. Wong, O'Toole GA. 2022. The Power of Touch: Type 4 Pili, the von Willebrand A Domain, and Surface Sensing by Pseudomonas aeruginosa. J Bacteriol 204.
5. Ha D-G, O'Toole GA. 2015. c-di-GMP and its Effects on Biofilm Formation and Dispersion: a <i>Pseudomonas Aeruginosa</i> Review. Microbiology Spectrum 3.
6. Bodey GP, Ricardo B, Fainstein V, Jadeja L. 1983. Infections Caused by Pseudomonas aeru. 5.
7. Burrows LL. 2012. Pseudomonas aeruginosa Twitching Motility: Type IV Pili in Action. Annual Review of Microbiology 66:493-520.

8.   Köhler T, Curty LK, Barja F, Delden Cv, Pechère J-C. 2000. Swarming of *Pseudomonas aeruginosa* is dependent on cell-to-cell signaling and requires Ffagella and pili. Journal of Bacteriology 182:5990-5996.

9.   Ha D-G, Kuchma SL, O'Toole GA. 2014. Plate-Based Assay for Swimming Motility in Pseudomonas aeruginosa, p 59-65 doi:10.1007/978-1-4939-0473-0_7. Springer New York.

10.   Toutain CM, Caizza NC, Zegans ME, O'Toole GA. 2007. Roles for flagellar stators in biofilm formation by Pseudomonas aeruginosa. Res Microbiol 158:471-7.

11.   Toutain CM, Zegans ME, O'Toole GA. 2005. Evidence for Two Flagellar Stators and Their Role in the Motility of <i>Pseudomonas aeruginosa</i>. Journal of Bacteriology 187:771-777.

12.   Baker AE, Webster SS, Diepold A, Kuchma SL, Bordeleau E, Armitage JP, O'Toole GA. 2019. Flagellar Stators Stimulate c-di-GMP Production by Pseudomonas aeruginosa. Journal of Bacteriology 201.

13.   Skerker JM, Berg HC. 2001. Direct observation of extension and retraction of type IV pili. Proceedings of the National Academy of Sciences 98:6901-6904.

14.   Talà L, Fineberg A, Kukura P, Persat A. 2019. Pseudomonas aeruginosa orchestrates twitching motility by sequential control of type IV pili movements. Nature Microbiology 4:774-780.

15.   Chiang P, Sampaleanu LM, Ayers M, Pahuta M, Howell PL, Burrows LL. 2008. Functional role of conserved residues in the characteristic secretion NTPase motifs of the Pseudomonas aeruginosa type IV pilus motor proteins PilB, PilT and PilU. Microbiology 154:114-126.

16.   Thomsen ND, Berger JM. 2008. Structural frameworks for considering microbial protein- and nucleic acid-dependent motor ATPases. Mol Microbiol 69:1071-90.

17.   McCallum M, Benlekbir S, Nguyen S, Tammam S, Rubinstein JL, Burrows LL, Howell PL. 2019. Multiple conformations facilitate PilT function in the type IV pilus. Nat Commun 10:5198.

18.   McCallum M, Tammam S, Khan A, Burrows LL, Howell PL. 2017. The molecular mechanism of the type IVa pilus motors. Nat Commun 8:15091.

19.   Craig L, Forest KT, Maier B. 2019. Type IV pili: dynamics, biophysics and functional consequences. Nat Rev Microbiol 17:429-440.

20.   Armbruster CR, Lee CK, Parker-Gilham J, De Anda J, Xia A, Zhao K, Murakami K, Tseng BS, Hoffman LR, Jin F, Harwood CS, Wong GC, Parsek MR. 2019. Heterogeneity in surface sensing suggests a division of labor in Pseudomonas aeruginosa populations. eLife 8.

21.   Lee CK, Vachier J, De Anda J, Zhao K, Baker AE, Bennett RR, Armbruster CR, Lewis KA, Tarnopol RL, Lomba CJ, Hogan DA, Parsek MR, O'Toole GA, Golestanian R, Wong GCL. 2020. Social Cooperativity of Bacteria during Reversible Surface Attachment in Young Biofilms: a Quantitative Comparison of Pseudomonas aeruginosa PA14 and PAO1. mBio 11.

22.   Kasetty S, Katharios-Lanwermeyer S, O'Toole GA, Nadell CD. 2021. Differential Surface Competition and Biofilm Invasion Strategies of Pseudomonas aeruginosa PA14 and PAO1. J Bacteriol 203:e0026521.

23.   Lee CK, De Anda J, Baker AE, Bennett RR, Luo Y, Lee EY, Keefe JA, Helali JS, Ma J, Zhao K, Golestanian R, O'Toole GA, Wong GCL. 2018. Multigenerational memory and adaptive adhesion in early bacterial biofilm communities. Proceedings of the National Academy of Sciences 115:4471-4476.

24.   Luo Y, Zhao K, Baker AE, Kuchma SL, Coggan KA, Wolfgang MC, Wong GC, O'Toole GA. 2015. A hierarchical cascade of second messengers regulates Pseudomonas aeruginosa surface behaviors. mBio 6.

25.   Comolli JC, Hauser AR, Waite L, Whitchurch CB, Mattick JS, Engel JN. 1999. <i>Pseudomonas aeruginosa</i> Gene Products PilT and PilU Are Required for Cytotoxicity In Vitro and Virulence in a Mouse Model of Acute Pneumonia. Infection and Immunity 67:3625-3630.

26.   Fuchs EL, Brutinel ED, Klem ER, Fehr AR, Yahr TL, Wolfgang MC. 2010. In Vitro and In Vivo Characterization of the Pseudomonas aeruginosa Cyclic AMP (cAMP) Phosphodiesterase CpdA, Required for cAMP Homeostasis and Virulence Factor Regulation. Journal of Bacteriology 192:2779-2790.

27.   Siryaporn A, Kuchma SL, O'Toole GA, Gitai Z. 2014. Surface attachment induces <i>Pseudomonas aeruginosa</i> virulence. Proceedings of the National Academy of Sciences 111:16860-16865.

28.   Bertrand JJ, West JT, Engel JN. 2010. Genetic Analysis of the Regulation of Type IV Pilus Function by the Chp Chemosensory System of <i>Pseudomonas aeruginosa</i>. Journal of Bacteriology 192:994-1010.

29. Whitchurch CB, Leech AJ, Young MD, Kennedy D, Sargent JL, Bertrand JJ, Semmler ABT, Mellick AS, Martin PR, Alm RA, Hobbs M, Beatson SA, Huang B, Nguyen L, Commolli JC, Engel JN, Darzins A, Mattick JS. 2004. Characterization of a complex chemosensory signal transduction system which controls twitching motility in Pseudomonas aeruginosa. Molecular Microbiology 52:873-893.

30. Katharios-Lanwermeyer S, O'Toole GA. 2022. Biofilm Maintenance as an Active Process: Evidence that Biofilms Work Hard to Stay Put. J Bacteriol 204.

31. Katharios-Lanwermeyer S, Whitfield GB, Howell PL, O'Toole GA. 2021. Pseudomonas aeruginosa Uses c-di-GMP Phosphodiesterases RmcA and MorA To Regulate Biofilm Maintenance. mBio 12.

32. Stefan Katharios-Lanwermeyer a, Sophia A. Koval aaKEB, a George A. O'Toolea. 2022. The Diguanylate Cyclase YfiNof Pseudomonas aeruginosa Regulates Biofilm Maintenance in Response to Peroxide. J Bacteriol 204.

33. Kim S-K, Lee J-H. 2016. Biofilm dispersion in Pseudomonas aeruginosa. Journal of Microbiology 54:71-85.

34. Rumbaugh KP, Sauer K. 2020. Biofilm dispersion. Nature Reviews Microbiology 18:571-586.

35. Fuchs EL, Brutinel ED, Jones AK, Fulcher NB, Urbanowski ML, Yahr TL, Wolfgang MC. 2010. The Pseudomonas aeruginosa Vfr Regulator Controls Global Virulence Factor Expression through Cyclic AMP-Dependent and -Independent Mechanisms. Journal of Bacteriology 192:3553-3564.

36. Inclan YF, Persat A, Greninger A, Von Dollen J, Johnson J, Krogan N, Gitai Z, Engel JN. 2016. A scaffold protein connects type IV pili with the Chp chemosensory system to mediate activation of virulence signaling in<i>Pseudomonas aeruginosa</i>. Molecular Microbiology 101:590-605.

37. Wolfgang MC, Lee VT, Gilmore ME, Lory S. 2003. Coordinate Regulation of Bacterial Virulence Genes by a Novel Adenylate Cyclase-Dependent Signaling Pathway. Developmental Cell 4:253-263.

38. Beatson SA, Whitchurch CB, Sargent JL, Levesque RC, Mattick JS. 2002. Differential Regulation of Twitching Motility and Elastase Production by Vfr in Pseudomonas aeruginosa. Journal of Bacteriology 184:3605-3613.

39. Chawla R, Gupta R, Lele TP, Lele PP. 2020. A Skeptic's Guide to Bacterial Mechanosensing. J Mol Biol 432:523-533.

40. Dufrêne YF, Persat A. 2020. Mechanomicrobiology: how bacteria sense and respond to forces. Nature Reviews Microbiology 18:227-240.

41. Purcell EM. 1977. Life at Low Reynolds Number. American Journal of Physics 45:3-11.

42. De Anda J, Lee EY, Lee CK, Bennett RR, Ji X, Soltani S, Harrison MC, Baker AE, Luo Y, Chou T, O'Toole GA, Armani AM, Golestanian R, Wong GCL. 2017. High-Speed "4D" Computational Microscopy of Bacterial Surface Motility. ACS Nano 11:9340-9351.

43. Lele PP, Hosu BG, Berg HC. 2013. Dynamics of mechanosensing in the bacterial flagellar motor. Proceedings of the National Academy of Sciences 110:11839-11844.

44. Tipping MJ, Delalez NJ, Lim R, Berry RM, Armitage JP. 2013. Load-dependent assembly of the bacterial flagellar motor. mBio 4.

45. Castillo DJ, Nakamura S, Morimoto YV, Che Y-S, Kami-Ike N, Kudo S, Minamino T, Namba K. 2013. The C-terminal periplasmic domain of MotB is responsible for load-dependent control of the number of stators of the bacterial flagellar motor. BIOPHYSICS 9:173-181.

46. Che YS, Nakamura S, Morimoto YV, Kami-Ike N, Namba K, Minamino T. 2014. Load-sensitive coupling of proton translocation and torque generation in the bacterial flagellar motor. Molecular Microbiology 91:175-184.

47. Chawla R, Ford KM, Lele PP. 2017. Torque, but not FliL, regulates mechanosensitive flagellar motor-function. Scientific Reports 7.

48. Block SM, Berg HC. 1984. Successive incorporation of force-generating units in the bacterial rotary motor. Nature 309:470-472.

49. Beeby M, Ribardo DA, Brennan CA, Ruby EG, Jensen GJ, Hendrixson DR. 2016. Diverse high-torque bacterial flagellar motors assemble wider stator rings using a conserved protein scaffold. Proceedings of the National Academy of Sciences 113:E1917-E1926.

50. Blair DF, Berg HC. 1988. Restoration of torque in defective flagellar motors. Science.

51. Leake MC, Chandler JH, Wadhams GH, Bai F, Berry RM, Armitage JP. 2006. Stoichiometry and turnover in single, functioning membrane protein complexes. Nature 443:355-358.

52. Nord AL, Gachon E, Perez-Carrasco R, Nirody JA, Barducci A, Berry RM, Pedaci F. 2017. Catch bond drives stator mechanosensitivity in the bacterial flagellar motor. Proceedings of the National Academy of Sciences 114:12952-12957.

53. De Anda J, Kuchma SL, Webster SS, Boromand A, Lewis KA, Lee CK, Contreras M, Pereira VFM, Hogan DA, O'Hern CS, O'Toole GA, Wong GCL. 2023. How individual *P. aeruginosa* cells with diverse stator distributions collectively form a heterogeneous macroscopic swarming population doi:10.1101/2023.04.10.536285. Cold Spring Harbor Laboratory.

54. Kuchma SL, Ballok AE, Merritt JH, Hammond JH, Lu W, Rabinowitz JD, O'Toole GA. 2010. Cyclic-di-GMP-Mediated Repression of Swarming Motility by *Pseudomonas aeruginosa*: the *pilY1* Gene and Its Impact on Surface-Associated Behaviors. Journal of Bacteriology 192:2950-2964.

55. O'Toole GA, Kolter R. 1998. Flagellar and twitching motility are necessary for *Pseudomonas aeruginosa* biofilm development. Molecular Microbiology 30:295-304.

56. Hug I, Deshpande S, Sprecher KS, Pfohl T, Jenal U. 2017. Second messenger–mediated tactile response by a bacterial rotary motor. Science 358:531-534.

57. Wu DC, Zamorano-Sánchez D, Pagliai FA, Park JH, Floyd KA, Lee CK, Kitts G, Rose CB, Bilotta EM, Wong GCL, Yildiz FH. 2020. Reciprocal c-di-GMP signaling: Incomplete flagellum biogenesis triggers c-di-GMP signaling pathways that promote biofilm formation. PLOS Genetics 16:e1008703.

58. Guttenplan SB, Kearns DB. 2013. Regulation of flagellar motility during biofilm formation. FEMS Microbiology Reviews 37:849-871.

59. Koch MD, Fei C, Wingreen NS, Shaevitz JW, Gitai Z. 2021. Competitive binding of independent extension and retraction motors explains the quantitative dynamics of type IV pili. Proceedings of the National Academy of Sciences 118:e2014926118.

60. Gibiansky ML, Conrad JC, Jin F, Gordon VD, Motto DA, Mathewson MA, Stopka WG, Zelasko DC, Shrout JD, Wong GCL. 2010. Bacteria Use Type IV Pili to Walk Upright and Detach from Surfaces. Science 330:197-197.

61. Maxsim L. Gibiansky JCC, 2* Fan Jin,1 Vernita D. Gordon,1 Dominick A. Motto,4 Margie A. Mathewson,3 Wiktor G. Stopka,3 Daria C. Zelasko,3 Joshua D. Shrout,4 Gerard C. L. Wong1,3†. 2010. Bacteria use type IV pili to walk upright and detach from surfaces. Science.

62. Conrad JC. 2012. Physics of bacterial near-surface motility using flagella and type IV pili: implications for biofilm formation. Res Microbiol 163:619-29.

63.   Jacinta, Maxsim, Jin F, Vernita, Dominick, Margie, Wiktor, Daria, Joshua, Gerard. 2011. Flagella and Pili-Mediated Near-Surface Single-Cell Motility Mechanisms in P. aeruginosa. Biophysical Journal 100:1608-1616.

64.   Maier B, Potter L, So M, Seifert HS, Sheetz MP. 2002. Single pilus motor forces exceed 100 pN. Proceedings of the National Academy of Sciences 99:16012-16017.

65.   Biais N, Ladoux B, Higashi D, So M, Sheetz M. 2008. Cooperative Retraction of Bundled Type IV Pili Enables Nanonewton Force Generation. PLoS Biology 6:e87.

66.   Ribbe J, Baker AE, Euler S, O'Toole GA, Maier B. 2017. Role of Cyclic Di-GMP and Exopolysaccharide in Type IV Pilus Dynamics. Journal of Bacteriology 199:JB.00859-16.

67.   Beaussart A, Baker AE, Kuchma SL, El-Kirat-Chatel S, O'Toole GA, Dufrêne YF. 2014. Nanoscale Adhesion Forces of <i>Pseudomonas aeruginosa</i> Type IV Pili. ACS Nano 8:10723-10733.

68.   Jin F, Conrad JC, Gibiansky ML, Wong GCL. 2011. Bacteria use type-IV pili to slingshot on surfaces. Proceedings of the National Academy of Sciences 108:12617-12622.

69.   Biais N, Higashi DL, Brujić J, So M, Sheetz MP. 2010. Force-dependent polymorphism in type IV pili reveals hidden epitopes. Proceedings of the National Academy of Sciences 107:11358-11363.

70.   Chlebek JL, Hughes HQ, Ratkiewicz AS, Rayyan R, Wang JC, Herrin BE, Dalia TN, Biais N, Dalia AB. 2019. PilT and PilU are homohexameric ATPases that coordinate to retract type IVa pili. PLoS Genet 15:e1008448.

71.   Evan Couser JLC, Ankur B. Daliaa. 2022. Retraction ATPase Motors from Three Orthologous Type IVa Pilus Systems Support Promiscuous Retraction of the Vibrio cholerae Competence Pilus. Journal of Bacteriology.

72.   Adams DW, Pereira JM, Stoudmann C, Stutzmann S, Blokesch M. 2019. The type IV pilus protein PilU functions as a PilT-dependent retraction ATPase. PLOS Genetics 15:e1008393.

73.   Whitchurch CB, Mattick JS. 1994. Characterization of a gene, pilU, required for twitching motility but not phage sensitivity in Pseudomonas aeruginosa. Molecular Microbiology 13:1079-1091.

74.   Zöllner R, Cronenberg T, Maier B. 2019. Motor Properties of PilT-Independent Type 4 Pilus Retraction in Gonococci. Journal of Bacteriology 201.

75. Chlebek JL, Denise R, Craig L, Dalia AB. 2021. Motor-independent retraction of type IV pili is governed by an inherent property of the pilus filament. Proceedings of the National Academy of Sciences 118:e2102780118.

76. Persat A, Inclan YF, Engel JN, Stone HA, Gitai Z. 2015. Type IV pili mechanochemically regulate virulence factors in Pseudomonas aeruginosa. Proc Natl Acad Sci U S A 112:7563-8.

77. Ellison CK, Kan J, Dillard RS, Kysela DT, Ducret A, Berne C, Hampton CM, Ke Z, Wright ER, Biais N, Dalia AB, Brun YV. 2017. Obstruction of pilus retraction stimulates bacterial surface sensing. Science 358:535-538.

78. Kuchma SL, O'Toole GA. 2022. Surface-Induced cAMP Signaling Requires Multiple Features of the Pseudomonas aeruginosa Type IV Pili. Journal of Bacteriology.

79. Cooley RB, Smith TJ, Leung W, Tierney V, Borlee BR, O'Toole GA, Sondermann H. 2016. Cyclic Di-GMP-Regulated Periplasmic Proteolysis of a Pseudomonas aeruginosa Type Vb Secretion System Substrate. Journal of Bacteriology 198:66-76.

80. Courtney Reichhardt, Holly M. Jacobs aMM, a Cynthis Wong,a Daniel J. Wozniak, Parsek MR. 2020. The Versatile Pseudomonas aeruginosa Biofilm Matrix Protein CdrA Promotes Aggregation through Different Extracellular Exopolysaccharide Interactions. J Bacteriol 202.

81. Bru J-L, Kasallis SJ, Zhuo Q, Høyland-Kroghsbo NM, Siryaporn A. 2023. Swarming of <i>P. aeruginosa</i>: Through the lens of biophysics. Biophysics Reviews 4.

82. Laventie B-J, Sangermani M, Estermann F, Manfredi P, Planes R, Hug I, Jaeger T, Meunier E, Broz P, Jenal U. 2019. A Surface-Induced Asymmetric Program Promotes Tissue Colonization by Pseudomonas aeruginosa. Cell Host & Microbe 25:140-152.e6.

83. Vrabioiu AM, Berg HC. 2022. Signaling events that occur when cells of <i>Escherichia coli</i> encounter a glass surface. Proceedings of the National Academy of Sciences 119:e2116830119.

84. Fulcher NB, Holliday PM, Klem E, Cann MJ, Wolfgang MC. 2010. The Pseudomonas aeruginosa Chp chemosensory system regulates intracellular cAMP levels by modulating adenylate cyclase activity. Molecular Microbiology 76:889-904.

85. Treuner-Lange A, Chang Y-W, Glatter T, Herfurth M, Lindow S, Chreifi G, Jensen GJ, Søgaard-Andersen L. 2020. PilY1 and minor pilins form a complex priming the type IVa pilus in Myxococcus xanthus. Nature Communications 11.

86. Ng D, Harn T, Altindal T, Kolappan S, Marles JM, Lala R, Spielman I, Gao Y, Hauke CA, Kovacikova G, Verjee Z, Taylor RK, Biais N, Craig L. 2016. The Vibrio cholerae Minor Pilin TcpB Initiates Assembly and Retraction of the Toxin-Coregulated Pilus. PLOS Pathogens 12:e1006109.

87. Webster SS, Lee CK, Schmidt WC, Wong GCL, O'Toole GA. 2021. Interaction between the type 4 pili machinery and a diguanylate cyclase fine-tune c-di-GMP levels during early biofilm formation. Proceedings of the National Academy of Sciences 118:e2105566118.

88. Shanice S. Webster aWCS, d,e,f, Marion Mathelié-Guinlet bGCLW, d,e,f, Andreia F. Verissimo cYFD, b, Daniel Schultz aAV, b George A. O'Toole. 2022. Force-Induced Changes of PilY1 Drive Surface Sensing by Pseudomonas aeruginosa. mBio 13.

89. McCallum M, Tammam S, Rubinstein JL, Burrows LL, Howell PL. 2021. CryoEM map of Pseudomonas aeruginosa PilQ enables structural characterization of TsaP. Structure 29:457-466.e4.

90. Lee CK, Schmidt WC, Webster SS, Chen JW, O'Toole GA, Wong GCL. 2022. Broadcasting of amplitude- and frequency-modulated c-di-GMP signals facilitates cooperative surface commitment in bacterial lineages. Proceedings of the National Academy of Sciences 119:e2112226119.

91. Moscoso JA, Jaeger T, Valentini M, Hui K, Jenal U, Filloux A. 2014. The Diguanylate Cyclase SadC Is a Central Player in Gac/Rsm-Mediated Biofilm Formation in Pseudomonas aeruginosa. Journal of Bacteriology 196:4081-4088.

92. Yahr TL, Vallis AJ, Hancock MK, Barbieri JT, Frank DW. 1998. ExoY, an adenylate cyclase secreted by the<i>Pseudomonas aeruginosa</i>type III system. Proceedings of the National Academy of Sciences 95:13899-13904.

93. Inclan YF, Huseby MJ, Engel JN. 2011. FimL Regulates cAMP Synthesis in Pseudomonas aeruginosa. PLoS ONE 6:e15867.

94. Topal H, Fulcher NB, Bitterman J, Salazar E, Buck J, Levin LR, Cann MJ, Wolfgang MC, Steegborn C. 2012. Crystal Structure and Regulation Mechanisms of the CyaB Adenylyl Cyclase from the Human Pathogen Pseudomonas aeruginosa. Journal of Molecular Biology 416:271-286.

95. Endoh T, Engel JN. 2009. CbpA: a Polarly Localized Novel Cyclic AMP-Binding Protein in Pseudomonas aeruginosa. Journal of Bacteriology 191:7193-7205.

96. Buensuceso RNC, Nguyen Y, Zhang K, Daniel-Ivad M, Sugiman-Marangos SN, Fleetwood AD, Zhulin IB, Junop MS, Howell PL, Burrows LL. 2016. The Conserved Tetratricopeptide Repeat-Containing C-Terminal Domain of Pseudomonas aeruginosa FimV Is Required for Its Cyclic AMP-Dependent and -Independent Functions. Journal of Bacteriology 198:2263-2274.

97. Carter T, Buensuceso RN, Tammam S, Lamers RP, Harvey H, Howell PL, Burrows LL. 2017. The Type IVa Pilus Machinery Is Recruited to Sites of Future Cell Division. mBio 8.

98. Bernhardt TG, De Boer PAJ. 2003. The Escherichia coli amidase AmiC is a periplasmic septal ring component exported via the twin-arginine transport pathway. Molecular Microbiology 48:1171-1182.

99. Heidrich C, Templin MF, Ursinus A, Merdanovic M, Berger J, Schwarz H, De Pedro MA, Höltje J-V. 2001. Involvement of N-acetylmuramyl-l-alanine amidases in cell separation and antibiotic-induced autolysis of Escherichia coli. Molecular Microbiology 41:167-178.

100. Peters NT, Dinh T, Bernhardt TG. 2011. A Fail-Safe Mechanism in the Septal Ring Assembly Pathway Generated by the Sequential Recruitment of Cell Separation Amidases and Their Activators. Journal of Bacteriology 193:4973-4983.

101. Buensuceso RNC, Daniel-Ivad M, Kilmury SLN, Leighton TL, Harvey H, Howell PL, Burrows LL. 2017. Cyclic AMP-Independent Control of Twitching Motility in Pseudomonas aeruginosa. Journal of Bacteriology 199.

102. Schniederberend M, Williams JF, Shine E, Shen C, Jain R, Emonet T, Kazmierczak BI. 2019. Modulation of flagellar rotation in surface-attached bacteria: A pathway for rapid surface-sensing after flagellar attachment. PLOS Pathogens 15:e1008149.

103. Darzins A. 1994. Characterization of a Pseudomonas aeruginosa gene cluster involved in pilus biosynthesis and twitching motility: sequence similarity to the chemotaxis proteins of enterics and the gliding bacterium Myxococcus xanthus. Molecular Microbiology 11:137-153.

104. Darzins A. 1993. The pilG gene product, required for Pseudomonas aeruginosa pilus production and twitching motility, is homologous to the enteric, single-domain response regulator CheY. Journal of Bacteriology 175:5934-5944.

105. Kearns DB, Robinson J, Shimkets LJ. 2001. <i>Pseudomonas aeruginosa</i> Exhibits Directed Twitching Motility Up Phosphatidylethanolamine Gradients. Journal of Bacteriology 183:763-767.

106. Limoli DH, Warren EA, Yarrington KD, Donegan NP, Cheung AL, O'Toole GA. 2019. Interspecies interactions induce exploratory motility in Pseudomonas aeruginosa. Elife 8.

107. Yarrington KD, Shendruk TN, Limoli DH. 2022. Twitching cells use a chemoreceptor to detect bacterial competitors doi:10.1101/2022.11.28.518211. Cold Spring Harbor Laboratory.

108. Nolan LM, McCaughey LC, Merjane J, Turnbull L, Whitchurch CB. 2020. ChpC controls twitching motility-mediated expansion of Pseudomonas aeruginosa biofilms in response to serum albumin, mucin and oligopeptides. Microbiology 166:669-678.

109. Jansari VH, Potharla VY, Riddell GT, Bardy SL. 2016. Twitching motility and cAMP levels: signal transduction through a single methyl-accepting chemotaxis protein. FEMS Microbiol Lett 363.

110. Kühn MJ, Macmillan H, Talà L, Inclan Y, Patino R, Pierrat X, Al-Mayyah Z, Engel JN, Persat A. 2023. Two antagonistic response regulators control <i>Pseudomonas aeruginosa</i> polarization during mechanotaxis. The EMBO Journal doi:10.15252/embj.2022112165.

111. Kühn MJ, Talà L, Inclan YF, Patino R, Pierrat X, Vos I, Al-Mayyah Z, Macmillan H, Negrete J, Engel JN, Persat A. 2021. Mechanotaxis directs <i>Pseudomonas aeruginosa</i> twitching motility. Proceedings of the National Academy of Sciences 118:e2101759118.

112. Koch MD, Black ME, Han E, Shaevitz JW, Gitai Z. 2022. Pseudomonas aeruginosa distinguishes surfaces by stiffness using retraction of type IV pili. Proc Natl Acad Sci U S A 119:e2119434119.

113. Geiger CJ, O'Toole GA. 2023. Evidence for the Type IV Pilus Retraction Motor PilT as a Component of the Surface Sensing System in Pseudomonas aeruginos. J Bacteriol 205.

114. McCallum M, Tammam S, Little DJ, Robinson H, Koo J, Shah M, Calmettes C, Moraes TF, Burrows LL, Howell PL. 2016. PilN Binding Modulates the Structure and Binding

Partners of the Pseudomonas aeruginosa Type IVa Pilus Protein PilM. Journal of Biological Chemistry 291:11003-11015.

115. Chang YW, Rettberg LA, Treuner-Lange A, Iwasa J, Sogaard-Andersen L, Jensen GJ. 2016. Architecture of the type IVa pilus machine. Science 351:aad2001.

116. Denise R, Abby SS, Rocha EPC. 2019. Diversification of the type IV filament superfamily into machines for adhesion, protein secretion, DNA uptake, and motility. PLOS Biology 17:e3000390.

117. Aukema KG, Kron EM, Herdendorf TJ, Forest KT. 2005. Functional Dissection of a Conserved Motif within the Pilus Retraction Protein PilT. Journal of Bacteriology 187:611-618.

118. Misic AM, Satyshur KA, Forest KT. 2010. P. aeruginosa PilT Structures with and without Nucleotide Reveal a Dynamic Type IV Pilus Retraction Motor. Journal of Molecular Biology 400:1011-1021.

119. Satyshur KA, Worzalla GA, Meyer LS, Heiniger EK, Aukema KG, Misic AM, Forest KT. 2007. Crystal Structures of the Pilus Retraction Motor PilT Suggest Large Domain Movements and Subunit Cooperation Drive Motility. Structure 15:363-376.

120. Cowles KN, Gitai Z. 2010. Surface association and the MreB cytoskeleton regulate pilus production, localization and function in Pseudomonas aeruginosa. Molecular Microbiology 76:1411-1426.

121. Jain R, Sliusarenko O, Kazmierczak BI. 2017. Interaction of the cyclic-di-GMP binding protein FimX and the Type 4 pilus assembly ATPase promotes pilus assembly. PLOS Pathogens 13:e1006594.

122. Sievers F, Higgins DG. 2018. Clustal Omega for making accurate alignments of many protein sequences. Protein Science 27:135-145.

123. Varadi M, Anyango S, Deshpande M, Nair S, Natassia C, Yordanova G, Yuan D, Stroe O, Wood G, Laydon A, Zidek A, Green T, Tunyasuvunakool K, Petersen S, Jumper J, Clancy E, Green R, Vora A, Lutfi M, Figurnov M, Cowie A, Hobbs N, Kohli P, Kleywegt G, Birney E, Hassabis D, Velankar S. 2022. AlphaFold Protein Structure Database: massively expanding the structural coverage of protein-sequence space with high-accuracy models. Nucleic Acids Res 50:D439-D444.

124. Evans R, O'Neill M, Pritzel A, Antropova N, Senior A, Green T, Žídek A, Bates R, Blackwell S, Yim J, Ronneberger O, Bodenstein S, Zielinski M, Bridgland A, Potapenko A, Cowie A, Tunyasuvunakool K, Jain R, Clancy E, Kohli P, Jumper J, Hassabis D. 2021.

Protein complex prediction with AlphaFold-Multimer
doi:10.1101/2021.10.04.463034. Cold Spring Harbor Laboratory.

125.   Jumper J, Evans R, Pritzel A, Green T, Figurnov M, Ronneberger O, Tunyasuvunakool K, Bates R, Žídek A, Potapenko A, Bridgland A, Meyer C, Kohl SAA, Ballard AJ, Cowie A, Romera-Paredes B, Nikolov S, Jain R, Adler J, Back T, Petersen S, Reiman D, Clancy E, Zielinski M, Steinegger M, Pacholska M, Berghammer T, Bodenstein S, Silver D, Vinyals O, Senior AW, Kavukcuoglu K, Kohli P, Hassabis D. 2021. Highly accurate protein structure prediction with AlphaFold. Nature 596:583-589.

126.   Ben Chorin A, Masrati G, Kessel A, Narunsky A, Sprinzak J, Lahav S, Ashkenazy H, Ben-Tal N. 2020. ConSurf-DB: An accessible repository for the evolutionary conservation patterns of the majority of PDB proteins. Protein Science 29:258-267.

127.   Ashkenazy H, Abadi S, Martz E, Chay O, Mayrose I, Pupko T, Ben-Tal N. 2016. ConSurf 2016: an improved methodology to estimate and visualize evolutionary conservation in macromolecules. Nucleic Acids Res 44:W344-50.

128.   Bradley D. 1980. a function of *Pseudomonas aeruginosa* PAO polar pili: twitching motility. Canadian Journal of Microbiology 26:146-154.

129.   Speers AM, Schindler BD, Hwang J, Genc A, Reguera G. 2016. Genetic Identification of a PilT Motor in Geobacter sulfurreducens Reveals a Role for Pilus Retraction in Extracellular Electron Transfer. Front Microbiol 7:1578.

130.   Black WP, Wang L, Jing X, Saldaña RC, Li F, Scharf BE, Schubot FD, Yang Z. 2017. The type IV pilus assembly ATPase PilB functions as a signaling protein to regulate exopolysaccharide production in Myxococcus xanthus. Scientific Reports 7.

131.   Dye KJ, Yang Z. 2020. Cyclic-di-GMP and ADP bind to separate domains of PilB as mutual allosteric effectors. Biochem J 477:213-226.

132.   Keane J. Dye, Safoura Salar UA, 1 Wraylyn Smith,1, Yang Z. 2023. Myxococcus xanthus PilB interacts with c-di-GMP and modulates motility and biofilm formation. J Bacteriol 205.

133.   Welker A, Cronenberg T, Zöllner R, Meel C, Siewering K, Bender N, Hennes M, Oldewurtel ER, Maier B. 2018. Molecular Motors Govern Liquidlike Ordering and Fusion Dynamics of Bacterial Colonies. Physical Review Letters 121.

134.   Berne C, Ellison CK, Ducret A, Brun YV. 2018. Bacterial adhesion at the single-cell level. Nature Reviews Microbiology 16:616-627.

135. Kreve S, Reis ACD. 2021. Bacterial adhesion to biomaterials: What regulates this attachment? A review. Jpn Dent Sci Rev 57:85-96.

136. Lee SW, Phillips KS, Gu H, Kazemzadeh-Narbat M, Ren D. 2021. How microbes read the map: Effects of implant topography on bacterial adhesion and biofilm formation. Biomaterials 268:120595.

137. Shah M, Taylor VL, Bona D, Tsao Y, Stanley SY, Pimentel-Elardo SM, McCallum M, Bondy-Denomy J, Howell PL, Nodwell JR, Davidson AR, Moraes TF, Maxwell KL. 2021. A phage-encoded anti-activator inhibits quorum sensing in Pseudomonas aeruginosa. Molecular Cell 81:571-583.e6.

138. Amelia K. Schmidt aADF, b Patrick R. Secora Caleb M. Schwartzkopf,a Dominick R. Faith,a Laura K. Jennings,a, Devin J. Hunt aLAM, a Aviv Hargil,c QingquanChen,c Paul L. Bollyky,c David W.Dorward,d Karen L. Maxwell,b, a. 2022. A Filamentous Bacteriophage Protein Inhibits Type IV Pili To Prevent Superinfection of Pseudomonas aeruginosa. mBio 13.

139. Chung I-Y, Jang H-J, Bae H-W, Cho Y-H. 2014. A phage protein that inhibits the bacterial ATPase required for type IV pilus assembly. Proceedings of the National Academy of Sciences 111:11503-11508.

140. Jean-Pierre F, Hampton TH, Schultz D, Hogan DA, Groleau M-C, Déziel E, O'Toole GA. 2023. Community composition shapes microbial-specific phenotypes in a cystic fibrosis polymicrobial model system. eLife 12.

Chapter 2

Introduction

Evidence for the Type IV Pili Retraction Motor PilT as a

Component of the Surface Sensing System in *Pseudomonas aeruginosa*

C.J. Geiger[1] and G.A. O'Toole[1]

[1]Department of Microbiology and Immunology, Geisel School of Medicine at Dartmouth

Author contributions:

C.J.G. and G.A.O. conceptualized and designed the overall study.

G.A.O. provided critical input on experimental design and data interpretation and assisted in writing and editing the chapter.

C.J.G. built all the strains, performed all experiments and data analysis, wrote all scripts for image processing and data analysis, and wrote the chapter.

2.1 Abstract

Biofilm formation begins when bacteria contacting a surface induce cellular changes to become better adapted for surface growth. One of the first changes to occur for *Pseudomonas aeruginosa* after surface contact is an increase in the nucleotide second messenger 3',5'-cyclic adenosine monophosphate (cAMP). It has been demonstrated that this increase in intracellular cAMP is dependent on functional Type IV pili (T4P) relaying a signal to the Pil-Chp system, but the mechanism by which this signal is transduced remains poorly understood. Here, we investigate the role of the Type IV pili retraction motor PilT in sensing a surface and relaying that signal to cAMP production. We show that mutations in PilT, and in particular impacting the ATPase activity of this motor protein, reduce surface-dependent cAMP production. We identify a novel interaction between PilT and PilJ, a member of the Pil-Chp system, and propose a new model whereby *P. aeruginosa* uses its PilT retraction motor to sense a surface and to relay that signal via PilJ to increased production of cAMP. We discuss these findings in light of current T4P-dependent surface sensing models for *P. aeruginosa*.

2.2 Importance

T4P are cellular appendages that allow *P. aeruginosa* to sense a surface leading to the production of cAMP. This second messenger not only activates virulence pathways but leads to further surface adaptation and irreversible attachment of cells. Here, we demonstrate the importance of the retraction motor PilT in surface sensing. We also present a new surface sensing model in *P. aeruginosa* whereby the T4P retraction motor PilT senses and transmits the surface signal, likely via its ATPase domain and interaction with PilJ, to mediate production of the second messenger cAMP.

2.3 Introduction

Biofilm formation is initiated when free swimming, planktonic cells contact a surface. This contact serves as a signal that must be transmitted across the cell envelope into the cytoplasm to initiate appropriate physiological changes to adapt to the biofilm mode of growth (1). For many bacteria this initial surface contact is mediated through motility appendages such as type IV pili (T4P) or flagella (61, 63, 76, 77, 87, 102, 141). Contact between these appendages and the surface creates forces that are not normally present in planktonic environments and can serve as a "surface signal" to the microbe (40).

Early work in *Vibrio parahaemolyticus* demonstrated that the signals encountered during surface contact could be mimicked by increasing the load on the flagellum either through changes in viscosity of the medium or by addition of antibodies specific to the flagellum (142, 143). Recent work in *Caulobacter crescentus* demonstrated that holdfast formation and DNA replication, which normally occurs during surface contact, could be stimulated by increasing the load on Tad pili during retraction. Furthermore, the baseline number of cells with a holdfast without prior pili obstruction was higher in mutants that were unable to rotate their flagellum (77). Others have demonstrated that the flagellar motor itself is able to sense surface contact to trigger c-di-GMP production leading to holdfast synthesis (56). Together, these data indicate that bacteria use their cellular appendages to help sense surface engagement and indicate that impeding the motion (i.e., retraction and/or rotation) of these appendages might serve as the proximal signal for surface engagement.

Pseudomonas aeruginosa also utilizes T4P as well as its polar flagellum to sense and traverse surfaces (7, 13, 24, 82, 87). One of the first changes to occur for many organisms upon surface contact is an increase in the second messenger cyclic-di-GMP (cdG) (144). In *P. aeruginosa* PA14, this initial increase in cdG is produced by the diguanylate cyclase SadC and recent work from our lab and others has shown that

SadC activity is regulated by both components of the flagellum and the T4P (12, 87). Prior to an increase in cdG level, *P. aeruginosa* PA14 increases the level of another second messenger, 3',5'-cyclic adenosine monophosphate (cAMP) (24).

The surface-dependent increase of cAMP by *P. aeruginosa* PA14 depends on functional T4P, the Pil-Chp chemotaxis-like system, and the adenylate cyclase CyaB, and to a lesser extent, the adenylate cyclase CyaA. The methyl-accepting chemotaxis protein (MCP) PilJ relays a signal to the kinase ChpA (84). Activation of the system causes ChpA to phosphorylate the response regulator PilG; phosphorylation of PilG as well as FimV and FimL are required to then activate the adenylate cyclases CyaAB to produce cAMP from ATP (36, 93, 145). The transcription factor Vfr then binds cAMP and activates genes necessary for further surface adaptation as well as for virulence (35, 37).

Recent work by Yarrington, Limoli and colleagues shows that the PilJ likely detects phenyl soluble modulins via its periplasmic domain as a ligand to trigger signaling, a finding that strongly suggests that PilJ can function like a classic MCP (107). Others have recently uncovered the function of PilG and PilH in twitching motility and surface adaptation (110, 111). In contrast, how surface engagement by T4P triggers cAMP signaling in a PilJ-dependent manner is still an open question. A previous study showed that the ligand binding domain (LBD) of PilJ is not required for surface-dependent cAMP production, although the extent of cAMP induction is significantly reduced relative to the WT (109). One model to explain T4P-mediated surface signaling includes interactions between PilA-PilJ via a mechanosensitive change in pilin conformation (76); we recently reported data at odds with this model (78).

P. aeruginosa utilizes the T4P as a cellular grappling hook that pulls the cell along a surface through rounds of pilus extension, surface binding and pilus retraction (13). Functional pili are also required for sensitivity to infection by the phage DMS3 (146). Extension and retraction are powered by three hexameric ATPases: PilB, PilT, and PilU (15, 17, 18). In a recent study from our group, we found that pili on the outside of the cell actively engaging a surface are required for surface-dependent phenotypes, consistent with previous studies (24, 28, 29, 37, 84). Furthermore, we

showed that the ability to retract pili with only enough force to allow phage infection was necessary for surface-dependent, cAMP production. That is, the force required for twitching motility was not necessary for cAMP signaling (78).

While the PilT and PilU proteins both power retraction of T4P through ATP hydrolysis, these ATPases individually have unique roles in T4P dynamics and surface sensing. PilU is the accessory retraction motor for T4P in *P. aeruginosa*, whose function is dependent on the presence of PilT (70, 72). Both PilT and PilU hydrolyze ATP to power retraction but only PilT can interact with the platform protein PilC to coordinate PilA disassembly from extended T4P (17, 72). Others have shown that PilC and PilU can interact via the Bacterial Adenylate Cyclase Two Hybrid (B2H) assay but there is no known functional consequence of this interaction in terms of T4P motility or surface dependent cAMP production (70, 114). While PilT alone is able to retract pili bound to phage (as judged by phage sensitivity assays), PilU in addition to PilT is required for T4P retraction that can pull the cell body along a surface to power twitching motility (TM) (13, 78, 146). Interestingly, deletion of *pilU* increases the amount of cAMP produced by *P. aeruginosa* when grown on a surface and is the only T4P protein, that when mutated, results in increased level of this second messenger. To investigate how PilU affects levels of cAMP during surface contact, we generated strains lacking one or both retraction motors and measured cAMP level via a transcriptional reporter. We found that like phage susceptibility, cAMP production was dependent on the pressence of PilT and that overexpression of PilU decreased cAMP levels when grown on a surface.

Since the effects of PilU on cAMP are dependent on PilT, we next explored the role of PilT in surface signaling. We began by characterizing the effect of different PilT mutations on surface-dependent cAMP production during biofilm formation. We found that mutations in PilT affecting ATP binding and hydrolysis affected cAMP production. A B2H screen revealed a novel interaction between PilT and PilJ. We report here a strong relationship between the extent of PilT-PilJ interaction for PilT mutants that are defective in ATPase activity and the magnitude of cAMP signaling. For strains with all T4P proteins, we also find a strong relationship between twitching motility zone size and the extent of cAMP production. We also identify a mutation in

PilT that disrupts its interaction with PilJ in a B2H assay in *E. coli* that does not appear to perturb signaling in *P. aeruginosa*, suggesting a possible unappreciated level of complexity in PilT-PilJ signaling. Our data are consistent with a model in which PilT senses a surface through tension on the pilus fiber and relays this signal, likely to PilJ, to modulate cAMP production.

2.4 Results

PilU levels significantly affect cAMP levels during surface attachment

To quantify cAMP levels during surface adaptation, the previously reported *PaQa* cAMP-responsive transcriptional reporter (76) was integrated onto the chromosome of *P. aeruginosa* PA14. This reporter is composed of two fluorescent proteins, mKate2 and EYFP, under the control of two different promoters, P_{rpoD} and P_{PaQa}, respectively. P_{PaQa} has been shown to be regulated by Vfr in a cAMP dependent manner and an increase in P_{PaQa}-*eyfp* expression is correlated with an increase in cAMP (76). P_{rpoD}-*mKate2* is used to normalize the EYFP levels for microscopy and used to gate on cells containing the reporter for flow cytometry (76). The *PaQa* reporter was integrated onto the chromosome at a neutral site of the *P. aeruginosa* PA14 chromosome using the mini-CTX1 system (76, 147). We validated this *PaQa* reporter using a mutant that is defective in cAMP production (Δ*cyaAB*) and a mutant lacking the phosphodiesterase that degrades cAMP (Δ*cpdA*), which leads to the accumulation of cAMP **(Figure S1A,B)**. After gating on single cells with P_{rpoD}-*mKate2* signal, the mean EYFP intensity was recorded and normalized to the WT signal. After five hours of surface growth on M8 agar, cells were scraped up and analyzed on a flow cytometer and as expected, the Δ*cyaAB* mutant showed reduced levels of the cAMP reporter compared to the WT, while the Δ*cpdA* mutant showed an increased signal **(Figure S1C).**
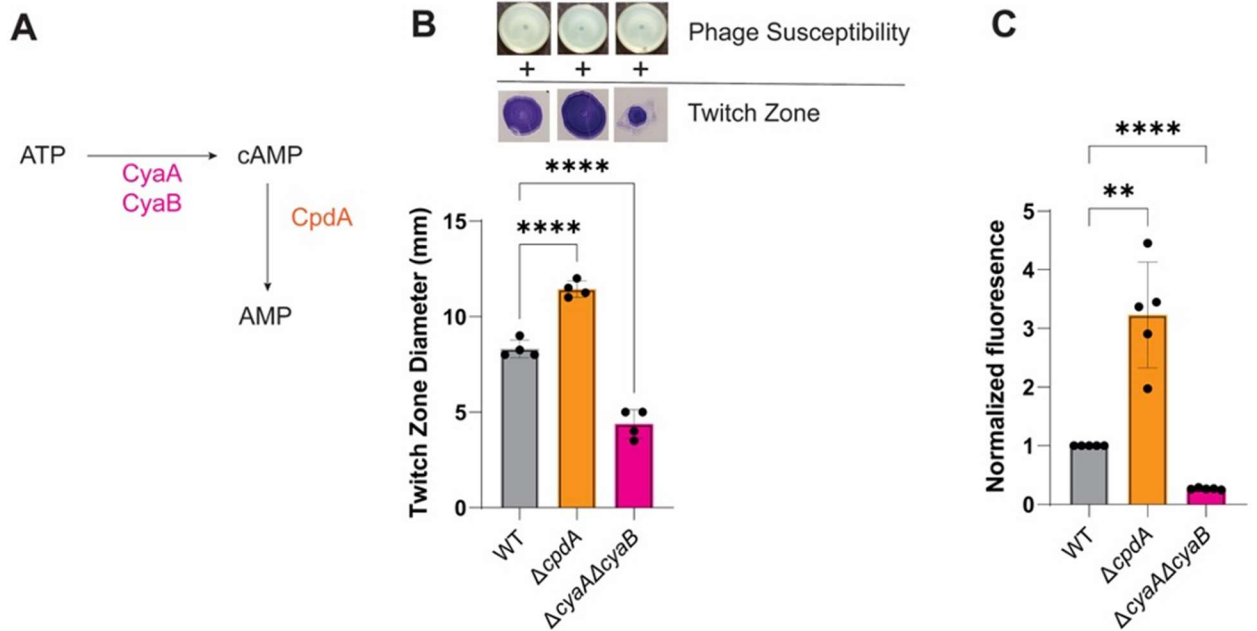
Figure S2.1 Analyzing cAMP levels to validate the reporter. A. A diagram representing the enzymes that make and degrade cAMP in *P. aeruginosa*. **B.** Phage susceptibility assay and twitching motility assay for the WT, Δ*cpdA,* and *ΔcyaAB* mutant backgrounds. Images of phage susceptibility plates (top panel, "+" indicates that strains are susceptible to phage infection) and twitching motility zones stained by crystal violet (middle panel) are above the quantification of the twitch zone diameter. Bars and errors bars represent the mean and standard deviation of 4 biological replicates when compared to the WT. Data were analyzed by one-way ANOVA followed by Tukey's post-test comparison. ****, P≤0.00001. **C.** Normalized fluorescence for WT as well as the Δ*cpdA* and *ΔcyaAB* mutant strains. Values were normalized to the WT for each biological replicate. Bars and errors bars represent the mean and standard deviation of 3 biological replicates compared to WT. Data were analyzed by one-way ANOVA followed by Tukey's post-test comparison. **, P≤0.001, ****, P≤0.00001.
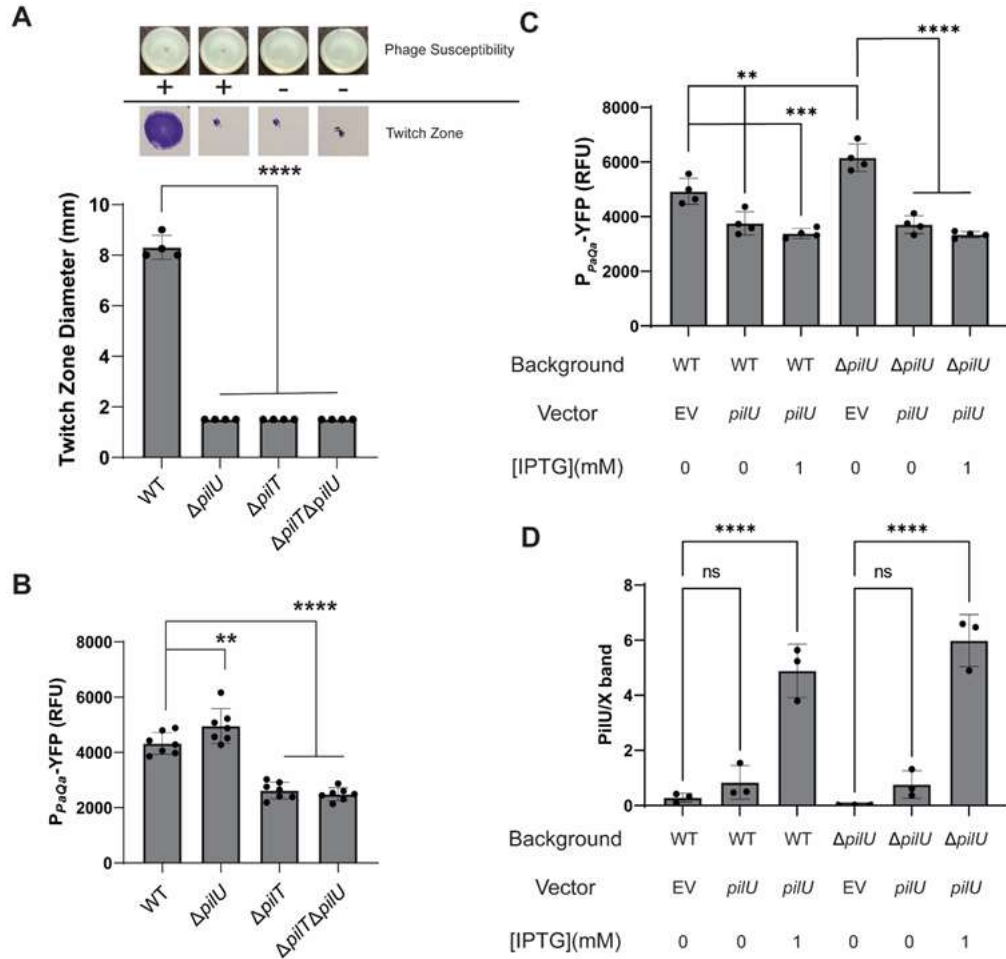
Figure 2.1. PilU levels affect surface-dependent cAMP production and T4P-related phenotypes. A. Images of phage sensitivity plates (top panel) and images of twitch zones stained with crystal violet (bottom panel). "+" indicates a phage susceptible strain and "–" indicates a phage resistant strain. Below is the quantification of the twitch zone diameter for each strain. Data are from four biological replicates. **B.** Quantification of *PaQa* reporter as measured by flow cytometry after 5 hours of growth on agar. Data are from six biological replicates. **C.** Quantification of the *PaQa* reporter as measured by flow cytometry after 5 hours of growth for the WT and Δ*pilU* mutant expressing the *pilU* gene from a multicopy plasmid or carrying the empty vector (EV) control. Growth was on M8 agar supplemented with 1mM or no IPTG and the appropriate antibiotics. **D.** Quantification of the normalized PilU protein levels of the cells in panel C. Values were normalized to a cross-reacting band. Data are from three biological replicates. Bars and error bars in all panels are the mean and standard deviation and statistical significance was determined by one-way ANOVA followed by Tukey's post hoc test, **$P \leq 0.001$, ***$P \leq 0.0001$, ****$P \leq 0.00001$; ns, not significant.

To better understand the respective contributions of PilT and PilU to surface-mediated cAMP production, we used single and double mutants and a series of phenotypic assays. The absence of PilT phenocopies a ΔpilTΔpilU double mutant in terms of TM, phage susceptibility and cAMP response (Figures 1A,B; and as reported previously by our group (78)). In contrast, a ΔpilU strain retains phage susceptibility due to the presence of PilT but shows an increase in surface-dependent cAMP response (**Figure 1A,B**; and as reported (15, 23, 24, 70, 72, 78, 114)). Given that PilU is the only T4P protein whose loss increases the level of surface-dependent cAMP and that this motor can only exert effects through PilT, we reasoned that PilT may be sensing the surface via forces occurring during retraction of surface bound pili and relaying this signal to the Pil-Chp system, a model we probe in more detail below.

As mentioned above, PilT appears capable of retracting T4P under low loads like that of a phage bound to the pilus, but is unable to power twitching motility, which requires ATP hydrolysis from both PilT and PilU (37, 41). We believe this to mean that the PilT hexamer is able to undergo conformational changes necessary for ATP hydrolysis while bound to PilC which in turn causes conformational changes that allow for the disassembly of PilA monomers into the IM for pili not bound to a surface. When pili are bound to a surface we believe the tension on each pilus resists the conformational changes in PilC that are necessary for disassembly and that the coordinated hydrolysis of ATP by both retraction motors are necessary to force PilC into the disassembly conformation that was achieved by just PilT for unbound pili. If PilT attempts to retract a T4P filament bound to a surface without PilU present, we hypothesize that the motor would stall and enter a force induced conformational change, potentially due to improper ATP binding to, ATP hydrolysis of and/or ADP release from the hexamer (32). This PilT signaling model makes several predictions. First, a ΔpilU strain should show increased cAMP but only on a surface, a finding we have reported previously (15, 29, 40) and shown here **(Figure 1B)**. Also, overexpression of PilU (a condition that is the opposite of deleting the *pilU* gene) should suppress the cAMP response. We predict that by increasing levels of PilU we will increase the frequency that this motor protein will assist in retraction events during surface contact and in turn lead to less stalled PilT and thus less cAMP.

To test this second prediction, we created the *pilU* expression plasmid, pVLT31-P$_{TAC}$-*pilU,* and transformed this construct into the WT and Δ*pilU* mutant backgrounds with the *PaQa* reporter on the chromosome. cAMP was measured via flow cytometry with *pilU* expressed from a multi-copy plasmid for surface-grown bacteria **(Figure 1C)**. Western blots were performed confirming levels of PilU greater than the wild type in all the analyzed strains **(Figure 1D)**.

All strains harboring the *pilU* overexpression construct had cAMP levels significantly lower than those with the vector control even in the absence of inducer. In the WT background, excess PilU significantly reduced the amount of cAMP when grown on a surface and the addition of inducer modestly further reduced the level of cAMP. The trends observed in the WT background were also observed in the Δ*pilU* mutant background. Interestingly, the level of cAMP production in the WT and Δ*pilU* backgrounds with the PilU expression construct were both significantly reduced from WT but not significantly different from each other. This observed decrease in surface-dependent cAMP is consistent with a model of PilT acting as a signaling protein during surface contact.

To determine whether the effects of PilU overexpression on cAMP levels are dependent on the ability of this retraction motor to bind and hydrolyze ATP, a PilU-K136A (this mutation is in the Walker A box, WA, of the ATPase domain) mutant was generated using the pVLT31-*pilU* plasmid and transformed into the WT and Δ*pilU* backgrounds. After 5 hours of surface growth, levels of cAMP were measured using flow cytometry. Interestingly, expressing PilU-WA in the WT and Δ*pilU* backgrounds significantly lowered cAMP to levels near that of the functional *pilU* allele (Figure S2A). Western blots confirmed the pressence of stable PilU-WA protein within cells with and without inducer **(Figure S2B)**. To determine how *pilU* overexpression affects T4P dynamics, TM assays were performed in strains expressing *pilU* and *pilU-WA.* In the WT background, increased levels of PilU and PilU-WA significantly decreased TM. Increased levels of PilU may bias T4P dynamics to a retracted state and limit the ability of PilB to extend T4P as seen with excess PilT (59). While we observe the same result with excess PilU-WA we interpret this to be due to the reduction of meaningful retraction events since PilU must now compete with PilU-WA

within the cell for retracting PilT. Expression of *pilU* in the Δ*pilU* background rescued TM and the size of the twitch zone increased with the addition of inducer. Complementing this background with *pilU-WA* did not rescue TM again demonstrating the need for both retraction motors to have ATPase activity to power twitching **(Figure S2C)**. The fact that PilU-WA is able to affect cAMP during surface contact without affecting T4P dynamics in the Δ*pilU* background indicates that binding of PilT to PilU even in the absence of PilU ATPase activity can affect surface signal transduction. One possible explanation is that PilU and PilJ share a binding interface on PilT and PilU-WA overexpression blocks signaling to PilJ without aiding in T4P retraction.
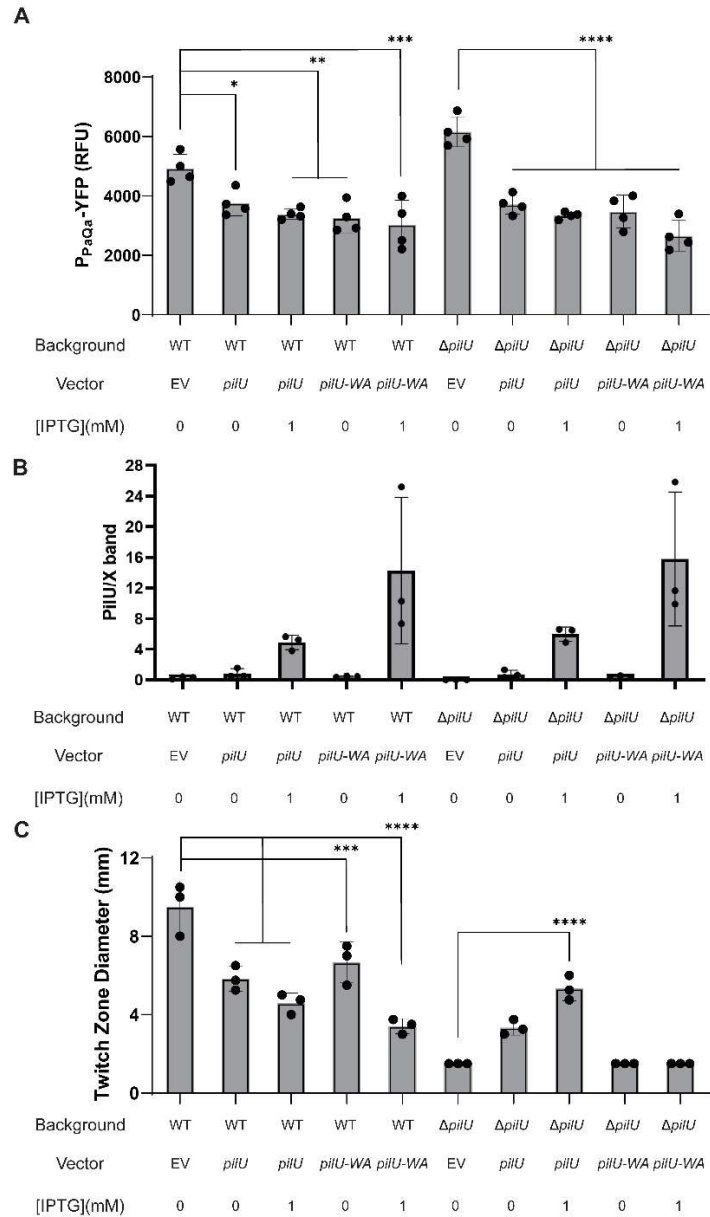
Figure S2.2. Expressing PilU-WA in the WT and Δ*pilU* background decreases twitching motility and cAMP. A. Quantification of the *PaQa* reporter as measured by flow cytometry after 5 hours of growth for the WT and Δ*pilU* mutant expressing the *pilU* gene, *pilU-K136A(WA)*, or carrying an empty vector (EV). Growth was on M8 agar supplemented with 1mM or no IPTG and the appropriate antibiotics. **B.** Quantification of the normalized PilU protein levels of the cells in panel A. Values were normalized to a cross-reacting band. Data are from three biological replicates. **C.** Quantification of twitch zone diameters for WT and Δ*pilU* mutant expressing the *pilU* gene, *pilU-K136A(WA)*, or carrying an empty vector (EV). Bars and errors bars represent the mean and standard deviation of 3 biological replicates. Data were analyzed by one-way ANOVA followed by Tukey's post-test comparison. ****, P<0.0001. ****, P≤0.0001, ***, P≤0.001, **, P≤0.01, *, P≤0.05.

To determine whether the increase in cAMP production in the Δ*pilU* background was due to improper PilT ATP hydrolysis during retraction, we expressed PilT-K136A from a multicopy plasmid in the WT background. PilT-K136A is unable to bind ATP and we hypothesized that the incorporation of this monomer into the functional hexamer would lead to hexameric conformations similar to those that occur for the WT PilT during pilus retraction in the absence of PilU. We observed a modest and non-significant increase in cAMP in strains containing the PilT- K136A expression vector relative to the empty vector control for the WT background (Figure S3, first 3 bars). While this negative result is difficult to interpret because we do not know if the mutant protein is indeed incorporated into the motor we believe it does as others have demonstrated that the PilT-K136A allele can still interact with the WT allele via B2H assay (70) and we observe a significant decrease in TM compared to the WT when expressing PilT-K136A from a multicopy plasmid **(Figure S3B).** Together, these data suggest that expression of the PilT-K136A (WA) mutation does not lock the TFP motor in an altered signaling conformation.
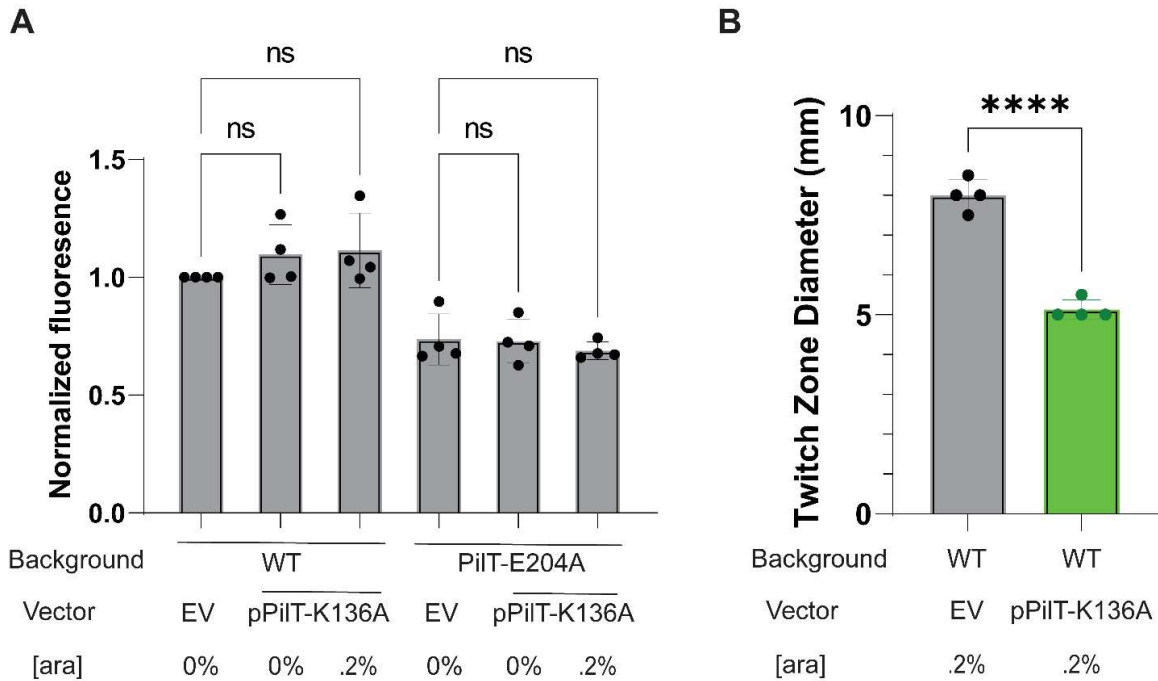
Figure S2.3. Co-expressing the Walker A (WA)/Walker B (WB) mutations does not impact cAMP signaling. A. Quantification of cAMP in WT (left) or PilT-E204A (right) strains carrying a plasmid expressing the PilT-K136A variant or the empty vector (EV) control, supplemented with 0 or 0.2% arabinose. Values were normalized to the WT for each corresponding biological replicate. Bars and errors bars represent the mean and standard deviation of 4 biological replicates. Data were analyzed by one-way ANOVA followed by Tukey's post-test comparison. ns, not significant. **B.** Quantification of twitch zone diameter of the WT carrying an empty vector (gray bar) or *pilT-K136A* (green bar) under an arabinose inducible promoter. Data were analyzed by student's t-test. ****, P≤0.0001.

Mutations in PilT change the dynamics of surface-dependent cAMP induction

We previously showed that mutating critical residues in the Walker A and Walker B motifs of PilT, which abolish ATP binding and hydrolysis, respectively, also disrupt the surface-dependent cAMP response (16, 78). To investigate the role of PilT in surface sensing, these mutations, as well as other previously published mutations in the PilT protein of *P. aeruginosa* that affect the protein's hexameric structure or retraction dynamics (15, 17, 59, 112), were inserted into the genome of *P. aeruginosa* PA14 at the gene's native locus with the *PaQa* cAMP reporter on the chromosome at the neutral *attB* site. A list of mutations tested here with their characteristics, either previously published or determined in this report, are summarized in Table 1 and mapped onto the PilT protein structure **(Figure 2A).**

For these mutants, we assessed protein stability, twitching motility, phage susceptibility and levels of cAMP when grown on a surface. The stability of each allele was assessed via Western blot and quantified by densitometry **(Figure 2B)**. As previously reported, alleles E204A and D31K showed decreased stability (or perhaps reduced antibody binding) (17). We also observed a significant decrease in the level of the protein with the PilT-H229A variant. The other alleles result in PilT levels that were reduced, but not significantly different relative to the level of the WT . The discrepancy in protein stability for some alleles could be due to the fact that previous reports used inducible promoters to express the *pilT* gene on multi-copy plasmids and/or perhaps due to the fact the experiments were performed in the PAO1 strain (15, 17, 59). Here we produce PilT from a single copy with the gene's native promoter to preserve endogenous regulation during surface sensing, and furthermore, to not perturb levels of PilU as the *pilU* gene is located directly downstream of the *pilT* gene.

To characterize the effects of these mutations on pilus retraction we performed twitching motility (TM) and phage susceptibility assays **(Figure 2C).** Twitching motility requires a fully functional PilT and PilU, while phage susceptibility requires only PilT (78, 128, 148). Despite the decrease in the level of the PilT proteins as measured by Western blot, all of the indicated PilT variants phenocopied previously published results in terms of twitching motility and phage susceptibility. Mutations that prevent ATP binding or hydrolysis (K136A, E204A; indicated in green) are unable

to power TM but remain phage susceptible due to the presence of a functional PilU (70, 78). Mutating the first histidine in the His-box reduced TM while mutating the second histidine completely abolished TM (H222A, H229A; indicated in magenta and blue, respectively), however both alleles maintained phage susceptibility (15, 17). Mutations in the N-terminus of PilT and mutations that affect the overall hexameric structure of the PilT protein (D31K, K58A, R123D, T216R; blue and magenta bars) maintained phage susceptibility but the D31K and R123D mutations exhibited reduced TM (17).
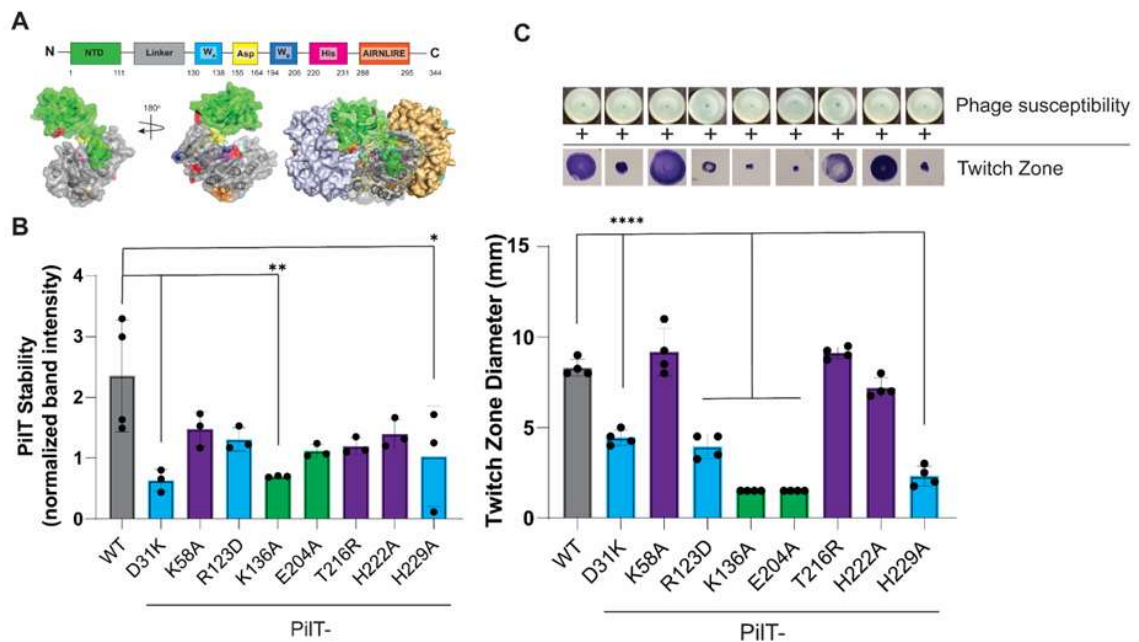
Figure 2.2. Characterization of PilT motor mutants. A. A schematic showing the domain architecture of PilT. Numbers represent the residue number of the beginning and ending of each domain. Below is the 3D structure of the *P. aeruginosa* PilT monomer and hexamer (PDB: 3jVV). **B.** Quantification of PilT protein levels via Western Blot analysis. The PilT band intensity from whole cells were normalized to a cross reacting band. Bars and errors bars represent the mean and SEM of 3 biological replicates. Data were analyzed by one-way ANOVA followed by Tukey's post-test comparison. *, P<0.05, **, P<0.01. Here and in panel C, strains that were able to twitch >75% of the WT have purple bars, strains that twitch between 25-75% of WT have blue bars, strains that twitch <25% WT have green bars. **C.** Assays for T4P function of *pilT* mutant strains. Images of phage sensitivity plates (top panel) and images of twitch zones stained with crystal violet (bottom panel). "+" denotes a phage susceptible strain and "-" denotes a phage resistant strain. The graph shows the quantification of twitch zone diameters for each strain. Bars and errors bars represent the mean and standard deviation of 4 biological replicates. Data were analyzed by one-way ANOVA followed by Tukey's post-test comparison. ****, P<0.0001.

Next, to capture the full dynamics of cAMP signaling during surface attachment, the first 6 hours of biofilm formation on the bottom of a glass bottom well was imaged using fluorescence microscopy. The average normalized fluorescent intensity per cell was plotted over time for cells harboring the *PaQa* reporter on the chromosome (77)(**Figure 3A, Figure S4**). All backgrounds initially start at the same level of intracellular cAMP (i.e., the lower levels associated with planktonic cells) and then begin to differ significantly for measured cAMP level within the first two hours. Throughout the time course, the Δ*pilT* (**Figure 3A**) and Walker box mutants (WA, PilT-K136A and WB, PilT-E204A; **Figure 3A, Figure S4**) maintained the lowest levels of cAMP. A strain carrying the PilT-D31K mutation (**Figure S4**) exhibited the greatest level of cAMP among all tested strains early and then decreased after three hours of growth. The H229A allele maintained an intermediate level of cAMP relative to the other mutants. The remaining PilT alleles converged with the WT allele around hour 3 and maintained this trajectory until the end of the experiment although their cAMP levels differed from WT at most time points (**Figure 3A, Figure S4**).
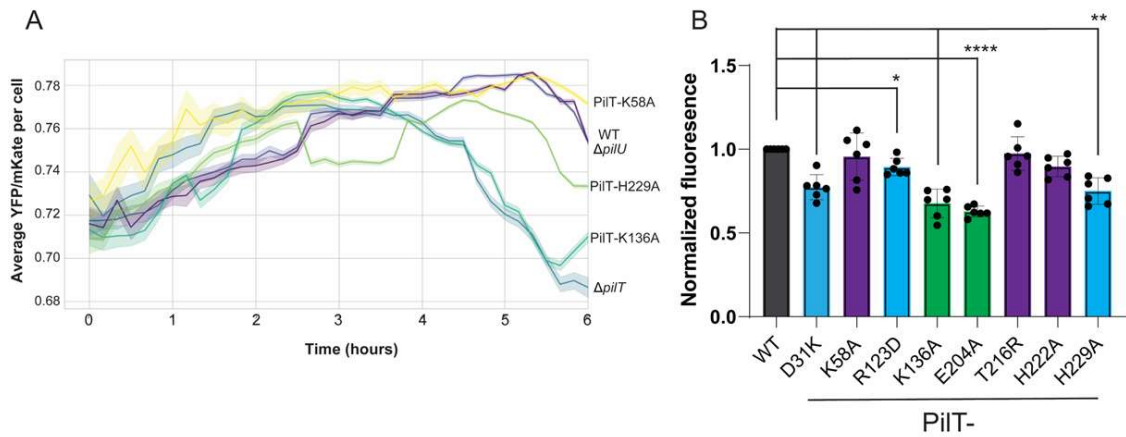
Figure 2.3. Measuring cAMP levels in strains carrying mutations in *pilT*. A. Graph depicting the average P*$_{PaQa}$YFP*/P*$_{rpoD}$mKate* per cell of selected strains during the first 6 hours of surface attachment in glass well dishes, as described in the text and Materials and Methods. Solid lines represent the mean YFP/mKate per cell and the shaded region represents the 95% confidence interval. At least 3 biological replicates were performed for each strain. A corresponding plot for all the *pilT* alleles described in this manuscript can be found in Figure S4. **B.** Cells were grown on an agar surface for 5 hours as described in the Materials and Methods and then analyzed by flow cytometer to quantify the amount of intracellular cAMP via the *PaQa* reporter. These values were then normalized by the WT value for that biological replicate. Bars and errors bars represent the mean and standard deviation of 6 biological replicates. Strains that were able to twitch >75% of the WT have purple bars, strains that twitch between 25-75% of WT have blue bars, strains that twitch <25% WT have green bars. Data were analyzed by one-way ANOVA followed by Tukey's post-test comparison. **, P≤0.01, ***, P≤0.001, ****, P≤0.0001.
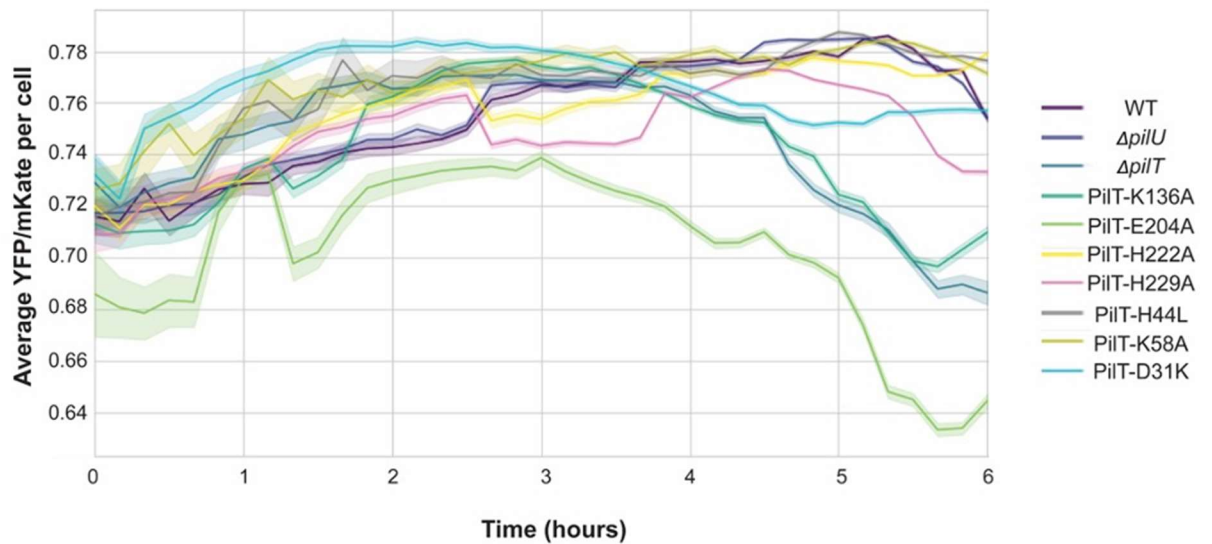
Figure S2.4. Time course measuring cAMP levels. Graph depicting the average $P_{PaQa}YFP/P_{rpoD}mKate$ per cell of selected strains during the first 6 hours of surface attachment in glass well dishes, as described in the text and Materials and Methods. Solid lines represent the mean YFP/mKate per cell and the shaded region represents the 95% confidence interval. At least 3 biological replicates were performed for each strain.

We noted that every genetic background that was unable to perform TM showed reduced levels of cAMP relative to WT (**Figure 3B**), with the exception of the Δ*pilU* mutant as shown above; this mutant background showed an increase in cAMP (**Figure 1B**) and as previously reported (23, 24, 78). cAMP was lowest in backgrounds that lacked the *pilT* gene followed by strains that expressed the Walker A (WA, PilT-K136A) and Walker B (WB, PilT-E204A) alleles of PilT. The PilT-D31K mutation resulted in a decrease in twitch zone and slight decrease in cAMP levels compared to that of WT. In contrast, PilT-H229A and R213D showed a significant decrease in twitching and cAMP levels. PilT-K58A, H222A, and T216R mutants displayed TM and cAMP not significantly different from WT.

As a control we measured cAMP levels in liquid grown cultures in the absence of a surface, and all strains carrying these *pilT* alleles were not significantly different from the WT. As an additional control we grew the Δ*cpdA* mutant (24) planktonically as well and it displayed high levels of cAMP (Figure S5A). We also showed that the cAMP measured in selected PilT alleles was PilJ-dependent, supporting the known role of PilJ in cAMP signaling (**Figure S5B**).

Together, these data show that mutations in various domains of the PilT motor alter cAMP signaling of bacteria grown on a surface, and these *pilT* alleles also impact pilus function by varying the extent of TM while retaining phage sensitivity.
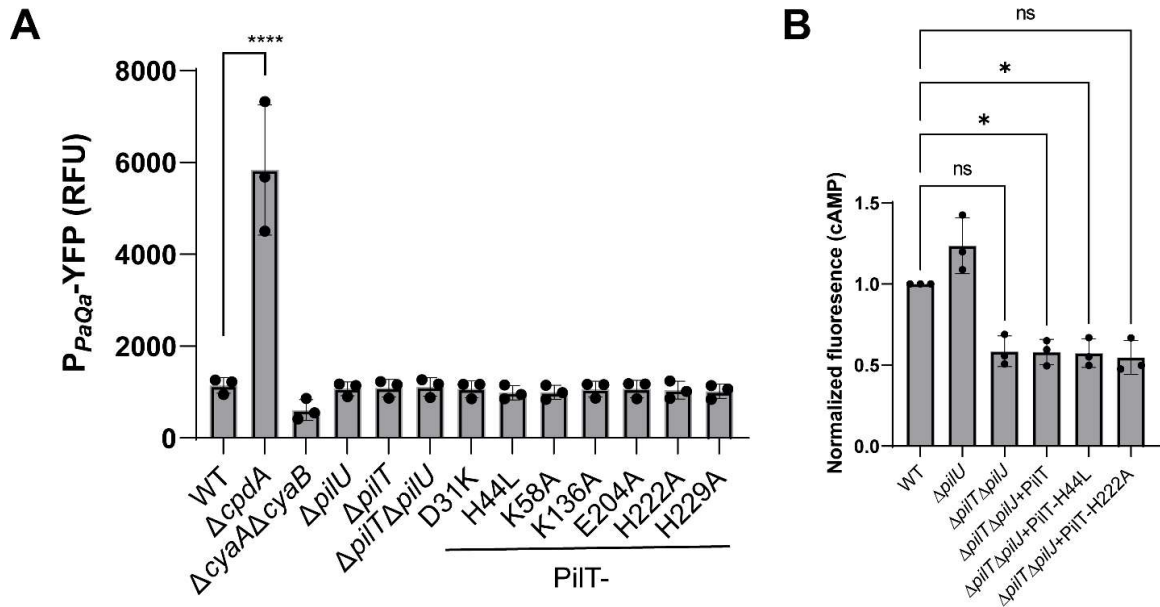
Figure S2.5. cAMP signaling is dependent on a surface and PilJ. A. Intracellular cAMP levels as measured by the *PaQa* reporter for the indicated mutants grown in planktonic culture. Bars and errors bars represent the mean and standard deviation of 3 biological replicates when compared to the WT. Data were analyzed by one-way ANOVA followed by Tukey's post-test comparison. ****, P≤0.00001. **B**. Signaling via selected PilT alleles is PilJ dependent. Quantification of cAMP as measured by the PaQa reporter using flow cytometry. Data were analyzed by one-way ANOVA followed by Tukey's post-test comparison. *, P≤0.05, ns, not significant.

Does PilT need to adopt both an ATP- (closed) and ADP- (open) bound state to support surface-dependent signaling?

Our previous work demonstrated that only the retractive force necessary for phage infection is necessary but not sufficient for surface-dependent cAMP induction (78). This conclusion was reached based on the observation that a Δ*pilU* mutant is phage susceptible, TM negative and has a cAMP level above that of the WT strain, while strains expressing the PilT-K136A (Walker A, WA) and PilT-E204A (Walker B, WB) mutations in a background with functional PilU are phage susceptible, TM negative but do *not* induce the cAMP response when grown on a surface (78).

While this observation could be due to a nuanced difference in the force threshold for cAMP induction versus phage infection, the lack of cAMP signaling in these PilT variants could also be due to the fact that these mutations limit the conformations that the PilT motor can adopt as a hexamer.   That is, a fully functional PilT hexamer exists as a mixture of ATP- and ADP-bound states, and we hypothesized that a mixture of ATP- (closed) and ADP-bound (open) states of PilT might be necessary for cAMP signaling.

Given that the Walker A mutation prevents ATP-binding and the Walker B mutation prevents hydrolysis of ATP to ADP (16, 17), based on previous studies (17), locking the hexamer in either a fully unbound or fully ATP bound state, respectively, might interfere with surface signaling. Furthermore, given the ADP-bound state is structurally similar to nucleotide free state we reasoned that we may be able to observe the cAMP response if we expressed both Walker A and B mutants of PilT within the same cell.

To perform this experiment, we transformed a multicopy plasmid expressing the PilT-WA mutation (P$_{BAD}$-*pilT*-K136A) in a background expressing the PilT-WB allele (PilT-E204A) integrated at its native locus with the *PaQa* reporter on the chromosome to measure the cAMP response. As shown in **Figure S3A (last 3 bars)**, these mutations had no impact on cAMP levels, indicating that locking the PilT motor in these particular mixed conformations does not alter cAMP signaling.

The retraction motor PilT binds to PilJ of the Pil-Chp system

The data presented so far are consistent with a model wherein PilT is required for the surface-dependent cAMP response. To determine how PilT might be influencing cAMP production, we screened for interactions between PilT and members of the Pil-Chp system using the Bacterial Adenylate Cyclase Two Hybrid System (B2H) and found an interaction between PilT and the protein at the top the Pil-Chp signaling system, PilJ (29) (**Figure 4A,B**). As a control we assessed binding between PilJ and the other retraction motor PilU and the extension motor PilB, but did not observe any such interaction (**Figure 4A,B**). We also assessed the interactions between PilT and the other components of the Pil-Chp system as well as other proteins that are known to influence surface attachment through T4P (**Figure S6** and Table 2). We only detected robust interaction between PilT and PilJ, as well as the previously reported interaction between PilU and PilT (114).
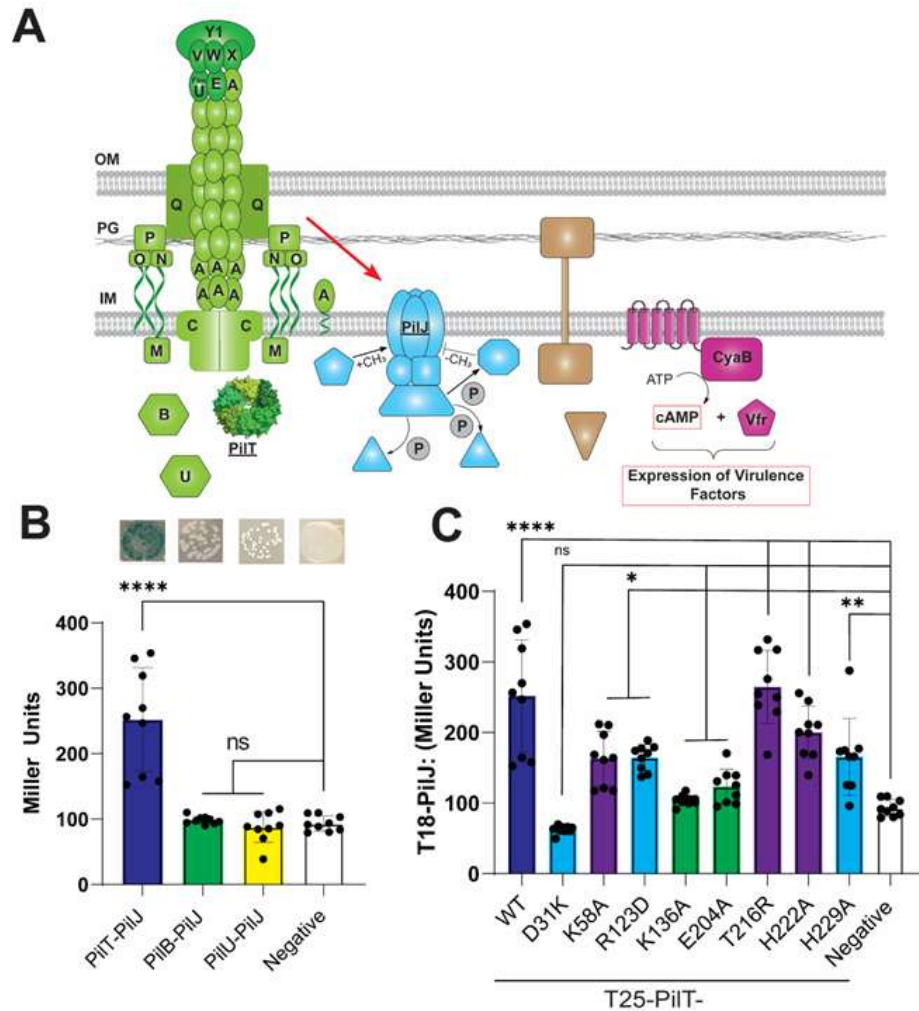
Figure 2.4. PilT interacts with PilJ. A. Schematic depicting the components of the TFP and cAMP-signaling pathway. **B.** Quantification of the B2H interaction between T4P motor proteins and PilJ in Miller Units. Shown are images of B2H colonies plated on X-gal plates (top of panel) and the interaction quantified (bottom of panel). Bars and errors bars represent the mean and standard deviation of 3 biological replicates. Data were analyzed by one-way ANOVA followed by Tukey's post-test comparison. ns, not significant, ****, $P<0.00001$. **C.** Quantification of the level of interaction between different PilT mutants and PilJ using the B2H system. Bars and errors bars represent the mean and standard deviation of 3 biological replicates. Data were analyzed by one-way ANOVA followed by Tukey's post-test comparison. *, $P<0.05$, **, $P\leq0.01$, ****, $P<0.00001$.
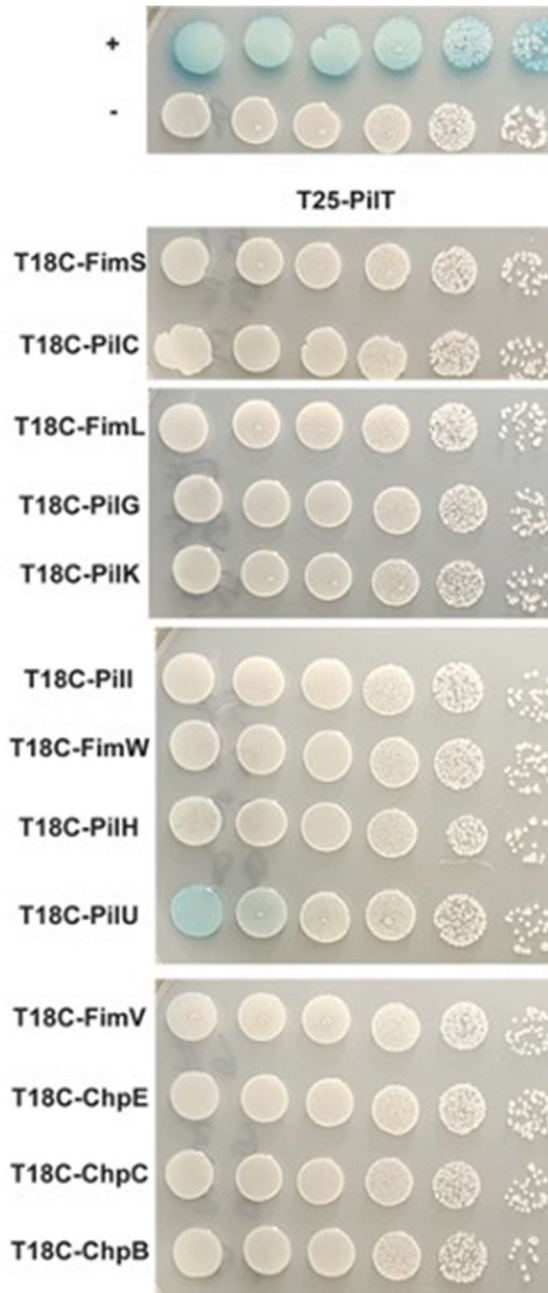
Figure S2.6. **PilT does not interact with other members of the Pil-Chp system as measured by B2H.** Images of plates from the B2H assay assessing interactions with PilT. As described in the Materials and Methods, BTH101 cells were co-transformed with the pUT25-PilT plasmid and the pUT18C plasmid fused to different components of the Pil-Chp system. Transformants were then serially diluted and plated on agar containing X-Gal and the appropriate antibiotics. The only observed interaction was between PilT and PilU. Positive (+) and negative (-) B2H controls are shown at the top of the figure.

To characterize this interaction with the *pilT* alleles described above, these mutants were cloned into the B2H system and the level of interaction with PilJ was measured via β-galactosidase activity. In general, PilT mutants that were able to perform TM and induce a surface-dependent cAMP response had higher levels of interaction with PilJ (**Figure 4C**). We explore the consequences of the changes in PilJ-PilT interaction for the PilT variants below.

Associations between PilT-related phenotypes and cAMP signaling.

We next examined associations between cAMP signaling and other measured phenotypes of the PilT variants. We first plotted the diameter of the twitch zone for each PilT allele versus the level of cAMP for surface-grown cells as measured by flow cytometry. Analyzing these data with a linear model we observed a highly significant, positive correlation between the twitch zone diameter and level of cAMP for strains with a functional PilU (**Figure 5A**). While this link between the production of cAMP and twitching motility is well known, the direct relationship between the levels of cAMP and the extent of TM, to our knowledge, has not been previously reported.

Importantly, using the data in Figures 3 and 4, we also observed a positive, significant relationship between cAMP levels and level of interaction between PilJ and PilT mutants that are completely or partially defective in ATPase activity (**Figure 5B**)(17).

As a control, we also quantified the strength of interaction between the PilT mutants shown in Figure 5 and PilU using the B2H assay (**Figure S7A**). These values were then used with cAMP data to build a linear model to evaluate the relationship between PilT-PilU interaction strength and cAMP production (**Figure S7B**). We did not find any significant relationship between PilT-PilU interaction strength and cAMP levels when analyzing either all the PilT alleles or only those that impact ATPase activity, indicating that the relationship between PilT-ATPase variants and interaction strength with cAMP levels is specific to the PilT-PilJ interaction.
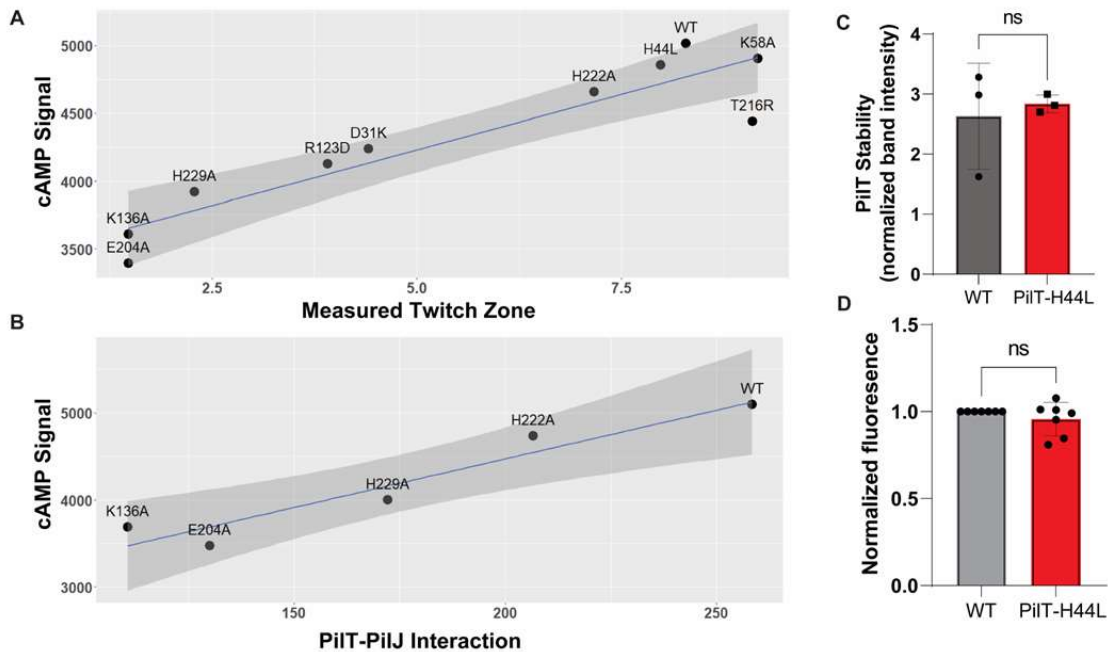
Figure 2.5. cAMP levels are positively associated with TM and the extent of PilT-PilJ interaction. A. A linear model depicting the relationship between twitching motility and surface induced cAMP production. Model is built using data from Figures 2, 3 and 4 using all tested alleles of *pilT* (R^2=0.8565, Adjusted R^2=0.8386, p-value=0.0001232). **B.** A linear model depicting the relationship between level of PilT-PilJ interaction as measured by the B2H system and surface induced cAMP production. Model is built using data from strains PilT-K136A, PilT-204A, PilT-H222A, PilT-H229A, and the WT strain (R^2=0.9176, Adjusted R^2=0.8902, p-value=0.01029). **C.** Quantification of PilT level for the PilT-H44L mutant compared to the WT strain. PilT bands were normalized by a cross reacting band. Bars and errors bars represent the mean and standard deviation of 3 biological replicates compared to WT. Data are from 3 biological replicates and were analyzed by one-way ANOVA followed by Tukey's post-test comparison. ns, not significant. **D**. Normalized fluorescence from the *PaQa* reporter for WT and PilT-H44L strains. Values were normalized by the WT for each biological replicate. Bars and errors bars represent the mean and standard deviation of 7 biological replicates compared to WT. Data were analyzed by one-way ANOVA followed by Tukey's post-test comparison. ns, not significant.
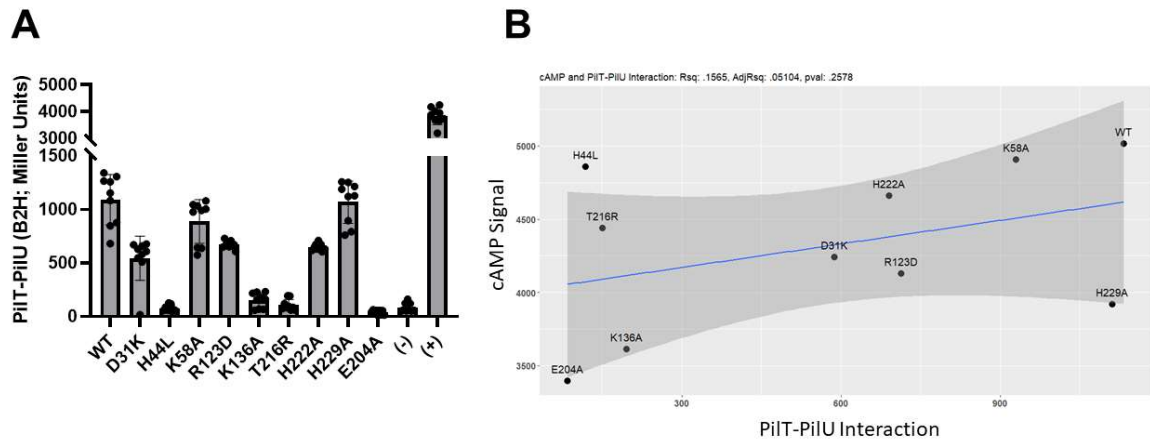
Figure S2.7. PilU and PilT interaction strength and cAMP level. **A.** Quantification of the interaction between PilT mutants and PilU as measured by the B2H assay. Bars and errors bars represent the mean and standard deviation of 3 biological replicates when compared to the WT. **B.** A linear model depicting the relationship between level of PilT-PilU interaction as measured by the B2H system and surface induced cAMP production. The model was built using data from all mutants of PilT in R (R^2: 0.1565, Adjusted R^2: 0.05104, p-value: 0.2578). When only considering the ATPase mutants, a similar not significant result is obtained (R^2: 0.5406, Adjusted R^2: 0.3875, p-value: 0.1569).

Together, these data indicate that the functional state of the ATPase domain of PilT alters the interaction of this motor protein with the PilJ. Furthermore, this association between interaction strength of these ATPase mutants with PilJ and cAMP signaling suggests a mechanism whereby PilT ATPase activity could be linked to PilJ-mediated cAMP signaling, a possibility we discuss further below.

Isolation of a mutation that disrupts PilJ-PilT interaction in *E. coli* using a B2H-based screen.

To attempt to further understand the interaction between PilT and PilJ, and to assess the impact of this interaction on the influence of the cAMP response in *P. aeruginosa*, we screened for mutants of PilT that were able to perform twitching motility but no longer able to interact with PilJ using a B2H-based assay. A schematic describing the screening process can be found in **Figure S8**. Briefly, random mutations were introduced into the *pilT* sequence using error-prone PCR and then the mutant library cloned into the B2H backbone. This pool was then co-transformed with the WT PilJ construct and we picked white colonies indicating a loss of interaction with PilJ. The PilJ non-interacting alleles were then pooled and screened for the ability to retract pili by cloning this population of mutant *pilT* alleles into an expression vector and transforming this pool of mutants into the Δ*pilT* background of *P. aeruginosa*. The transformants were then screened for twitching motility. The *pilT* alleles that were able to twitch and did not interact with PilJ using a plate-based B2H assay were sequenced.
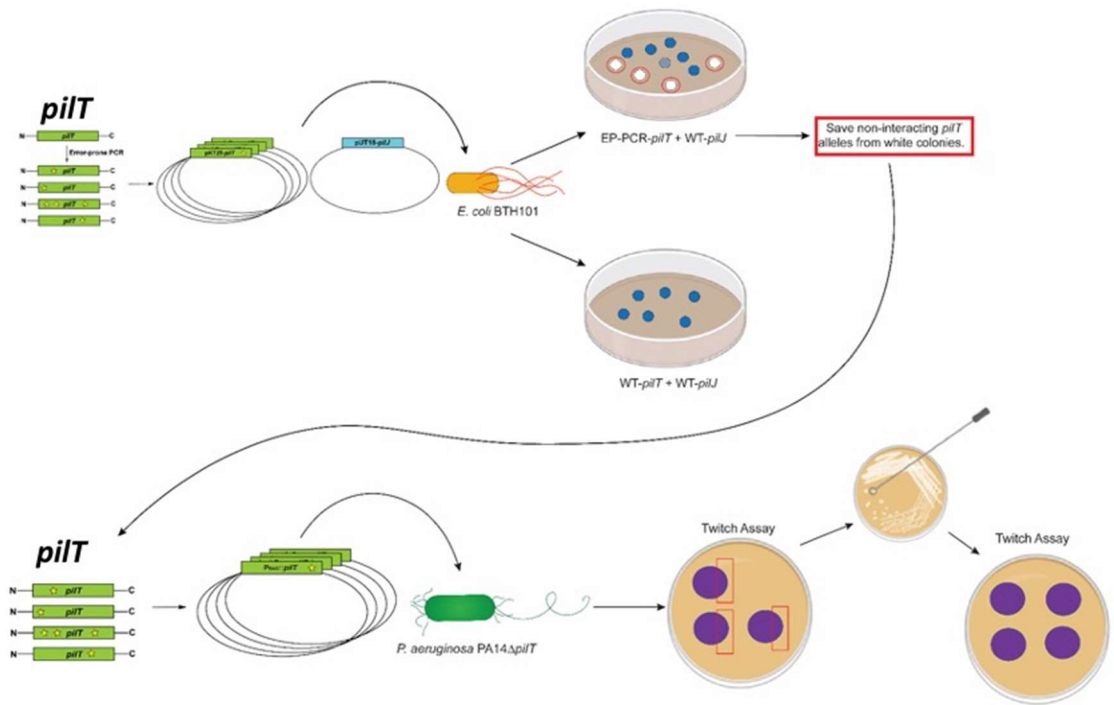
Figure S2.8. Isolating a mutation that disrupts PilT-PilJ interaction. A schematic depicting the screening process to isolate functional *pilT* alleles that no longer bind to PilJ in the B2H assay. The screen is described in detail in the main text.

The extent of interaction of PilJ with candidate PilT alleles was then quantified using the B2H assay (**Figure S9A**), the stability of the proteins assessed by Western Blot (**Figure S9B**), and the mutations were mapped onto the PilT hexameric structure (**Figure S9C**). The majority of these mutations mapped to a patch on the surface of the N-terminal domain of the PilT protein.

As mentioned above, these mutant variants of PilT were checked for their stability via Western blotting, and unfortunately, the only stable allele was PilT-H44L (**Figure 5C, Figure S9B**). The *P. aeruginosa* strain carrying the H44L showed levels of TM similar to the WT and the strain expressing this allele is phage susceptible (Figure S9D). The H44 residue maps to the N-terminal domain of PilT and should not impact ATPase activity. Although this allele does not interact with PilJ by B2H in *E. coli*, it appears to have phenotypes identical to the WT *P. aeruginosa* for twitching and phage susceptibility, and it produces cAMP levels that are not significantly different from the WT (**Figure 5D**). These data suggest that the relationship between PilT and PilJ interaction and cAMP signaling may be complex, or that for this allele, the lack of interaction is *E. coli*-specific, points we discuss below.
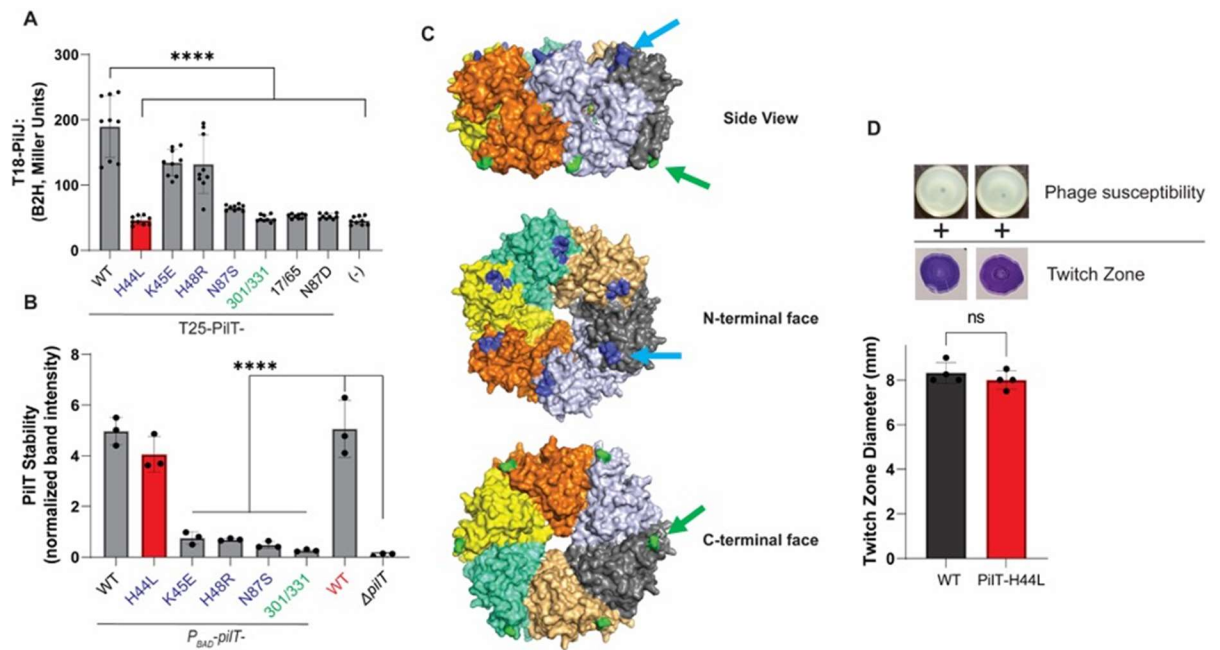
Figure S2.9. Analysis of mutants from the genetic screen. **A**. Quantification of the level of interaction between different PilT mutants and PilJ using the B2H system. Mutations in blue map to the blue patch on the N-terminal face of PilT shown in panel C. Mutations in green localize to the C-terminal face as shown in panel C. Bars and errors bars represent the mean and standard deviation of 3 biological replicates. The red bar represents the PilT-H44L mutant. Data were analyzed by one-way ANOVA followed by Tukey's post-test comparison. ****, P≤0.0001. **B.** PilT levels expressed from a multi-copy plasmid and quantified via Western blot. Bars and errors bars represent the mean and standard deviation of 3 biological replicates. All PilT intensity values were normalized by a cross-reacting band. Data were analyzed by one-way ANOVA followed by Tukey's post-test comparison. ****, P<0.0001. **C**. Hexameric structure of PilT (PDB: 3jVV) side view (top panel), N-terminal face (middle panel), and C-terminal face (bottom panel) are shown. Each monomer is in a different color. The mutations listed in blue in panels A and B cluster on the N-terminal face of the hexamer and highlighted in blue with a blue arrow indicating where the mutations map. The mutations listed in green form a patch on the C-terminal face of the hexamer and colored green with a green arrow indicating where the mutations map. **D.** T4P assays to assess PilT-H44L function in *P. aeruginosa*. Images of phage susceptibility plates (top panel) and twitching motility zones stained by crystal violet (middle panel) are above the quantification of the twitch zone diameter. Bars and errors bars represent the mean and standard deviation of 3 biological replicates when compared to the WT. Data were analyzed by one-way ANOVA followed by Tukey's post-test comparison. ns, not significant.

2.5 Discussion

Here we examine the contribution of the T4P retraction motor PilT to surface sensing and present a model whereby PilT transmits a surface signal to the Pil-Chp system to activate cAMP production upon surface contact. Data presented here and from previous studies indicate that PilT is involved in sensing a surface, promoting at least minimal T4P retraction activity (as judged by phage susceptibility), and that PilT's role may extend beyond its function in TFP retraction. We show that mutations in PilT that affect its structure and/or T4P-related phenotypes also impact the surface-dependent cAMP response as measured through kinetic and endpoint assays. We also describe a novel interaction between PilT and PilJ of the Pil-Chp system. We then quantified the level of interaction between these PilT variants and PilJ using a B2H assay. A linear model showed a positive, significant correlation between cAMP level and twitching motility, and importantly, cAMP level and the strength or PilJ-PilT interaction for variants of PilT with known deficiencies in ATPase activity. We interpret this latter finding to mean that ATP binding and hydrolysis is critical, not only for retraction activity, but for PilT to bind and transmit a signal to PilJ. Alternatively, PilJ could be transmitting a signal to PilT that affects twitching motility, or alternatively, this interaction could also facilitate localization of PilT to the poles of the cell. However, we believe that the simplest interpretation of our data is that the flow of information is from PilT to PilJ since the interaction strength between the PilT ATPase mutants and PilJ MCP is positively correlated with cAMP level. We did not observe this correlation when examining mutant variants of PilT with full ATPase activity or for the interaction between PilT and PilU. Together, these data support a model whereby the retraction motor PilT participates in sensing the surface during T4P retraction and relays this signal to PilJ in a mechanism that incorporates the PilT ATPase activity.

Any model involving T4P retraction must incorporate both retraction motors, PilT and PilU. We and others have shown that loss of PilU results in an increase in surface-dependent cAMP levels while retaining phage sensitivity (23, 24, 78). These data indicate that PilT can facilitate some level of T4P retraction even in the absence of PilU. We believe these data mean that in the absence of PilU, the PilT hexamer is

able to undergo conformational changes necessary for ATP hydrolysis while bound to PilC, for unbound pili (or a pilus bound to phage), which in turn results in conformational changes in PilT and/or PilC that allow for the disassembly of PilA monomers into the IM and retraction of the pilus. Consistent with this idea, previous studies have shown that in the absence of PilU, PilT is still able to bind PilC and begin retraction in a manner similar to that of the wild type (14). Furthermore, the two retraction motors do not always localize to the same pole, indicating that PilT and PilU are not necessarily always bound to each other when engaging PilC (15, 121). Thus, even for the WT, there may be instances when PilT is attempting to retract a pilus in the absence of PilU.

In contrast to planktonic cells, when *P. aeruginosa* is bound to a surface, we propose that the tension on a pilus might prevent the typical conformational changes in PilC and/or the PilT motor that are necessary for disassembly of the pilus. For the WT with a bound T4P, this model proposes that the coordinated hydrolysis of ATP by both retraction motors PilT/PilU is necessary for PilC to attain the needed conformation for T4P disassembly. Indeed, the measured binding force of this pilus to a surface is at or above retraction force of the T4P pilus of *P. aeruginosa* (66, 67), indicating that the retraction motors operate at the cusp of their ability to unbind a pilus from the surface. That is, it is difficult for *P. aeruginosa* to pull a pilus off the surface to which it is attached. Finally, we propose that during retraction, PilT may undergo a force-induced conformational change, perhaps through stalling of the motor (i.e., an incomplete cycle of ATP binding, ATP hydrolysis and/or ADP release) while attempting to retract a bound pilus, in turn transmitting a signal of surface engagement to the Pil-Chp system via the PilT-PilJ interaction. This conformational change may occur even when PilU is present for a surface-engaged cell with bound pili, but the observation that loss of PilU results in an increase in cAMP levels suggests that PilT is more likely to attain (or less likely to leave) a signaling conformation in the absence of its accessory motor, whether PilU is absent via mutation or for instances when PilU is not complexed with PilT in the WT. The fact that PilU-WA, which is unable to bind ATP and restore TM, in a Δ*pilU* background still reduces cAMP to levels similar to the functional PilU suggests that PilU and PilJ may share a binding interface on the N-terminal of PilT.

Our model makes several predictions that have been confirmed in previous publications (23, 24, 78) and this study. First, we demonstrated that cAMP levels when grown on a surface are dependent on the presence of PilT and PilJ. Second, the absence of PilU leads to elevated cAMP levels, a finding made by others and confirmed here (23, 24, 78). Lastly, our data show that excess PilU, has the opposite effect, reducing the surface-dependent cAMP response.

We also observed a strong, positive correlation between twitching ability as measured through twitch zone diameter and cAMP production for multiple mutants when analyzed with a linear model. This finding is consistent with previous studies that demonstrated that twitching motility requires cAMP production, and that at the single cell level, oscillations of T4P activity and cAMP level are highly correlated (23). While cAMP production is dependent on T4P activity, this second messenger activates a positive feedback loop whereby Vfr and cAMP positively regulate FimS-AlgR, which in turn leads to increased expression of minor pilins and the number of active T4P complexes per cell. This positive regulatory loop is part of the rapid surface adaptation response of *P. aeruginosa*, and we now know that part of this signaling cascade is initiated by the retraction motor PilT. Thus, PilT appears to play integrated roles in surface sensing and the control of TM in response to surface inputs.

To complement our candidate mutant approach for studying the PilT-PilJ interaction, we performed a genetic screen to identify PilT variants that could promote TM despite a defect in interaction with PilJ. This screen yielded two interesting findings. First, most of the mutations mapped to a surface exposed region on the N-terminus of PilT. The N-terminus of PilT binds to the C-terminus of the adjacent monomer to form the hexamer. This interface also undergoes the major conformational change during ATP binding and also makes contacts that facilitate open and closed motor conformations. Unfortunately, most of these PilT variants were unstable thus we could not unwind whether the lack of signaling was due to reduced levels of the PilT protein, or the inability of these mutant proteins to interact with PilJ.

We did isolate one allele of *pilT* that was able to perform TM but did not interact with PilJ in *E. coli* using a B2H assay; for this allele (H44L) we still observed WT surface-dependent cAMP production in *P. aeruginosa*. This mutation was near the N-terminal region of PilT and

not in proximity to any parts of the protein thought to contribute to its ATPase activity. Consistent with this idea, this allele was able to perform TM at a level similar to that of WT, indicating that this mutant variant does not have a defect in its ATPase activity. A similar phenotype was observed for the PilT-D31K allele, which retains ATPase activity (17). This PilT-D31K allele, which also maps to the N-terminus of PilT, was able to perform TM at WT levels and induce cAMP production when on a surface, but had very low levels of interaction with PilJ when measured through the B2H assay in *E. coli*. Thus, it is possible that mutations at the N-terminus of PilT can impact its ability to interact with PilJ in the B2H, but perhaps not impact PilT-PilJ interaction when this allele is expressed in *P. aeruginosa* in the presence of the rest of the T4P machinery or in the context of the hexamer. We believe it is important to acknowledge that while our findings here allow us to posit a model connecting T4P to surface sensing and cAMP signaling, we still lack key pieces of information to build a model which explains all of the current data. We look forward to interrogating our model further.

We believe our findings are consistent with previous studies, as T4P motors as signaling proteins is not unprecedented. For example, *Mxyococcus xanthus* requires T4P for exopolysaccharide (EPS) production as well as a type of surface-based motility known as S-motility. Researchers performed a suppressor screen for EPS production in a T4P-deficient background. Mutations in the T4P assembly ATPase PilB were isolated that led to the production of EPS without S-motility. A Walker-A mutation in PilB phenocopied this mutation and was dominant over the WT allele (130). Consistent with our studies of T4P/PilY1 regulating surface-dependent cdG signaling (87), these data link a T4P and motor function to second messenger signaling, and may represent a more general strategy whereby T4P (and perhaps other pili families) serve double duty as adhesins and signal transduction machinery.

Others have suggested that the surface signal is transmitted from the T4P pilin, PilA, to PilJ to activate cAMP production (76). Although we have previously shown no correlation between PilA-PilJ binding strength and cAMP production (78) this does not exclude a role for PilA signaling through a different mechanism. Regardless of the extent of signaling through PilA, the pilin remains a critical part of our motor signaling model, as the motor relies on the presence of a pilus fiber to extend and bind to the surface to create tension during PilT-mediated retraction. Overall, we have presented

evidence for a new model of surface signal sensing and transduction through the T4P motor PilT and we will continue to investigate the mechanism by which this signaling occurs.

Table 2.1. Mutant alleles characterized in this report.

pilT allele	Phenotypes	Reference
D31K	Decreased stability, increased twitching, Decreased Closed Conformation, partial phage sensitivity.	(17)
K58A	Increase in the Open Conformation, increased twitching, increased OOCOOC[a] hexamer conformation.	(17)
R123D	Decreased stability of OOOOOO and CCCCCC hexameric[b] conformations	(17)
K136A(WA)	Cannot bind ATP	(70, 78)
E204A (WB)	Cannot hydrolyze ATP	(70)
T216R	Eliminates OOOOOO hexameric conformation	(17)
H222A	Decreased twitching, phage sensitive, decreased retraction velocity, increase in falling off T4P complex	(15, 59)
H229A	No twitching, phage sensitive, DEC ATPase in vitro	(15, 17)

[a]OOCOOC indicates open, open, closed, open, open, closed for the conformation of the 6 hexamers of PilT.

[b]OOOOOO or CCCCCC indicates all open or all closed conformations, respectively, of the 6 hexamers of PilT.

Table 2.2. Interaction status with PilT using B2H assay

pUT18C-	Interaction status with T25-PilT	Colony
FimS	-	
PilC	-	
FimL	-	
PilG	-	
PilK	-	
PilI	-	
FimW	-	
PilH	-	
PilU	+	
FimV	-	
ChpE	-	
ChpC	-	

ChpB	-	

2.6 Materials and Methods

Strains and media. *Pseudomonas aeruginosa* UCBPP PA14 was used as the WT strain. Mutations were made in this background using *E. coli* S17-1 λpir. *E. coli* BTH101 was used for Bacterial Adenylate Cyclase Two Hybrid assays. Strains used in this study are listed in Supplemental Table S1. Bacterial strains were routinely cultured in 5ml of lysogeny broth (LB) medium or plated on 1.5% agar with antibiotics when necessary. Tetracycline (tet) was used at 15ug/ml for *E. coli* and 120 ug/ml during *P. aeruginosa* selection and maintained with 75ug/ml. Gentamicin (Gm) was used at 30 μg/ml for *P. aeruginosa* and 10 μg/ml for *E. coli*. Carbenicillin (Cb) was used at 250 ug/ml for *P. aeruginosa* and 100 ug/ml for *E. coli*. Kanamycin (Kan) was used at 50 ug/ml for *E. coli*. M8 minimal salts medium supplemented with $MgSO_4$ (1mM), glucose (0.2%) and casamino acids (0.5%) was used for all assays (8). Plasmids were induced with either 0.2% arabinose for P_{BAD} promoter induction or 0.5 mM isopropyl-D-thiogalactopyranoside (IPTG) was added to agar or liquid media for P_{TAC} promoter induction unless otherwise stated. β-galactosidase activity from B2H assays was visualized using plates supplemented with 5-bromo-4-chloro-3-indolyl-β-D-galactopyranoside (X-Gal; 40 μg/ml).

Construction of mutant strains and plasmids. Plasmids used in this study are listed in Supplemental Table S2 and primers are listed in Supplemental Table S3. Plasmids were constructed using Gibson assembly of purified PCR products. Chromosomal mutations were made using homologous recombination with the pMQ30 vector. Insertions at neutral sites in the *P. aeruginosa* genome were made using the mini-Tn7 vector (149, 150) and the mini-CTX1 vector (147). Resistance markers were removed using the pFLP2 plasmid followed by sucrose counter selection (147). Point mutations were generated using QuikChange ® site-directed mutagenesis followed by Gibson assembly. Expression vectors were generated using Gibson assembly of purified PCR products into pMQ72 or pVLT31 and then transformed into *P. aeruginosa* or *E. coli* using electroporation.

Twitching motility. Twitching motility plates were made using M8 medium supplemented with casamino acids, MgSO4, glucose and 1% agar. Plates were inoculated from liquid cultures using a sterile toothpick plunged through the agar to the bottom of the plate. Plates were incubated for 24 hours at 37C and then 24 hours at room temperature. The agar was then removed and the twitch zones were stained with 0.1% crystal violet. Images were obtained and the twitch zone diameter was measured twice using a ruler.

Phage plaque assay. Phage susceptibility assays were performed in (60 x 15 mm) plates using M8 medium supplemented with casamino acids, MgSO4, glucose, and 1% agar. 1ml of 0.5% M8 molten agar was then inoculated with 50 ul from a *P. aeruginosa* overnight culture. This mixture was poured over the solidified 1% M8 agar to form a bacterial lawn. After solidifying, 2ul of phage DMS3$_{vir}$ lysate was pipetted onto the bacterial lawn and incubated for 24 hours at 37C.

Bacterial Adenylate Cyclase Two Hybrid assays. The B2H system from Euromedex (151) was used to assess protein-protein interactions in *E. coli* BTH101. Alleles of *pilT* and other T4P proteins were cloned into the pKT25 vector and PilJ along with other Pil-Chp proteins were cloned into the pUT18 and pUT18C vectors. A pair of pKT25 and pUT18/UT18C vectors were then co-transformed into *E. coli* BTH101. To visualize the interaction, transformants were plated on LB agar containing Cb, Kan, X-Gal (5-bromo-4-chloro-3-indolyl-β-D-galactopyranoside) (40 g/ml) and IPTG (isopropyl-D-thiogalactopyranoside) (0.5 mM) and incubated at 30C until an interaction was observed through the transformation of X-Gal to a blue pigment or until the negative control began to produce a blue pigment. To quantify the level of interaction between proteins, transformants were plated on LB agar with Cb, Kan and IPTG. After incubation at 30C, cells were harvested and β-galactosidase assays were performed as previously described (151).

Protein detection and quantification. Strains were grown in M8 liquid medium supplemented with arabinose or IPTG and grown at 37C for 6 hours. Whole cell

lysates were prepared as previously described (152). Cultures were OD normalized to 1 and an equal volume was resolved on either a 12% or 10% polyacrylamide gel. Proteins were then transferred to a nitrocellulose membrane and probed with either anti-PilT or anti-PilU antisera. Detection of proteins was performed using fluorescence detection with IR-Dye®-labeled fluorescent secondary antibodies and imaged using the Odyssey CLx Imager (LICOR Biosciences, Inc., Lincoln, NE). Quantification of protein bands was performed using Image Studio Lite software (LICOR Biosciences, Inc., Lincoln, NE). Protein levels were then normalized by a cross-reacting band.

Flow cytometry measurements. Bacterial strains harboring the *PaQa* reporter on the chromosome were subcultured into liquid M8 medium supplemented with glucose, casamino acids, and MgSO4 and incubated at 37C until an OD of 0.5 was reached, ~3 hours. Gm, Tet, IPTG, or arabinose was added to the liquid medium when indicated. 200ul of the culture was then spread onto M8 agar plates and allowed to incubate for 5 hours at 37C. Cells were then harvested from these plates, washed, diluted, and analyzed on a Beckman Coulter Cytoflex S. FlowJo software version 10.8.1 was used to gate on populations of single cells that had mKate fluorescence. The EYFP fluorescence from the P*PaQa* promoter was then measured on the gated population. A workflow of the gating strategy can be found in **Figure S10**. For plots reporting the normalized fluorescent intensity, the average P*PaQa*-*eyfp* value for each gated mutant subpopulation was normalized by the wild type value for that biological replicate.
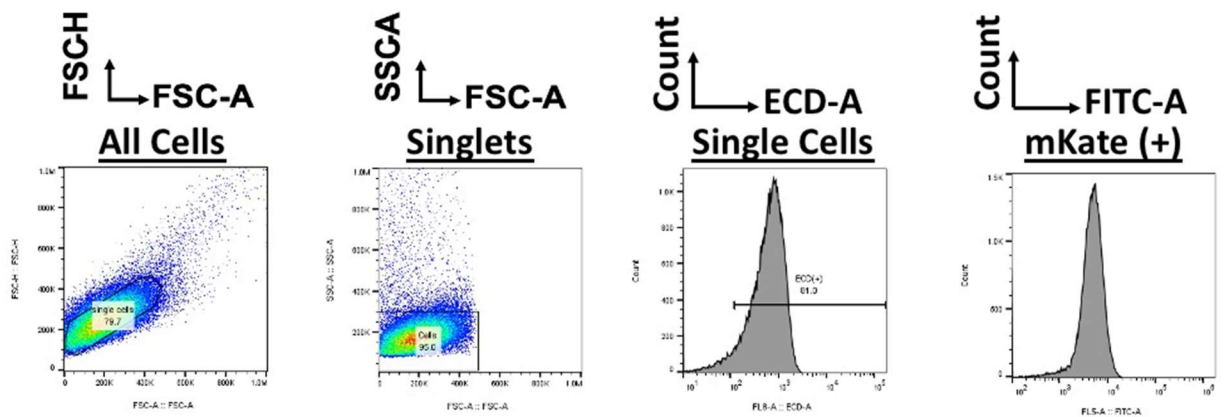
Figure S2.10. Gating strategy for flow cytometry assays. Single cells were first selected by gating on the FSC-H to FSC-A scatter plot and then gating by size in the SSC-A by FSC-A scatter plot. This population was then further gated to only include mKate positive cells by gating cells with an ECD-A value of 1000 RFU or greater. The resulting population was then used to calculate the geometric mean and standard deviation of the FITC-A population.

Microscopy experiments using 8-well dishes. Bacterial strains were subcultured in liquid M8 supplemented with glucose, MgSO4, and casamino acids after being cultured overnight in liquid LB at 37C. After reaching an OD600~0.5, cultures were diluted 1:100 into fresh, liquid M8 and then 300ul was used to fill a glass bottom chamber (Cellvis 8 chambered cover glass system). The chamber was then mounted on a Nikon Ti Eclipse epifluorescence microscope in an environmental chamber set to 37C. Images of at least 3 FOV were taken every 5 minutes for the first 8 hours of surface attachment. Images were then analyzed using a python script, which can be found at https://github.com/GeiselBiofilm.

Statistical analysis. Data visualization and statistical analysis were performed in GraphPad Prism 9 (version 9.2.0). Linear mixed models were built in R (v4.0.2) and visualized using ggplot2 (v3.3.2). The script used to perform the analysis can be found at https://github.com/GeiselBiofilm.

Data Accessibility Statement. All code is available on Github at https://github.com/GeiselBiofilm.

2.8 Supplemental Tables

Supplementary Table S2.1. Strains used in this study.

Strain name	Relevant genotype, description	Source
E. coli strains		
DH5α	*supE44 ΔlacU169(f80lacZΔM15) hsdR17 thi-1 relA1 recA1*	Life Technologies
S17-1(λpir)	*thi pro hsdR- hsdM+ ΔrecA RP4-2::TcMu-Km::Tn7*	(153)
BTH101	*F-, cya-99, araD139, galE15, galK16, rpsL1 (Str r), hsdR2, mcrA1, mcrB1*	(151)Euromedex
SM10	*thi thr leu tonA lacY supE recA::RP4-2-Tc::Mu Km λpir*	(153)
P. aeruginosa strains (SMC#)		
232	PA14 wild type (WT)	(154)
7302	Δ*pilT;* unmarked in-frame deletion	(23)
7304	Δ*pilU;* unmarked in-frame deletion	(24)
8856	Δ*pilT*Δ*pilU;* unmarked in-frame deletion	(78)
9652	Δ*pilT*Δ*pilJ;* unmarked in-frame deletions	This study
6707	Δ*cyaA*Δ*cyaB;* unmarked in-frame deletions	(24)
6851	Δ*cpdA;* unmarked in-frame deletion	(24)
9462	PA14 *attTn7::P1-lacZ, attB::P$_{PaQa}$-eyfp, P$_{rpoD}$-mKate2;* Tetracycline-resistance (Tc^r) cassette	This study

9463	Δ*pilU attB::P_{PaQa}-eyfp, P_{rpoD}-mKate2;* Tc^r	This study
9464	Δ*pilT attB::P_{PaQa}-eyfp, P_{rpoD}-mKate2;* Tc^r	This study
9465	Δ*pilTΔpilU attB::P_{PaQa}-eyfp, P_{rpoD}-mKate2;* Tc^r	This study
9466	Δ*cpdA attTn7::P1-lacZ, attB::P_{PaQa}-eyfp, P_{rpoD}-mKate2;* Tc^r	This study
9467	Δ*cyaAΔcyaB attTn7::P1-lacZ, attB::P_{PaQa}-eyfp, P_{rpoD}-mKate2;* Tc^r; Tc^r	This study
9653	*pilT-D31K attTn7::P1-lacZ, attB::P_{PaQa}-eyfp, P_{rpoD}-mKate2;* Tc^r	This study
9654	*pilT-H44L attTn7::P1-lacZ, attB::P_{PaQa}-eyfp, P_{rpoD}-mKate2;* Tc^r	This study
9655	*pilT-K58A attTn7::P1-lacZ, attB::P_{PaQa}-eyfp, P_{rpoD}-mKate2;* Tc^r	This study
9656	*pilT-R123D attTn7::P1-lacZ, attB::P_{PaQa}-eyfp, P_{rpoD}-mKate2;* Tc^r	This study
9665	*pilT-K136A attTn7::P1-lacZ, attB::P_{PaQa}-eyfp, P_{rpoD}-mKate2;* Tc^r	This study
9657	*pilT-E204A attTn7::P1-lacZ, attB::P_{PaQa}-eyfp, P_{rpoD}-mKate2;* Tc^r	This study
9658	*pilT-T216R attTn7::P1-lacZ, attB::P_{PaQa}-eyfp, P_{rpoD}-mKate2;* Tc^r	This study
9659	*pilT-H222A attTn7::P1-lacZ, attB::P_{PaQa}-eyfp, P_{rpoD}-mKate2;* Tc^r	This study
9660	*pilT-H229A attTn7::P1-lacZ, attB::P_{PaQa}-eyfp, P_{rpoD}-mKate2;* Tc^r	This study

9661	PA14 *attTn7::P1-lacZ, attB::P$_{PaQa}$-eyfp, P$_{rpoD}$-mKate2*	This study
9662	Δ*pilU attB::P$_{PaQa}$-eyfp, P$_{rpoD}$-mKate2*	This study
9663	Δ*pilT*Δ*pilJ attB::P$_{PaQa}$-eyfp, P$_{rpoD}$-mKate2,* Tc[r]	This study
9664	Δ*pilT*Δ*pilU attB::P$_{PaQa}$-eyfp, P$_{rpoD}$-mKate2*	This study

Supplementary Table S2.2. Plasmids used in this study.

Plasmid name	Description	Source
pMQ72	Vector for cloning in yeast, *E. coli*, and *P. aeruginosa* with arabinose-inducible gene expression system; Gentamycin-resistance (Gm[r]) cassette	(155)
pMQ30	Shuttle vector for cloning in yeat and allelic exchange in Gram-negatives; Gm[r]	(155)
miniCTX1	Suicide vector for integration into the *Pseudomonas attB* site on the chromosome; Tetracycline-resistance (Tc[r]) cassette	(147)
pMQ56-mTn7	Suicide vector for insertion of the mini-Tn7 element from pUT18-mTn7-Gm into the *attTn7* site on the chromosome of *P. aeruginosa*	(78)
pFLP2	For removal of antibiotic resistance cassettes flanked by FRT sites with Flipase; sacB for plasmid counterselection; Carbenicillin-resistance (Cb[r]) cassette	(156)
pUT18C	BACTH vector for fusions with the C-terminus of the T18 fragment of *cyaA*, Cb[r]	Euromedex

pUT18	BACTH vector for fusions with the N-terminus of the T18 fragment of *cyaA*, Cb[r]	Euromedex
pKT25	BACTH vector for fusions with the C-terminus of the T25 fragment of *cyaA*, Kanamycin resistance (Kn[r]) cassette	Euromedex
pKNT25	BACTH vector for fusions with the N-terminus of the T25 fragment of *cyaA*, Kanamycin resistance (Kn[r]) cassette	Euromedex
pKT25-zip	BACTH positive control, leucine zipper of GCN4 fused to T25, Kn[r]	Euromedex
pUT18C-zip	BACTH positive control, leucine zipper of GCN4 fused to T18, Cb[r]	Euromedex
pVLT31	Vector for cloning in *E. coli* and *P. aeruginosa* with IPTG-inducible gene expression system; Tc[r]	(157)
pMQ72-*pilT*	For arabinose-inducible expression of *pilT* in *P. aeruginosa;* Gm[r]	This study
pMQ72-*pilT-H44L*	For arabinose-inducible expression of *pilT-H44L* in *P. aeruginosa;* Gm[r]	This study
pMQ72-*pilT-H222A*	For arabinose-inducible expression of *pilT-H222A* in *P. aeruginosa;* Gm[r]	This study
pVLT31-*pilU*	For IPTG-inducible expression of *pilU* in *P. aeruginosa;* Tc[r]	This study
pVLT31-*pilU-K136A(WA)*	For IPTG-inducible expression of *pilU* in *P. aeruginosa;* Tc[r]	This study
pKT25-*pilT*	*pilT* gene cloned into pKT25; Kn[r]	This study

pKT25-*pilT-D31K*	*pilT-D31K* gene cloned into pKT25; Kn[r]	This study
pKT25-*pilT-K58A*	*pilT-K58A* gene cloned into pKT25; Kn[r]	This study
pKT25-*pilT-K136A*	*pilT-K136A* gene cloned into pKT25; Kn[r]	This study
pKT25-*pilT-E204A*	*pilT-E204A* gene cloned into pKT25; Kn[r]	This study
pKT25-*pilT-H222A*	*pilT-H222A* gene cloned into pKT25; Kn[r]	This study
pKT25-*pilT-H229A*	*pilT-H229A* gene cloned into pKT25; Kn[r]	This study
pKT25-*pilT-H44L*	*pilT-H44L* gene cloned into pKT25; Kn[r]	This study
pKT25-*pilT-K45E*	*pilT-K45E* gene cloned into pKT25; Kn[r]	This study
pKT25-*pilT-H48R*	*pilT-H48R* gene cloned into pKT25; Kn[r]	This study
pKT25-*pilT-N87S*	*pilT-N87S* gene cloned into pKT25; Kn[r]	This study
pKT25-*pilT-N87D*	*pilT-N87D* gene cloned into pKT25; Kn[r]	This study
pKT25-*pilT-D17G/E65K*	*pilT-D17G/E65K* gene cloned into pKT25; Kn[r]	This study
pKT25-*pilT-M301T/R331H*	*pilT-M301T/R331H* gene cloned into pKT25; Kn[r]	This study
pUT18-*pilJ*	*pilJ* gene cloned into pUT18; Cb[r]	
pUT18C-*fimS*	*fimS* gene cloned into pUT18C; Cb[r]	This study
pUT18C-*pilC*	*pilC* gene cloned into pUT18C; Cb[r]	This study
pUT18C-*fimL*	*fimL* gene cloned into pUT18C; Cb[r]	This study
pUT18C-*pilG*	*pilG* gene cloned into pUT18C; Cb[r]	This study
pUT18C-*pilK*	*pilK* gene cloned into pUT18C; Cb[r]	This study
pUT18C-*pilI*	*pilI* gene cloned into pUT18C; Cb[r]	This study
pUT18C-*fimW*	*fimW* gene cloned into pUT18C; Cb[r]	This study
pUT18C-*pilH*	*pilH* gene cloned into pUT18C; Cb[r]	This study
pUT18C-*pilU*	*pilU* gene cloned into pUT18C; Cb[r]	This study

pUT18C-*fimV*	*fimV* gene cloned into pUT18C; Cb^r	This study
pUT18C-*chpE*	*chpE* gene cloned into pUT18C; Cb^r	This study
pUT18C-*chpC*	*chpC* gene cloned into pUT18C; Cb^r	This study
pUT18C-*chpB*	*chpB* gene cloned into pUT18C; Cb^r	This study
pMQ72-*pilT-H44L*	For arabinose-inducible expression of *pilT-H44L* in *P. aeruginosa;* Gm^r	This study
pMQ72-*pilT-K45E*	For arabinose-inducible expression of *pilT-K45E* in *P. aeruginosa;* Gm^r	This study
pMQ72-*pilT-H48R*	For arabinose-inducible expression of *pilT-H48R* in *P. aeruginosa;* Gm^r	This study
pMQ72-*pilT-N87S*	For arabinose-inducible expression of *pilT-N87S* in *P. aeruginosa;* Gm^r	This study
pMQ72-*pilT-M301T/R331H*	For arabinose-inducible expression of *pilT-M301T/R331H* in *P. aeruginosa;* Gm^r	This study
miniCTX1-*PaQa*	For integration of the *PaQa* reporter into the *attB* site of the chromosome of *P. aeruginosa*. P_{PaQa}-*eyfp,* P_{rpoD}-*mKate2*	This study
pMQ56-mTn7-*P1-lacZ*	For integration of the cAMP transcriptional reporter into the *attTn7* site on the chromosome of *P. aeruginosa. P1-lacZ*	(78)
pMQ30-*pilT-D31K*	For performing allelic exchange at the native locus of the *pilT* gene in *P. aeruginosa* PA14 to introduce the mutation *pilT-D31K*	This study

pMQ30-*pilT-H44L*	For performing allelic exchange at the native locus of the *pilT* gene in *P. aeruginosa* PA14 to introduce the mutation *pilT-H44L*	This study
pMQ30-*pilT-K58A*	For performing allelic exchange at the native locus of the *pilT* gene in *P. aeruginosa* PA14 to introduce the mutation *pilT-K58A*	This study
pMQ30-*pilT-R123D*	For performing allelic exchange at the native locus of the *pilT* gene in *P. aeruginosa* PA14 to introduce the mutation *pilT-R123D*	This study
pMQ30-*pilT-E204A*	For performing allelic exchange at the native locus of the *pilT* gene in *P. aeruginosa* PA14 to introduce the mutation *pilT-E204A*	This study
pMQ30-*pilT-T216R*	For performing allelic exchange at the native locus of the *pilT* gene in *P. aeruginosa* PA14 to introduce the mutation *pilT-T216R*	This study
pMQ30-*pilT-H222A*	For performing allelic exchange at the native locus of the *pilT* gene in *P. aeruginosa* PA14 to introduce the mutation *pilT-H222A*	This study
pMQ30-*pilT-H229A*	For performing allelic exchange at the native locus of the *pilT* gene in *P. aeruginosa* PA14 to introduce the mutation *pilT-H22A*	This study
pMQ30-*pilT-K136A*	For performing allelic exchange at the native locus of the *pilT* gene in *P. aeruginosa* PA14 to introduce the mutation *pilT-K136A*	This study

Supplementary Table S2.3. Primers used in this study.

Primer name	Primer sequence (5'->3')
D17G_pilT_F	CAAACAGGGCGCTTCGGGCCTGCACCTCTCCGCCGGC
D17G_pilT_R	GCCGGCGGAGAGGTGCAGGCCCGAAGCGCCCTGTTTG
K45E_pilT_F	CCACCGCTGGAACACGAGCAGGTGCATGCGC
K45E_pilT_R	GCGCATGCACCTGCTCGTGTTCCAGCGGTGG
H48R_pilT_F	GGAACACAAGCAGGTGCGTGCGCTGATCTACGACATC
H48R_pilT_R	GATGTCGTAGATCAGCGCACGCACCTGCTTGTGTTCCAG
E65K_pilT_F	GCAGCGCAAGGACTTCGAGAAATTCCTCGAGACCGACTTCTCC
E65K_pilT_R	GGAGAAGTCGGTCTCGAGGAATTTCTCGAAGTCCTTGCGCTGC
N87S_pilT_F	CGGGTCAACGCCTTCAGCCAGAACCGTGGCGC
N87S_pilT_R	GCGCCACGGTTCTGGCTGAAGGCGTTGACCCG
N87D_pilT_F	CGGGTCAACGCCTTCGACCAGAACCGTGGCGC
N87D_pilT_R	GCGCCACGGTTCTGGTCGAAGGCGTTGACCCG
H222A_pilT_F	CGCGGCGGAGACCGGCGCCCTGGTATTCGGCACCC
H222A_pilT_R	GGGTGCCGAATACCAGGGCGCCGGTCTCCGCCGCG
M301T_pilT_F	CGAGGACAAGGTCGCGCAGACGTATTCGGCGATCCAGACC
M301T_pilT_R	GGTCTGGATCGCCGAATACGTCTGCGCGACCTTGTCCTCG

R331H_pilT_F	GGGCCTGATCAGCCACGAGAATGCCCGCGAGAAGG
R331H_pilT_R	CCTTCTCGCGGGCATTCTCGTGGCTGATCAGGCCC
YFP_K213E_F	gcaaactgtctaaagacccgaacgaaaaacgtgaccacatgg
YFP_K213E_R	ccatgtggtcacgttttttcgttcgggtctttagacagtttgc
LBB2H_pT_5'	GCGTCTAGAGATGGATATTACCGAGCTGCTCG
LBB2H_pT_3'	GCGGGTACCTCAGAAGTTTTCCGGGATCTTC
LBB2H_pU_5'	GCGTCTAGAGATGGAATTCGAAAAGCTGCTGC
LBB2H_pU_3'	GCGGGTACCGCTGGCCTACTGAAGACGGT
LBB2H_pC_5'	TATATAACTCTAGAGATGGCGGACAAAGCGTTAAAAACCAG
LBB2H_pC_3'	TATATATGGAATTCGTTATCCGACGACGTTGCCGA
LBB2H_pB_5'	TATATATATCTAGAGATGAACGACAGCATCCAACTG
LBB2H_pB_3'	TATATATAGAATTCGTTAATCCTTGGTCACGCGGTT
K58A_pilT_F	gatctaCGACATCATGAACGACgcGCAGCGCAAGGACTTCGAGGAATTCC
K58A_pilT_R	GGAATTCCTCGAAGTCCTTGCGCTGCgcGTCGTTCATGATGTCGTAGATC
H229A_pilT_F	cctGGTATTCGGCACCCTGGCCACCACCTCGGCGGCGAAGACC
H229A_pilT_R	GGTCTTCGCCGCCGAGGTGGTggcCAGGGTGCCGAATACCAGG

30pT_1	CGAATTCGAGCTCGGTACCCCCACGGCCTCGGCGTTGGAC
30pT_6	GTCGACTCTAGAGGATCCCCCGAACACAGCACCCTGCAACTGGA AACC
30pT_7	GTCGACTCTAGAGGATCCCCCCAGACCAACTCGACCCGCC
30pT_2COR	GAGCAGCTCGGTAATATCCAT
30pT_3COR	ATGGATATTACCGAGCTGCTC
30pT_4COR	GAAGTTTTCCGGGATCTTCGC
30pT_5COR	GCGAAGATCCCGGAAAACTTC
pilT_D31K_F_COR	CCGCCCATGATCCGGGTGAAGGGCGATGTACGCCGGATCAACCT GCC
pilT_D31K_R_COR	GGCAGGTTGATCCGGCGTACATCGCCCTTCACCCGGATCATGGGC GG
72RBS_pilT5'	gGTACCgaaggagatatacatATGGATATTACCGAGCTGCTCGC
72RBS_pilT3'	ccaaaacagccaAGCTTTCAGAAGTTTTCCGGGATCTTCGCC
18C_pilC_XbaI_5'	TATATAACTCTAGAGatggcggacaaagcgttaaagacc
18C_pilC_EcoRI_3'	TATATATGGAATTCGTTAcacaacggaacccagttggaagatcg
72toVLT31_Gib1_5'	CAGAATTCGAGCTCGGTACCctactgtttctccatacccgttttttttg
72toVLT31_Gib2_5'	ACACAGGAAACAGAATTCGGctactgtttctccatacccgttttttttg
PaQaRpoD_CTX1_A	ctagaactagtggatcccctaataaccaggcatcaaataaaacgaaaggctc

PaQaRpoD_CTX1_B2	atatcgaattcctgcagccgcggccgcaaaaggaaaagatc
72rbs_pT_5'	TcgagctcggtacccCAGGAGGAATTTTCCATGGATATTACCGAGCTG CTCGC
72rbs_pT_3'	CgactctagaggatcccctcaGAAGTTTTCCGGGATCTTCgc
T18C_fimL_5'	CGACTCTAGAGGATCCCCGGatggtcacaggagccacgtc
T18C_fimL_3'	AATTCGAGCTCGGTACCCTggcggccaccggcag
T18C_pilK_5'	CGACTCTAGAGGATCCCCGGatgcaggcgaacggcgtc
T18C_pilK_3'	AATTCGAGCTCGGTACCCTtgtgcctgagtaccccttacg
T18C_chpB_5'	CGACTCTAGAGGATCCCCGGatgagtgagcgcgccac
T18C_chpB_3'	AATTCGAGCTCGGTACCCTtgtttcgactcctgtcggcg
T18C_fimW_5'	CGACTCTAGAGGATCCCCGGatggaaaaccagagcccccac
T18C_fimW_3'	AATTCGAGCTCGGTACCCTcagagacttccagagcgagtcaaaatc
VLT31rbs_pilU_5'	TTCGAGCTCGGTACCCCAGGAGGAATTTTCCatggaattcgaaaagct gctgc
VLT31rbs_pilU_3'	CGACTCTAGAGGATCCCCtcagcggaagcgccg
T18C_pilG_5'	CGACTCTAGAGGATCCCCGGatggaacagcaatccgacggt
T18C_pilG_3'	AATTCGAGCTCGGTACCCTggaaacggcgtccaccg
T18C_pilH_5'	CGACTCTAGAGGATCCCCGGatggctcgtattttgattgttgatgact

T18C_pilH_3'	AATTCGAGCTCGGTACCCTgcccgccagcaccg
T18C_pilC_L_5'	CGACTCTAGAGGATCCCCGGatggcggacaaagcgttaaagac
T18C_pilC_S_5'	CGACTCTAGAGGATCCCCGGatgctggtgaaggctcaactg
T18C_pilC_3'	AATTCGAGCTCGGTACCCTcacaacggaacccagttggaag
T18C_pilU_5'	CGACTCTAGAGGATCCCCGGatggaattcgaaaagctgctgcg
T18C_pilU_3'	AATTCGAGCTCGGTACCCTgcggaagcgccgg
T18C_pilI_5'	CGACTCTAGAGGATCCCCGGatgtcggacgttcagaccc
T18C_pilI_3'	AATTCGAGCTCGGTACCCTtacggcgacgtcgagga
T18C_chpC_5'	CGACTCTAGAGGATCCCCGGatgaaccaggccgtgatcgag
T18C_chpC_3'	AATTCGAGCTCGGTACCCTgatcaggccggcgtcg
T18C_chpD_5'	CGACTCTAGAGGATCCCCGGatggccggcctgcaac
T18C_chpD_3'	AATTCGAGCTCGGTACCCTgccgcgcacagcg
T18C_chpE_5'	CGACTCTAGAGGATCCCCGGatgctcgccatcttcctcg
T18C_chpE_3'	AATTCGAGCTCGGTACCCTcagcccgcgcagc
QC_pilT_R123D_5'	CGTGTTTCAGACGTCCCGgaCGGGCTGGTACTGGTCACCG
QC_pilT_R123D_3'	CGGTGACCAGTACCAGCCCGtcCGGGACGTCTGAAACACG
QC_PilU_K136A_fwd	GCGCCACCGGCACCGGCgcGTCCACCTCGCTGGCGGC
QC_PilU_K136A_rev	GCCGCCAGCGAGGTGGACgcGCCGGTGCCGGTGGCGC

QC_pilT_T216R_5'	CGCCTGGCCCTGAgaGCGGCGGAGACCGGCC
QC_pilT_T216R_3'	GGCCGGTCTCCGCCGCtcTCAGGGCCAGGCG

2.9 Supplemental References.

1.   Simon R, Priefer U, Pühler A. 1983. A broad host range mobilization system for in vivo genetic engineering: transposon mutagenesis in gram negative bacteria. Bio/Technology 1:784-791.

2.   Karimova G, Pidoux J, Ullmann A, Ladant D. 1998. A bacterial two-hybrid system based on a reconstituted signal transduction pathway. Proceedings of the National Academy of Sciences 95:5752-5756.

3.   Rahme LG, Stevens EJ, Wolfort SF, Shao J, Tompkins RG, Ausubel FM. 1995. Common virulence factors for bacterial pathogenicity in plants and animals. Science 268:1899-1902.

4.   Lee CK, De Anda J, Baker AE, Bennett RR, Luo Y, Lee EY, Keefe JA, Helali JS, Ma J, Zhao K, Golestanian R, O'Toole GA, Wong GCL. 2018. Multigenerational memory and adaptive adhesion in early bacterial biofilm communities. Proceedings of the National Academy of Sciences 115:4471-4476.

5.   Luo Y, Zhao K, Baker AE, Kuchma SL, Coggan KA, Wolfgang MC, Wong GC, O'Toole GA. 2015. A hierarchical cascade of second messengers regulates Pseudomonas aeruginosa surface behaviors. mBio 6:e02456-14.

6.   Kuchma SL, O'Toole GA. 2022. Surface-induced cAMP signaling requires multiple features of the *Pseudomonas aeruginosa* Type IV Pili. Journal of Bacteriology 204:e0018622.

7.   Shanks RMQ, Caiazza NC, Hinsa SM, Toutain CM, O'Toole GA. 2006. *Saccharomyces cerevisiae*-based molecular tool kit for manipulation of genes from gram-negative bacteria. Applied and Environmental Microbiology 72:5027-5036.

8.   Hoang TT, Kutchma AJ, Becher A, Schweizer HP. 2000. Integration-proficient plasmids for *Pseudomonas aeruginosa*: site-specific integration and use for engineering of reporter and expression strains. Plasmid 43:59-72.

9.   Hoang TT, Karkhoff-Schweizer RR, Kutchma AJ, Schweizer HP. 1998. A broad-host-range Flp-FRT recombination system for site-specific excision of chromosomally-

located DNA sequences: application for isolation of unmarked *Pseudomonas aeruginosa* mutants. Gene 212:77-86.

10. De Lorenzo V, Eltis L, Kessler B, Timmis KN. 1993. Analysis of *Pseudomonas* gene products using lacP/Ptrp-lac plasmids and transposons that confer conditional phenotypes. Gene 123:17-24.

Chapter 3

Introduction

Atomic Force Microscopy Measurements of Pel Polysaccharide- and Type IV pili-Mediated Adhesion of *Pseudomonas aeruginosa* PA14 to an Abiotic Surface

Audrey Beaussart[1,3], Telmo Manuel Oliveira Paiva[1], Christopher J. Geiger[2], Amy E. Baker[2], George A. O'Toole[2,#] and Yves Dufrêne[1,#]

[1]Institute of Life Sciences, Université catholique de Louvain, B-1348 Louvain-la-Neuve, Belgium.

[2]Department of Microbiology and Immunology, Geisel School of Medicine at Dartmouth

[3]Current Address: *Interdisciplinary Laboratory for Continental Environments,* UMR 7360 CNRS - Université de Lorraine, 15 avenue du Charmois, 54500 Vandoeuvre-Lès-nancy, France

Running Title: Measuring surface adhesion by AFM

Author contributions:

C.J.G. performed phenotypic assays and analyzed data.

3.1 Abstract. Type IV pili (TFP) use ATP-driven motors to extend and retract, thereby contributing to the ability of microbes such as *Pseudomonas aeruginosa* to engage with and move across surfaces. We reported previously that TFP of *P. aeruginosa* generates retractive forces of ~30 pN, and in this same publication, provided indirect evidence that TFP-mediated surface attachment was enhanced in the presence of the Pel polysaccharide. We first show that mutating the flagellum (D*flgK* mutant) results in an increase in Pel polysaccharide production, but this increase in Pel does not result in an increase in surface adhesive properties compared to those previously described for the WT strain (158). By blocking the ability to produce Pel in the D*flgK* mutant background, we show direct evidence using atomic force microscopy that Pel mediates two distinct mechanisms of early surface attachment by *P. aeruginosa*. First, Pel can mediate direct adhesive forces of up to ~1000 pN between the cell and an abiotic substratum. Second, the presence of Pel results in TFP-mediated attachment displaying a long-range (~1 um) median adhesive force of ~150 pN compared to ~75 pN in the absence of Pel. Thus, Pel increases TFP-substratum binding by ~2-fold. Because the TFP retraction force is on the order of ~30 pN, a relatively low value compared to TFP/Pel adhesive forces, our data suggest that the ability to retract the TFP might depend on changing TFP properties under force, perhaps as a consequence of the spring-like properties of the TFP we identify here. Alternatively, TFP depolymerization may also contribute to loss of TFP-Pel adhesion. We propose that given the role of TFP in bacterial surface sensing, the Pel-dependent increase in TFP-mediated surface interaction could have a profound impact on the ability of *P. aeruginosa* to detect surface engagement.

3.2 Importance. The Pel polysaccharide and the type IV pili (TFP) of *P. aeruginosa* play critical roles in biofilm formation by this opportunistic pathogen. Here we present the direct measurement of the bacteria-surface adhesive force mediated by these two extracellular, biofilm-promoting factors. Furthermore, we show that TFP-mediated adherence is enhanced by the presence of Pel. These force measurements, together with the force retraction data reported for the TFP, provide critical values for developing models whereby TFP, perhaps together with the Pel polysaccharide, participate in surface sensing by *P. aeruginosa.*

3.3 Introduction

P. aeruginosa is an important opportunistic pathogen with the ability to form biofilms in a variety of contexts, including on medical impacts and in the context of chronic infections such as cystic fibrosis and diabetic wounds (159-163). A number of factors have been identified that contribute to biofilm formation by this microbe, including the production of type IV pili (TFP) and exopolysaccharides (EPS) such as Pel and Psl (164-169). These factors have also been shown to contribute to colonization of human airway cells, as well as pathogenesis (170).

Interestingly, despite the important role for TFP and EPS in biofilm formation, the extent to which these extracellular factors contribute to the adhesion of bacteria to a substratum has not been examined for this organism. One means of directly measuring adhesive force is via atomic force microscopy (AFM). We have used AFM previously to document that the cell surface-localized LapA protein is a bacterial adhesin (171-173). Several other studies have examined biofilm-related factors by AFM, including pili, adhesins and polysaccharides (172, 174-180). Using a laser trap, Maier, O'Toole and colleagues demonstrated that the retraction force of TFP of *P. aeruginosa* could exert a force of ~30 pN (181). Finally, we examined the role of TFP in adhesion of *P. aeruginosa* to a surface; these studies indicated that a TFP could mediate an adhesive force of up to 250 pN (158). In this previous report, using *P. aeruginosa* strain PA14, TFP-mediated adhesion was measured in the context of a strain that was capable of producing the EPS known as Pel (158).

Here, we use AFM to investigate the relative contribution of the Pel EPS, as well as TFP-mediated adhesion in the presence and absence of Pel. Our data indicate that Pel can enhance TFP-mediated adhesion, a finding consistent with our previous report (181). The adhesive forces measured here are critical to generate an overall model for how TFP engage the surface, particularly given the role for TFP in surface sensing (182).

3.4 Results

AFM analysis of TFP-mediated adhesion in the absence of Pel. In a previous report from our team, we examined TFP adhesion parameters by the wild-type strain of *P. aeruginosa* PA14 using an abiotic, hydrophobic tip. In these studies, we observed maximal adhesive events of ~ 250 pN and rupture length of >1500 pN for the WT *P. aeruginosa* PA14 when interacting with a hydrophobic surface.

Importantly, the WT *P. aeruginosa* PA14 strain produces the Pel polysaccharide, which has been previously reported as critical for biofilm formation (168, 169, 183). Thus, it was possible that we observed combined adhesive forces of the TFP with Pel. Furthermore, the flagellum has been implicated in early biofilm formation and surface sensing for *P. aeruginosa* (164, 184). To address the relative contribution of all of these factors we examined mutants defective in flagellar biosynthesis, Pel production or TFP production, alone or in combination.

The Δ*flgK* mutant shows a robust increase in Pel polysaccharide production as assessed by the Congo red (CR) assay (**Figure 1a**). Furthermore, mutating the *flgK* gene, which blocks synthesis of the flagellar hook and filament, as expected, results in a strain that is defective for swimming and swarming motility, and biofilm formation but shows near WT levels of TFP-mediated twitching motility (**Figure 1b**). Given this increase in production of the Pel adhesion, we investigated the impact on adhesion of this mutant to a hydrophobic surface using AFM.
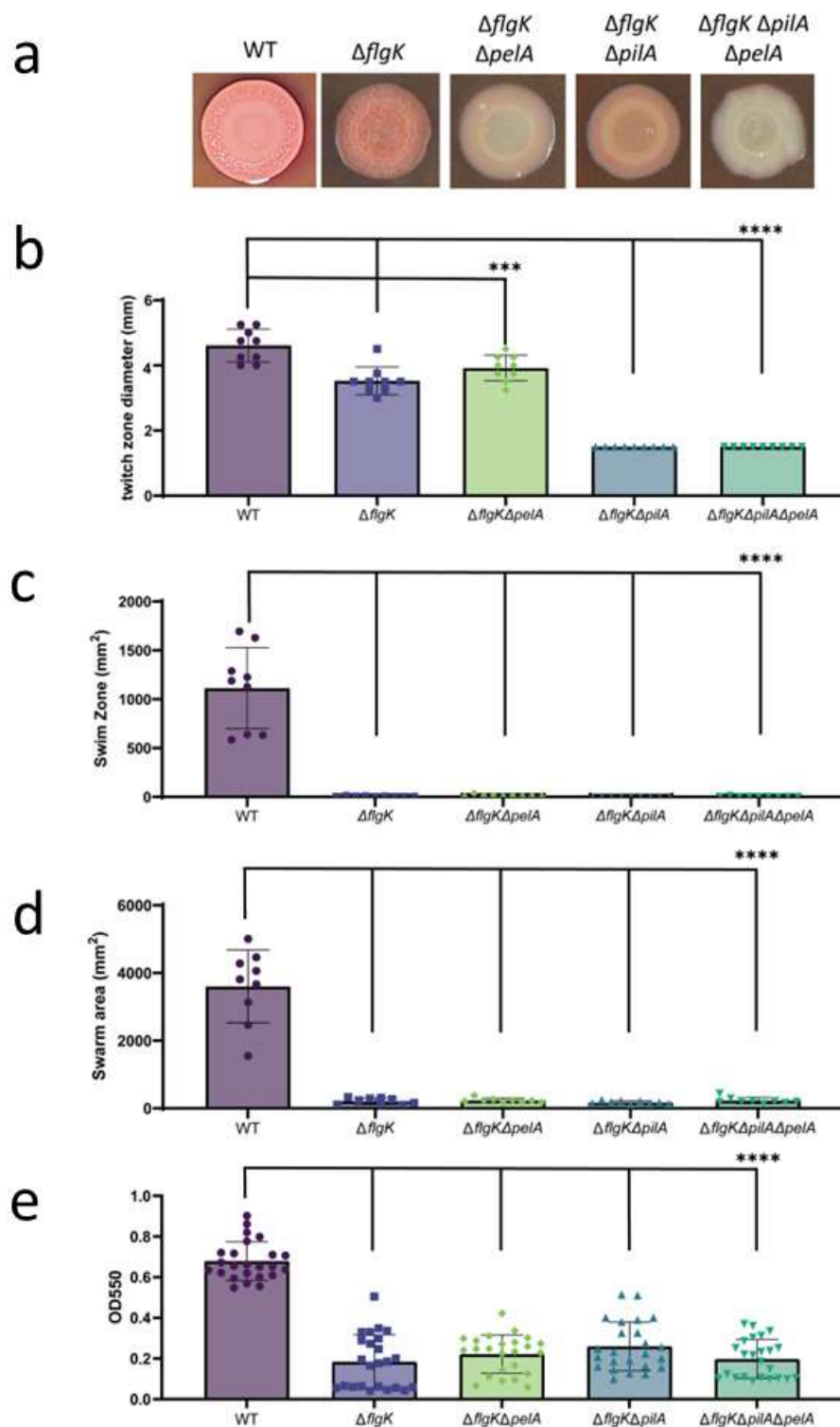
Figure 3.1. **Phenotypes of mutants used in these studies**. a. Binding to congo red (CR) serves a surrogate for the production of the Pel exopolysaccharide. b-c. Shown are the twitching (top), swimming (below), swarming (below), and biofilm formation

(bottom) phenotypes of the mutants shown in this experiment. Data were analyzed by one-way ANOVA followed by Tukey's post-test comparison. ***, $P<0.001$; ****, $P<0.0001$.

A representative cell of the Δ*flgK* mutant shows the TFP (**Figure 2b,left, inset**).The

maximum adhesion force (~250pN) and maximum rupture length (~1500 nm) of the

Δ*flgK* mutant (**Figure 2b,c**) is similar to that previously reported for the WT strain

(158). These data indicate that loss of this appendage does not markedly change the

strength and nature of the interaction between the bacterial cell and a hydrophobic

surface.
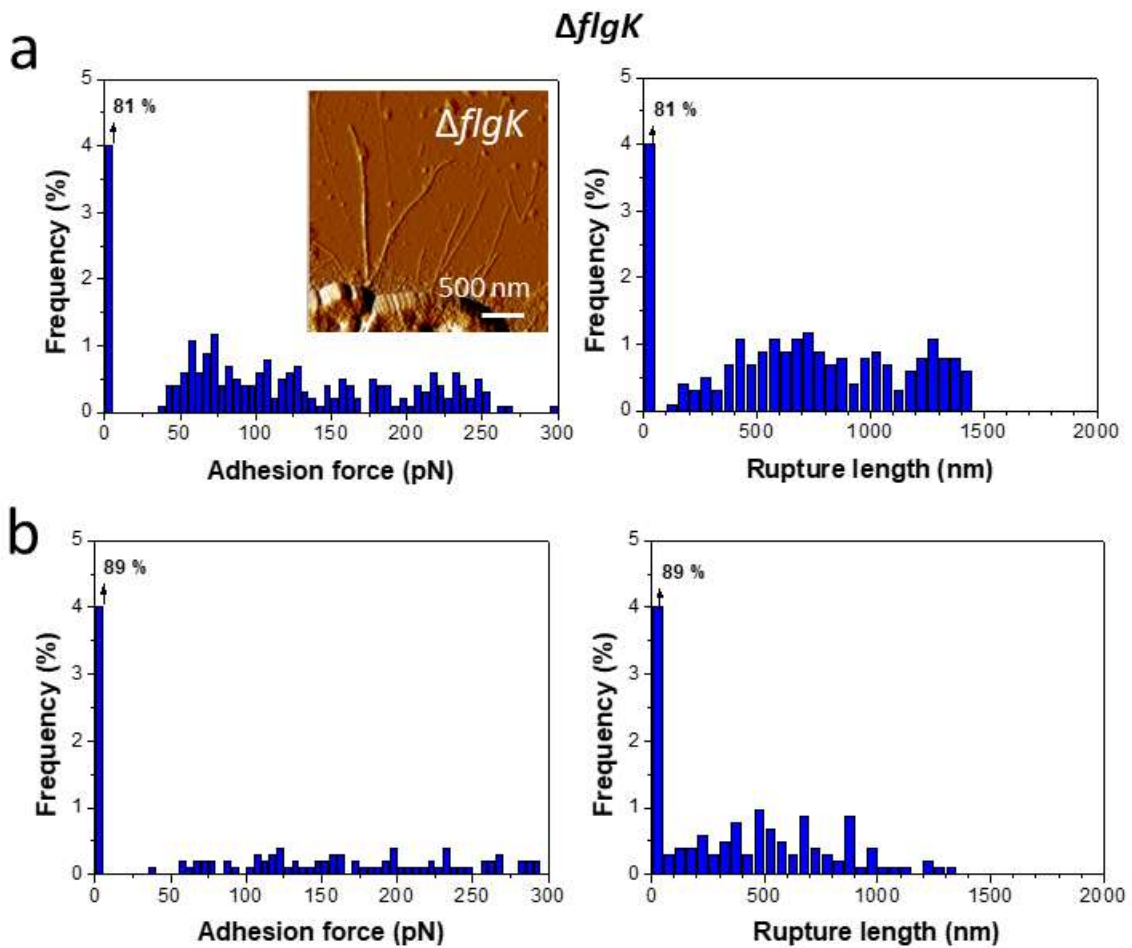
Figure 3.2. **Analysis of the Δ*flgK* mutant**. Shown are two independent replicates (a,b) of the adhesion force and rupture distance histograms for multiple cells of the Δ*flgK* mutant on a hydrophobic surface. This strain lacks a functional flagellum. Inset: representative image of the Δ*flgK* mutant.

We next addressed the impact of mutating Pel polysaccharide production. The lack of motility with the Δ*flgK* provides an advantage in terms of reducing cell movement and eliminating any contribution of the flagellum to cell-to-substratum adhesion, so we examined the loss of Pel in the Δ*flgK* genetic background; this strain is incapable of Pel production but still can produce TFP and shows near WT levels of twitching motility (**Figure 1b**).

The Δ*flgK* Δ*pelA* double mutant results in a maximal adhesive force of ~200 with most cells showing an adhesive force of ~75 pN (**Figure 3**). The WT, in contrast, shows a relatively even distribution of adhesive forces topping out at ~250 pN (158). The rupture distance in this mutant is extended to ~2000 nM, which can be attributed to the TFP; a value almost twice that reported for the WT (158).
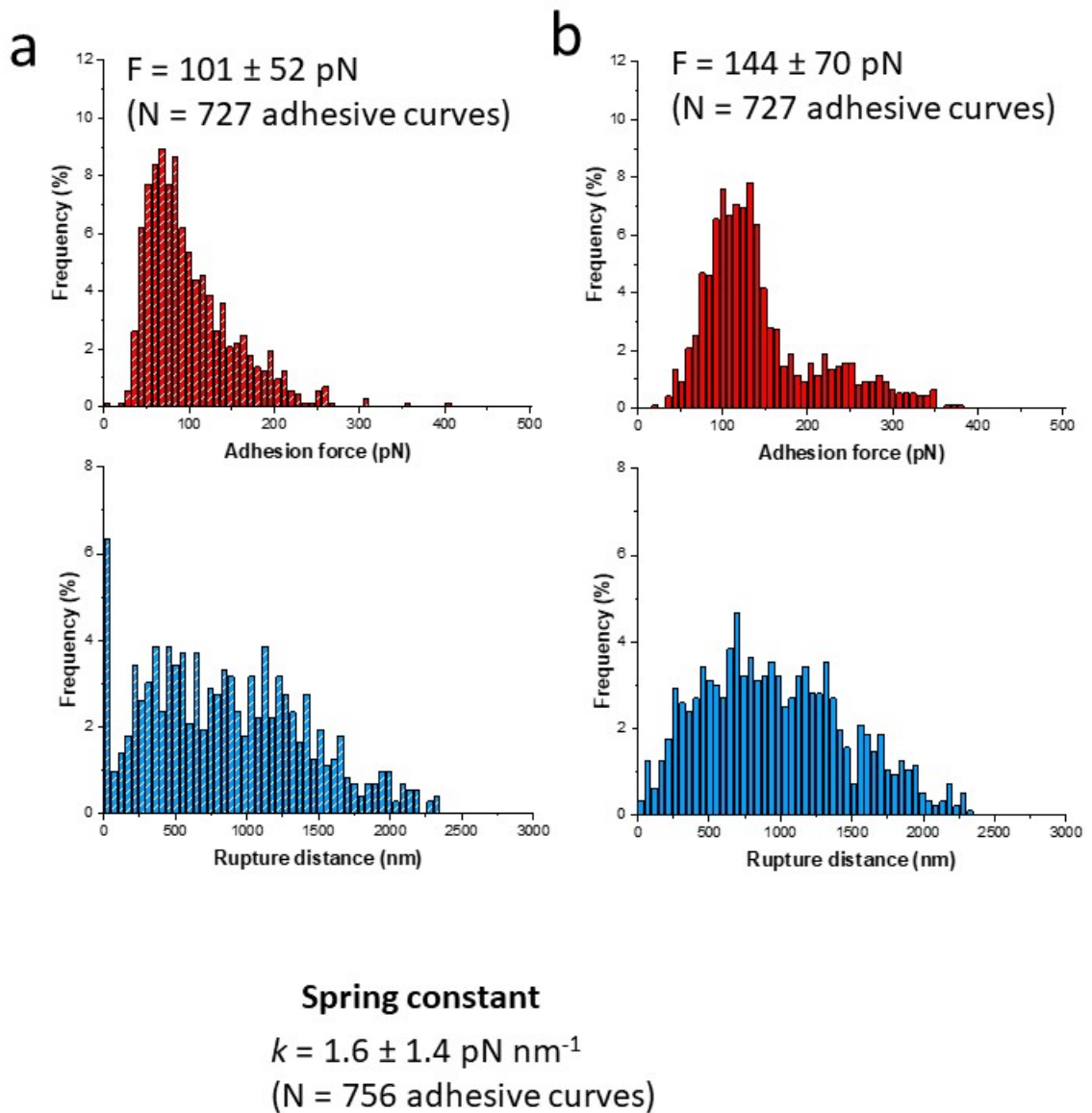
Figure 3.3. AFM analysis of TFP-mediated adhesion. Shown are two independent replicates (a,b) of the adhesion force and rupture distance histograms for the Δ*flgK*Δ*pelA* double mutant on a hydrophobic surface. This strains lacks a functional flagellum and the ability to produce the Pel polysaccharide.

AFM analysis of Pel-mediated adhesion reveals strong, short-distance adhesive forces. We next examined the impact of Pel mediated adhesion using a Δ*flgK* Δ*pilA* double mutant. This strain is still capable of producing the Pel polysaccharide, but at levels less than Δ*flgK* mutant (**Figure 1a**). This strain lacks the TFP as well as the flagellum and thus cannot swim, swarm or twitch (**Figure 1b**).

AFM analysis of the Δ*flgK* Δ*pilA* double mutant revealed two key findings. First, we observed a time-dependent increase in adhesive force, increasing from a median force of ~500 pN at 1 sec to ~1000 pN at 3 sec (**Figure 4a,b**). The measured rupture distance at 0 and 1 sec varied between 100-200 nm (**Figure 4a,b**). Interestingly, by 3 sec there was an increase in adhesion force with a maximum of ~1800 pN and bimodal distribution of the rupture distance at ~200 and ~400 nm (**Figure 4c**).

Inspection of individual force curves (**Figure 4c, inset**) showed that bacteria fell into two discreet groups with a rupture distance of ~200 and 400 nM, rather than single bacteria displaying two, step-wise rupture events. These data indicate a potential difference in the quantity, or perhaps quality, of the Pel polysaccharide produced. No such bimodal distribution was observed for the rupture distance for the WT; rather, a broad flat distribution of rupture lengths, varying from close to 0 to >2000 nm were measured (158).
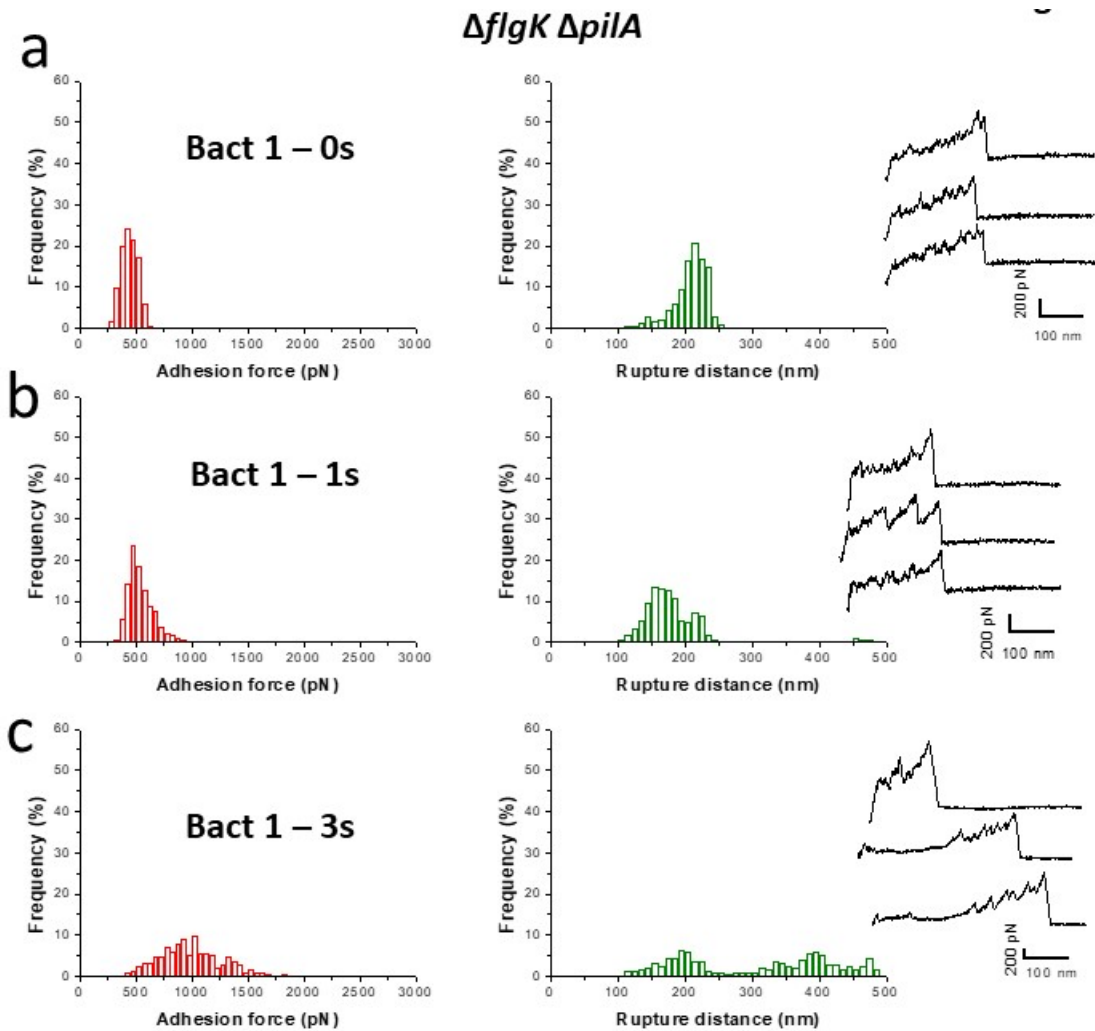
Figure 3.4. **AFM analysis of Pel-mediated adhesion**. Shown are the adhesion force and rupture distance histograms at 0, 1 and 3s post-adherence for the Δ*flgK*Δ*pilA* double mutant on a hydrophobic surface. This strains lacks a functional flagellum and the ability to produce TFP. Inset: representative force curves at each time point.

Loss of Pel and TFP effectively eliminate adhesion. It is formally possible that in addition to the flagellum, TFP and Pel polysaccharide, there are other factors that contribute to early attachment events by *P. aeruginosa*. As shown in **Figure 5**, the Δ*flgK*Δ*pilA*Δ*pelA* triple mutant shows essentially no measurable adhesion events at 0 sec, with 98% of cells having an interaction with the hydrophobic tip of 0 pN. Few such events (~30% of cells) are observed at 1 and 3 sec, and those measured events were <250 pN. These data suggest that TFP and Pel polysaccharide make a substantial contribution to early bacteria-substratum interaction events.
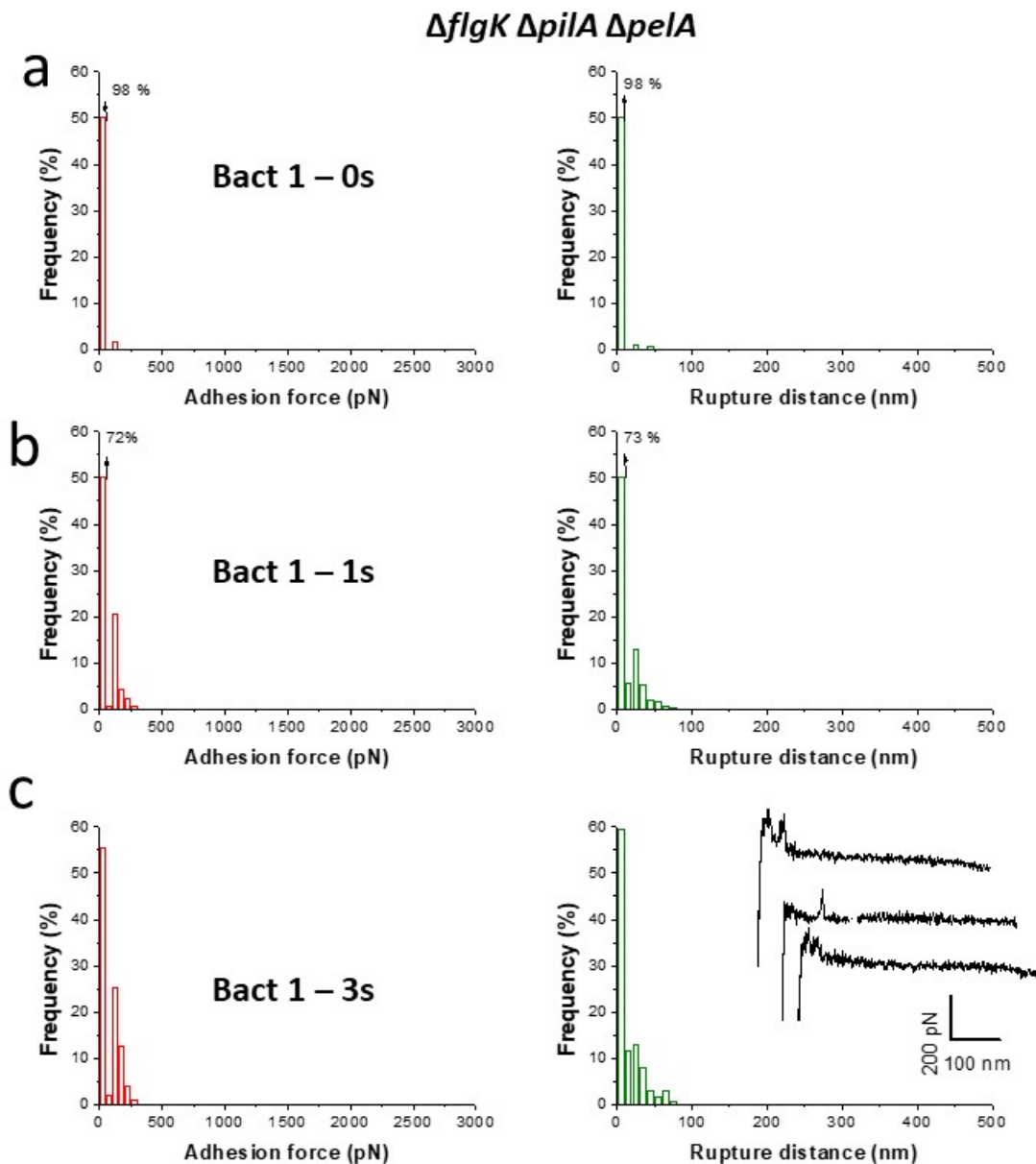
Figure 3.5. **Loss of Pel and TFP effectively eliminate adhesion.** Shown are the adhesion force and rupture distance histograms at 0, 1 and 3s post-adherence for the ΔflgKΔpilAΔpelA triple mutant on a hydrophobic surface. This strains lacks a functional flagellum and the ability to produce the Pel polysaccharide. This strains lacks a functional flagellum, and the ability to produce theTFP and Pel polysaccharide. Inset: representative force curves at each time point.

3.5 Discussion.

In this study, we examined the impact of mutating the flagellum, TFP and/or Pel EPS on early surface interactions, allowing us to refine our model of factors driving interaction of P. aeruginosa PA14 with a surface (**Figure 6**). Using the D*flgK* mutant we showed that, despite the increase in Pel production in this strain, that the measured interaction of this mutant with a hydrophobic substratum is very similar to the WT, as we previously reported (158). These data suggest that: (i) the flagellum is not a critical adhesive structure under these conditions and (ii) increasing Pel does not increase the measured adhesion parameters, that is, the baseline Pel production of the WT appears to maximize surface binding. Furthermore, analysis of the D*flgK*D*pilA*D*pelA* mutant results in almost a complete loss of binding to the hydrophobic substratum, indicating that the TFP and Pel are the major adhesive factors under these conditions. This observation has allowed us to focus on the roles of Pel and TFP during initial surface engagement.
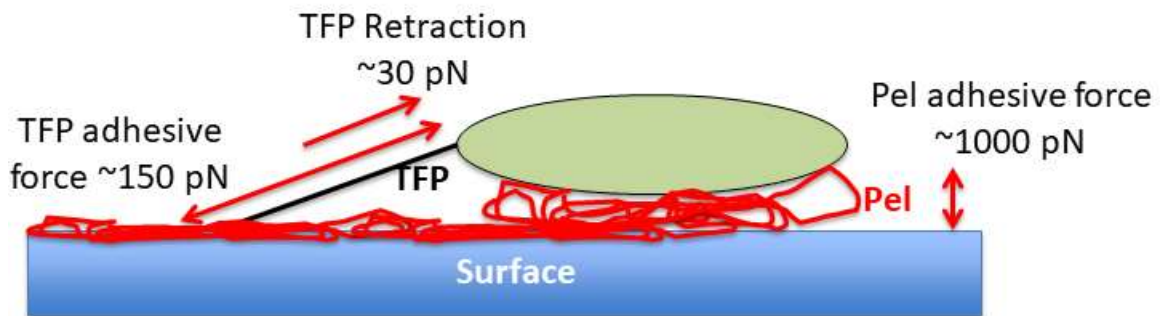
Figure 3.6. **Model for Pel and TFP-mediated adhesion.** Our current model of factors contributing to initial attachment events of *P. aeruginosa* PA14 to a hydrophobic surface, a common substratum used in biofilm studies. Work here and in previous studies (158) indicate that type IV pili (TFP), in the context of Pel-producing strains, can mediate up to 250 pN of adhesive force. In contrast, TFP mediate ~125 pN of force in the absence of Pel, a reduction of ~2-fold. Adhesive force in the absence of TFP, but in a strain capable of Pel production, can reach ~1000pN. The retractile force generated by these pili is ~30pN (185).

Interestingly, we observe that in the absence of TFP (the D*flgK*D*pilA* mutant), the initial Pel-mediated attachment is more robust (~1000 pN), but with a much shorter rupture length (~200 nm) compared to the strain expressing both TFP and Pel, which displays a maximal adhesive force of ~250 pN and a rupture length maximum of ~1500 nm (158). These data suggest that TFP, or perhaps TFP-mediated movement, may modulate Pel-mediated early attachment. That is, in the absence of TFP and/or TFP-mediated movement, perhaps the strains become hyper-adhesive. Such a model is consistent with a report showing a *pel* mutant strain of *P. aeruginosa* PA14 makes a flat, uniform biofilm compared to the typical "mushroom-like" colony biofilm morphology (183), where colonies of bacteria are separated by channels. Perhaps the TFP help prevent immediate bacterial adhesion with the surface, and thus moderate what would otherwise be robust, short-range, Pel-mediated initial adherence events.

Why would the cell develop a strategy to block Pel-mediated adherence early on during surface engagement? *P. aeruginosa* is well known to undergo initial "reversible" attachment events, wherein the bacteria readily return to the motile, planktonic phase (164, 182, 186). Our previous studies are consistent with such a conclusion, in that TFP-mediate cAMP signaling requires extended, multi-generational signaling to promote biofilm formation (187). Presumably, the ability to transiently adhere to the surface via TFP-mediated process would allow the bacteria to sample the surface, but not fully commit to a surface lifestyle immediately. That is, Pel-mediated adherence may play a role in tightly securing the bacteria to a surface once the decision to commit is fully embraced by the microbe. Presumably, this "decision" occurs only after the appropriate surveying of the environment by the

microbe is complete, and signals that promote biofilm formation are sensed and integrated. Interestingly, for the PAO1 strain of *P. aeruginosa*, the Psl EPS does seem to be a major driver of early attachment (188, 189) and the PAO1 strain typically shows less robust twitching motility in standard assays (190-193). These different mechanisms of initial attachment likely impact what are clearly distinct strategies for biofilm formation used by these two strains (22, 188).

An important implication of our findings is the observed TFP-mediated adherence in the absence of Pel compared to the recently measured retractile force generated by these TFP at $\sim$30 pN (185). The measured adherence of TFP in the presence of Pel at 250 pN would make it difficult to envision how TFP could detach from the surface. Thus, early surface engagement events, and the ability to continue to move across the surface via TFP-mediated movement may necessarily require that little/no Pel is deposited on the surface early on. These findings also have important implications for understanding surface-sensing pathways in *P. aeruginosa* (24, 39, 76, 182, 194, 195). While the mechanistic basis of such surface-sensing systems are not yet understood, the values determined here (TFP-mediated adherence with and without Pel) and the TFP retractile force measurements (185) set critical constraints on any models we develop in the future.

3.6 Methods and Materials

Strains and media. The strains used in this report are Δ*flgK* (SMC5845; (185)), Δ*flgK*Δ*pelA* (SMC7297; (185)), Δ*flgK*Δ*pilA* (SMC6595), and Δ*flgK*Δ*pelA*Δ*pilA* (SMC7296), built previously as reported in the respective references or constructed as reported (ref) for this study. Bacteria were routinely grown on M63 minimal medium supplemented with glucose (0.2%), magnesium sulfate (1 mM) and casamino acids (0.5%) at 37°C, as reported (164).

Phenotypic assays. Congo red (196), swarming motility (192), swimming motility (197), twitching motility (198), biofilm (199), and phage resistance (200) assays were performed as reported.

Atomic force microscopy. Atomic force microscopy experiments were performed as previously described (158)

3.8 Literature Cited

1. Beaussart A, Baker AE, Kuchma SL, El-Kirat-Chatel S, O'Toole GA, Dufrene YF. Nanoscale adhesion forces of *Pseudomonas aeruginosa* type IV Pili. ACS nano. 2014;8(10):10723-33.

2. Palmer GC, Whiteley M. Metabolism and pathogenicity of *Pseudomonas aeruginosa* infections in the lungs of individuals with Cystic Fibrosis. Microbiology spectrum. 2015;3(4).

3. Bergan T. Pathogenetic factors of Pseudomonas aeruginosa. Scand J Infect Dis Suppl. 1981;29:7-12.

4. Costerton JW, Stewart PS, Greenberg EP. Bacterial biofilms: a common cause of persistent infections. Science. 1999;284(5418):1318-22.

5. Giamarellou H, Kanellakopoulou K. Current therapies for *Pseudomonas aeruginosa*. Crit Care Clin. 2008;24(2):261-78, viii.

6. Govan JR, Deretic V. Microbial pathogenesis in cystic fibrosis: mucoid Pseudomonas aeruginosa and Burkholderia cepacia. Microbiol Rev. 1996;60(3):539-74.

7. O'Toole GA, Kolter R. Flagellar and twitching motility are necessary for Pseudomonas aeruginosa biofilm development. Mol Microbiol. 1998;30(2):295-304.

8. Burrows LL. *Pseudomonas aeruginosa* twitching motility: type IV pili in action. Annual review of microbiology. 2012;66:493-520.

9. Leighton TL, Buensuceso RN, Howell PL, Burrows LL. Biogenesis of Pseudomonas aeruginosa type IV pili and regulation of their function. Environmental microbiology. 2015;17(11):4148-63.

10.   Matsukawa M, Greenberg EP. Putative exopolysaccharide synthesis genes influence *Pseudomonas aeruginosa* biofilm development. J Bacteriol. 2004;186(14):4449-56.

11.   Friedman L, Kolter R. Genes involved in matrix formation in *Pseudomonas aeruginosa* PA14 biofilms. Mol Microbiol. 2004;51(3):675-90.

12.   Friedman L, Kolter R. Two genetic loci produce distinct carbohydrate-rich structural components of the *Pseudomonas aeruginosa* biofilm matrix. J Bacteriol. 2004;186(14):4457-65.

13.   Moreau-Marquis S, Bomberger JM, Anderson GG, Swiatecka-Urban A, Ye S, O'Toole GA, et al. The DeltaF508-CFTR mutation results in increased biofilm formation by Pseudomonas aeruginosa by increasing iron availability. Am J Physiol Lung Cell Mol Physiol. 2008;295(1):L25-37.

14.   El-Kirat-Chatel S, Beaussart A, Boyd CD, O'Toole GA, Dufrene YF. Single-cell and single-molecule analysis deciphers the localization, adhesion, and mechanics of the biofilm adhesin LapA. ACS chemical biology. 2014;9(2):485-94.

15.   El-Kirat-Chatel S, Boyd CD, O'Toole GA, Dufrene YF. Single-molecule analysis of *Pseudomonas fluorescens* footprints. ACS nano. 2014;8(2):1690-8.

16.   Boyd CD, Smith TJ, El-Kirat-Chatel S, Newell PD, Dufrene YF, O'Toole GA. Structural features of the *Pseudomonas fluorescens* biofilm adhesin LapA required for LapG-dependent cleavage, biofilm formation, and cell surface localization. J Bacteriol. 2014;196(15):2775-88.

17.   Ciesluk M, Deptula P, Piktel E, Fiedoruk K, Suprewicz L, Paprocka P, et al. Physics comes to the aid of medicine-clinically-relevant microorganisms through the eyes of atomic force microscope. Pathogens. 2020;9(11).

18.   Viljoen A, Mignolet J, Viela F, Mathelie-Guinlet M, Dufrene YF. How microbes use force to control adhesion. J Bacteriol. 2020;202(12).

19. Dufrene YF. Sticky microbes: forces in microbial cell adhesion. Trends in microbiology. 2015;23(6):376-82.

20. Dufrene YF, Ando T, Garcia R, Alsteens D, Martinez-Martin D, Engel A, et al. Imaging modes of atomic force microscopy for application in molecular and cell biology. Nat Nanotechnol. 2017;12(4):295-307.

21. Puchner EM, Gaub HE. Force and function: probing proteins with AFM-based force spectroscopy. Curr Opin Struct Biol. 2009;19(5):605-14.

22. Touhami A, Jericho MH, Boyd JM, Beveridge TJ. Nanoscale characterization and determination of adhesion forces of Pseudomonas aeruginosa pili by using atomic force microscopy. J Bacteriol. 2006;188(2):370-7.

23. Ivanov IE, Boyd CD, Newell PD, Schwartz ME, Turnbull L, Johnson MS, et al. Atomic force and super-resolution microscopy support a role for LapA as a cell-surface biofilm adhesin of *Pseudomonas fluorescens*. Res Microbiol. 2012;163(9-10):685-91.

24. Maier B, Wong GC. How bacteria use Type IV pili machinery on surfaces. Trends in microbiology. 2015;23(12):775-88.

25. O'Toole GA, Wong GC. Sensational biofilms: surface sensing in bacteria. Current opinion in microbiology. 2016;30:139-46.

26. Colvin KM, Gordon VD, Murakami K, Borlee BR, Wozniak DJ, Wong GC, et al. The Pel polysaccharide can serve a structural and protective role in the biofilm matrix of *Pseudomonas aeruginosa*. PLoS pathogens. 2011;7(1):e1001264.

27. Hug I, Deshpande S, Sprecher KS, Pfohl T, Jenal U. Second messenger-mediated tactile response by a bacterial rotary motor. Science. 2017;358(6362):531-4.

28. Monds RD, O'Toole GA. The developmental model of microbial biofilms: ten years of a paradigm up for review. Trends in microbiology. 2009;17(2):73-87.

29. Lee CK, de Anda J, Baker AE, Bennett RR, Luo Y, Lee EY, et al. Multigenerational memory and adaptive adhesion in early bacterial biofilm communities. Proceedings of the National Academy of Sciences of the United States of America. 2018;115(17):4471-6.

30. Lee CK, Vachier J, de Anda J, Zhao K, Baker AE, Bennett RR, et al. Social cooperativity of bacteria during reversible surface attachment in young biofilms: a quantitative comparison of *Pseudomonas aeruginosa* PA14 and PAO1. mBio. 2020;11(1).

31. Zhao K, Tseng BS, Beckerman B, Jin F, Gibiansky ML, Harrison JJ, et al. Psl trails guide exploration and microcolony formation in *Pseudomonas aeruginosa* biofilms. Nature. 2013;497(7449):388-91.

32. Doyle TB, Hawkins AC, McCarter LL. The complex flagellar torque generator of P*seudomonas aeruginosa*. J Bacteriol. 2004;186(19):6341-50.

33. Toutain CM, Zegans ME, O'Toole GA. Evidence for two flagellar stators and their role in the motility of *Pseudomonas aeruginosa*. J Bacteriol. 2005;187(2):771-7.

34. Ha DG, Kuchma SL, O'Toole GA. Plate-based assay for swarming motility in *Pseudomonas aeruginosa*. Methods Mol Biol. 2014;1149:67-72.

35. Morris JD, Hewitt JL, Wolfe LG, Kamatkar NG, Chapman SM, Diener JM, et al. Imaging and analysis of *Pseudomonas aeruginosa* swarming and rhamnolipid production. Appl Environ Microbiol. 2011;77(23):8310-7.

36. Kasetty S, Katharios-Lanwermeyer S, O'Toole GA, Nadell CD. Differential surface competition and biofilm invasion strategies of *Pseudomonas aeruginosa* PA14 and PAO1. J Bacteriol. 2021;203(22):e0026521.

37. Ribbe J, Baker AE, Euler S, O'Toole GA, Maier B. The role of cyclic di-GMP and exopolysaccharide in type IV pilus dynamics. J Bacteriol. 2017.

38. Luo Y, Zhao K, Baker AE, Kuchma SL, Coggan KA, Wolfgang MC, et al. A hierarchical cascade of second messengers regulates *Pseudomonas aeruginosa* surface behaviors. mBio. 2015;6(1).

39. Persat A, Inclan YF, Engel JN, Stone HA, Gitai Z. Type IV pili mechanochemically regulate virulence factors in Pseudomonas aeruginosa. Proceedings of the National Academy of Sciences of the United States of America. 2015;112(24):7563-8.

40. Siryaporn A, Kuchma SL, O'Toole GA, Gitai Z. Surface attachment induces Pseudomonas aeruginosa virulence. Proceedings of the National Academy of Sciences of the United States of America. 2014;111(47):16860-5.

41. Webster SS, Wong GCL, O'Toole GA. The power of touch: Type 4 Pili, the von Willebrand A domain, and surface sensing by *Pseudomonas aeruginosa*. J Bacteriol. 2022;204(6):e0008422.

42. Chawla R, Gupta R, Lele TP, Lele PP. A skeptic's guide to bacterial mechanosensing. J Mol Biol. 2020;432(2):523-33.

43. Merritt JH, Brothers KM, Kuchma SL, O'Toole GA. SadC reciprocally influences biofilm formation and swarming motility via modulation of exopolysaccharide production and flagellar function. J Bacteriol. 2007;189(22):8154-64.

44. Ha DG, Kuchma SL, O'Toole GA. Plate-based assay for swimming motility in *Pseudomonas aeruginosa*. Methods Mol Biol. 2014;1149:59-65.

45. Caiazza NC, O'Toole GA. SadB is required for the transition from reversible to irreversible attachment during biofilm formation by *Pseudomonas aeruginosa* PA14. J Bacteriol. 2004;186(14):4476-85.

46. Cady KC, Bondy-Denomy J, Heussler GE, Davidson AR, O'Toole GA. The CRISPR/Cas adaptive immune system of *Pseudomonas aeruginosa* mediates resistance to naturally occurring and engineered phages. J Bacteriol. 2012;194(21):5728-38.

Table 3.1. Strains used in this study.

Organism/ Strain Number	Genotype/Description	Reference
Pseudomonas aeruginosa PA14		
SMC6595	Δ*flgK* Δ*pilA*	This study
SMC7296	Δ*flgK* Δ*pilA* Δ*pelA*	(185)
SMC7297	Δ*flgK* Δ*pelA*	(185)
SMC5845	Δ*flgK*	(37)

Chapter 4

Final Conclusions and Outlook

Final Conclusions

Biofilms are not only the dominant mode of cellular life on planet earth, but they also highlight the intricacy of sensing and signaling pathways that have evolved in microbes over billions of years (1, 2). The biofilm mode of growth was first described by Henrici and then later by Zobell and Allen in the 1930s but it wasn't until the 1980's that the field as a whole gained insight into how these microorganisms were actually able to sense a surface in order initiate the biofilm lifestyle (142, 143, 201, 202). By manipulating the viscosity of liquid medium researchers were able to generate multi-flagellated *Vibrio parahaemolyticus*, a phenotype previously only observed for cells grown on a surface (142, 143). Since then, the physical manipulation of motility appendages has resulted in biofilm-associated phenotypes indicating that the obstruction of these motility appendages were allowing cells to sense the surface and initiate the biofilm mode of growth.

In this thesis I present mechanistic insight by which two motility appendages encoded by *Pseudomonas aeruginosa* are able to sense a surface. The physical strain on these molecular machines when these appendages interact with a surface is transmitted to the proteins that power locomotion. We present data that support a model whereby the proteins that power motility in these molecular machines are required for surface sensing and directly sense and transmit a surface contact signal. I demonstrate that the type IV pili retraction motor of PilT senses and transmits a surface signal culminating in cAMP production. I also show that the accessory retraction motor PilU modulates the surface signal by aiding in retraction as well as modulating signal transduction from PilT to PilJ. We also show that Pel can significantly enhance T4P retractive forces on abiotic surfaces. Below I discuss three main conclusions and future directions:

- Demonstrate direct interaction of PilT and PilJ in *P. aeruginosa* for surface grown cells. PilT and PilJ were shown to interact within a heterologous system in the absence of the rest of T4P and Pil-Chp machinery. Future studies should confirm

this interaction for surface grown *P. aeruginosa*. A pulldown assay should be performed with His-tagged PilJ on a Cobalt-NTA column. After eluting the solution should then be probed for the presence of PilT using our α-PilT antibody from Chapter 2.

- Determine the residues of PilT that facilitate interaction with PilU. Comparative genomics examining the conserved surface residues of PilT as well as structural predictions have indicated that PilT likely interacts with PilU through the PilT-N-terminal face of the hexamer but experiments must be performed to validate interaction through these residues. To identify residues on PilT that facilitate interaction with PilU a genetic screen should be designed to isolate mutants of PilT that are deficient in twitching motility but remain phage susceptible. Twitching motility requires interaction with PilU as well as the rest of the pilus machinery whereas phage susceptibility only requires that PilT retains ATPase activity and binding with PilC. To perform this screen, I would first perform error-prone PCR on the PilT sequence, clone the mutagenized *pilT* sequences into a *Pseudomonas*-specific expression vector, and then transform this pool of *pilT* mutants into the *P. aeruginosa* PA14 Δ*pilTU* background, and then perform phage susceptibility assays in a 96 well format as previously described (82), which allows for higher throughput than the traditional phage susceptibility plate assays. Cells with a variant of PilT that remain phage susceptible in the absence of PilU will be stable, retain the ability to interact with PilC, and perform ATPase activity to power pilus retraction. I would then prep the plasmids from these strains, pool them, and then transform them into the Δ*pilT* background and select for mutants that are unable to perform twitching motility. This approach then select for mutants that are functional but unable to bind PilU. I would then sequence these mutants and map the mutations onto the surface of PilT as done in Chapter 2. This strategy will allow us to verify the interaction predicted by alphafold multimer and conservation information.

- Perform lineage studies on PilT mutants to identify how the frequency and amplitude of cAMP oscillations vary with changes in PilT-PilJ interaction strength. The frequency and amplitude of c-di-GMP oscillations within single cells during biofilm formation has been shown to depend on the binding strength between the alignment complex protein PilO and the diguanylate cyclase SadC. *P. aeruginosa* PA14 also undergoes oscillations of cAMP at the single cell level during biofilm formation. To determine if the frequency and amplitude of these cAMP oscillations are controlled by the binding strength of the PilT-PilJ interaction, lineage experiments of *pilT* mutants with varying degrees of interaction with PilJ should be performed. To generate stable alleles of PilT with varying degrees of PilJ interaction, NNK mutagenesis should be performed on the PilT-PilJ interaction residues identified in Chapter 2 via the B2H system: H44, K45, H48, N87 (113). Alleles will then be subjected to Western assays as well as twitching motility to identify stable, functional alleles when expressed at physiological levels before lineage testing.

- Determine if expression of *pilU* increases independently of *pilT* during high levels of cAMP as a mechanism to aid in lowering levels to baseline after surface adaptation. We have previously shown that overexpressing *pilU* decreases cAMP levels. Furthermore, previous studies have shown that expression and protein levels of PilU increase with increasing cAMP levels (37, 96, 101). By mining microarray and RNAseq datasets we will be able to determine if transcription of *pilU* is independent of *pilT*, which is located directly upstream. Since all cellular changes in *P. aeruginosa* due to cAMP are mediated through its binding protein Vfr, we can predict that any transcriptional change due to cAMP is mediated through this protein (35, 95). We can also swap the chromosomal promoter of *pilU* for an inducible promoter that will not respond to Vfr, for example P_{tac}. We will then be able to express *pilU* without the promoter being subject to Vfr regulation and determine

whether cAMP dynamics are altered during surface adaptation. Furthermore, we can perform an electrophoretic mobility shift assay to assess if the promoter of the *pilU* gene is bound by purified Vfr in the presence of cAMP. Finally, we can perform qRT-PCR experiments to verify the increase in *pilU* expression for surface grown cells and see if the expression tracks with cAMP levels using our fluorescent cAMP reporter described in Chapter 2. In this way we will be able to determine if *Pa* elevates levels of PilU in order to bring cAMP levels back down during biofilm formation.

Outlook

It has been nearly 25 years since bacterial flagella were first demonstrated to be capable of sensing a mechanical load on the flagellar filament (142). By manipulating culture conditions either through the change in viscosity or the addition of antibodies specific to the flagellum, phenotypes associated with surface growth were able to be achieved in liquid conditions. Since then, the field of bacterial surface sensing has grown tremendously (142, 143). Recently, several surface sensing studies that use polar monotricious flagellates as their model organisms have uncovered striking similarities in mechanisms and outputs among these bacteria - this has been nicely summarized recently (203).

Studies investigating the mechanism of flagellar mediated surface sensing by *Caulobacter crescentus*, *Vibrio cholerae*, and *P. aeruginosa* have displayed similarities in their requirement for certain genetic elements as well as functional outputs during surface contact (57, 204, 205). One similarity among these model organisms is that mutations in the flagellum lead to biofilm related phenotypes, specifically the production of EPS or a holdfast. In *V. cholerae*, deleting the flagellin gene *flaA* leads to a rugose colony morphology due to the increased expression of *vps* genes responsible for regulating EPS production (57). In *P. aeruginosa*, deletion of the flagellin gene *fliC* leads to RSCV colony morphology due to the overproduction of pel and psl EPS when grown on VBMM agar and we have demonstrated in Chapter 3 that mutating the hook associated protein FlgK results in increased pel production as observed through congo red binding (205). In *C. crescentus*, flagellar synthesis mutants have been shown to be more adhesive than WT cells following transposon mutagenesis and selection (206).

Another similarity among these three systems is that the increased EPS production phenotype in these flagellar mutants are dependent on functional stator units. In order for stators to function in flagellar torque generation they must first be able to bind the ion whose gradient it uses to power flagellar rotation. It has been shown in *E. coli* that the ability to bind and conduct protons is necessary for stators to be

recruited to flagella when they are under high load (47). In *P. aeruginosa* and *C. crescentus* this means stators units must be able to bind and conduct protons and in *V. cholerae* they must be able to conduct Na⁺ (56, 57). Stators must also be able to engage the peptidoglycan layer as well as the C-ring in order to convert the ion motive force into flagellar torque. Disruption of either of these critical stator interactions also eliminates the overproduction of EPS in these backgrounds. In *V. cholerae*, mutating the flagellar components that aid in stator binding of the peptidoglycan, MotX, eliminates the EPS overproduction of flagellar mutants and in *P. aeruginosa* we have demonstrated that mutating the PG binding domain or the residues facilitating interaction with FliG eliminate Pel EPS overproduction as judged by Congo Red binding (Chapter 3) (57). In *C. crescentus*, mutating the residues results in non-functional stators, MotB-D33N, results in cells that no longer attach to surfaces or activate the DGC DgcB (56).

It has also been demonstrated that in all three of these model organisms, the overproduction of EPS caused by flagellar mutations are due to increases in c-di-GMP, usually through DGC activation. In *C. crescentus*, stator units have been shown to physically interact with the DGC DgcB which leads to increased c-di-GMP when the flagellum interacts with a surface (56). In *V. cholerae*, three different DGCs, CdgA, CdgL, and CdgO, all contribute to the flagellum dependent increase in c-di-GMP (57). *P. aeruginosa* has several DGCs shown to influence c-di-GMP levels in *fliC* mutants (GcbA, PA3177, SiaD) but the one with a known mechanism and physical link to a stator set itself is SadC (12, 205). We have previously shown that interaction of MotC and SadC leads to stimulation of diguanylate cyclase activity (12). Even in non-model organisms such as *Bordetella pertussis*, physically impeding flagellar rotation has been shown to lead to stator diffusion out of the flagellum allowing for physical interaction with DgcB that leads to stimulation of DGC activity and increased levels of c-di-GMP (207). These data demonstrate that the stator-dependent increase in c-di-GMP upon surface contact is a widespread mechanism of surface adaptation in the bacterial world.

While these aspects of flagellar mediated surface sensing have been well documented, a less appreciated facet of the flagellar mutations in these organisms are

their effect on the function or regulation of the other surface sensing appendage responsible for biofilm formation in these organisms: type four filaments. For *V. cholerae*, mutating the flagellin results in decreased levels of MSHA pili (57). The homologous mutation in *P. aeruginosa* has been shown to increase the number of extended T4aP pili by ~4-5X (14). Furthermore, in screens identifying suppressor of the flagellar mutant EPS overproduction phenotype in *P. aeruginosa*, T4P and Pil-Chp components were shown to be necessary in both the *P. aeruginosa* PAO1 and PA14 backgrounds (Chapter 3) (205). There are also several cases in *P. aeruginosa* where a T4P mutation affected a flagellar-mediated motility like swarming (208). Finally in *C. crescentus*, deleting either the flagellin or the flagellar hook protein results in reduction in Tad (T4cP) pilus synthesis due to reduced transcription of *tad* pili genes (209). Just like the similarities in flagellar-mediated signaling among these three organisms, there also exists regulatory links between these two motility appendages to coordinate surface behavior and biofilm formation. Below I will propose experiments to elucidate the mechanisms by which T4P and the flagellum of *P. aeruginosa* coordinate their efforts during surface attachment in order to build a robust biofilm.

One well studied mechanism by which T4P can be influenced by flagella is through manipulating levels of the second messenger c-di-GMP. The flagella of *V. cholerae, P. aeruginosa*, and *C. crescentus* have all been shown to stimulate c-di-GMP production when on a surface and this c-di-GMP can affect type 4 filament extension and retraction dynamics. In *P. aeruginosa* it has been shown that the protein FimX is able to bind c-di-GMP and affect pilus extension by interacting with PilB (121). The c-di-GMP binding protein immediately upstream of FimX, FimW, has also been shown to affect pili dynamics in a c-di-GMP-dependent manner but the mechanism by which FimW exerts its effects on pili remains unknown (82). In *V. cholerae* c-di-GMP directly binds the extension motor MshE to affect pilus extension and retraction dynamics with high levels of c-di-GMP being correlated with MSHA pili being in the retracted state resulting in increased levels of surface detachment (210). For *C. crescentus* the extension and retraction of T4cP are mediated by the same ATPase, CpaF (211). Low to medium levels of cdG has been associated pili extension but elevated levels of cdG

is associated with Tad pili retraction, although the exact mechanism by which c-di-GMP influence CpaF remains unknown (77, 212).

Clearly c-di-GMP from flagellar mediated-surface sensing can influence T4P dynamics but so can cAMP in *P. aeruginosa* as shown in Chapter 2. Vfr bound to cAMP activates the two-component system FimS-AlgR that is necessary for minor pilin production (24). The minor pilins are thought to serve as an initiation complex for T4P extension, thus increased cAMP leads to increased T4P activity as shown in Chapter 2, with *cpdA* mutants exhibiting the highest levels of cAMP and twitching motility (85, 113). Recent studies have also demonstrated that cAMP can affect flagellar dynamics as well. Deleting both adenylate cyclases in *P. aeruginosa* decreases swimming motility and the addition of extracellular cAMP increases the number of reversals for surface attached bacteria and increased the counter clockwise rotational speed of the flagellum in MotAB and FlhF dependent manner (102). Furthermore, mutations in the flagellum have recently been shown to affect cAMP as well as c-di-GMP as discussed above. These mutations are thought to lead to an increase in the load on the flagellum and require the structural polar hub protein FimV as well as FlhF. By deleting the regulator of flagellum number, FleN, the cell produces multiple polar flagella that bundle together resulting in an increased load and increased cAMP although the exact mechanisms by which this occurs remains unknown (102).

In order to determine how the flagella and/or pili regulate each other's activity through cAMP and c-di-GMP, a dual fluorescent reported has been developed by the Parsek lab to report the normalized relative amounts of c-di-GMP and cAMP within the same cell. This reporter can be used with previously employed microscopy techniques to track *P. aeruginosa* motility and behavior during surface adaptation in order to correlate a certain second messenger with a type of surface behavior. I would first establish that a Δ*fleN* overproduces cAMP as measured by our fluorescent reporter and that this strain twitches above or near that of WT. These findings would establish another mechanism by which a flagellar mutation influences T4P activity for *P. aeruginosa*.

To identify the mechanisms by which the flagellum contributes to cAMP production during surface contact I propose performing the following genetic screen. Using the Δ*fleN* background, I would perform chemical mutagenesis with EMS to screen for mutants that no longer have increased levels of cAMP. The reason behind using chemical mutagenesis instead of transposon mutagenesis is the hope that subtle missense mutations will sever key signal transduction pathways without eliminating the entire protein. The pool of mutants will then be transformed with the dual reporter plasmid and mutants that no longer have high levels of cAMP will be sorted using the MACS Quant Tyto sorter. This approach allows us to sort 110,000 cells/hr which is much more high throughput than our current plating methods. Cells with low cAMP will be collected in the waste container of the sorter. Whole genome sequencing (WGS) can be performed to identify mutations that prevented the cAMP production for cells with Δ*fleN* background. Before WGS, the *fimV*, *flhF*, *cyaA*, and *cyaB* genes can be sequenced first to identify if mutations occurred in these likely targets leading to disruption of cAMP signaling. Not only will we identify new proteins involved in this pathway, but we will also likely select for stable point mutants that prevent signal transduction that are not achieved using other methods of random mutagenesis such as a transposon.

An alternative model to consider is that the complex formed by FimV+FlhF(GDP)+flagellum performs a similar role to the FimV+FimL+PilG(P) complex and that alone is enough to stimulate CyaB activity (36, 102). To test this model, we could express *fimV* and *flhF* with *cyaB* and look for an interaction in the B2H system. If we observe an interaction we could co-express both *fimV* and *flhF* in the same cell with *cyaB* to assess if there is enhanced interaction with CyaB, indicating that FlhF and FimV make a complex that is able to interact with CyaB. We can then isolate mutants of FimV or FlhF that no longer interact with CyaB, put them into the *fleN* mutant background and determine if this mutant no longer overproduces cAMP.

I am currently working on generating control plasmids for the dual reporter to generate a compensation matrix for flow cytometry and sorting experiments. I am also in the process of generating the *fleN* mutation as well as other mutations known

to affect surface mediated c-di-GMP or cAMP production such as *tsaP*, *fimW*, and *flhF-R251G*. TsaP is a protein involved in T4P dependent c-di-GMP production that also affects the extent of twitching motility (35). This protein could significantly affect the pool of c-di-GMP during surface contact and that could in turn affect stator dynamics through FlgZ. FimW is a protein whose unipolar localization occurs in a c-di-GMP dependent manner within seconds of surface contact in *P. aeruginosa* (7). The presence of this protein has been shown to affect initial surface contact through a T4P dependent mechanism although the exact mechanism is unknown. By deleting this early effector of c-di-GMP signaling we may be able to identify new proteins involved in the surface sensing pathway. The GTPase FlhF is involved in flagellar biosynthesis and has recently been shown to associate with FliG of the flagellar C-ring and FimV when bound to GDP. Binding of FliG and FimV leads to the cessation of flagellar rotation for surface bound *P. aeruginosa*. The GDP bound state can be mimicked by generating the FlhF-R251G mutation which leads to constitutive binding of FliG and FimV and no flagellar rotation (33). I will introduce this mutation into PA14 and see if there is an overproduction of cAMP like in the *fleN* background and then look for suppressor mutations using the screening method outline above.

Putting it all together

My thesis work has provided mechanistic insight into how *P. aeruginosa* uses its motility appendages to sense a surface and form a biofilm. T4P and flagella have been shown to coordinate surface behavior in several model organisms and *P. aeruginosa* is no different. The production of cAMP and c-di-GMP are dependent on T4P and flagella but these second messengers also control appendage behavior. The studies above demonstrate that critical protein-protein interactions mediate surface sensing in *P. aeruginosa* and future work will identify how surface sensing system influence each other to produce a biofilm over multiple generations and across an entire population of cells (12, 23, 87, 90, 102, 113).

Literature Cited.

1.   Flemming H-C, Wuertz S. 2019. Bacteria and archaea on Earth and their abundance in biofilms. Nature Reviews Microbiology 17:247-260.

2.   O'Toole GA, Wong GC. 2016. Sensational biofilms: surface sensing in bacteria. Current Opinion in Microbiology 30:139-146.

3.   Henrici AT. 1933. Studies of Freshwater Bacteria. Journal of Bacteriology 25:277-287.

4.   Zobell CE, Allen EC. 1935. The Significance of Marine Bacteria in the Fouling of Submerged Surfaces. Journal of Bacteriology 29:239-251.

5.   L. McCarter, M. Hilmen, Silverman M. 1988. Flagellar dynamometer controls swarmer cell defferentiation of V. parahaemolyticus. Cell 54:345-351.

6.   McCarter L, Silverman M. 1990. Surface-induced swarmer cell differentiation of Vibrio parahaemoiyticus. Molecular Microbiology 4:1057-1062.

7.   Laventie B-J, Sangermani M, Estermann F, Manfredi P, Planes R, Hug I, Jaeger T, Meunier E, Broz P, Jenal U. 2019. A Surface-Induced Asymmetric Program Promotes Tissue Colonization by Pseudomonas aeruginosa. Cell Host & Microbe 25:140-152.e6.

8.   Geiger CJ, O'Toole GA. 2023. Evidence for the Type IV Pilus Retraction Motor PilT as a Component of the Surface Sensing System in Pseudomonas aeruginos. J Bacteriol 205.

9.   Wolfgang MC, Lee VT, Gilmore ME, Lory S. 2003. Coordinate Regulation of Bacterial Virulence Genes by a Novel Adenylate Cyclase-Dependent Signaling Pathway. Developmental Cell 4:253-263.

10.   Buensuceso RNC, Nguyen Y, Zhang K, Daniel-Ivad M, Sugiman-Marangos SN, Fleetwood AD, Zhulin IB, Junop MS, Howell PL, Burrows LL. 2016. The Conserved Tetratricopeptide Repeat-Containing C-Terminal Domain of Pseudomonas aeruginosa FimV Is Required for Its Cyclic AMP-Dependent and -Independent Functions. Journal of Bacteriology 198:2263-2274.

11.   Buensuceso RNC, Daniel-Ivad M, Kilmury SLN, Leighton TL, Harvey H, Howell PL, Burrows LL. 2017. Cyclic AMP-Independent Control of Twitching Motility in Pseudomonas aeruginosa. Journal of Bacteriology 199.

12.   Endoh T, Engel JN. 2009. CbpA: a Polarly Localized Novel Cyclic AMP-Binding Protein in Pseudomonas aeruginosa. Journal of Bacteriology 191:7193-7205.

13. Fuchs EL, Brutinel ED, Jones AK, Fulcher NB, Urbanowski ML, Yahr TL, Wolfgang MC. 2010. The Pseudomonas aeruginosa Vfr Regulator Controls Global Virulence Factor Expression through Cyclic AMP-Dependent and -Independent Mechanisms. Journal of Bacteriology 192:3553-3564.

14. Hershey DM. 2021. Integrated control of surface adaptation by the bacterial flagellum. Curr Opin Microbiol 61:1-7.

15. Wu DC, Zamorano-Sánchez D, Pagliai FA, Park JH, Floyd KA, Lee CK, Kitts G, Rose CB, Bilotta EM, Wong GCL, Yildiz FH. 2020. Reciprocal c-di-GMP signaling: Incomplete flagellum biogenesis triggers c-di-GMP signaling pathways that promote biofilm formation. PLOS Genetics 16:e1008703.

16. Hershey DM, Fiebig A, Crosson S. 2021. Flagellar Perturbations Activate Adhesion through Two Distinct Pathways in Caulobacter crescentus. mBio 12.

17. Harrison JJ, Almblad H, Irie Y, Wolter DJ, Eggleston HC, Randall TE, Kitzman JO, Stackhouse B, Emerson JC, McNamara S, Larsen TJ, Shendure J, Hoffman LR, Wozniak DJ, Parsek MR. 2020. Elevated exopolysaccharide levels in Pseudomonas aeruginosa flagellar mutants have implications for biofilm growth and chronic infections. PLoS Genet 16:e1008848.

18. Hershey DM, Fiebig A, Crosson S. 2019. A Genome-Wide Analysis of Adhesion in Caulobacter crescentus Identifies New Regulatory and Biosynthetic Components for Holdfast Assembly. mBio 10.

19. Chawla R, Ford KM, Lele PP. 2017. Torque, but not FliL, regulates mechanosensitive flagellar motor-function. Scientific Reports 7.

20. Hug I, Deshpande S, Sprecher KS, Pfohl T, Jenal U. 2017. Second messenger–mediated tactile response by a bacterial rotary motor. Science 358:531-534.

21. Baker AE, Webster SS, Diepold A, Kuchma SL, Bordeleau E, Armitage JP, O'Toole GA. 2019. Flagellar Stators Stimulate c-di-GMP Production by Pseudomonas aeruginosa. Journal of Bacteriology 201.

22. Yukihiro Hiramatsu1* TN, Dendi Krisna Nugraha1, Mayuko Osada-Oka2, Daisuke Nakane3, Katsumi Imada4, Yasuhiko Horiguchi1,. 2022. Interference of flagellar rotation up-regulates the expression of small RNA contributing to Bordetella pertussis infection. Science.

23. Talà L, Fineberg A, Kukura P, Persat A. 2019. Pseudomonas aeruginosa orchestrates twitching motility by sequential control of type IV pili movements. Nature Microbiology 4:774-780.

24. Lewis K, Vermilyea, D. M., Webster, S. S., Geiger, C. J., de Anda, J., Wong, G. C. L., O'Toole, G. A., Hogan, D. 2022. Nonmotile Subpopulations of Pseudomonas aeruginosa Repress Flagellar Motility in Motile Cells through a Type IV Pilus- and Pel-Dependent Mechanism. Journal of Bacteriology.

25. Ellison CK, Rusch DB, Brun YV. 2019. Flagellar Mutants Have Reduced Pilus Synthesis in Caulobacter crescentus. Journal of Bacteriology 201.

26. Jain R, Sliusarenko O, Kazmierczak BI. 2017. Interaction of the cyclic-di-GMP binding protein FimX and the Type 4 pilus assembly ATPase promotes pilus assembly. PLOS Pathogens 13:e1006594.

27. Floyd KA, Lee CK, Xian W, Nametalla M, Valentine A, Crair B, Zhu S, Hughes HQ, Chlebek JL, Wu DC, Hwan Park J, Farhat AM, Lomba CJ, Ellison CK, Brun YV, Campos-Gomez J, Dalia AB, Liu J, Biais N, Wong GCL, Yildiz FH. 2020. c-di-GMP modulates type IV MSHA pilus retraction and surface attachment in Vibrio cholerae. Nat Commun 11:1549.

28. Courtney K. Ellison1*† JK, 3, Jennifer L. Chlebek1, Katherine R. Hummels1, Gaël Panis4, Patrick H. Viollier4, Nicolas Biais2,3, Ankur B. Dalia1, Yves V. Brun1,5*. 2019. A bifunctional ATPase drives tad pilus extension and retraction. Science.

29. Sangermani M, Hug I, Sauter N, Pfohl T, Jenal U. 2019. Tad Pili Play a Dynamic Role in Caulobacter crescentus Surface Colonization. mBio 10.

30. Ellison CK, Kan J, Dillard RS, Kysela DT, Ducret A, Berne C, Hampton CM, Ke Z, Wright ER, Biais N, Dalia AB, Brun YV. 2017. Obstruction of pilus retraction stimulates bacterial surface sensing. Science 358:535-538.

31. Luo Y, Zhao K, Baker AE, Kuchma SL, Coggan KA, Wolfgang MC, Wong GC, O'Toole GA. 2015. A hierarchical cascade of second messengers regulates Pseudomonas aeruginosa surface behaviors. mBio 6.

32. Treuner-Lange A, Chang Y-W, Glatter T, Herfurth M, Lindow S, Chreifi G, Jensen GJ, Søgaard-Andersen L. 2020. PilY1 and minor pilins form a complex priming the type IVa pilus in Myxococcus xanthus. Nature Communications 11.

33. Schniederberend M, Williams JF, Shine E, Shen C, Jain R, Emonet T, Kazmierczak BI. 2019. Modulation of flagellar rotation in surface-attached bacteria: A pathway for rapid surface-sensing after flagellar attachment. PLOS Pathogens 15:e1008149.

34. Inclan YF, Persat A, Greninger A, Von Dollen J, Johnson J, Krogan N, Gitai Z, Engel JN. 2016. A scaffold protein connects type IV pili with the Chp chemosensory system to mediate activation of virulence signaling in *Pseudomonas aeruginosa*. Molecular Microbiology 101:590-605.

35. Webster SS, Lee CK, Schmidt WC, Wong GCL, O'Toole GA. 2021. Interaction between the type 4 pili machinery and a diguanylate cyclase fine-tune c-di-GMP levels during early biofilm formation. Proceedings of the National Academy of Sciences 118:e2105566118.

36. Lee CK, De Anda J, Baker AE, Bennett RR, Luo Y, Lee EY, Keefe JA, Helali JS, Ma J, Zhao K, Golestanian R, O'Toole GA, Wong GCL. 2018. Multigenerational memory and adaptive adhesion in early bacterial biofilm communities. Proceedings of the National Academy of Sciences 115:4471-4476.

37. Lee CK, Schmidt WC, Webster SS, Chen JW, O'Toole GA, Wong GCL. 2022. Broadcasting of amplitude- and frequency-modulated c-di-GMP signals facilitates cooperative surface commitment in bacterial lineages. Proceedings of the National Academy of Sciences 119:e2112226119.

Appendices

Appendix 1

Biofilm, cAMP, and c-di-GMP measurements for single point mutants in type IV pili that restore twitching motility in the mPAO1 ΔpilU background.

In an attempt to better characterize the contribution of PilU to T4P function and twitching motility, the Burrows Lab performed chemical mutagenesis with EMS on the mPAO1 Δ*pilU* mutant background and selected for suppressor mutants with restored twitching motility. Whole genome sequencing revealed that point mutants in the T4P pilin *pilA* and the protein at the tip of the T4P fiber and involved in surface sensing, *pilY1*, were able to restore twitching motility. To further characterize these mutations in biofilm formation and surface sensing, I transformed the cAMP and c-di-GMP fluorescent reporter plasmids discussed in chapters 2. I then looked at biofilm levels, cAMP, and c-di-GMP levels during surface attachment in these strains. Biofilms were performed in liquid M8 medium for 24 hours and then stained with crystal violet, de-stained, and measured on a spectrophotometer at an absorbance of OD550 (n=6). For cAMP and c-di-GMP measurements, strains were prepared as described in Chapter 2. Briefly, after a 3 hour liquid subculture in M8 medium, cells were grown on M8 agar for five hours before being harvested and measured on a flow cytometer (n=3). A linear mixed effect model was developed to examine the relationship between cAMP and c-di-GMP levels in these strains. We observed a significant negative correlation between the amount of cAMP produced and the amount of c-di-GMP produced during surface adaptation. We also see that strains that produced more cAMP also were able to form thicker biofilms. The PilA mutants M13I and P48L produced the most cAMP when grown on agar. Not only are the population means altered in these strains but the overall bimodal distribution is also altered relative to both the WT mPAO1 and Δ*pilU* backgrounds.
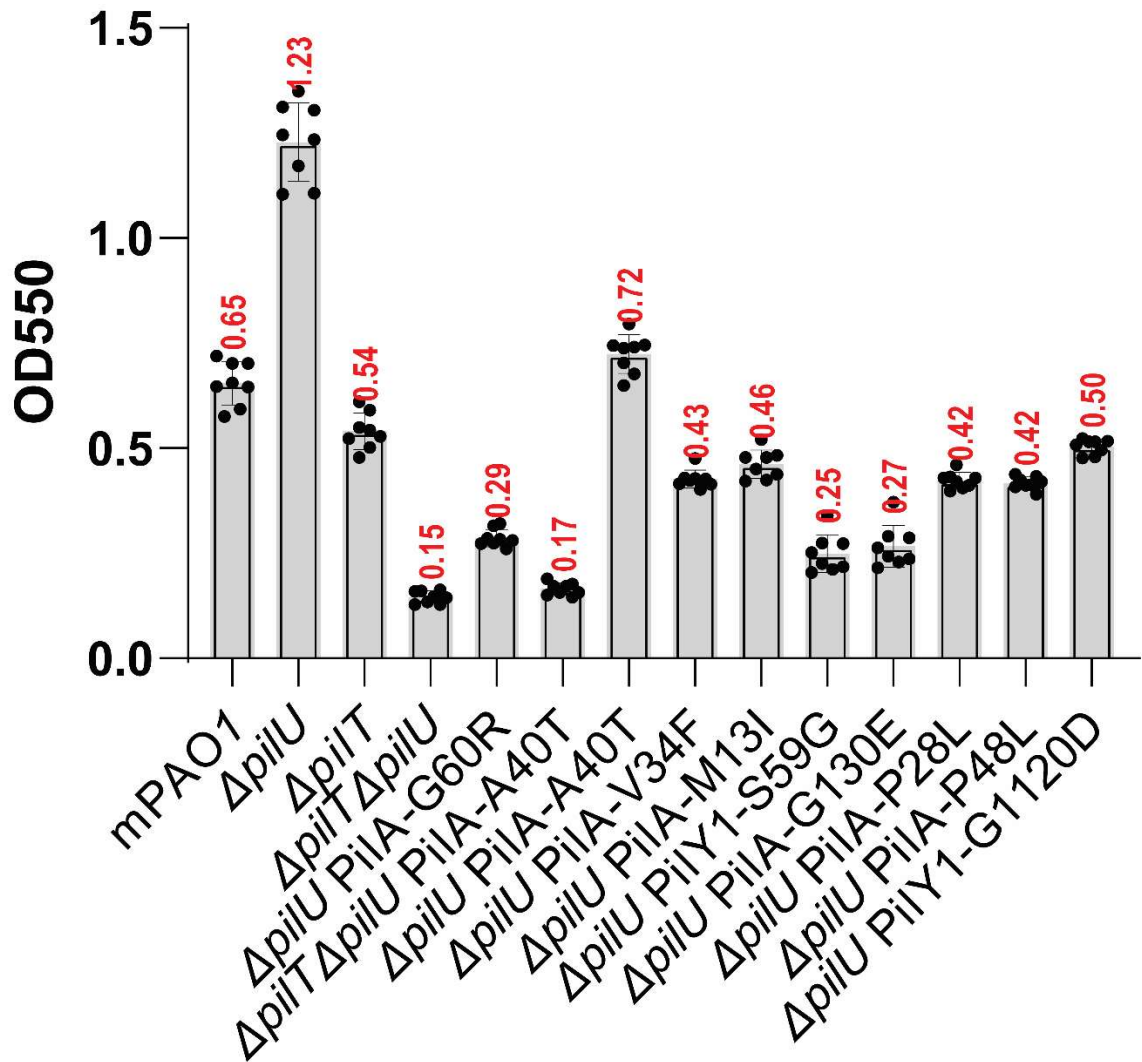
Figure A1.1. Biofilm formation by WT and suppressor mutants for twitching motility in the Δ*pilU* background. Biofilm assays were performed as previously described in Chapter 3.
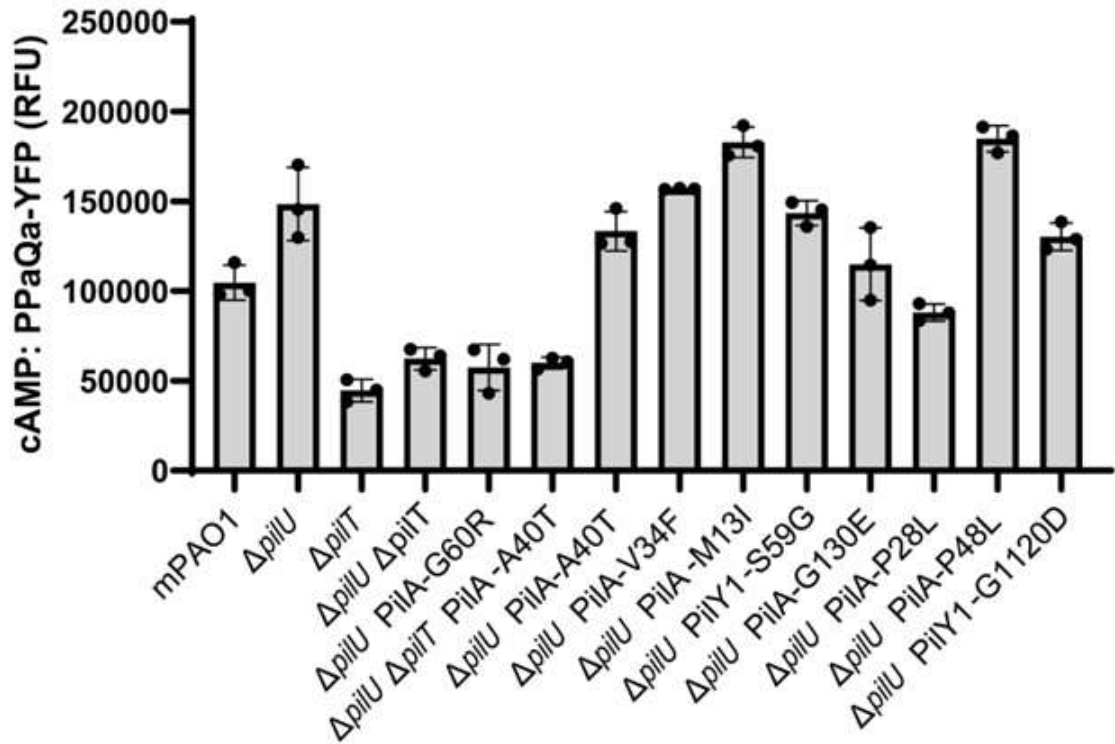
Figure A1.2. cAMP levels during surface growth for WT and suppressor mutants for twitching motility in the Δ*pilU* background. cAMP was measured using plasmid based PaQa fluorescent reporter transformed into each strain. Fluorescence was measured using flow cytometry as previously described in Chapter 2.
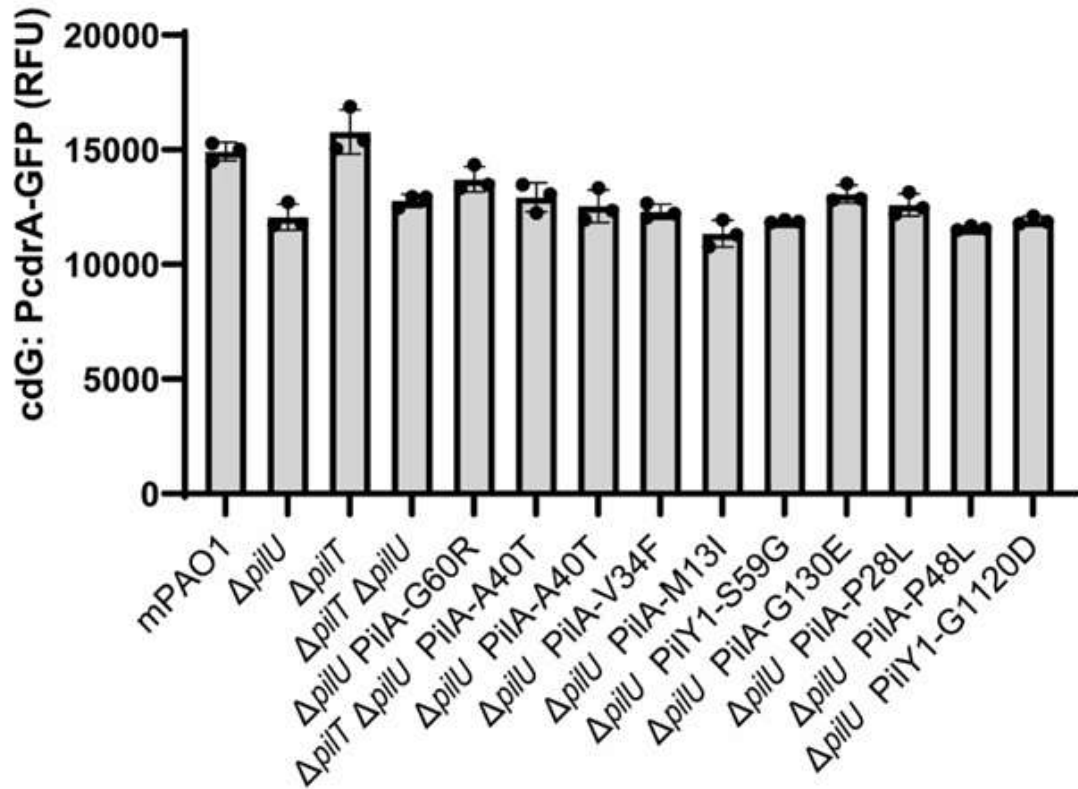
Figure A1.3. c-di-GMP levels during surface growth for WT and suppressor mutants for twitching motility in the Δ*pilU* background. c-di-GMP was measured using plasmid based *PcdrA-gfp* fluorescent reporter transformed into each strain. Fluorescence was measured using flow cytometry as previously described in Chapter 2.
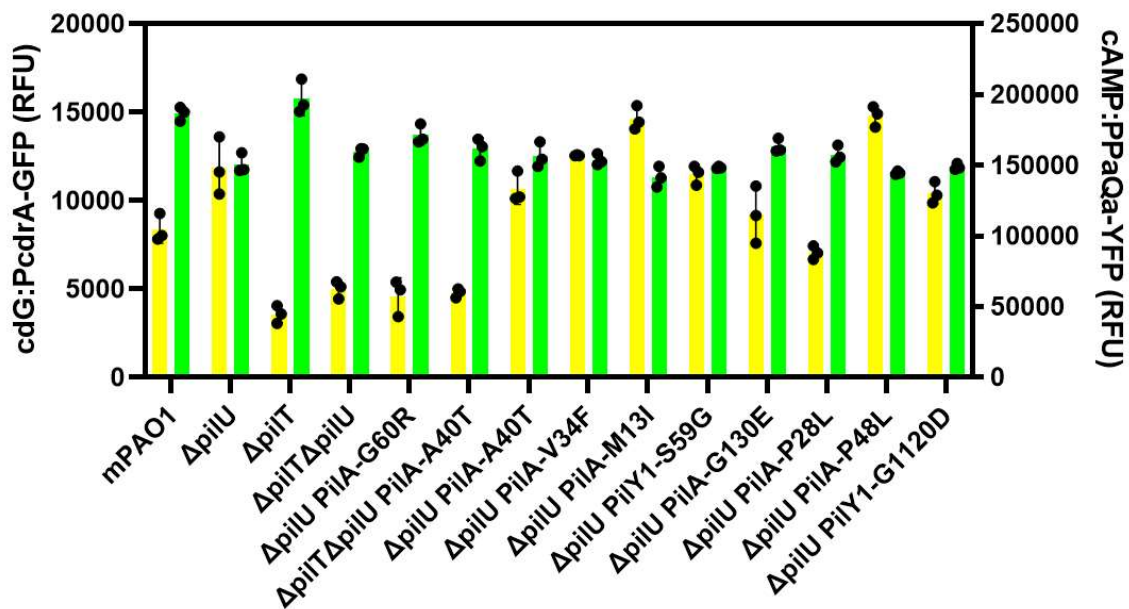
Figure A1.4. c-di-GMP and cAMP levels during surface growth for WT and suppressor mutants for twitching motility in the Δ*pilU* background.
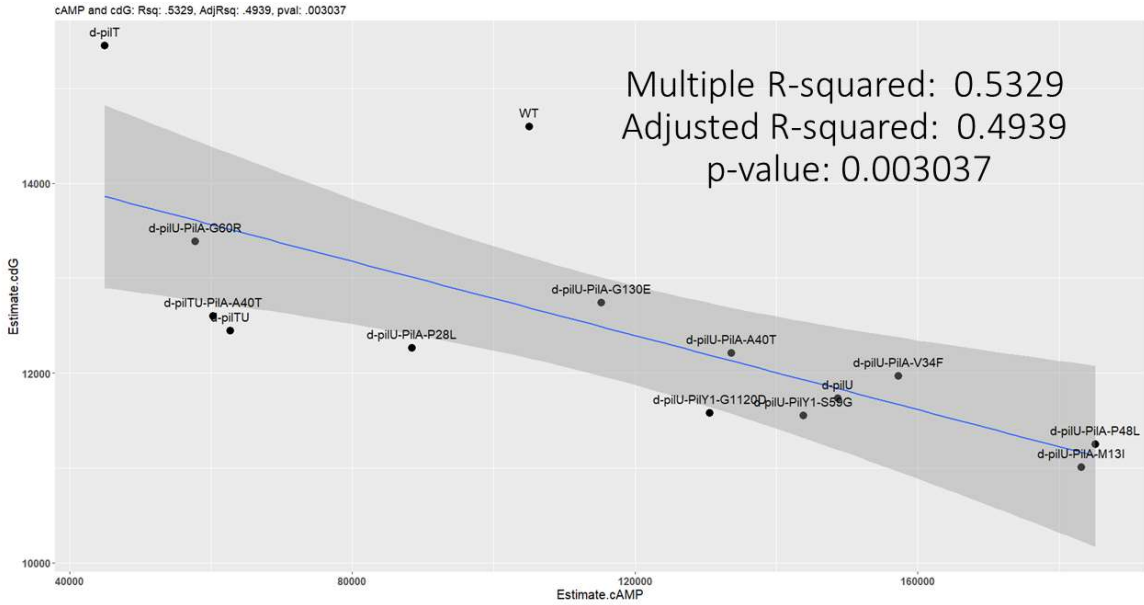
Figure A1.5. Linear mixed model describing the relationship between cAMP and c-di-GMP during the first 6 hours of surface growth for WT and suppressor mutants for twitching motility in the Δ*pilU* background. There is a significant negative correlation between the amount of cAMP produced during surface growth and the extent of c-di-GMP produced.
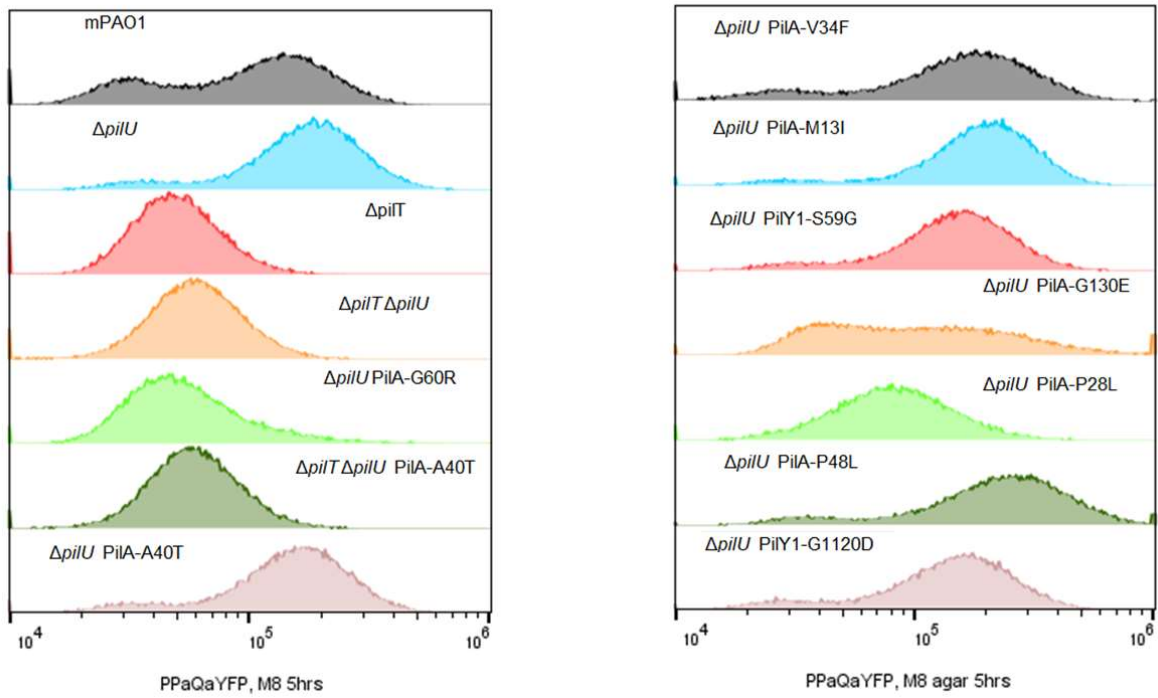
Figure A1.6. The distribution of fluorescence intensities representing cAMP levels for 50,000 cells of each strain as measured by flow cytometry. After 5 hours of surface growth, WT cells displayed a bimodal distribution of cAMP levels. Other strains displayed deviations from this bimodal distribution at this timepoint.

Appendix 2

cAMP kinetics during surface adaptation for PA14 and mPAO1 WT and Δ*pilU* strains

To determine the kinetics of cAMP during surface adaptation on agar surfaces, strains were incubated on M8 agar for different lengths of time as described in Chapter 2 and then cAMP was measured using the plasmid based PaQa reporter. This assay was performed for the *Pseudomonas aeruginosa* PA14 and mPAO1 WT and Δ*pilU* backgrounds. The average pPaQa-YFP intensity per cell was reported as well as the distribution for ~50,000 surface grown cells on M8 agar. For PA14 backgrounds, we observed a single peak at all measured timepoints. The maximum average YFP intensity per cell occurred at 5 hours of incubation for the PA14 backgrounds. The ΔpilU cells displayed more cAMP than WT cells after 3 hours of growth and this difference increased until the last timepoint at 6 hours. The mPAO1 background displayed similar trends to the PA14 background at the population level with an average maximum cAMP level measured after 5 hours of growth on agar. Unlike the PA14 background, the mPAO1 strains displayed a bimodal peak at all measured timepoints, and as cells become adapted to the surface, the population of cells with high levels of cAMP increases while the population with low cAMP decreases. We also note that the signal in the mPAO1 background was much higher than the PA14 background at all time points. This is expected as the *PPaQa* promoter was isolated from the PAO1 background and likely functions better with mPAO1-Vfr than the PA14-Vfr.

PA14:WT; 2-6hrs

Sample Name	Subset Name	Count	Geometric Mean : FL1-A	SD : FL1-A
[04-Well-A1.fcs]	mKatePos	47741	40206	31926
[04-Well-B5.fcs]	mKatePos	45703	53079	31018
[04-Well-B9.fcs]	mKatePos	48270	56929	29443
[04-Well-E1.fcs]	mKatePos	46578	57481	28136
[04-Well-E5.fcs]	mKatePos	42904	50143	24039
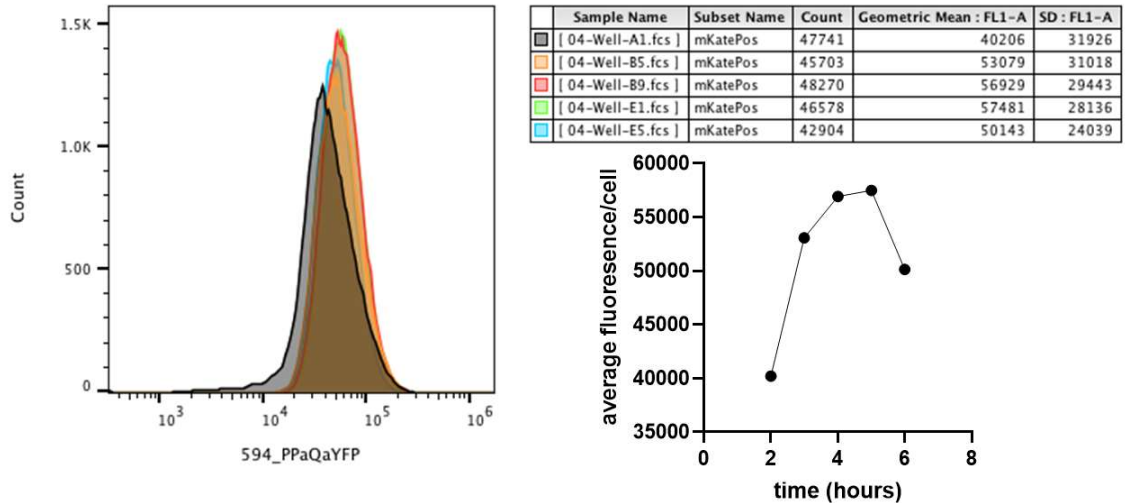
Figure A2.1. cAMP levels for 50,000 cells of PA14-WT during the first six hours of surface growth. Fluorescence intensities were measured by flow cytometry as previously described in Chapter 2. On the left is the distribution of fluorescence intensities at each time point. On the right is the average fluorescence intensity of the population plotted for 2 to 6 hours of surface growth.

PA14: Δ*pilU;* 2-6hrs

Sample Name	Subset Name	Count	Geometric Mean : FL1-A	SD : FL1-A
[04-Well-A4.fcs]	mKatePos	48359	41982	29928
[04-Well-B8.fcs]	mKatePos	48701	55691	34022
[04-Well-B12.fcs]	mKatePos	49725	62568	33566
[04-Well-E4.fcs]	mKatePos	47813	67157	35422
[04-Well-E8.fcs]	mKatePos	48668	64293	33753
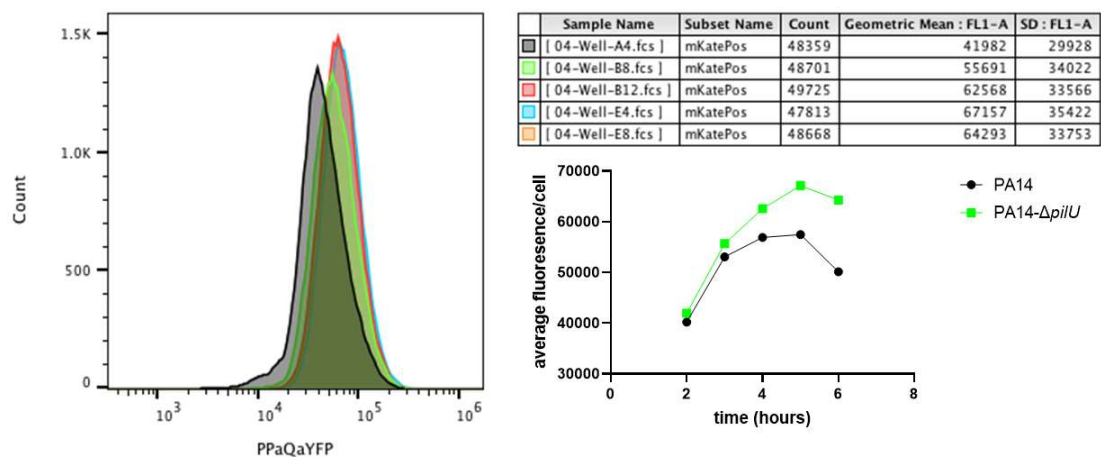
Figure A2.2. cAMP levels for 50,000 cells of PA14-Δ*pilU* during the first six hours of surface growth. Fluorescence intensities were measured by flow cytometry as

previously described in Chapter 2. On the left is the distribution of fluorescence intensities at each time point. On the right is the average fluorescence intensity of the population plotted for 2 to 6 hours of surface growth.

mPAO1: WT; 2-6hrs

	Sample Name	Subset Name	Count	Geometric Mean : FL1–A	SD : FL1–A
	[04–Well–A2.fcs]	mKatePos	48373	58956	70034
	[04–Well–B6.fcs]	mKatePos	51991	96078	128920
	[04–Well–B10.fcs]	mKatePos	58988	122962	129877
	[04–Well–E2.fcs]	mKatePos	63118	122002	107413
	[04–Well–E6.fcs]	mKatePos	54193	95958	85885

Figure A2.3. cAMP levels for 50,000 cells of mPAO1-WT during the first six hours of surface growth. Fluorescence intensities were measured by flow cytometry as previously described in Chapter 2. On the left is the distribution of fluorescence intensities at each time point. On the right is the average fluorescence intensity of the population plotted for 2 to 6 hours of surface growth.

mPAO1: Δ*pilU*, 2-6hrs

	Sample Name	Subset Name	Count	Geometric Mean : FL1–A	SD : FL1–A
	[04–Well–A3.fcs]	mKatePos	46532	72355	87521
	[04–Well–B7.fcs]	mKatePos	50081	108807	107531
	[04–Well–B11.fcs]	mKatePos	54780	142690	115057
	[04–Well–E3.fcs]	mKatePos	52446	165544	111812
	[04–Well–E7.fcs]	mKatePos	51178	104336	84102

Figure A2.4. cAMP levels for 50,000 cells of mPAO1-Δ*pilU* during the first six hours of surface growth. Fluorescence intensities were measured by flow cytometry as previously described in Chapter 2. On the left is the distribution of fluorescence intensities at each time point. On the right is the average fluorescence intensity of the population plotted for 2 to 6 hours of surface growth.
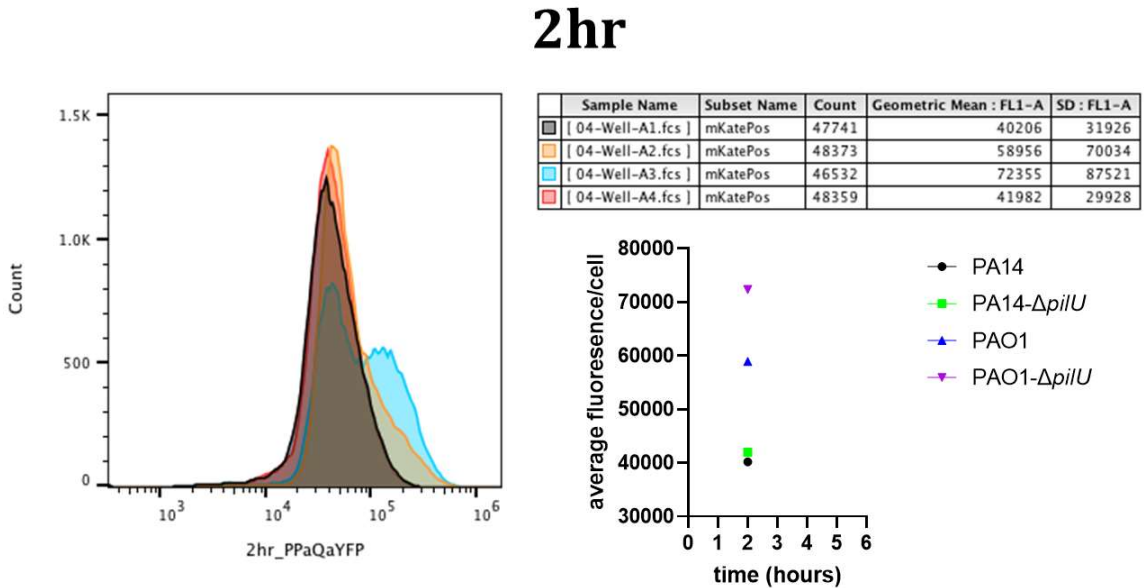
Figure A2.5. cAMP levels for mPAO1-WT and Δ*pilU* as well as PA14-WT and Δ*pilU* after 2 hours of surface growth. Fluorescence intensities were measured by flow cytometry as previously described in Chapter 2. On the left is the distribution of fluorescence intensities of each strain at 2 hours. On the right is the average fluorescence intensity of the population plotted for 2 hours of surface growth.

3hr

	Sample Name	Subset Name	Count	Geometric Mean : FL1–A	SD : FL1–A
■	[04–Well–B5.fcs]	mKatePos	47039	51630	31212
■	[04–Well–B6.fcs]	mKatePos	51991	96078	128920
■	[04–Well–B7.fcs]	mKatePos	50081	108807	107531
■	[04–Well–B8.fcs]	mKatePos	48701	55691	34022

Figure A2.6. cAMP levels for mPAO1-WT and Δ*pilU* as well as PA14-WT and Δ*pilU* after 3 hours of surface growth. Fluorescence intensities were measured by flow cytometry as previously described in Chapter 2. On the left is the distribution of fluorescence intensities of each strain at 3 hours. On the right is the average fluorescence intensity of the population plotted for 3 hours of surface growth.

4hr

	Sample Name	Subset Name	Count	Geometric Mean : FL1–A	SD : FL1–A
■	[04–Well–B9.fcs]	mKatePos	48737	56326	29576
■	[04–Well–B10.fcs]	mKatePos	58988	122962	129877
■	[04–Well–B11.fcs]	mKatePos	54780	142690	115057
■	[04–Well–B12.fcs]	mKatePos	49725	62568	33566
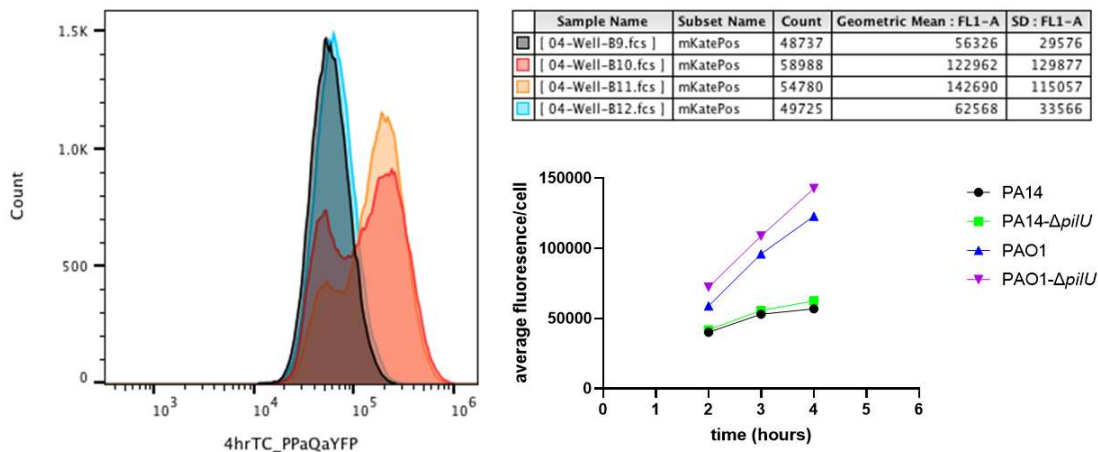
Figure A2.7. cAMP levels for mPAO1-WT and Δ*pilU* as well as PA14-WT and Δ*pilU* after 4 hours of surface growth. Fluorescence intensities were measured by flow cytometry as previously described in Chapter 2. On the left is the distribution of

fluorescence intensities of each strain at 4 hours. On the right is the average fluorescence intensity of the population plotted for 4 hours of surface growth.

5hr

	Sample Name	Subset Name	Count	Geometric Mean : FL1–A	SD : FL1–A
■	[04–Well–E1.fcs]	mKatePos	47376	56629	28303
■	[04–Well–E2.fcs]	mKatePos	63118	122002	107413
■	[04–Well–E3.fcs]	mKatePos	52446	165544	111812
■	[04–Well–E4.fcs]	mKatePos	47813	67157	35422
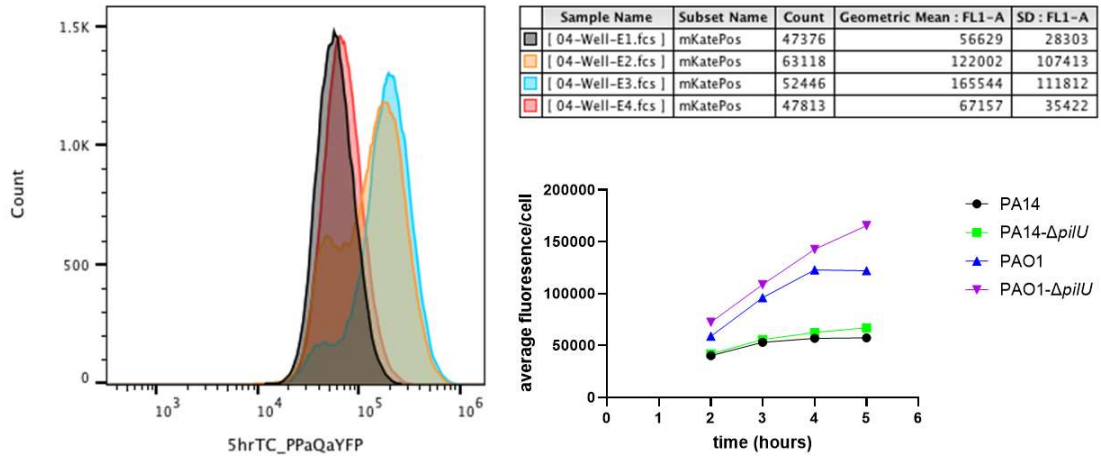
Figure A2.8. cAMP levels for mPAO1-WT and Δ*pilU* as well as PA14-WT and Δ*pilU* after 5 hours of surface growth. Fluorescence intensities were measured by flow cytometry as previously described in Chapter 2. On the left is the distribution of fluorescence intensities of each strain at 5 hours. On the right is the average fluorescence intensity of the population plotted for 5 hours of surface growth.

6hr

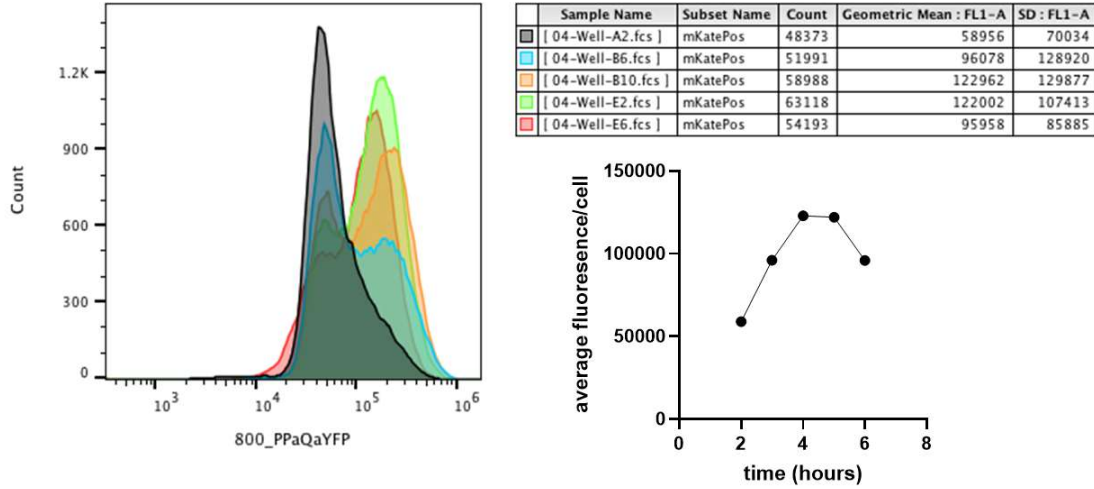|	Sample Name	Subset Name	Count	Geometric Mean : FL1–A	SD : FL1–A
■	[04–Well–E5.fcs]	mKatePos	45720	48477	24196
■	[04–Well–E6.fcs]	mKatePos	54193	95958	85885
■	[04–Well–E7.fcs]	mKatePos	51178	104336	84102
■	[04–Well–E8.fcs]	mKatePos	48668	64293	33753
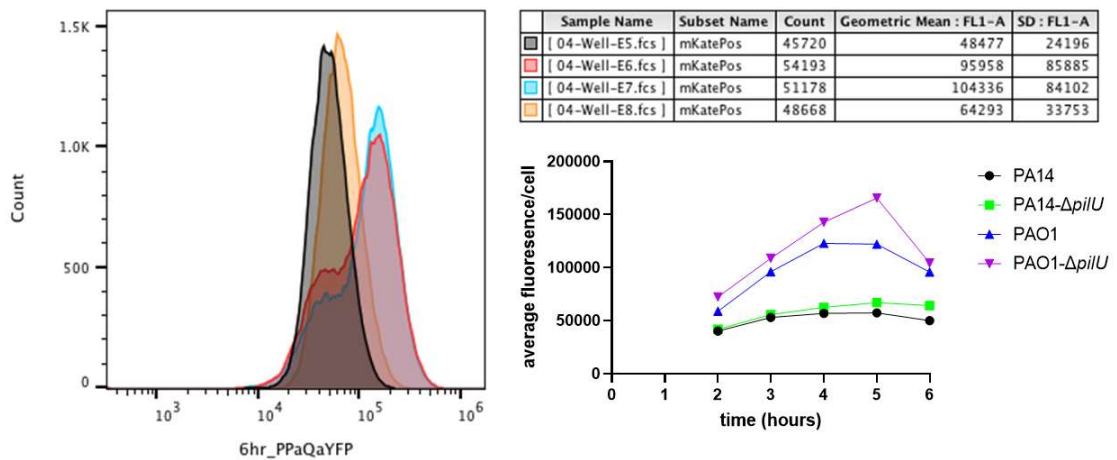
Figure A2.9. cAMP levels for mPAO1-WT and Δ*pilU* as well as PA14-WT and Δ*pilU* after 6 hours of surface growth. Fluorescence intensities were measured by flow cytometry as previously described in Chapter 2. On the left is the distribution of fluorescence intensities of each strain at 6 hours. On the right is the average fluorescence intensity of the population plotted for 6 hours of surface growth.
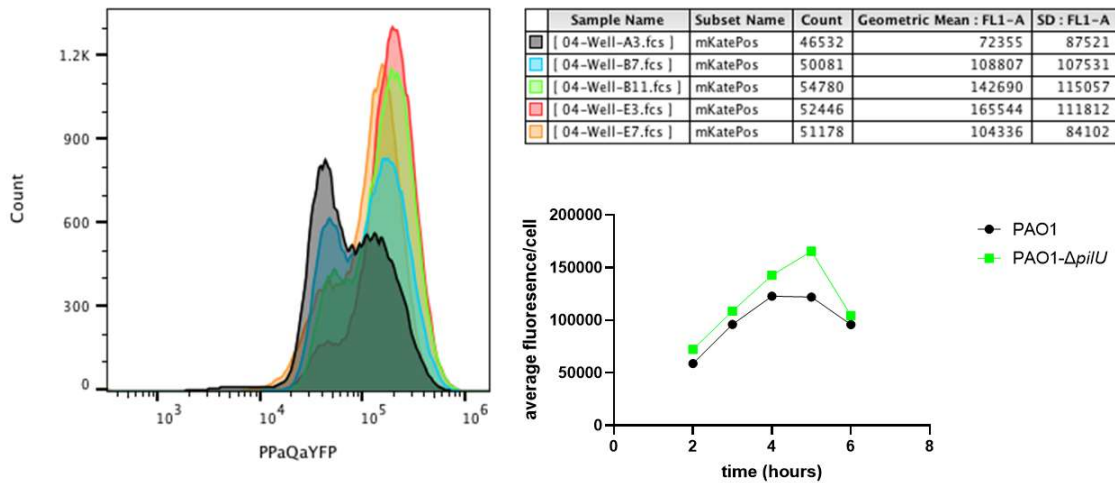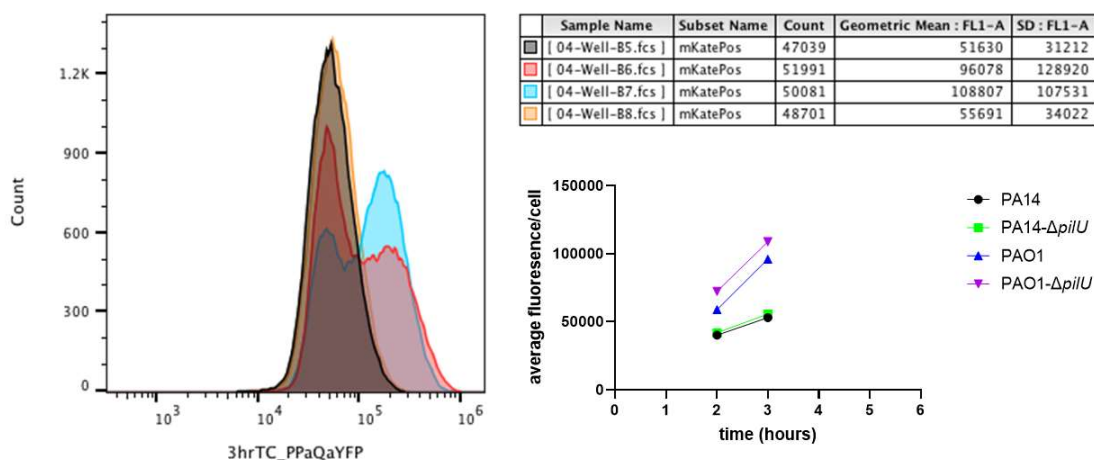
Appendix 3

Swimming and swarming motility assays for PA14 PilT motor mutants

To determine how *pilT* mutations may affect flagellar mediated motility, swim and swarm assays were performed to quantify the extent of flagellar mediated motility in these backgrounds. These assays were performed as previously described in chapter 3. Deletion of the primary retraction motor PilT eliminates swimming and swarming motility. Deletion of the accessory retraction motor PilU eliminates swimming motility but swarming motility is maintained. For PilT mutants that are still able to perform twitching motility, swimming and swarming motility is near that of WT. Deleting both adenylate cyclases increases flagellar mediated motility while deleting the lone cAMP phosphodiesterase eliminates swimming and swarming. These data indicate that mutations affecting T4P or cAMP can significantly affect swimming and swarming motility.
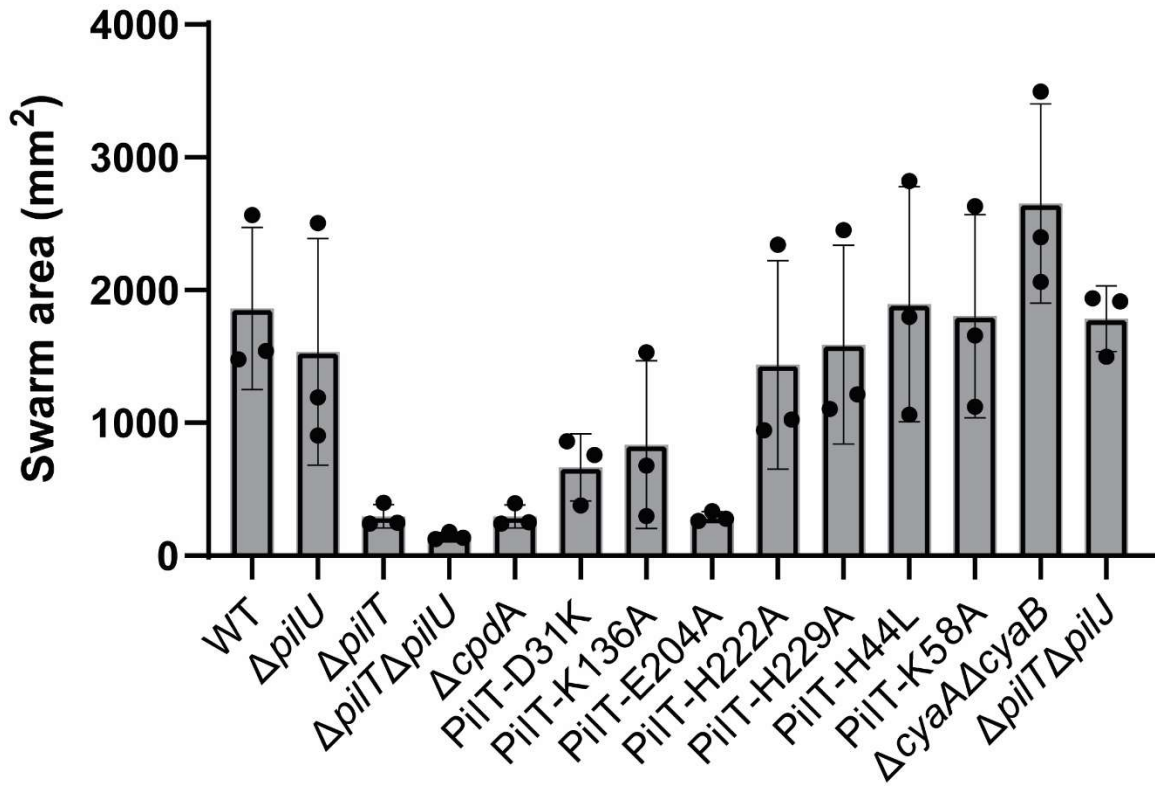
Figure A3.1. Swarming motility assay for PilT and cAMP mutants. Swarming motility was measured as previously described in (213).
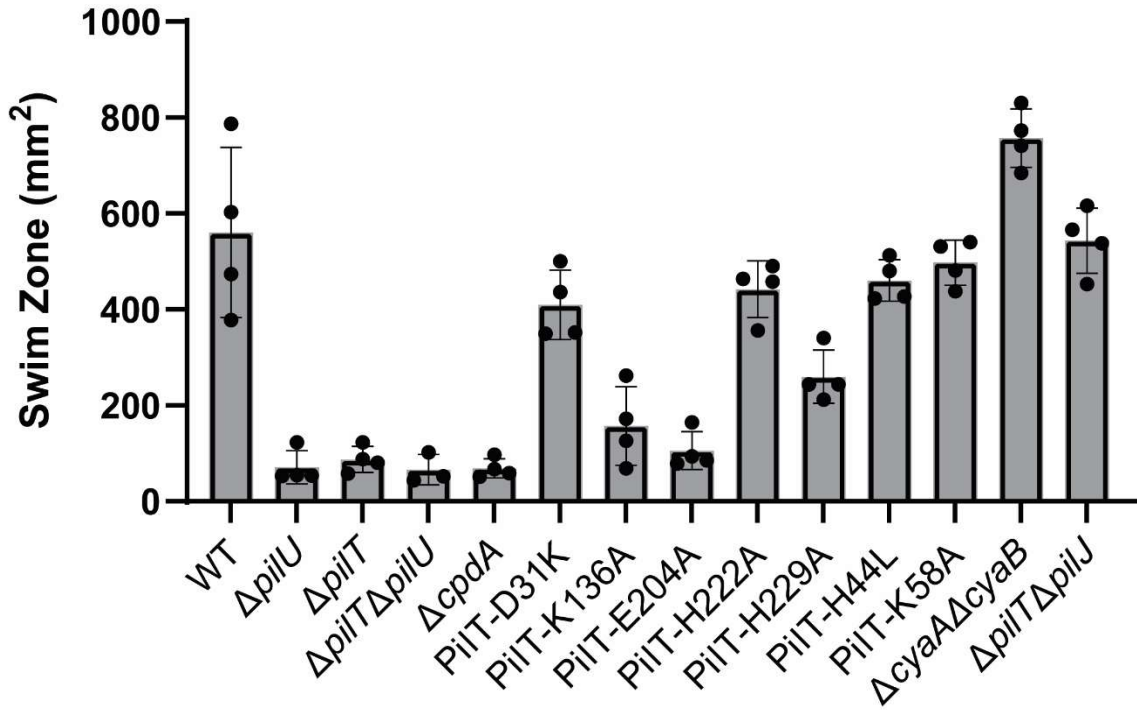
Figure A3.2. Swimming motility assay for PilT and cAMP mutants. Swimming motility was measured as previously described in (9).

Appendix 4

cAMP for flagellar and stator mutants in PA14

In order to determine how flagellar mutations affect levels of cAMP for surface grown cells, cAMP was measured using flow cytometer and the genomic encoded PaQa reporter as previously described in Chapter 2. Mutating FimV or FlhF resulted in decreased cAMP for surface grown cells but mutating the hook associated protein, FlgK, or the flagellar filament, FliC, or the stators, MotABCD, did not significantly affect cAMP levels for surface grown cells.
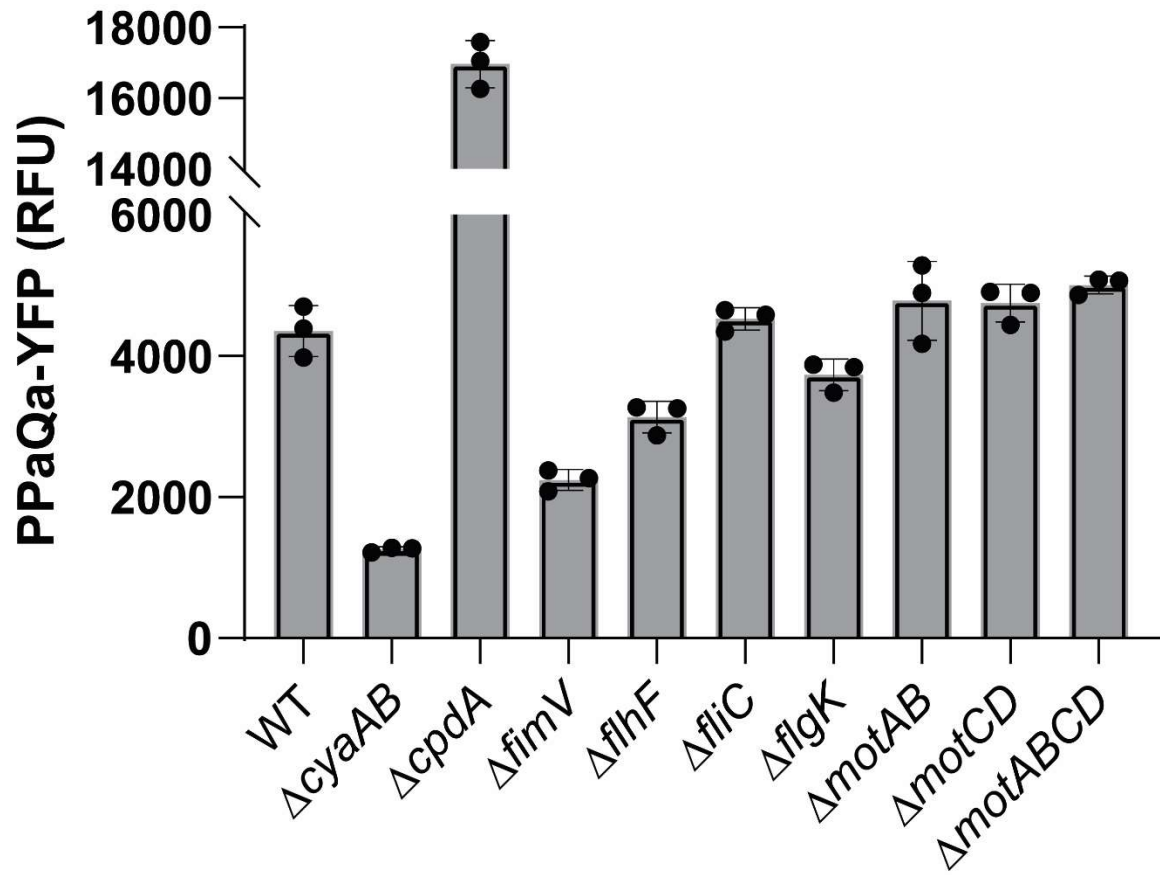
Figure A4. cAMP levels for surface grown flagellar mutants.

Appendix 5

Investigating the mechanism of flagellar-mediated surface sensing by Pseudomonas aeruginosa PA14

Introduction

Bacterial biofilms were first described in the 1930s and since then this ubiquitous mode of sessile bacterial growth has been shown to be important in both medical and industrial settings (201, 202, 214, 215). The first step in the transition from free swimming planktonic cells to the biofilm mode of growth is the microbe contacting the surface and relaying this input signal to the cell to initiate the biofilm mode of growth, a process known as "surface sensing" (5, 34).

Many bacteria rely on motility appendages such as flagella and type IV pili to sense and traverse surfaces (55). These molecular machines have been shown to be necessary for proper biofilm formation and have been implicated in surface sensing, but the mechanism(s) by which these appendages sense and transmit the surface sensing signal are just beginning to emerge. Several early studies demonstrated that the bacterial flagellum can respond to mechanical load, which in turn can serve as the signal of surface engagement. For example, by manipulating the viscosity of the liquid culture or by adding antibodies specific to the flagellum, surface-associated phenotypes were achieved during liquid culture conditions (142, 143) indicating that it is the interference in bacterial flagellum function that is the proximal means whereby microbes detect surface engagement.

Bacterial flagella are used to propel the cell body in both liquid and across surfaces (8-10). A flagellum is composed of hook-basal-body (HBB) structure that spans the cellular envelope in bacteria. A hook and flagellar filament extend from the cell body, and upon rotation, propels the cell body forward (216). This molecular machine uses ion motive force, generated by a gradient of protons or sodium across

the cytoplasmic membrane, to generate torque on the flagellar filament (217-219). This conversion of chemical potential to flagellar torque is achieved by stator units that can dynamically bind and dissociate from the flagellar machinery (44, 45, 47, 220, 221). Stators are composed of an inner membrane (IM) pentamer and a central dimer unit that plugs the ion pore when stators are not incorporated in the flagellum. Upon incorporation into the flagellum, the inner dimer binds the peptidoglycan (PG) layer, unplugging the ion channel within the stator unit, which allows for ion flow down the concentration gradient into the cytoplasm. This chemical energy is harnessed by the stator units in the form of torque that is transferred to the C-ring of the flagellum via electrostatic interactions with FliG (222). It has been demonstrated that when flagella experiences a mechanical load, it is able to remodel itself and recruit additional stator units to aid in rotation. In *E. coli* a stalled stator unit does not conduct protons, however, mutations that prevent proton flow also prevent recruitment of stator units to the flagellum machinery, so it is unclear if the effects of such mutations is due to lack of ion flow or stator recruitment (47).

Recently, studies using different polarly flagellated, monotrichous bacteria have revealed striking similarities in the mechanism by which they use their flagellum to sense surfaces (57, 203, 205, 206). *Vibrio cholerae*, *Caulobacter crescentus* and *Pseudomonas aeruginosa* have all been used as model organisms to study flagellar-mediated surface sensing and biofilm initiation. One similarity is that mutating the genes required for flagellar biosynthesis results in surface-associated phenotypes such as exopolysaccharide (EPS) over-production. For flagellar mutants that are able to form a HBB, EPS production also requires functional stator units. Finally, EPS

production was dependent on an increase in the second messenger c-di-GMP (cdG) which was often caused by activation of a diguanylate cyclase (DGC) (57, 203-205).

P. aeruginosa uses its single polar flagellum to sense and traverse surfaces. Unlike other microbes, the flagella of P. aeruginosa contains two sets of stators, MotAB and MotCD. These two sets of stators have different roles in surface motility as MotAB have been shown to be necessary for maximum velocity during swimming motility but MotCD has been shown to be absolutely required for swarming motility (8, 10, 11, 81, 223, 224). Furthermore, MotCD has been shown to be directly involved in surface sensing by binding to the diguanylate cyclase (DGC) SadC and stimulating c-di-GMP production upon surface contact. This interaction is mediated by FlgZ bound to c-di-GMP, and the FlgZ·c-di-GMP complex has been shown to be required for the removal of stator units from the flagellum, leading to shutdown of flagellar rotation while stimulating c-di-GMP production (12). These data indicate that the flagella, stators, and SadC are important for surface sensing but there remains missing links in how these complexes coordinate during surface contact.

A recent study demonstrated that deleting the gene encoding the flagellar filament fliC, results in a rugose-small colony variant (RSCV) morphology when plated on Vogel-Bonner Minimal Media (VBMM) agar. This colony morphology was shown to be due to overproduction of both Pel and Psl EPS in a c-di-GMP-dependent manner. A genetic screen for suppressor mutations in the fliC background revealed that the RSCV phenotype required both stator units as well as type IV pili and 2 different DGCs: SadC and SiaD (205). While proteins involved in flagella-mediated surface sensing in P. aeruginosa have been identified, the mechanism by c-di-GMP is initially increased

due to surface contact by the flagellum remains a mystery. Here we use a combination of genetic screens and phenotypic assays to investigate how *P. aeruginosa* uses its flagellum to sense a surface.

Results

A recent publication from our lab demonstrated that a flagellar mutation in the hook associated protein, FlgK, in the PA14 *P. aeruginosa* background has a similar phenotype to the *fliC* mutation (208). When plated on Congo Red agar (CR), *flgK* strains demonstrate enhanced congo red uptake due to an increase in Pel production as well as a wrinkled colony morphology **(Figure 1)**. To identify other cellular components that were necessary for this phenotype, we made mutations in the *flgK* background via random transposon mutagenesis or by targeted deletion and plated them on CR agar. We identified two DGCs, SadC and RoeA, that were important for the CR phenotype **(Figure 1)**. As previously described in other bacteria, this phenotype was also dependent on the pressence of functional stator units. Deletion of either set of stators reduced the amount of CR dye uptake and extent of wrinkles of the colony. Stators must also be able to interact with the flagellar motor via FliG as mutants that abolish this interaction phenocopied deleting the full stator protein. Mutations that prevent proton binding also suppress the CR phenotype in the *flgK* background. The amount of c-di-GMP was shown to correlate with the CR phenotype as determined by mass spectroscopy **(Figure 1)**. These data indicate the enhanced CR uptake in the *flgK* background was due to an increase in c-di-GMP by two DGCs, SadC and RoeA. This phenotype also required functional stator units that are able to bind the flagellar

motor and conduct protons. Interestingly, a mutation in FliG that is able to restore interaction with a MotA-R89E mutation, FliG-D295A, shows enhanced CR binding and c-di-GMP levels greater than that of the *flgK* background.

Of the cellular components shown to be important for increased c-di-GMP and CR in the flgK background, only SadC and MotC have been shown to directly interact to stimulate DGC activity. In order to identify other potential interactions between these proteins, Bacterial Adenylate Cyclase Two Hybrid (B2H) assays were performed. Through this we identified a novel interaction between the two DGCs SadC and RoeA **(Figure 2)**. It is unknown whether this interaction affects the diguanylate cyclase activity of either of these DGCs.

In order to identify other cellular components that are necessary for this phenotype in the *flgK* background, transposon mutagenesis was performed to generate a pool of random mutants and then plated on CR to evaluate pel production and colony morphology. A table to mutants that either suppressed or exacerbated the CR phenotype in the flgK background can be found in Table 1. Many of the hits in this screen mapped to genes in the Pel biosynthesis and secretion machinery as expected. We also hit genes involved in c-di-GMP production or degradation including RoeA, which was shown to be important for this phenotype. Lastly we hit genes involved in type IV pili function which indicate to us that this CR phenotype is likely mediated through the coordinated efforts of these two surface sensing and motility appendages.

Materials and Methods

Strains and media. *P. aeruginosa* UCBPP PA14 was used as the WT strain and all mutations were made in this background unless stated otherwise. Mutations were made using *E. coli* S17-1 λpir. All strains used in this study are listed in Supplemental Table S1. Bacterial strains were cultured in 5ml of lysogeny broth (LB) medium or plated on 1.5% LB agar with antibiotics, when necessary. Tetracycline (tet) was used at 15ug/ml for *E. coli* and 120 ug/ml for initial selections for *P. aeruginosa,* and *P. aeruginosa* was maintained with 75ug/ml. Gentamicin (Gm) was used at 30 μg/ml for *P. aeruginosa* and 10 μg/ml for *E. coli*. Carbenicillin (Cb) was used at 200 ug/ml for *P. aeruginosa* and 100 ug/ml for *E. coli*. Kanamycin (Kan) was used at 50 ug/ml for *E. coli*. M8 minimal salts medium supplemented with $MgSO_4$ (1mM), glucose (0.2%) and casamino acids (0.5%) was used for all assays (8). Plasmids were induced with either 0.2% arabinose for P_{BAD} promoter induction or 0.5 mM isopropyl-D-thiogalactopyranoside (IPTG) was added to agar or liquid media for PTAC promoter induction unless otherwise stated.

Construction of mutant strains and plasmids. Plasmids used in this study are listed in Table S2 and primers used in this study are listed in Table S3. In-frame deletions were generated using allelic exchange as previously described (155). Plasmids were generated either by ligation or Gibson assembly (225). Insertions were made at neutral sites in the *P. aeruginosa* genome using the mini-Tn7 vector and the mini-CTX1 vector (147, 149, 150). Resistance markers were removed using the pFLP2 plasmid and sucrose counterselection (156). Point mutants were generated

using QuikChange site-directed mutagenesis and cloned into expression vectors pMQ72 or pVLT31.

Transposon mutagenesis and identification of integration site. Transposon mutants were generated with the Mariner transposon as previously described (226, 227). Briefly, *E. coli* S17 harboring the pBT20 plasmid harboring the Mariner transposon was co-incubated with *P. aeruginosa* PA14 Δ*flgK* on LB agar for 1 hour for conjugation to occur at 30°C. Cells were then scraped-up, diluted, and plated on LB agar plates supplemented with 30 μg/ml Gm, 20 μg/ml Triclosan, 0.04 mg/ml Congo Red, and 0.01 mg/ml Coomassie blue. Plates were then incubated at 37C for 24 hours and then at room temperature for 48 hours. Colonies that displayed altered colony morphology or Congo Red uptake relative to the Δ*flgK* strain were selected and confirmed with a second round of plating on Congo Red agar with selection. After confirmation of the phenotype, arbitrary primed PCR was then performed and sequenced using Sanger sequencing to identify the location and direction of the transposon as previously described (55, 226, 228, 229).

Bacterial adenylate cyclase two hybrid assays. The B2H system from Euromedex was used to evaluate protein-protein interactions within the BTH101 *E. coli* background (151). Genes were cloned into either the pKT25/pKNT25 or pUT18/pUT18C vector backgrounds. Transformants were plated on LB agar containing Cb (50ug/ml), Kn (50ug/ml), X-Gal (5-bromo-4-chloro-3-indolyl-β-d-galactopyranoside) (40 g/mL) and IPTG (isopropyl-d-thiogalactopyranoside)

(0.5 mM) and incubated at 30°C until an interaction was observed through the transformation of X-Gal to a blue pigment or until the negative control began to produce a blue pigment. Quantification of the level of interaction between proteins was performed as previously described (151).

Congo Red assay. Congo red stain uptake was adapted from previously published protocols (230, 231). Briefly, LB agar plates supplemented with Congo Red 0.04 mg/ml, and 0.01 mg/ml Coomassie blue were spotted with 2.5 ul of an overnight culture and incubated at 37°C for 24 hours and then at room temperature for 48 hours. Colony morphology and extent of Congo Red uptake was then noted and photographs were taken.

Swimming motility assay. Swimming assays were performed as previously described (9). M8 medium was supplemented with 0.3% agar. Swim plates were inoculated with sterile tips dipped into an overnight culture and incubated at 37° C for 16 to 18 hours. No more than two plates were stacked together. Swim zones were then imaged and quantified using ImageJ.

Protein detection and quantification. Proteins were transferred to a nitrocellulose membrane and probed with antiserum. Proteins were detected using fluorescence detection with IRDye-labeled fluorescent secondary antibodies and imaged using the Odyssey CLx Imager (LICOR Biosciences, INC., Lincoln, NE). Image Studio Lite software (LICOR Biosciences, Inc., Lincoln, NE) were used to quantify protein bands.

Flow cytometry measurements.   Bacterial strains harboring the *PcdrA-gfp* c-di-GMP reporter plasmid were subcultured into M8 liquid medium supplemented with glucose (.2%), casamino acids (.5%), and $MgSO_4$ (1mM) and incubated at 37°C until an OD of 0.5 was reached (~3h). Gm, Tet, IPTG, or arabinose was added to the liquid medium when indicated. 200 µl of the culture was then spread on M8 agar plates and incubated at 37°C for. Cells were then harvested, washed, diluted, and analyzed on a Biorad 27-color YETI flow cytometer. FlowJo software v.10.8.1 was used to measure the GFP fluorescent intensity for at least 50,000 cells.

Literature Cited

1.   Zobell CE, Allen EC. 1935. The Significance of Marine Bacteria in the Fouling of Submerged Surfaces. Journal of Bacteriology 29:239-251.
2.   Henrici AT. 1933. Studies of Freshwater Bacteria. Journal of Bacteriology 25:277-287.
3.   Chattopadhyay I, J RB, Usman TMM, Varjani S. 2022. Exploring the role of microbial biofilm for industrial effluents treatment. Bioengineered 13:6420-6440.

4. Sharma S, Mohler J, Mahajan SD, Schwartz SA, Bruggemann L, Aalinkeel R. 2023. Microbial Biofilm: A Review on Formation, Infection, Antibiotic Resistance, Control Measures, and Innovative Treatment. Microorganisms 11:1614.

5. Ha D-G, O'Toole GA. 2015. c-di-GMP and its Effects on Biofilm Formation and Dispersion: a *Pseudomonas Aeruginosa* Review. Microbiology Spectrum 3.

6. Rumbaugh KP, Sauer K. 2020. Biofilm dispersion. Nature Reviews Microbiology 18:571-586.

7. O'Toole GA, Kolter R. 1998. Flagellar and twitching motility are necessary for *Pseudomonas aeruginosa* biofilm development. Molecular Microbiology 30:295-304.

8. L. McCarter, M. Hilmen, Silverman M. 1988. Flagellar dynamometer controls swarmer cell defferentiation of V. parahaemolyticus. Cell 54:345-351.

9. McCarter L, Silverman M. 1990. Surface-induced swarmer cell differentiation of Vibrio parahaemoiyticus. Molecular Microbiology 4:1057-1062.

10. Ha D-G, Kuchma SL, O'Toole GA. 2014. Plate-Based Assay for Swimming Motility in Pseudomonas aeruginosa, p 59-65 doi:10.1007/978-1-4939-0473-0_7. Springer New York.

11. Köhler T, Curty LK, Barja F, Delden Cv, Pechère J-C. 2000. Swarming of *Pseudomonas aeruginosa* is dependent on cell-to-cell signaling and requires Ffagella and pili. Journal of Bacteriology 182:5990-5996.

12. Toutain CM, Caizza NC, Zegans ME, O'Toole GA. 2007. Roles for flagellar stators in biofilm formation by Pseudomonas aeruginosa. Res Microbiol 158:471-7.

13. Aldridge P, Hughes K. 2002. Regulation of flagellar assembly. Cell regulation.

14. Homma M, Kojima S. 2022. The Periplasmic Domain of the Ion-Conducting Stator of Bacterial Flagella Regulates Force Generation. Front Microbiol 13:869187.

15. Guo S, Liu J. 2022. The Bacterial Flagellar Motor: Insights Into Torque Generation, Rotational Switching, and Mechanosensing. Front Microbiol 13:911114.

16. Deme JC, Johnson S, Vickery O, Aron A, Monkhouse H, Griffiths T, James RH, Berks BC, Coulton JW, Stansfeld PJ, Lea SM. 2020. Structures of the stator complex that drives rotation of the bacterial flagellum. Nature Microbiology 5:1553-1564.

17. Wadhwa N, Phillips R, Berg HC. 2019. Torque-dependent remodeling of the bacterial flagellar motor. Proceedings of the National Academy of Sciences 116:11764-11769.

18. Tipping MJ, Delalez NJ, Lim R, Berry RM, Armitage JP. 2013. Load-dependent assembly of the bacterial flagellar motor. mBio 4.

19. Castillo DJ, Nakamura S, Morimoto YV, Che Y-S, Kami-Ike N, Kudo S, Minamino T, Namba K. 2013. The C-terminal periplasmic domain of MotB is responsible for load-dependent control of the number of stators of the bacterial flagellar motor. BIOPHYSICS 9:173-181.

20. Chawla R, Ford KM, Lele PP. 2017. Torque, but not FliL, regulates mechanosensitive flagellar motor-function. Scientific Reports 7.

21. Zhu S, Takao M, Li N, Sakuma M, Nishino Y, Homma M, Kojima S, Imada K. 2014. Conformational change in the periplamic region of the flagellar stator coupled with the assembly around the rotor. Proceedings of the National Academy of Sciences 111:13523-13528.

22. Morimoto YV, Nakamura S, Hiraoka KD, Namba K, Minamino T. 2013. Distinct Roles of Highly Conserved Charged Residues at the MotA-FliG Interface in Bacterial Flagellar Motor Rotation. Journal of Bacteriology 195:474-481.

23. Harrison JJ, Almblad H, Irie Y, Wolter DJ, Eggleston HC, Randall TE, Kitzman JO, Stackhouse B, Emerson JC, McNamara S, Larsen TJ, Shendure J, Hoffman LR, Wozniak DJ, Parsek MR. 2020. Elevated exopolysaccharide levels in Pseudomonas aeruginosa flagellar mutants have implications for biofilm growth and chronic infections. PLoS Genet 16:e1008848.

24.   Hershey DM, Fiebig A, Crosson S. 2019. A Genome-Wide Analysis of Adhesion in Caulobacter crescentus Identifies New Regulatory and Biosynthetic Components for Holdfast Assembly. mBio 10.

25.   Wu DC, Zamorano-Sánchez D, Pagliai FA, Park JH, Floyd KA, Lee CK, Kitts G, Rose CB, Bilotta EM, Wong GCL, Yildiz FH. 2020. Reciprocal c-di-GMP signaling: Incomplete flagellum biogenesis triggers c-di-GMP signaling pathways that promote biofilm formation. PLOS Genetics 16:e1008703.

26.   Hershey DM. 2021. Integrated control of surface adaptation by the bacterial flagellum. Curr Opin Microbiol 61:1-7.

27.   Hershey DM, Fiebig A, Crosson S. 2021. Flagellar Perturbations Activate Adhesion through Two Distinct Pathways in Caulobacter crescentus. mBio 12.

28.   Hook AL, Flewellen JL, Dubern JF, Carabelli AM, Zaid IM, Berry RM, Wildman RD, Russell N, Williams P, Alexander MR. 2019. Simultaneous Tracking of Pseudomonas aeruginosa Motility in Liquid and at the Solid-Liquid Interface Reveals Differential Roles for the Flagellar Stators. mSystems 4.

29.   Bru J-L, Kasallis SJ, Zhuo Q, Høyland-Kroghsbo NM, Siryaporn A. 2023. Swarming of <i>P. aeruginosa</i>: Through the lens of biophysics. Biophysics Reviews 4.

30.   Toutain CM, Zegans ME, O'Toole GA. 2005. Evidence for Two Flagellar Stators and Their Role in the Motility of <i>Pseudomonas aeruginosa</i>. Journal of Bacteriology 187:771-777.

31.   Zhengyu Wu aaMT, a Rongjing Zhang,a Junhua Yuana. 2021. Dynamics of the Two Stator Systems in the Flagellar Motor of Pseudomonas aeruginosa Studied by a Bead Assay. Applied and Environmental Microbiology 87.

32.   Baker AE, Webster SS, Diepold A, Kuchma SL, Bordeleau E, Armitage JP, O'Toole GA. 2019. Flagellar Stators Stimulate c-di-GMP Production by Pseudomonas aeruginosa. Journal of Bacteriology 201.

33.   Lewis K, Vermilyea, D. M., Webster, S. S., Geiger, C. J., de Anda, J., Wong, G. C. L., O'Toole, G. A., Hogan, D. 2022. Nonmotile Subpopulations of Pseudomonas

aeruginosa Repress Flagellar Motility in Motile Cells through a Type IV Pilus-and Pel-Dependent Mechanism. Journal of Bacteriology.

34. Shanks RMQ, Caiazza NC, Hinsa SM, Toutain CM, O'Toole GA. 2006. <i>Saccharomyces cerevisiae</i>-Based Molecular Tool Kit for Manipulation of Genes from Gram-Negative Bacteria. Applied and Environmental Microbiology 72:5027-5036.

35. Gibson DG, Young L, Chuang R-Y, Venter JC, Hutchison CA, Smith HO. 2009. Enzymatic assembly of DNA molecules up to several hundred kilobases. Nature Methods 6:343-345.

36. Choi K-H, Gaynor JB, White KG, Lopez C, Bosio CM, Karkhoff-Schweizer RR, Schweizer HP. 2005. A Tn7-based broad-range bacterial cloning and expression system. Nature Methods 2:443-448.

37. Choi K-H, Schweizer HP. 2006. mini-Tn7 insertion in bacteria with single attTn7 sites: example Pseudomonas aeruginosa. Nature Protocols 1:153-161.

38. Hoang TT, Kutchma AJ, Becher A, Schweizer HP. 2000. Integration-proficient plasmids for Pseudomonas aeruginosa: site-specific integration and use for engineering of reporter and expression strains. Plasmid 43:59-72.

39. Hoang TT, Karkhoff-Schweizer RR, Kutchma AJ, Schweizer HP. 1998. A broad-host-range Flp-FRT recombination system for site-specific

excision of chromosomally-located DNA sequences: application for

isolation of unmarked Pseudomonas aeruginosa mutants. Gene 212:77-86.

40. Wong SM, Mekalanos JJ. 2000. Genetic footprinting with <i>mariner</i> -based transposition in <i>Pseudomonas</i> <i>aeruginosa</i>. Proceedings of the National Academy of Sciences 97:10191-10196.

41. Kulasekara HD, Ventre I, Kulasekara BR, Lazdunski A, Filloux A, Lory S. 2005. A novel two-component system controls the expression of <i>Pseudomonas aeruginosa</i> fimbrial <i>cup</i> genes. Molecular Microbiology 55:368-380.

42. Pastora A, O'Toole GA. 2023. The regulator FleQ both transcriptionally and posttranscriptionally regulates the level of RTX adhesins of Pseudomonas fluorescens. Journal of Bacteriology 205.

43. O'Toole GA, Pratt LA, Watnick PI, Newman DK, Weaver VB, Kolter R. 1999. Genetic Approaches To Study of Biofilms, p 91-109, Methods in Enzymology, vol 310.

44. Karimova G, Pidoux J, Ullmann A, Ladant D. 1998. A bacterial two-hybrid system based on a reconstituted signal transduction pathway. Proceedings of the National Academy of Sciences 95:5752-5756.

45. Spiers AJ, Bohannon J, Gehrig SM, Rainey PB. 2003. Biofilm formation at the air–liquid interface by the *Pseudomonas fluorescens* SBW25 wrinkly spreader requires an acetylated form of cellulose. Molecular Microbiology 50:15-27.

46. Ghafoor A, Hay ID, Rehm BHA. 2011. Role of Exopolysaccharides in Pseudomonas aeruginosa Biofilm Formation and Architecture. Applied and Environmental Microbiology 77:5238-5246.

Table 1. Hits from Congo red transposon screen in *flgK* background

Candidate	Function
pelB	forms part of the Pel secretion complex
pelD	cdG binding protein; important for Pel secretion
pelA	Component of the Pel secretion complex
pelE	Component of the Pel secretion complex
pelC	Component of the Pel secretion complex
pelF	Component of the Pel secretion complex
pelG	Component of the Pel secretion complex
PA14_11290	Putative Permease – membrane transport proteins
thdF	Putative GTP binding protein - GTPase
PA14_16550 (PA3699)	Putative transcriptional regulator
ppK	Polyphosphate kinase – responsible for the synthesis of inorganic polyphosphate from ATP
pvrS	pvrS part of a two component system with pvrR (a PDE)
PA14_43670 (PA1611)	Signal transduction histidine kinase, Part of a two component system
pilQ	OM T4P secretin protein
pilW	Minor pilin, forms the T4P assembly
pilY1	Important in pili assembly and mechanosensing
ptsP	phosphoenolpyruvate protein phosphotransferase, downstream gene (PA14_04420) has PAS/GGDEF domain, enhanced CR
hflX	Role in lysogeny
pilV	minor pilin
hepP	heparanase
PA14_30470	periplasmic aliphatic sulfonate binding protein

PA14_02890	nucleoside channel forming protein near pcaFTBDCK
pilX	minor pilin
roeA	our second fave DGC
retS	regulator of EPS & T3SS, Part of Gac-Rsm pathway, (inhibits GacS autophos and dephos gacS, inhibit dimerization)
PA14 72870	aminotransferase, biosyn of secondary metabolites,
PA14 08600	23S rRNA,
PA14 08570	16S rRNA
pelA	glycohydrolase
orfN	(NAD dependent epimerase/dehydrase), glycosylation, group 4 glycosyl transferase
bifA-sodB	Motility/attachment
PelE	
aguR	TF, negative regulation of hydrolase activity
PA14_08580	tRNA-Ile
pvrS	phosphodiesterase (breaks down ci-d-gmp
PA14_44350	cbb3-type cytochrome c oxidase subunit II
speA	arginine dearboxylase, putrescine from arg
PA14_40660	Tse1, amidase activity, (Pa T6SS effector, hydrolase, PDB: 3VPI, complex with immune protein Tsi1
PA14_32820	PA2462 from PAO1
PA14_70870	5s rRNA
PA14_30100	50S ribosomal protein L16 3-hydroxylase
sodM	superoxide dismutase
PA14_57570	cytochrome c reductase, iron-sulfur subun, ubiquinol-cytochrome-c reductase, Ubiquinol—cytochrome-c reductase catalyzes the chemical reaction

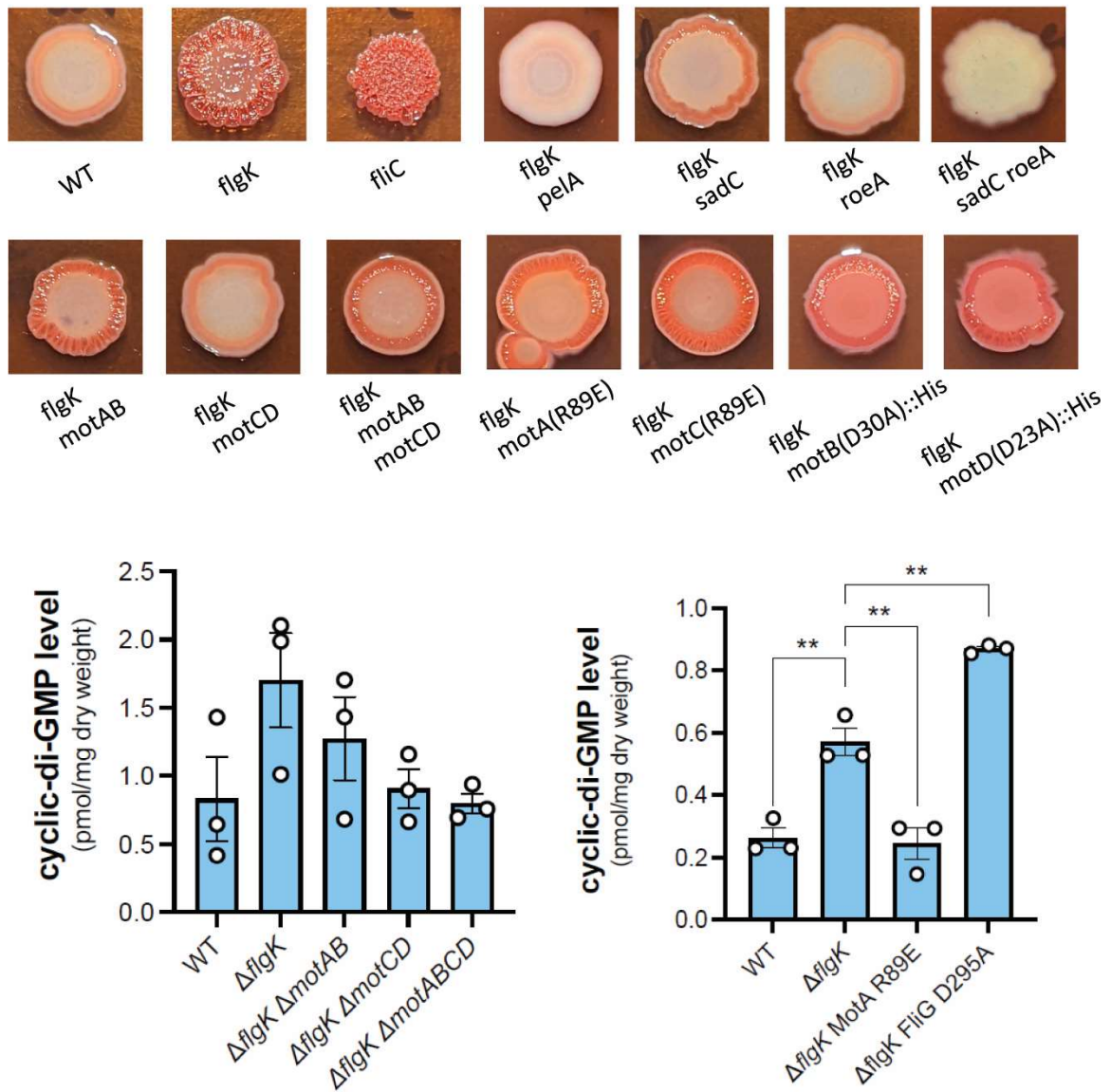|	
	QH2 + 2 ferricytochrome c ⇌ \rightleftharpoons Q + 2 ferrocytochrome c + 2 H+
PA14_66100	O-antigen ligase, WaaL, critical for cell wall integrity and motility
purM	phosphoribosylaminoimidazole
katA	catalase
PA14_41280	beta-lactamase

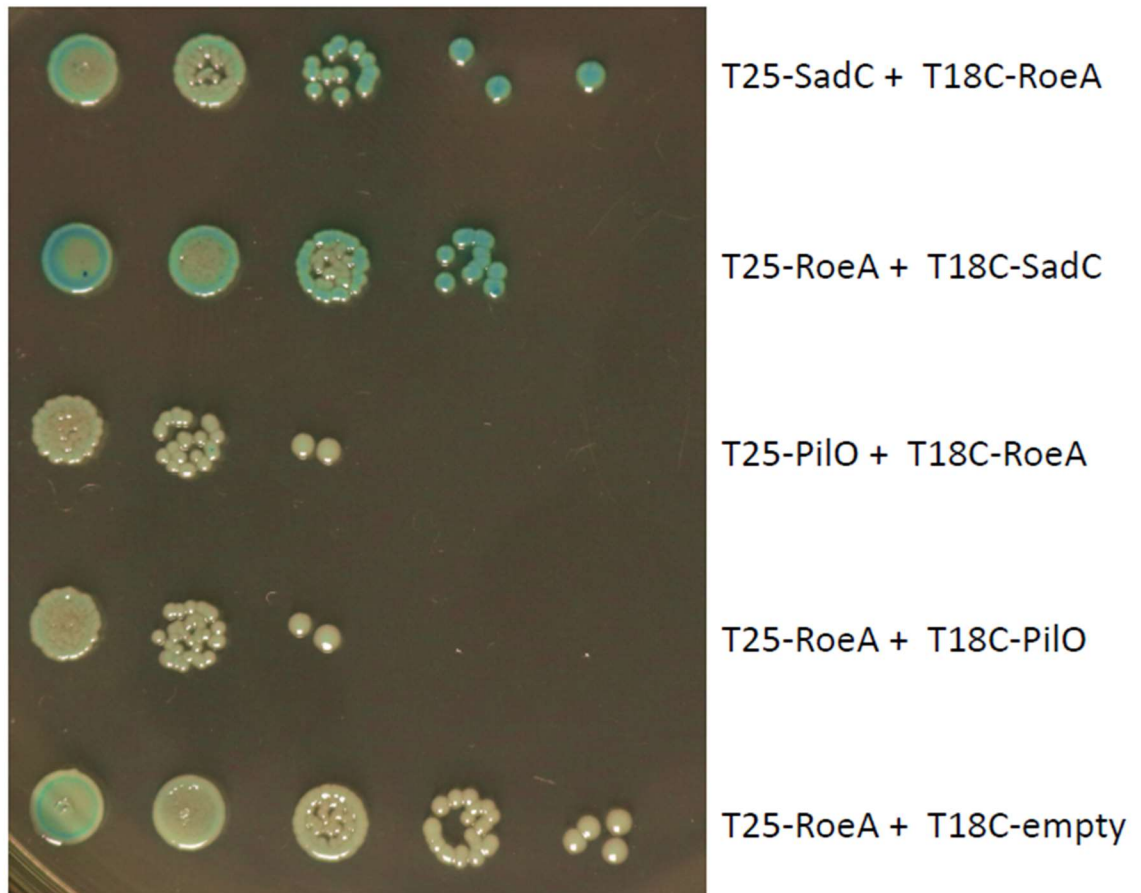**Figure 1. Congo red phenotype and c-di-GMP measurements for flagellar mutants.**

Figure 2. Bacterial Adenylate Cyclase Two Hybrid Interactions between SadC, RoeA, and PilO.

Appendix 6

Nonmotile Subpopulations of *Pseudomonas aeruginosa* Repress Flagellar Motility in Motile Cells through a Type IV Pilus- and Pel-Dependent Mechanism

Nonmotile Subpopulations of *Pseudomonas aeruginosa* Repress Flagellar Motility in Motile Cells through a Type IV Pilus- and Pel-Dependent Mechanism

Kimberley A. Lewis,[a] Danielle M. Vermilyea,[a] Shanice S. Webster,[a] Christopher J. Geiger,[a] Jaime de Anda,[b,c,d] Gerard C. L. Wong,[b,c,d] George A. O'Toole,[a] Deborah A. Hogan[a]

[a]Department of Microbiology and Immunology, Geisel School of Medicine at Dartmouth, Hanover, New Hampshire, USA
[b]Department of Bioengineering, University of California Los Angeles, Los Angeles, California, USA
[c]Department of Chemistry and Biochemistry, University of California Los Angeles, Los Angeles, California, USA
[d]California NanoSystems Institute, University of California Los Angeles, Los Angeles, California, USA

Kimberley A. Lewis and Danielle M. Vermilyea contributed equally to this article. Author order was determined by who conceptualized and started the project.

ABSTRACT The downregulation of *Pseudomonas aeruginosa* flagellar motility is a key event in biofilm formation, host colonization, and the formation of microbial communities, but the external factors that repress motility are not well understood. Here, we report that on soft agar, swarming motility can be repressed by cells that are nonmotile due to the absence of a flagellum or flagellar rotation. Mutants that lack either flagellum biosynthesis or rotation, when present at as little as 5% of the total population, suppressed swarming of wild-type cells. Non-swarming cells required functional type IV pili and the ability to produce Pel exopolysaccharide to suppress swarming by the flagellated wild type. Flagellated cells required only type IV pili, but not Pel production, for their swarming to be repressed by non-flagellated cells. We hypothesize that interactions between motile and nonmotile cells may enhance the formation of sessile communities, including those involving multiple genotypes, phenotypically diverse cells, and perhaps other species.

IMPORTANCE Our study shows that, under the conditions tested, a small population of non-swarming cells can impact the motility behavior of a larger population. The interactions that lead to the suppression of swarming motility require type IV pili and a secreted polysaccharide, two factors with known roles in biofilm formation. These data suggest that interactions between motile and nonmotile cells may enhance the transition to sessile growth in populations and promote interactions between cells with different genotypes.

KEYWORDS swarming, *Pseudomonas aeruginosa*, motility, type IV pili, Pel, microbe-microbe interaction

icrobial localization through processes other than cell division are critical for the formation of spatially structured populations and communities. Thus, motility and its regulation by diverse chemical and physical stimuli is a major driver of intraspecies and interspecies microbial interactions (1, 2). Previously, we found that exogenous ethanol, a common product secreted by many microbes, markedly reduced *Pseudomonas aeruginosa* swimming and swarming motilities at the population level, but only decreased the motile fraction of cells in the population by 16% when individual cells were examined (3). Prompted by this finding, we sought to determine the impact of a subpopulation of nonmotile cells on the motility of the larger motile *P. aeruginosa* population.

During *P. aeruginosa* biofilm formation, motile cells are recruited to microcolonies

195

of sessile cells via a combination of processes which may differ between strains with distinct early biofilm-forming strategies (4, 5) or in response to different experimental conditions. For *P. aeruginosa* strain PA14, retractile type IV pili (T4P) participate in surface sensing, which results in the upregulation of cAMP and the subsequent induction of cyclic-di-GMP (6–8); flagellar motility is then downregulated in order to facilitate surface attachment (6, 7, 9, 10) followed by Pel exopolysaccharide matrix production (11), which can connect cells to one another (10, 12). Both matrix production and T4P function have been shown to participate in motility repression (10, 12–14), suggesting that matrix materials may mediate physical interactions between neighboring cells. T4P also mediate cell-cell interactions in swarms (15).

Boyle et al. (16) previously showed that a Δ*flgK* mutant lacking a flagellum repressed swarming (i.e., decreased the swarm radius) when present in excess (83%) compared to the flagellated wild type (WT; 17%). In support of the observation that a non-motile subpopulation can suppress population-wide swarming, our previously published findings (3) showed that while WT strain PA14 was able to swim in soft agar, an average of only 38% of flagellated cells were motile at any given time. Furthermore, we showed that ethanol reduced the motile fraction of the *P. aeruginosa* population from 38% to 22%. Ethanol also strongly repressed swarming, and this repression required some T4P components (3). Thus, we proposed that a reduction in the motile fraction of cells was sufficient to repress swarming by the entire population, and sought to explore the interactions between motile and non-motile cells in the context of swarms.

In this study, we show that non-motile cells lacking a flagellum, when added to a population at 5% to 75% of the total inoculum, resulted in repression of swarming by WT cells. To repress flagellar motility, non-motile cells required the ability to produce Pel polysaccharide, and both motile and non-motile cells required functional T4P for this interaction. These data have implications for factors which contribute to population-level behaviors and intra- and interspecies interactions. Conditions that promote cell-cell interactions may be relevant in situations where non-motile and motile cells can be found together, such as in cystic fibrosis (CF)-associated lung infections (17–19), wounds (20), and ear infections (18).

RESULTS

The absence of flagellar motility in a subpopulation of cells is sufficient to suppress wild-type *P. aeruginosa* swarming. To explore the effects of a subpopulation of non-motile cells on swarming motility, mixtures containing different proportions of flagellated *P. aeruginosa* strain PA14 (WT) cells and non-flagellated Δ*flgK* mutant cells lacking the flagellar hook protein were grown on 0.5% M8 agar, which supports swarming motility by the WT strain. The percentage of Δ*flgK* mutant cells ranged from 5% to 75% in these mixtures, and single strains were included as controls. As expected, cultures with 100% WT swarmed readily, while cultures with 100% Δ*flgK* showed no swarming (Fig. 1A). We found that swarming motility was completely repressed by the addition of 5 to 75% Δ*flgK* cells under the conditions tested (Fig. 1A and C). The addition of 1 to 4% Δ*flgK* was insufficient to repress population-wide swarming (Fig. S1 in the supplemental material), though it is worth noting that a swarming phenotype was variable between technical and biological replicates when the fraction of nonmotile cells was small. This finding is consistent with the variability in swarming ability among replicates that has been previously reported even for single-strain cultures (21, 22), and thus all data for all experiments are summarized in Fig. S1. The Δ*flgK* mutant, when added at 5% of the population, regularly repressed WT swarming (Fig. S1). In contrast to our finding, work by Boyle et al. (16) reported that Δ*flgK* repressed swarming only when it was present in excess of the WT. Specifically, the authors reported repression, measured by a reduction in swarm radius, when there was a 1:5 ratio of WT to the Δ*flgK* mutant; however, images for 1:1 WT:Δ*flgK* mixes may also suggest a reduction of the swarm area even though swarm radius was not yet affected.

To determine whether the lack of swarming in WT:Δ*flgK* co-cultures was due to faster growth of the non-flagellated cells compared to the WT, we competed both the

196
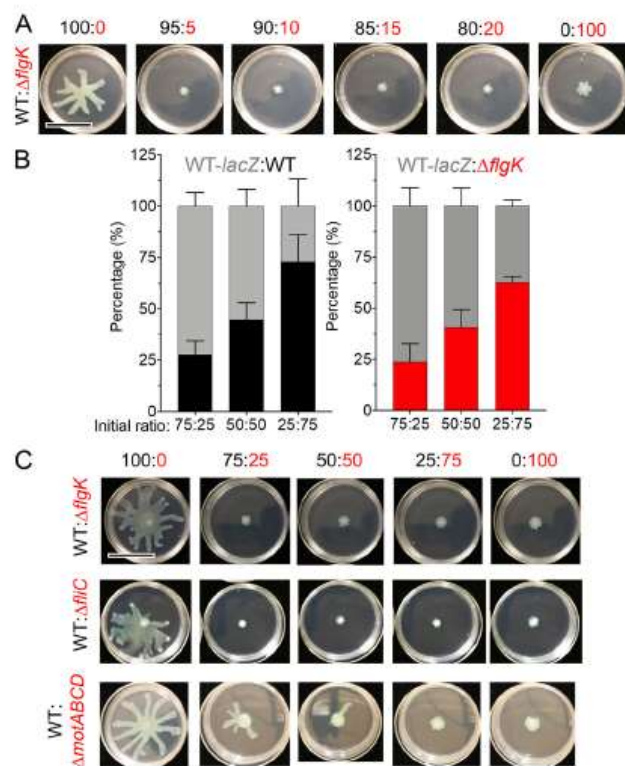
FIG 1 Motility heterogeneity represses swarming motility independent of competition. (A) Representative images from swarm assay of wild-type (WT) *P. aeruginosa* strain PA14 (flagellated) mixed with Δ*flgK* (non-flagellated) at the indicated ratios on M8 agar. WT and derivatives are labeled in black, flagellar mutants are labeled in red. Data are representative of three individual experiments. (B) Competition growth assay between WT tagged with a *lacZ* reporter (gray) and either an untagged WT (black) or Δ*flgK* mutant strain (red). Data show the average of three individual experiments. Error bars represent standard deviations between the replicate values. Statistical analysis using one-way analysis of variance showed no difference between input and output for each ratio analyzed. (C) Representative images from swarm assay of WT (flagellated) mixed with Δ*flgK* (non-flagellated), Δ*fliC* (non-flagellated), or Δ*motABCD* (paralyzed flagellum) at the indicated ratios on M8 agar. Data are representative of three individual experiments. Scale bar, 30 mm.

WT and the Δ*flgK* mutant against a WT strain tagged with a *lacZ* reporter at different ratios atop a 0.22-μm filter placed on 0.5% M8 agar. After 16 h, the colony was disrupted and the CFU for each strain were enumerated on blue/white screening plates containing X-Gal. At all ratios tested, neither untagged WT nor the Δ*flgK* mutant could outgrow the *lacZ*-expressing WT strain (Fig. 1B), indicating that the lack of swarming observed in WT:Δ*flgK* mixes was not due to increased growth of non-flagellated cells and thus, to overgrowth of the population. Rather, our data suggest that a subpopulation of cells incapable of flagellar motility inhibits the motility of the larger flagellated WT population.

Using conditions in which the non-motile strain comprised 25%, 50%, or 75% of the population, we also found that, like the Δ*flgK* mutant, the Δ*fliC* mutant, another strain incapable of flagellar motility due to a lack of the flagellin protein used to make the flagellar filament, inhibited WT swarming at all ratios tested (Fig. 1C). Similarly, the

197

FIG 2 Flagellated *P. aeruginosa* requires functional T4P to be repressed by the non-motile subpopulation. Representative images from swarm assays 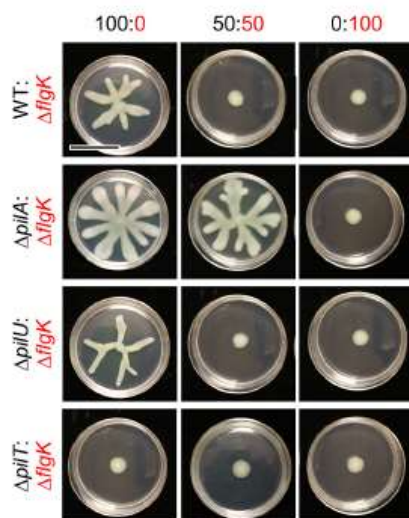of the non-flagellated Δ*flgK* mutant (functional T4P) mixed with either wild-type (WT) *P. aeruginosa* strain PA14 (functional T4P), Δ*pilA* mutant (lacking T4P), Δ*pilT* mutant (no T4P retraction), or Δ*pilU* mutant (reduced T4P retraction) at the indicated ratios on M8 agar. Data are representative of three individual experiments. Scale bar, 30 mm.

Δ*motABCD* mutant, which produces a flagellum that is unable to rotate due to the absence of stators, repressed swarming of the WT; however, compared to Δ*flgK* and Δ*fliC*, the Δ*motABCD* mutant was slightly less effective at repressing WT swarming (Fig. 1C). Together, these data suggest that the absence of flagellar motility in a subpopulation of cells is sufficient to suppress WT swarming in co-culture.

Functional T4P in flagellated cells are required for non-flagellated cells to repress swarming in co-culture. Several studies have shown that *P. aeruginosa* strains which are deficient in T4P tend to have a hyper-swarming phenotype (23–25), while hyperpiliated strains (those that overproduce elongated pili due to a defect in retraction) have inhibited swarming (15, 26). Additionally, *P. aeruginosa* cells have been shown to interact via their T4P to form close cell associations that facilitate directional swarming (15). Therefore, we determined whether flagellated cells require T4P in order to facilitate the ability of Δ*flgK* to inhibit population-wide swarming motility. To do this, we analyzed the ability of Δ*flgK* to repress swarming when co-cultured with the following mutants: Δ*pilA*, which lacks T4P; Δ*pilMNOP*, which lacks the alignment complex required for T4P function (27) and cyclic-di-GMP signaling (28); and both Δ*pilT* and Δ*pilU*, hyperpiliated mutants which lack either of the ATPases that mediate T4P retraction (29). Strains lacking *pilA*, *pilMNOP*, *pilT*, and *pilU* were all defective for twitching motility (Fig. S2 and S3). The swarming motility of strains lacking *pilA* or *pilMNOP* was no longer inhibited by the Δ*flgK* mutant in co-culture (Fig. 2 and Fig. S4). Interestingly, despite its reported hyperpiliation and in contrast to previous reports (15), Δ*pilU* was capable of swarming, but had an altered morphology compared to the WT (Fig. 2). Swarming by Δ*pilU* was inhibited by the Δ*flgK* mutant in co-culture, similar to the WT (Fig. 2 and Fig. S5). However, the hyperpiliated Δ*pilT* mutant was incapable of swarming (Fig. 2), in agreement with previous models (15). Complementation of the Δ*pilU* and Δ*pilT* mutants restored twitching in both strains as well as swarming in Δ*pilT* (Fig. S6).

PilT is the main retractile ATPase, and the Δ*pilT* mutant completely lacks pilus retraction (26, 30), while the Δ*pilU* mutant has reduced retraction but still retains some

198

function (26). This accessory role is supported by previous observations that the Δ*pilU* mutant retained sensitivity to infection by phage PO4, while the Δ*pilT* mutant became resistant to infection (26). We confirmed that the WT and the Δ*pilU* mutant were sensitive to phage DMS3 infection and that the Δ*pilA* and Δ*pilT* mutants were resistant to infection under our experimental conditions (Fig. S2B). Additionally, while the Δ*pilU* mutant can form dense biofilms under static conditions (30), its ability to form a biofilm under flow conditions varies by strain (30, 31), possibly due to differences in Δ*pilU* T4P strength compared to WT and Δ*pilT* T4P. Differences in T4P strength may allow Δ*pilU* T4P to readily detach from the cell surface (26, 30). Overall, the data show that Δ*pilU* displays an intermediate phenotype in that it is hyperpiliated due to reduced T4P retraction, which still results in inhibition of T4P-mediated twitching motility, but not swarming motility. Together, these data indicate that motile cells require T4P, and likely functional T4P, for the non-flagellated subpopulation to inhibit the swarming motility of the WT strain when they are grown in co-culture.

P. aeruginosa T4P participate in a cAMP-dependent signaling pathway (see Fig. S7A for pathway) which involves FimS, PilJ, CyaAB adenylate cyclases, and the cAMP-binding transcription factor Vfr (6). We found that this pathway was not required for the repression of WT swarming motility by the Δ*flgK* mutant (Fig. S7B), using published mutants lacking components of the cAMP signaling pathway (Δ*pilJ*, Δ*fimS*, Δ*cyaAB*, and Δ*vfr*) which retained expression of partially functional T4P, as evidenced by their sensitivity to phage DMS3 (Fig. S7C). Taken together, these data show that flagellated WT cells require functional T4P, but not the cAMP-dependent surface-sensing pathway, for non-flagellated cells to be able to repress swarming in co-culture.

Non-flagellated cells require functional T4P to repress swarming motility of flagellated cells in co-culture. Consistent with published results (4, 32, 33), the Δ*flgK* mutant has functional T4P, as evidenced by the formation of a large twitching motility zone using an agar-plastic interface assay (Fig. S2A and Fig. S3). While both the WT and Δ*flgK* formed twitch zones that were significantly larger than those formed by the T4P-null Δ*pilA* mutant, the Δ*flgK* twitch zone was ~25% smaller than that formed by the WT ($P < 0.05$; Fig. S3A). Using Δ*flgK* and Δ*flgK*Δ*pilA* strains, we found that *pilA*, which encodes the major pilin component of T4P, was required for the Δ*flgK* mutant to suppress WT swarming on 0.5% M8 agar (Fig. 3A). To assess whether Δ*flgK* cells needed functional pili to repress the WT, Δ*flgK* lacking either *pilU* (reduced T4P retraction) or *pilT* (no T4P retraction) were mixed with the WT. At all ratios tested, Δ*flgK*Δ*pilU* and Δ*flgK*Δ*pilT* were no longer able to repress WT swarming, like Δ*flgK*Δ*pilA*, indicating that the Δ*flgK* mutant required fully functional pili to repress population-wide swarming (Fig. 3A and Fig. S8). Complementation of *pilU* and *pilT* in Δ*flgK*Δ*pilU* and Δ*flgK*Δ*pilT*, respectively, was confirmed to restore twitching motility (Fig. S9); the effect of complementation on swarming motility was not assessed given that Δ*flgK* does not swarm. In a similar assay using 0.3% M63 agar, which supports both flagellum-mediated swimming and swarming, we found that inoculated spots of Δ*flgK* cells (Fig. 3B, red dots) decreased local expansion of the motile WT population, while spots of the Δ*flgK*Δ*pilA* mutant (Fig. 3B, purple dots) did not. In contrast to the effects of Δ*flgK* cells on flagellar motility, the Δ*flgK* mutant did not alter T4P-dependent twitching motility of the WT in a 50:50 ratio compared to the that of the WT alone (Fig. S3B). Therefore, the data show that functional T4P are required for non-flagellated cells to inhibit flagellar motility (swimming and swarming) of WT cells in co-culture.

Non-flagellated *P. aeruginosa* requires Pel matrix production to repress swarming motility in the flagellated population. We next explored whether Pel matrix production played a role in swarming repression by using a Δ*pelA* mutant, which is capable of robust swarming but lacks PelA-mediated deacetylase and hydrolase activities and, subsequently, secretion of properly modified Pel polysaccharide (34). We found that swarming by the Δ*pelA* mutant was repressed by Δ*flgK* in co-culture, similar to the WT (Fig. 4A). In contrast, Δ*flgK*Δ*pelA* did not repress WT swarming (Fig. 4A). Flagellar mutants, such as Δ*fliC*, have been reported to overexpress Pel and Psl polysaccharides (35). Both Δ*flgK* and Δ*fliC*, which repress WT swarming (Fig. 1), had increased Congo red-binding,
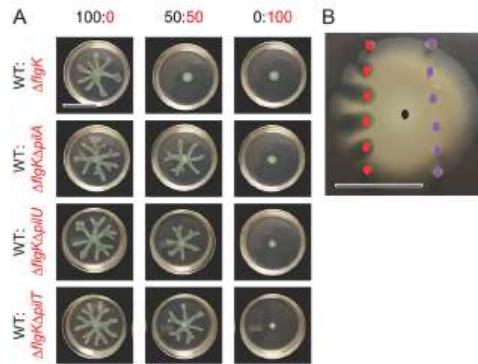
199

FIG 3 Non-flagellated *P. aeruginosa* requires functional T4P to repress flagellum-mediated motility of motile strains on soft agar. (A) Representative images of swarm assays for wild-type (WT) *P. aeruginosa* strain PA14 (swarmer, T4P+) mixed with Δ*flgK* (non-swarmer, T4P+), Δ*flgK*Δ*pilA* (non-swarmer, T4P–), Δ*flgK*Δ*pilU* (non-swarmer, reduced T4P retraction), or Δ*flgK*Δ*pilT* (non-swarmer, no T4P retraction) on M8 agar at the indicated ratios. WT is labeled in black, Δ*flgK* and derivatives are labeled in red. (B) Representative image showing the interaction between WT (black dot), Δ*flgK* (red dots), and Δ*flgK*Δ*pilA* (purple dots) for flagellum-mediated swimming motility in soft agar (03% M63 agar) after 42 h incubation. Colored dots indicate points of inoculation for the respective strains. Data are representative of three individual experiments. Scale bar, 30 mm.

which is consistent with increased Pel exopolysaccharide production (Fig. 4B and Fig. S10). Additionally, while Δ*flgK*Δ*pilA* (no T4P), Δ*flgK*Δ*pilU* (reduced T4P retraction), and Δ*flgK*Δ*pilT* (no T4P retraction) no longer repressed population-wide swarming motility (Fig. 2A), this did not appear to be due to a change in Pel production, as all Δ*flgK* mutants displayed an increase in Congo red-binding (Pel production) (Fig. 4B and Fig. S10). Together, these data show that the non-flagellated strain needs to produce Pel matrix to repress swarming motility, but the flagellated strain does not.

DISCUSSION

Based on the data presented here, we propose a model (Fig. 5) whereby a subpopulation of cells defective in flagellar motility limits the swarming motility of the entire
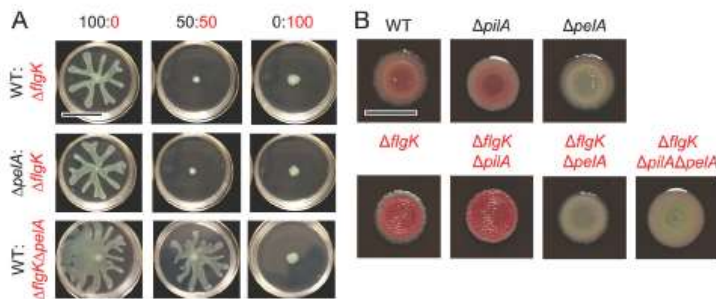
FIG 4 Pel matrix is required by the non-flagellated *P. aeruginosa* subpopulation alone to repress overall swarming motility. (A) Representative images from swarm assays of Δ*flgK* (non-flagellated, Pel+) mixed with wild-type (WT) *P. aeruginosa* strain PA14 (flagellated, Pel+) or Δ*pelA* (flagellated, Pel–), and of WT mixed with Δ*flgK*Δ*pelA* (non-flagellated, Pel–), at the indicated ratios on M8 agar. Scale bar, 30 mm. (B) Representative images of WT (flagellated, Pel+, T4P+), Δ*pilA* (flagellated, Pel+, T4P–), Δ*pelA* (flagellated, Pel–, T4P+), Δ*flgK* (non-flagellated, Pel+, T4P+), Δ*flgK*Δ*pilA* (non-flagellated, Pel+, T4P–), Δ*flgK*Δ*pelA* (non-flagellated, Pel–, T4P+), and Δ*flgK*Δ*pilA*Δ*pelA* (non-flagellated, Pel–, T4P–) grown on Congo red plates to assess Pel production. WT and derivatives are labeled in black, Δ*flgK* and derivatives are labeled in red. Scale bar, 10 mm.

200
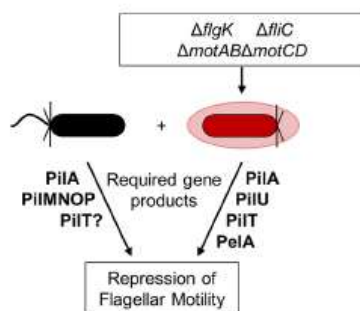
FIG 5 Summary model describing genes and gene products needed for repression of flagellum-mediated motility by non-flagellated cells in *P. aeruginosa* strain PA14. We show that a subpopulation of *P. aeruginosa* cells defective in flagellar motility (red) in co-culture with flagellated cells (black) impedes flagellum-mediated swarming motility in a retractable T4P-dependent manner (PilMNOP, PilA, PilU, PilT). We also show that Pel matrix (PelA), but only that from the non-flagellated strain, is required. PilU, PilJ, FimS, CyaAB, and Vfr were not required for repression of swarming motility.

population. Like Boyle et al. (16), we found that non-motile mutants (e.g., Δ*flgK*, Δ*fliC*) can repress WT swarming and, in our assays, only 5% of the population needed to lack flagellar motility to repress swarming by motile cells. Thus, our published findings (3) that ethanol repression of *P. aeruginosa* flagellar motility may be the result of a combination of direct motility reduction in some cells and interactions between motile and non-motile cells. The number of non-flagellated cells needed to repress WT motility may vary due to experimental conditions, such as medium type and composition. Our analyses revealed that non-flagellated cells required retractile T4P and Pel polysaccharide to inhibit the larger swarming population, and that flagellated cells required retractile T4P, but not the Vfr/cAMP signaling system, to respond to the non-flagellated population. The involvement of T4P and Pel in the recruitment of cells parallels previous studies on microcolony formation during biofilm development and aggregate formation, which has been reported in numerous contexts (e.g., O'Toole and Kolter [4]). While cAMP was not required for the repression of swarming, our previous findings showed that ethanol decreased swarming motility by increasing cyclic-di-GMP (3). Future studies will investigate the role of cyclic-di-GMP levels in the Δ*flgK*-mediated repression of WT swarming. Furthermore, given that Δ*flgK* requires retractile T4P and Pel to repress WT swarming, and overproduces Pel compared to the WT, additional studies will test how varying the amount of Pel and TFP in WT and mutant populations contributes to repression of population-wide swarming.

The involvement of T4P in swarming cells was previously reported by Anyan et al. (15), who reported that T4P impact cell-cell interactions in swarms in ways which limit the movement of cells away from the population front. T4P-null mutants have been shown to have increased swarming motility (23–25), while hyperpiliated mutants have been shown to have decreased swarming motility, compared to the WT (15, 26), suggesting that the intercellular T4P interactions we reported between flagellated and non-flagellated genotypes may also be occurring in single-strain swarms in which all cells have the potential for flagellar motility. Not only may intercellular T4P interactions be occurring in single-strain swarms, but also appropriate flagellum-mediated shear forces during swarming motility (36). This could account for the ability of Δ*pilU*, a hyperpiliated mutant with fragile and readily sheared T4P, to swarm; unlike Δ*pilT*, a hyperpiliated mutant with more robust T4P (26, 30). Future studies will determine whether T4P play direct roles in cell-cell interactions or indirect roles in structuring the community.

The WT and Δ*pelA* mutant responded similarly to non-flagellated cells, while Δ*flgK*Δ*pelA* was no longer able to repress swarming, suggesting that not all cells need

201

to produce exopolysaccharide to repress swarming. Our findings that Pel production is only necessary in the non-flagellated subpopulation is supported by published data showing that ethanol not only decreases *P. aeruginosa* flagellar motility (3), but increases Pel production (37). Pel has been suggested to repress motility via the steric hindrance of flagella (3, 38), but further studies are needed to test this hypothesis. The involvement of Pel in the interaction between flagellated and non-flagellated cells is particularly interesting in light of recent work by Whitfield et al. (39), which found that the Pel biosynthetic locus is widespread across Gram-positive and Gram-negative bacteria. Future studies will determine whether Pel is specifically detected by a T4P-dependent mechanism.

In the studies here, we seeded a low percentage of non-swarming cells into a swarming population, reminiscent of genetically heterogeneous populations in the CF airway or other chronic infections (19, 40, 41), as well as during normal environmental growth (41, 42). Additionally, clinical *P. aeruginosa* isolates from the CF lung have diverse motility phenotypes (19). This diversity in motility is even observed within single patients (19). We hypothesize that such a mechanism promotes inter- and intraspecies interactions. The strong implication of these findings is that in a mixed population with a subpopulation of cells deficient in flagellar motility, the entire population can be brought to a halt. Similarly, in a population in which a significant number of cells have stopped swimming or swarming, the further addition of even a few flagellar-mutant cells can suppress the motility of the entire population (e.g., the ethanol studies mentioned above). As *P. aeruginosa* populations inherently have some number of non-motile or inactive cells (3), future studies are required to determine how strain background or mutant genotype affects phenotypic heterogeneity among isogenic cells.

MATERIALS AND METHODS

Strains and media. Strains used in this study are listed in Table 1. *P. aeruginosa* strain PA14 and derivatives were routinely cultured on lysogeny broth (LB; 1% tryptone [wt/vol], 0.5% yeast extract [wt/vol], and 0.5% NaCl [wt/vol]) solidified with 1.5% agar or in LB broth at 37°C with shaking. For *P. aeruginosa* phenotypic assays, either M63 [22 mM KH_2PO_4, 40 mM K_2HPO_4, and 15 mM $(NH_4)_2SO_4$] or M8 (42 mM Na_2PO_4, 22 mM KH_2PO_4, and 8.5 mM NaCl) minimal salts medium supplemented with $MgSO_4$ (1 mM), glucose (0.2%), and Casamino acids (CAA; 0.5%) were used as indicated. Complemented strains containing genes regulated by an arabinose-inducible promoter (P_{BAD}) were grown in the presence of 0.25% arabinose.

Construction and complementation of mutant strains. Plasmids used in this study are listed in Table 1. Plasmid constructs for making in-frame deletions and arabinose-inducible complementation strains were constructed using either a *Saccharomyces cerevisiae* recombination technique, described previously (43), or Gibson assembly. All plasmids were sequenced at the Molecular Biology Core at the Geisel School of Medicine at Dartmouth. Plasmids were introduced into *P. aeruginosa* by conjugation via S17/lambda pir *E. coli*. Merodiploids were selected by drug resistance, and double recombinants were obtained using sucrose counter-selection and genotype screening by PCR.

Swarming motility assays. Swarm assays were performed as previously described (44). Briefly, 9 mL of M8 medium with 0.5% agar (swarm agar) was poured into 60 × 15 mm plates and allowed to dry at room temperature (~25°C) for 3 h prior to inoculation. The indicated strains were grown for 16 h, then each was washed in 1× phosphate-buffered saline (PBS) and then normalized to an OD_{600} (optical density at 600 nm) of 1. Indicated isolates were then mixed at the indicated ratios to a final volume of 100 μL. Each plate was inoculated with 0.5 μL of the liquid culture mixture, and the plates were incubated face-up at 37°C for up to 22 h, in stacks of no more than four plates. Each mixture was inoculated in three to four replicates and assessed on at least three separate days. Images were captured using a Canon EOS Rebel T6i camera and images assessed for swarm repression.

Swimming motility assays. Swim assays were performed as previously described (44). Briefly, M63 medium solidified with 0.3% agar (soft agar) was poured into 100 × 15 mm petri plates and allowed to dry at room temperature (~25°C) for 3 h prior to inoculation. The indicated strains were grown for 16 h, then each was washed in 1× PBS and then normalized to an OD_{600} of 1. Indicated isolates were then mixed at the indicated ratios to a final volume of 100 μL. Sterile toothpicks or P20 pipette tips were used to inoculate bacterial mixes into the center of the agar without touching the bottom of the plate. No more than four bacterial mixtures were assayed per plate. Plates were incubated upright at 37°C in stacks of no more than four plates per stack for 18 to 20 h.

Twitching motility assays. T-broth (1% tryptone [wt/vol], 0.5% NaCl [wt/vol]) medium solidified with 1.5% agar was poured into petri plates and allowed to dry at room temperature (~25°C) for 3 h. Overnight (16 h) cultures were washed once in 1× PBS and then normalized to an OD_{600} of 1. Plates were inoculated by dipping a sterile toothpick or P20 pipette tip into the washed and normalized cultures and then inserting the toothpick into the agar until it touched the bottom of the plate. Plates were then incubated at 37°C for 46 h after which time the agar was removed and the plate incubated in 0.1% (wt/vol) crystal violet

202

TABLE 1 Strains and plasmids used in this study[a]

Strain or plasmid	Lab strain	Description	Source or reference
P. aeruginosa			
PA14	DH123	WT	45
PA14 *att::lacZ*	DH22	WT with constitutive expression of *lacZ*	46
Δ*flgK*	DH1075	*flgK*::Tn5B30(Tc); nonmotile	4
Δ*fliC*	DH3543	Unmarked deletion of *fliC*	This study
Δ*motABCD*	SMC7230	Unmarked deletion of *motABCD*	This study
Δ*pilMNOP*	DH2705	Unmarked deletion of *pilMNOP*	6
Δ*pilA*	DH2636	Unmarked deletion of *pilA*	24
Δ*pelA*	DH97 or SMC2893	Unmarked deletion of *pelA*	47
Δ*flgK*Δ*pelA*	DH3541	Unmarked deletion of *flgK* and *pelA*	11
Δ*flgK*Δ*pilA*	DH3539	Unmarked deletion of *flgK* and *pilA*	11
Δ*flgK*Δ*pilA*Δ*pelA*	DH3542	Unmarked deletion of *flgK*, *pilA*, and *pelA*	11
Δ*pilT*	DH3591 or SMC7302	Unmarked deletion of *pilT*	31
Δ*pilU*	DH3592 or SMC7304	Unmarked deletion of *pilU*	31
Δ*pilJ*	DH2637 or SMC2992	Unmarked deletion of *pilJ*	48
Δ*fimS*	SMC6967	Unmarked deletion of *fimS*	6
Δ*cyaAB*	DH2648 or SMC6707	Unmarked deletion of *cyaAB*	6
Δ*vfr*	DH2701 or SMC6722	Unmarked deletion of *vfr*	6
Δ*pilU att::*P$_{BAD}$-ara	SMC7826	Unmarked Δ*pilU* (DH3592/SMC7304) with arabinose-inducible promoter at the *att*Tn7 site, control, Gm^R	This study
Δ*pilU att::*P$_{BAD}$-*pilU*	SMC7827	Unmarked Δ*pilU* (DH3592/SMC7304) complemented with arabinose-inducible *pilU* at the *att*Tn7 site, Gm^R	This study
Δ*pilT att::*P$_{BAD}$-ara	SMC8882	Unmarked Δ*pilT* (DH3591/SMC7302) with arabinose-inducible promoter at the *att*Tn7 site, control, Gm^R	This study
Δ*pilT att::*P$_{BAD}$-*pilT*	SMC8883	Unmarked Δ*pilT* (DH3591/SMC7302) complemented with arabinose-inducible *pilT* at the *att*Tn7 site, Gm^R	This study
Δ*flgK*Δ*pilU*	DH3950	Unmarked deletion of *flgK* and *pilU*	This study
Δ*flgK*Δ*pilT*	DH3951	Unmarked deletion of *flgK* and *pilT*	This study
Δ*flgK*Δ*pilU att::*P$_{BAD}$-ara	DH3952	Unmarked deletion of *flgK* and *pilU* with arabinose-inducible promoter at the *att*Tn7 site, control, Gm^R	This study
Δ*flgK*Δ*pilU att::*P$_{BAD}$-*pilU*	DH3953	Unmarked deletion of *flgK* and *pilU* complemented with arabinose-inducible *pilU* at the *att*Tn7 site, control, Gm^R	This study
Δ*flgK*Δ*pilT att::*P$_{BAD}$-ara	DH3954	Unmarked deletion of *flgK* and *pilT* with arabinose-inducible promoter at the *att*Tn7 site, control, Gm^R	This study
Δ*flgK*Δ*pilT att::*P$_{BAD}$-*pilT*	DH3955	Unmarked deletion of *flgK* and *pilT* complemented with arabinose-inducible *pilT* at the *att*Tn7 site, control, Gm^R	This study
E. coli			
S17 λpir	DH71	Used as a conjugation partner for introducing pMQ30- and GH121-based plasmids	
Plasmids			
pUX-BF13	SMC1852	Helper plasmid that provides the transposition functions for Tn7 in *trans*, Ap^R	49
pMQ56	SMC3242	pMQ56-miniTn7 for insertion at the *att*Tn7 site, Ap^R	43
pBAD-ara	SMC7453	pMQ56-miniTn7 plasmid containing arabinose-inducible P$_{BAD}$ and *araC* for insertion at the *att*Tn7 site, Ap^R	This study
pPilU-His	SMC7777	pMQ56-miniTn7 plasmid containing 6× His-tagged *pilU* regulated by arabinose-inducible P$_{BAD}$ and *araC* for insertion at the *att*Tn7 site, Ap^R, Gm^R	This study
pPilT-His	SMC8873	pMQ56-miniTn7 plasmid containing 6× His-tagged *pilT* regulated by arabinose-inducible P$_{BAD}$ and *araC* for insertion at the *att*Tn7 site, Ap^R, Gm^R	This study
pMQ30	DH2620	Suicide vector for allelic replacement; Gm^R	43
pMQ30-del-pilT	SMC7298	Construct for in-frame deletion of *pilT*	31
pMQ30-del-pilU	SMC7299	Construct for in-frame deletion of *pilU*	31

[a]WT, wild type.

for 10 min. Plates were then washed three times in water and dried at room temperature. Images of the dried, stained twitch area were taken and twitch diameter was measured.

Competition experiments. Competition assays were performed to determine relative growth of selected *P. aeruginosa* strains. Strains were grown for 16 h and then 1 mL of culture was pelleted at 15,682 × *g* for 2 min, washed once in 1 mL 1× PBS, and then resuspended in 1 mL 1× PBS. The OD$_{600}$ of each culture was

203

normalized to 1. The strains to be competed were mixed at the indicated ratios to a final volume of 100 μl, and then 0.5 μL of the combined suspension was spotted onto a 0.22-μm polycarbonate filter (Millipore) placed on the surface of a swarm plate, in triplicate. Plates were incubated at 37°C. Filters were then transferred to a 1.5-mL microcentrifuge tube, and filter-associated cells were resuspended by adding 1 mL 1× PBS + 0.05% Triton X-100 detergent and agitating the tubes at high speed for 2 min using a Disruptor Genie (Zymo). This suspension as well as the starting inoculum were diluted, spread on LB plates supplemented with 150 μg/mL 5-bromo-4-chloro-3-indolyl-β-D-galactopyranoside (X-Gal) using glass beads, and incubated at 30°C until blue colonies were visible (~ 24 h). The numbers of blue and white colonies per plate were counted and recorded to determine the relative abundance of each strain.

Phage susceptibility assays. Phage susceptibility was analyzed by the cross-streak method or by spotting phage directly onto a lawn of *P. aeruginosa*. For the cross-streak method, *P. aeruginosa* strains were grown for 16 h in LB, diluted 1:100 in LB, and then grown to an OD$_{600}$ of 0.5 to 0.7. Then, 4 μL of phage DMS3 vir strain was spotted on the side of an LB agar plate and dragged across the agar surface in a straight line before being allowed to absorb into the agar. Once absorbed, 4 μL of each *P. aeruginosa* strain was spotted at the top of the agar and dragged downward in a straight line through the phage line. Plates were incubated at 37°C for 16 h.

Alternatively, 1% M8 agar plates (60 × 15 mm) containing 0.2% glucose (vol/vol), 0.5% Casamino Acids (vol/vol), and 1 mM MgSO$_4$ were prepared and cooled to room temperature. A 50-μL volume of *P. aeruginosa* 16 h cultures was added to 1 mL of 0.5% warm top agar (M8 medium and supplements). The mixture was gently mixed and quickly poured onto M8 agar plates. Plates were swirled to ensure even spreading of top agar. Once cooled, 2 μL of phage DMS3 vir strain was spotted onto the center of the plate and allowed to dry before incubating plates at 37°C for 16 h.

Congo red-binding assay. Cultures were grown in 5 mL LB for 16 h at 37°C with rolling. Culture aliquots were washed once and resuspended in sterile deionized water. Washed cells were spotted (3 μL) onto Congo red plates (1% tryptone [wt/vol], 1.5% agar, 40 μg/mL Congo red, 20 μg/mL Coomassie blue). Plates were grown for 16 h at 37°C and then moved to room temperature for 3 days to allow for color development.

Statistical analysis. A one-way analysis of variance with multiple comparisons was performed pairwise between all isolates and mixtures using GraphPad Prism 6 software (GraphPad, La Jolla, CA).

SUPPLEMENTAL MATERIAL

Supplemental material is available online only.
SUPPLEMENTAL FILE 1, PDF file, 0.8 MB.

REFERENCES

1. Hogan DA, Kolter R. 2002. *Pseudomonas-Candida* interactions: an ecological role for virulence factors. Science 296:2229–2232. https://doi.org/10.1126/science.1070784.
2. Limoli DH, Warren EA, Yarrington KD, Donegan NP, Cheung AL, O'Toole GA. 2019. Interspecies interactions induce exploratory motility in *Pseudomonas aeruginosa*. Elife 8:e47365. https://doi.org/10.7554/eLife.47365.
3. Lewis KA, Baker AE, Chen AI, Harty CE, Kuchma SL, O'Toole GA, Hogan DA. 2019. Ethanol decreases *Pseudomonas aeruginosa* flagellar motility through the regulation of flagellar stators. J Bacteriol 201:e00285-17. https://doi.org/10.1128/JB.00285-19.
4. O'Toole GA, Kolter R. 1998. Flagellar and twitching motility are necessary for *Pseudomonas aeruginosa* biofilm development. Mol Microbiol 30:295–304. https://doi.org/10.1046/j.1365-2958.1998.01062.x.
5. Zhao K, Tseng BS, Beckerman B, Jin F, Gibiansky ML, Harrison JJ, Luijten E, Parsek MR, Wong GCL. 2013. Psl trails guide exploration and microcolony formation in *Pseudomonas aeruginosa* biofilms. Nature 497:388–391. https://doi.org/10.1038/nature12155.
6. Luo Y, Zhao K, Baker AE, Kuchma SL, Coggan KA, Wolfgang MC, Wong GCL, O'Toole GA. 2015. A hierarchical cascade of second messengers regulates *Pseudomonas aeruginosa* surface behaviors. mBio 6:e02456-14. https://doi.org/10.1128/mBio.02456-14.
7. O'Toole GA, Wong GC. 2016. Sensational biofilms: surface sensing in bacteria. Curr Opin Microbiol 30:139–146. https://doi.org/10.1016/j.mib.2016.02.004.
8. Lee CK, Vachier J, de Anda J, Zhao K, Baker AE, Bennett RR, Armbruster CR, Lewis KA, Tarnopol RL, Lomba CJ, Hogan DA, Parsek MR, O'Toole GA,

204

Golestanian R, Wong GCL. 2020. Social cooperativity of bacteria during reversible surface attachment in young biofilms: a quantitative comparison of *Pseudomonas aeruginosa* PA14 and PAO1. mBio 11:e02644-19. https://doi.org/10.1128/mBio.02644-19.

9. Boyd CD, Smith TJ, El-Kirat-Chatel S, Newell PD, Dufrene YF, O'Toole GA. 2014. Structural features of the *Pseudomonas fluorescens* biofilm adhesin LapA required for LapG-dependent cleavage, biofilm formation, and cell surface localization. J Bacteriol 196:2775–2788 https://doi.org/10.1128/JB.01629-14.

10. Parsek MR. 2016. Controlling the connections of cells to the biofilm matrix. J Bacteriol 198:12–14. https://doi.org/10.1128/JB.00865-15.

11. Ribbe J, Baker AE, Euler S, O'Toole GA, Maier B. 2017. Role of cyclic di-GMP and exopolysaccharide in type IV pilus dynamics. J Bacteriol 199:e00859-16. https://doi.org/10.1128/JB.00859-16.

12. Ma L, Conover M, Lu H, Parsek MR, Bayles K, Wozniak DJ. 2009. Assembly and development of the *Pseudomonas aeruginosa* biofilm matrix. PLoS Pathog 5:e1000354. https://doi.org/10.1371/journal.ppat.1000354.

13. Colvin KM, Irie Y, Tart CS, Urbano R, Whitney JC, Ryder C, Howell PL, Wozniak DJ, Parsek MR. 2012. The Pel and Psl polysaccharides provide *Pseudomonas aeruginosa* structural redundancy within the biofilm matrix. Environ Microbiol 14:1913–1928. https://doi.org/10.1111/j.1462-2920.2011.02657.x.

14. Wei Q, Ma LZ. 2013. Biofilm matrix and its regulation in *Pseudomonas aeruginosa*. Int J Mol Sci 14:20983–21005. https://doi.org/10.3390/ijms141020983.

15. Anyan ME, Amiri A, Harvey CW, Tierra G, Morales-Soto N, Driscoll CM, Alber MS, Shrout JD. 2014. Type IV pili interactions promote intercellular association and moderate swarming of *Pseudomonas aeruginosa*. Proc Natl Acad Sci U S A 111:18013–18018. https://doi.org/10.1073/pnas.1414661111.

16. Boyle KE, Monaco HT, Deforet M, Yan J, Wang Z, Rhee K, Xavier JB. 2017. Metabolism and the evolution of social behavior. Mol Biol Evol 34:2367–2379. https://doi.org/10.1093/molbev/msx174.

17. Lozano C, Azcona-Gutierrez JM, Van Bambeke F, Saenz Y. 2018. Great phenotypic and genetic variation among successive chronic *Pseudomonas aeruginosa* from a cystic fibrosis patient. PLoS One 13:e0204167. https://doi.org/10.1371/journal.pone.0204167.

18. Mahenthiralingam E, Campbell ME, Speert DP. 1994. Nonmotility and phagocytic resistance of *Pseudomonas aeruginosa* isolates from chronically colonized patients with cystic fibrosis. Infect Immun 62:596–605. https://doi.org/10.1128/iai.62.2.596-605.1994.

19. Workentine ML, Sibley CD, Glezerson B, Purighalla S, Norgaard-Gron JC, Parkins MD, Rabin HR, Surette MG. 2013. Phenotypic heterogeneity of *Pseudomonas aeruginosa* populations in a cystic fibrosis patient. PLoS One 8:e60225. https://doi.org/10.1371/journal.pone.0060225.

20. Turner KH, Everett J, Trivedi U, Rumbaugh KP, Whiteley M. 2014. Requirements for *Pseudomonas aeruginosa* acute burn and chronic surgical wound infection. PLoS Genet 10:e1004518. https://doi.org/10.1371/journal.pgen.1004518.

21. Ha DG, Kuchma SL, O'Toole GA. 2014. Plate-based assay for swarming motility in *Pseudomonas aeruginosa*. Methods Mol Biol 1149:67–72. https://doi.org/10.1007/978-1-4939-0473-0_8.

22. Tremblay J, Deziel E. 2008. Improving the reproducibility of *Pseudomonas aeruginosa* swarming motility assays. J Basic Microbiol 48:509–515. https://doi.org/10.1002/jobm.200800030.

23. Shrout JD, Chopp DL, Just CL, Hentzer M, Givskov M, Parsek MR. 2006. The impact of quorum sensing and swarming motility on *Pseudomonas aeruginosa* biofilm formation is nutritionally conditional. Mol Microbiol 62:1264–1277. https://doi.org/10.1111/j.1365-2958.2006.05421.x.

24. Kuchma SL, Ballok AE, Merritt JH, Hammond JH, Lu W, Rabinowitz JD, O'Toole GA. 2010. Cyclic-di-GMP-mediated repression of swarming motility by *Pseudomonas aeruginosa*: the *pilY1* gene and its impact on surface-associated behaviors. J Bacteriol 192:2950–2964. https://doi.org/10.1128/JB.01642-09.

25. Kuchma SL, Griffin EF, O'Toole GA. 2012. Minor pilins of the type IV pilus system participate in the negative regulation of swarming motility. J Bacteriol 194:5388–5403. https://doi.org/10.1128/JB.00899-12.

26. Whitchurch CB, Mattick JS. 1994. Characterization of a gene, *pilU*, required for twitching motility but not phage sensitivity in *Pseudomonas aeruginosa*. Mol Microbiol 13:1079–1091. https://doi.org/10.1111/j.1365-2958.1994.tb00499.x.

27. Tammam S, Sampaleanu LM, Koo J, Sundaram P, Ayers M, Chong PA, Forman-Kay JD, Burrows LL, Howell PL. 2011. Characterization of the PilN, PilO and PilP type IVa pilus subcomplex. Mol Microbiol 82:1496–1514. https://doi.org/10.1111/j.1365-2958.2011.07903.x.

28. Webster SS, Lee CK, Schmidt WC, Wong GCL, O'Toole GA. 2021. Interaction between the type 4 pili machinery and a diguanylate cyclase fine-

tune c-di-GMP levels during early biofilm formation. Proc Natl Acad Sci U S A 118:e2105566118. https://doi.org/10.1073/pnas.2105566118.

29. Burrows LL. 2005. Weapons of mass retraction. Mol Microbiol 57:878–888. https://doi.org/10.1111/j.1365-2958.2005.04703.x.

30. Chiang P, Burrows LL. 2003. Biofilm formation by hyperpiliated mutants of *Pseudomonas aeruginosa*. J Bacteriol 185:2374–2378. https://doi.org/10.1128/JB.185.7.2374-2378.2003.

31. Lee CK, de Anda J, Baker AE, Bennett RR, Luo Y, Lee EY, Keefe JA, Helali JS, Ma J, Zhao K, Golestanian R, O'Toole GA, Wong GCL. 2018. Multigenerational memory and adaptive adhesion in early bacterial biofilm communities. Proc Natl Acad Sci U S A 115:4471–4476. https://doi.org/10.1073/pnas.1720071115.

32. Shen Y, Siryaporn A, Lecuyer S, Gitai Z, Stone HA. 2012. Flow directs surface-attached bacteria to twitch upstream. Biophys J 103:146–151. https://doi.org/10.1016/j.bpj.2012.05.045.

33. Landry RM, An D, Hupp JT, Singh PK, Parsek MR. 2006. Mucin-*Pseudomonas aeruginosa* interactions promote biofilm formation and antibiotic resistance. Mol Microbiol 59:142–151. https://doi.org/10.1111/j.1365-2958.2005.04941.x.

34. Marmont LS, Whitfield GB, Rich JD, Yip P, Giesbrecht LB, Stremick CA, Whitney JC, Parsek MR, Harrison JJ, Howell PL. 2017. PelA and PelB proteins form a modification and secretion complex essential for Pel polysaccharide-dependent biofilm formation in *Pseudomonas aeruginosa*. J Biol Chem 292:19411–19422. https://doi.org/10.1074/jbc.M117.812842.

35. Harrison JJ, Almblad H, Irie Y, Wolter DJ, Eggleston HC, Randall TE, Kitzman JO, Stackhouse B, Emerson JC, McNamara S, Larsen TJ, Shendure J, Hoffman LR, Wozniak DJ, Parsek MR. 2020. Elevated exopolysaccharide levels in *Pseudomonas aeruginosa* flagellar mutants have implications for biofilm growth and chronic infections. PLoS Genet 16:e1008848. https://doi.org/10.1371/journal.pgen.1008848.

36. Rodesney CA, Roman B, Dhamani N, Cooley BJ, Katira P, Touhami A, Gordon VD. 2017. Mechanosensing of shear by *Pseudomonas aeruginosa* leads to increased levels of the cyclic-di-GMP signal initiating biofilm development. Proc Natl Acad Sci U S A 114:5906–5911. https://doi.org/10.1073/pnas.1703255114.

37. Chen AI, Dolben EF, Okegbe C, Harty CE, Golub Y, Thao S, Ha DG, Willger SD, O'Toole GA, Harwood CS, Dietrich LE, Hogan DA. 2014. *Candida albicans* ethanol stimulates *Pseudomonas aeruginosa* WspR-controlled biofilm formation as part of a cyclic relationship involving phenazines. PLoS Pathog 10:e1004480. https://doi.org/10.1371/journal.ppat.1004480.

38. Merritt JH, Brothers KM, Kuchma SL, O'Toole GA. 2007. SadC reciprocally influences biofilm formation and swarming motility via modulation of exopolysaccharide production and flagellar function. J Bacteriol 189:8154–8164. https://doi.org/10.1128/JB.00585-07.

39. Whitfield GB, Marmont LS, Bundalovic-Torma C, Razvi E, Roach EJ, Khursigara CM, Parkinson J, Howell PL. 2020. Discovery and characterization of a Gram-positive Pel polysaccharide biosynthetic gene cluster. PLoS Pathog 16:e1008281. https://doi.org/10.1371/journal.ppat.1008281.

40. Darch SE, McNally A, Harrison F, Corander J, Barr HL, Paszkiewicz K, Holden S, Fogarty A, Crusz SA, Diggle SP. 2015. Recombination is a key driver of genomic and phenotypic diversity in a *Pseudomonas aeruginosa* population during cystic fibrosis infection. Sci Rep 5:7649. https://doi.org/10.1038/srep07649.

41. Head NE, Yu H. 2004. Cross-sectional analysis of clinical and environmental isolates of *Pseudomonas aeruginosa*: biofilm formation, virulence, and genome diversity. Infect Immun 72:133–144. https://doi.org/10.1128/IAI.72.1.133-144.2004.

42. Grosso-Becerra MV, Santos-Medellin C, Gonzalez-Valdez A, Mendez JL, Delgado G, Morales-Espinosa R, Servin-Gonzalez L, Alcaraz LD, Soberon-Chavez G. 2014. *Pseudomonas aeruginosa* clinical and environmental isolates constitute a single population with high phenotypic diversity. BMC Genomics 15:318. https://doi.org/10.1186/1471-2164-15-318.

43. Shanks RM, Caiazza NC, Hinsa SM, Toutain CM, O'Toole GA. 2006. Saccharomyces cerevisiae-based molecular tool kit for manipulation of genes from gram-negative bacteria. Appl Environ Microbiol 72:5027–5036. https://doi.org/10.1128/AEM.00682-06.

44. Ha DG, Richman ME, O'Toole GA. 2014. Deletion mutant library for investigation of functional outputs of cyclic diguanylate metabolism in *Pseudomonas aeruginosa* PA14. Appl Environ Microbiol 80:3384–3393. https://doi.org/10.1128/AEM.00299-14.

45. Rahme LG, Stevens EJ, Wolfort SF, Shao J, Tompkins RG, Ausubel FM. 1995. Common virulence factors for bacterial pathogenicity in plants and animals. Science 268:1899–1902. https://doi.org/10.1126/science.7604262.

205

46. Clay ME, Hammond JH, Zhong F, Chen X, Kowalski CH, Lee AJ, Porter MS, Hampton TH, Greene CS, Pletneva EV, Hogan DA. 2020. *Pseudomonas aeruginosa lasR* mutant fitness in microoxia is supported by an Anr-regulated oxygen-binding hemerythrin. Proc Natl Acad Sci U S A 117:3167–3173. https://doi.org/10.1073/pnas.1917576117.

47. Friedman L, Kolter R. 2004. Genes involved in matrix formation in *Pseudomonas aeruginosa* PA14 biofilms. Mol Microbiol 51:675–690. https://doi.org/10.1046/j.1365-2958.2003.03877.x.

48. Belete B, Lu H, Wozniak DJ. 2008. *Pseudomonas aeruginosa* AlgR regulates type IV pilus biosynthesis by activating transcription of the *fimU-pilVWXY1Y2E* operon. J Bacteriol 190:2023–2030. https://doi.org/10.1128/JB.01623-07.

49. Hojberg O, Schnider U, Winteler HV, Sorensen J, Haas D. 1999. Oxygen-sensing reporter strain of *Pseudomonas fluorescens* for monitoring the distribution of low-oxygen habitats in soil. Appl Environ Microbiol 65:4085–4093. https://doi.org/10.1128/AEM.65.9.4085-4093.1999.

206
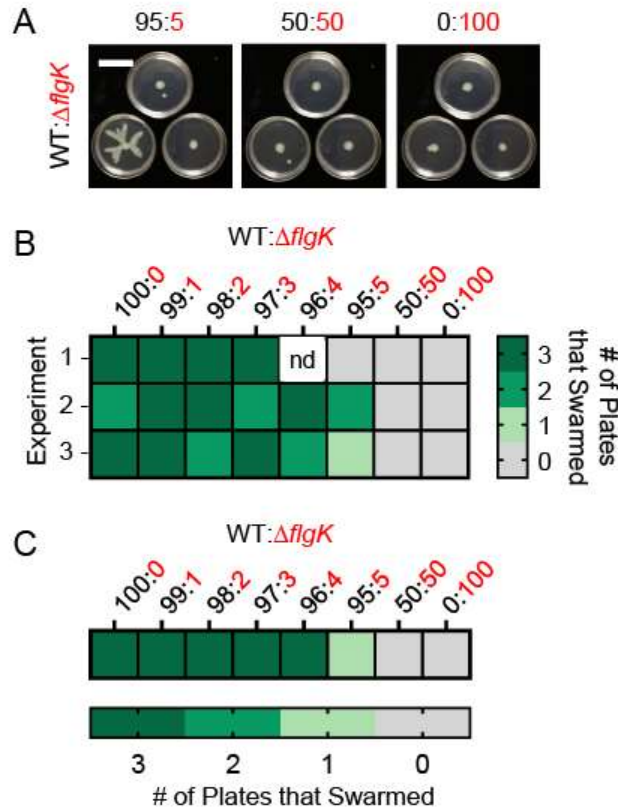
Fig. S1. Establishing the lower limit of Δ*flgK* cells that is sufficient to repress motility A. Representative images from swarm assays of wild-type *P. aeruginosa* strain PA14 (WT) mixed with Δ*flgK* (non-swarmer) at 95:5, 50:50, and all Δ*flgK* mutant. Images show three technical replicates from a single experiment. Consistent with published observations, there can be heterogeneity in swarm phenotypes despite best efforts for uniform assay conditions. Scale bar: 30 mm. **B.** Heatmap showing the number of plates (technical replicates) that swarmed at each ratio in three individual experiments (1-3). **C.** Heatmap showing the average number of plates (technical replicates) that swarmed at each ratio using data in **B**. nd, not determined.
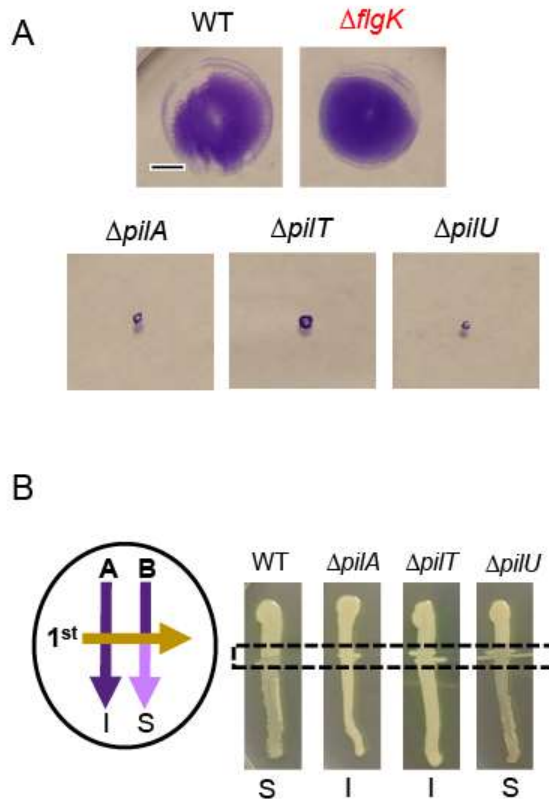
Fig. S2. A. Representative images from twitch assays of wild-type (WT) *P. aeruginosa* strain PA14, Δ*flgK*, Δ*pilA*, Δ*pilT*, and Δ*pilU* on T-broth agar after 46 h incubation at 37ºC. **B.** Cross-streak assay set up. On an LB plate, the phage lysate is first streaked horizontally (orange arrow) followed by vertical streaks of each bacterial strain. "S" denotes strains that are sensitive to phage uptake and lysis (lighter cell density, light purple) and "I" denotes strains that are insensitive to phage uptake and lysis (heavier cell density, dark purple). Representative images of the cross-streak assay of WT, Δ*pilA*, Δ*pilT*, and Δ*pilU* showing sensitivity and insensitivity to phage DMS3. Dashed line indicates phage line. WT and derivatives are labeled in black while Δ*flgK* is labeled in red. Data are representative of three individual experiments showing similar results. Scale bar: 5 mm
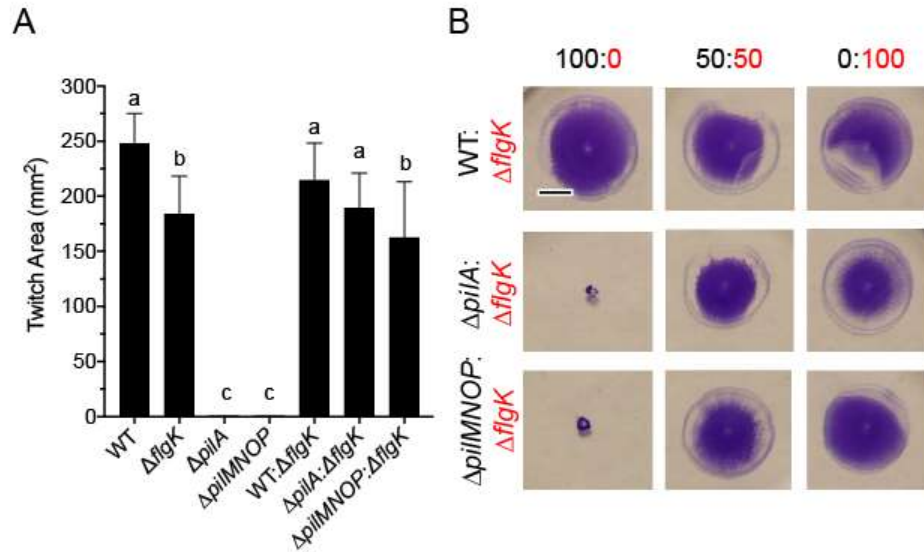
Fig. S3. Motility heterogeneity does not impact T4P-mediated twitching motility.
A. Quantified results of the twitch assay of individual and mixed samples of the
following strains: wild-type (WT) *P. aeruginosa* strain PA14, Δ*flgK*, Δ*pilA*, and
Δ*pilMNOP*. Mixed samples were done at a 50:50 ratio. Same letters indicate samples
that are not significantly different, while different letters indicate significant differences
($p<0.05$), as determined by One-way ANOVA with multiple comparisons. **B.**
Representative images from twitch assays of WT (flagellated and T4P+), Δ*pilA*
(flagellated and T4P-), and Δ*pilMNOP* (flagellated and T4P-) mixed with Δ*flgK* (non-
flagellated and T4P+) at the indicated ratios on T-broth agar. WT and derivatives are
labeled in black while Δ*flgK* is labeled in red. Data are **A.** the average or **B.**
representative of three individual experiments. Scale bar: 5 mm
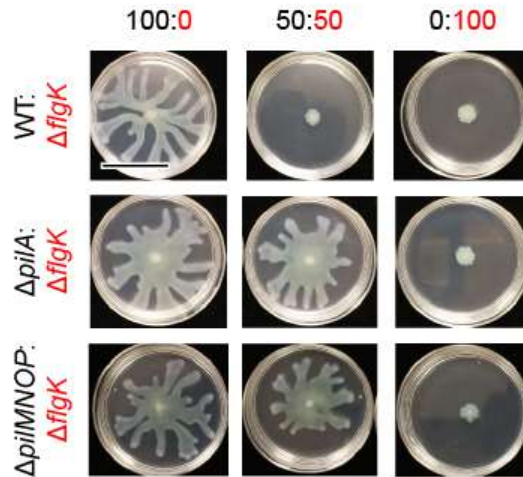
Fig. S4. Flagellated *P. aeruginosa* requires both *pilA* and *pilMNOP* for non-flagellated Δ*flgK* to repress swarming. Representative images from swarm assays of wild-type (WT) *P. aeruginosa* strain PA14 (flagellated and T4P+), Δ*pilA* (flagellated and T4P-), or Δ*pilMNOP* (flagellated and T4P-) mixed with Δ*flgK* (non-flagellated and T4P+) at ratios indicated. WT and derivatives are labeled in black while Δ*flgK* is labeled in red. Data are representative of three individual experiments showing similar results. Scale bar: 30 mm
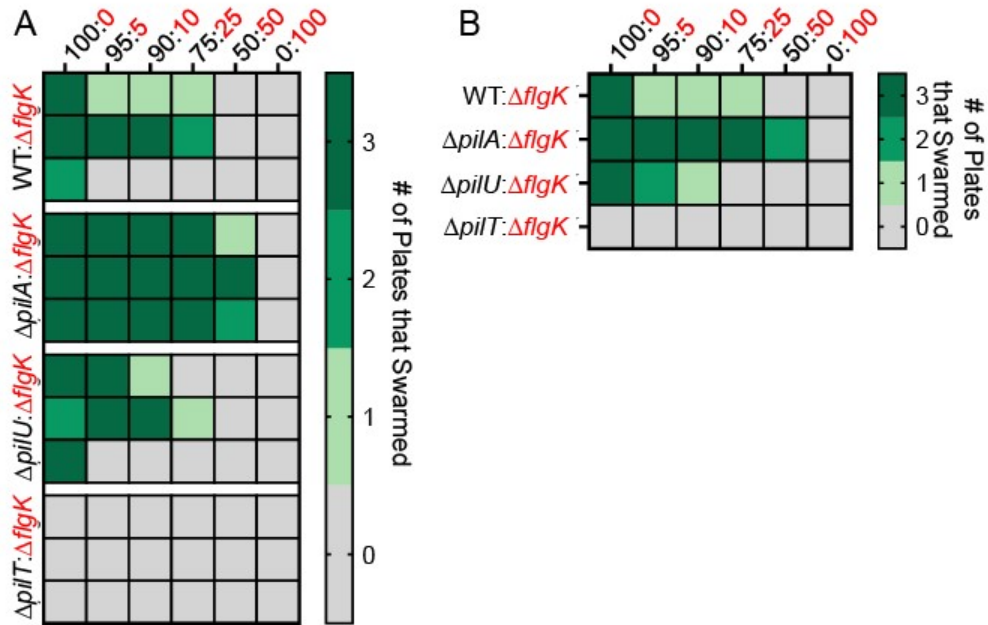
Fig. S5. The hyperpiliated Δ*pilU* mutant with reduced T4P retraction swarms and is repressed by Δ*flgK*, but the hyperpiliated Δ*pilT* mutant with no T4P retraction is unable to swarm. A. Heatmap showing the number of plates (technical replicates) that swarmed at each ratio for three individual experiments represented by three different rows. **B.** Heatmap showing the average number of plates (technical replicates) that swarmed at each ratio using data in **A**. WT and its derivatives are labeled in black while Δ*flgK* is labeled in red.
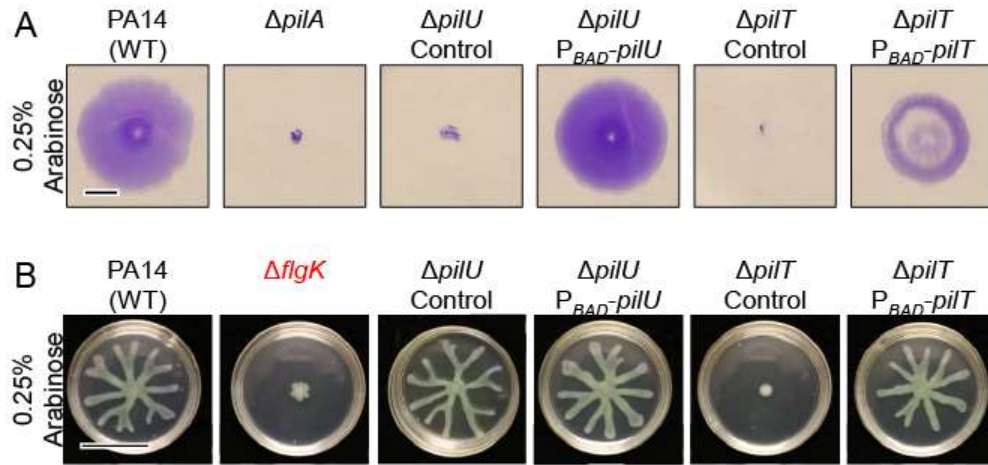
Fig. S6. Complementation of Δ*pilU* and Δ*pilT*. Representative images from **A.** twitch assays and **B.** swarm assays of wild-type (WT) *P. aeruginosa* strain PA14, Δ*pilA*, Δ*pilU*, Δ*pilU* P$_{BAD}$-*pilU* (complemented), Δ*pilT*, and Δ*pilT* P$_{BAD}$-*pilT* on T-broth agar containing 0.25% arabinose after 46 h incubation at 37°C. Data are representative of three individual experiments. **A.** Scale bar: 5 mm **B.** Scale bar: 30 mm
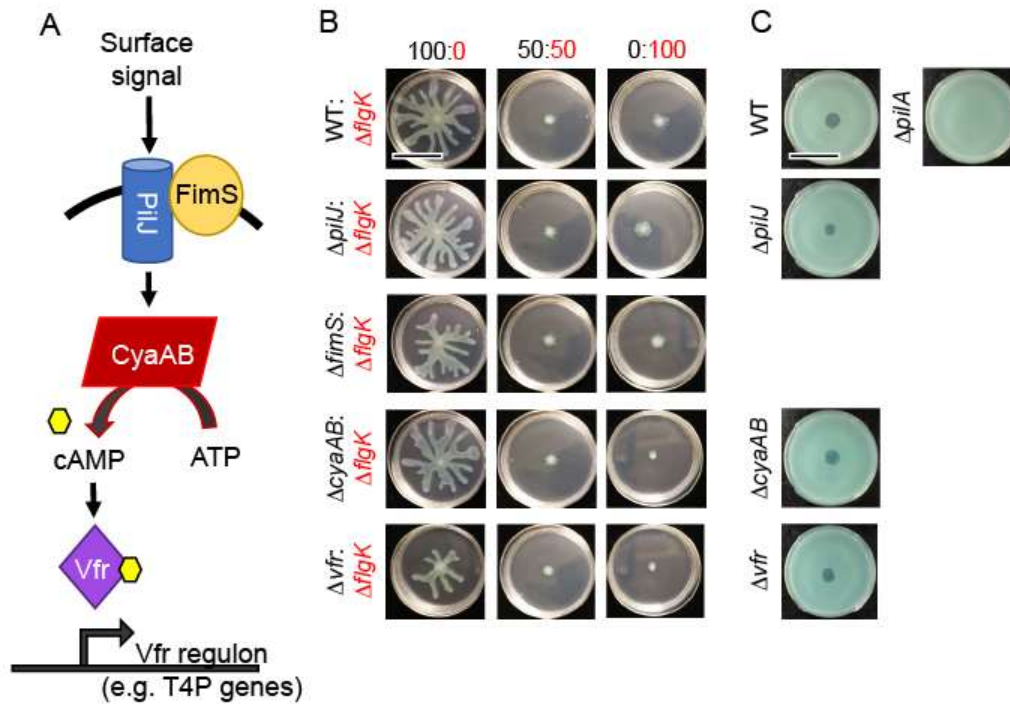
Fig. S7. Surface-sensing and cAMP signaling is not involved in mixed motility repression. A. Schematic of genes involved in surface sensing in *P. aeruginosa*. This pathway is dependent on the perception of a surface followed by cAMP induction and transcriptional activation of the Vfr regulon. Schematic was adapted from Luo *et al.,* 2015. **B.** Representative images from swarm assays of wild-type (WT) *P. aeruginosa* strain PA14, ΔflgK, ΔpilJ, ΔfimS, ΔcyaAB, and Δvfr mixed at the indicated combinations and ratios on M8 agar. **C.** Representative images from plaque assays of WT, ΔpilJ, ΔcyaAB, Δvfr, and ΔpilA (negative control) showing sensitivity (T4P+) and insensitivity (T4P-) to phage DMS3 lysis. Data are representative of three individual experiments. WT and derivatives are labeled in black while ΔflgK is labeled in red. Scale bar: 30 mm

213
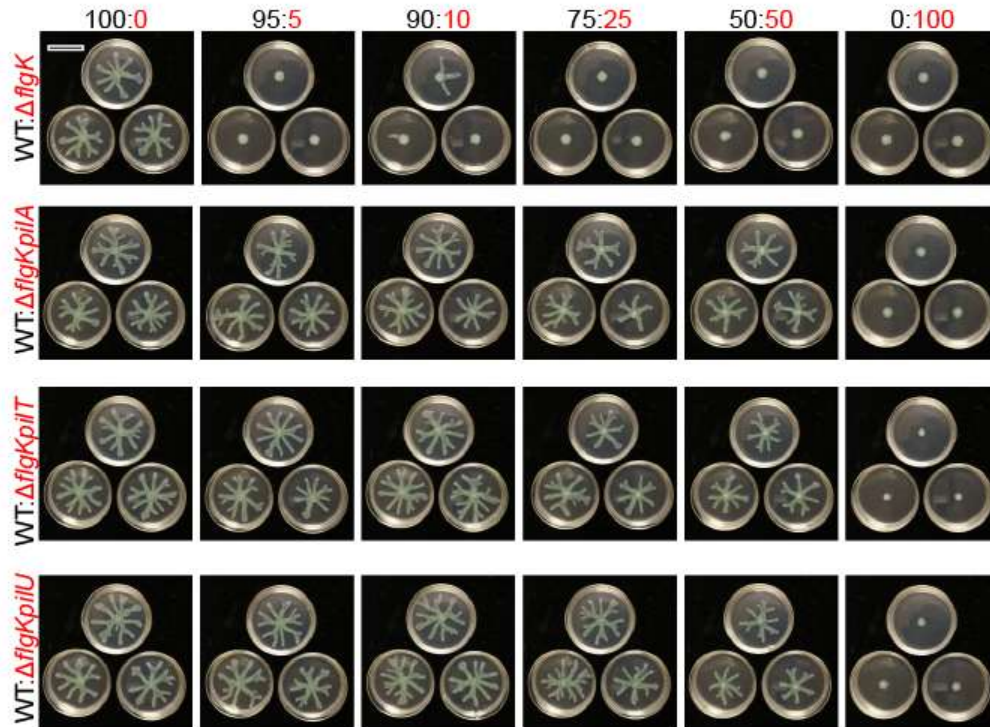
Fig. S8. Non-flagellated *P. aeruginosa* requires functional T4P to repress swarming by flagellated strains on soft agar. Representative images from swarm assays of wild-type (WT) *P. aeruginosa* strain PA14 (flagellated and T4P+) mixed with Δ*flgK* (non-flagellated and T4P+), Δ*flgK*Δ*pilA* (non-flagellated and T4P-), Δ*flgK*Δ*pilT* (non-flagellated with no T4P retraction), or Δ*flgK*Δ*pilU* (non-flagellated with reduced T4P retraction) at ratios indicated. Images show three technical replicates from a single experiment. Images are representative of three individual experiments. WT and derivatives are labeled in black while Δ*flgK* is labeled in red. Scale bar: 30 mm
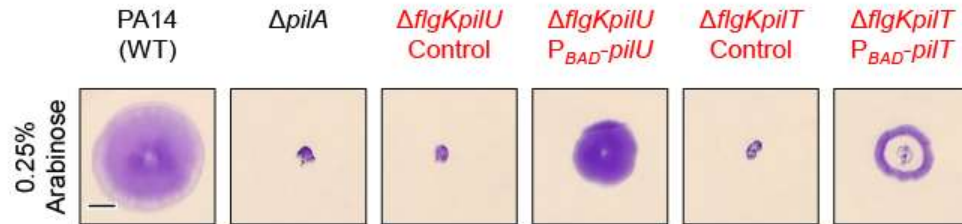
Fig. S9. Complementation of ΔflgKpilU and ΔflgKpilT. Representative images from twitch assays of wild-type (WT) *P. aeruginosa* strain PA14, Δ*pilA*, Δ*flgKpilU*, Δ*flgKpilU* P$_{BAD}$-*pilU* (complemented), Δ*flgKpilT*, and Δ*flgKpilT* P$_{BAD}$-*pilT* (complemented) on T-broth agar containing 0.25% arabinose after 46 h incubation at 37ºC. Data are representative of three individual experiments. Scale bar: 5 mm
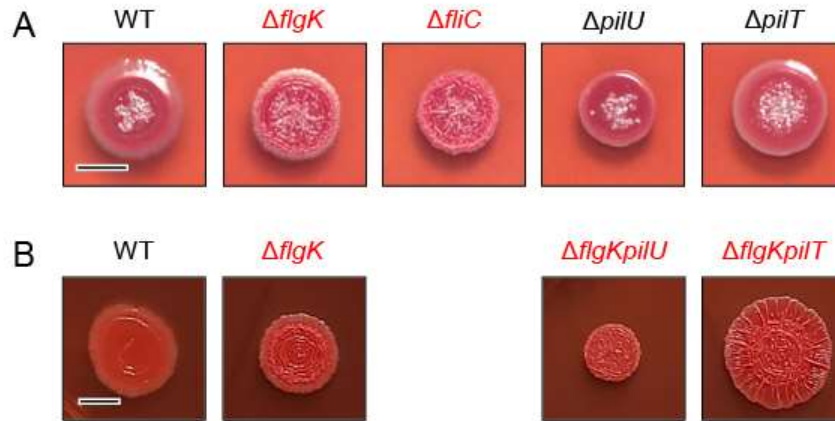
Fig. S10. Non-flagellated mutants have increased Congo Red binding indicative of increased Pel production. Representative images of **A.** wild-type (WT) *P. aeruginosa* strain PA14 (flagellated and T4P+), *ΔflgK* (non-flagellated and T4P+), *ΔfliC* (non-flagellated and T4P+), *ΔpilU* (flagellated with reduced T4P retraction), *ΔpilT* (flagellated with no T4P retraction) and **B.** WT, *ΔflgK, ΔflgKΔpilU* (non-flagellated with reduced T4P retraction), and *ΔflgKΔpilT* (non-flagellated with no T4P retraction) from two separate experiments grown on Congo Red plates to assess Pel production. WT and derivatives are labeled in black while *ΔflgK* and derivatives are labeled in red. Scale bar: 5 mm

Appendix 7

The accumulation and growth of *Pseudomonas aeruginosa* on surfaces is modulated by surface mechanics via cyclic-di-GMP signaling

ARTICLE OPEN
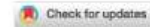
The accumulation and growth of *Pseudomonas aeruginosa* on surfaces is modulated by surface mechanics via cyclic-di-GMP signaling

Liyun Wang[1,12], Yu-Chern Wong[1,2,12], Joshua M. Correira[3], Megan Wancura [3], Chris J. Geiger[4], Shanice S. Webster[4], Ahmed Touhami[5], Benjamin J. Butler[6], George A. O'Toole[4], Richard M. Langford[6], Katherine A. Brown[6,7], Berkin Dortdivanlioglu[8], Lauren Webb [3], Elizabeth Cosgriff-Hernandez[9] and Vernita D. Gordon [1,10,11 ✉]

Attachment of bacteria onto a surface, consequent signaling, and accumulation and growth of the surface-bound bacterial population are key initial steps in the formation of pathogenic biofilms. While recent reports have hinted that surface mechanics may affect the accumulation of bacteria on that surface, the processes that underlie bacterial perception of surface mechanics and modulation of accumulation in response to surface mechanics remain largely unknown. We use thin and thick hydrogels coated on glass to create composite materials with different mechanics (higher elasticity for thin composites; lower elasticity for thick composites) but with the same surface adhesivity and chemistry. The mechanical cue stemming from surface mechanics is elucidated using experiments with the opportunistic human pathogen *Pseudomonas aeruginosa* combined with finite-element modeling. Adhesion to thin composites results in greater changes in mechanical stress and strain in the bacterial envelope than does adhesion to thick composites with identical surface chemistry. Using quantitative microscopy, we find that adhesion to thin composites also results in higher cyclic-di-GMP levels, which in turn result in lower motility and less detachment, and thus greater accumulation of bacteria on the surface than does adhesion to thick composites. Mechanics-dependent c-di-GMP production is mediated by the cell-surface-exposed protein PilY1. The biofilm lag phase, which is longer for bacterial populations on thin composites than on thick composites, is also mediated by PilY1. This study shows clear evidence that bacteria actively regulate differential accumulation on surfaces of different stiffnesses *via* perceiving varied mechanical stress and strain upon surface engagement.

INTRODUCTION

Mechanosensing, including but not limited to responding to surface mechanics, is well-established to be an important cellular function in eukaryotes[1,2]. Much less is known about mechanosensing by prokaryotes[3–5]. Some recent studies have shown that during early biofilm formation, bacteria can sense and respond to mechanical cues, such as those arising from contacting a surface[6–12] and varying fluid flow over surface-bound bacteria[13,14]. For the biofilm-forming pathogen *Pseudomonas aeruginosa*, previous research has shown two categories of sensing pathways. One is through cell envelope-associated proteins, the membrane-bound protein WspA, which might sense cell envelope stress upon surface attachment[12], and the cell-surface-exposed protein PilY1, which has been proposed as a possible mechanosensor of surface adhesion[10,13] and fluid shear[13]. PilY1 is localized at the outer membrane[9,10] and found at the tip of type-IV pili (TFP)[15]. The second is through the extension and retraction of TFP, which power the twitching motility of *P. aeruginosa* on surfaces and are contribute to bacterial mechanosensing of surfaces[8,11] and fluid shear[13].

In vivo, bacteria can experience a wide range of surface mechanics, from ultrasoft (dermal fillers have elastic moduli 0.02–3 kPa and living tissues 0.2–30 kPa) to hard (orthopedic implants have elastic moduli 5–300 GPa)[16,17]. In such diverse settings, biofilm formation commonly causes chronic infection, resulting in prolonged illness and high medical costs[18–20]. Recent research has indicated connections between bacterial behavior and the physical properties of the substrates to which they are attached, as follows: Other researchers have shown that the extension and retraction of TFP of *P. aeruginosa* actively regulates virulence-related genes in a stiffness-dependent manner indicating by a *PaQa* reporter[21]. A second research group has shown that increasing gel substrate stiffness above ~30 kPa correlates with increases in the speed of TFP-driven twitching in *P. aeruginosa*[22]. However, using the same *PaQa* reporter, intracellular signaling was not found to correlate with changes in substrate gel compositions (*i.e.* changed stiffness)[22]. These findings imply that surface mechanics seem to affect bacteria behaviors in a complicated way, and we therefore need a better understanding

[1]Department of Physics, Center for Nonlinear Dynamics, The University of Texas at Austin, Austin, TX 78712, USA. [2]Department of Mechanical Engineering, The University of Texas at Austin, Austin, TX 78712, USA. [3]Department of Chemistry, The University of Texas at Austin, Austin, TX 78712, USA. [4]Geisel School of Medicine at Dartmouth, Hanover, NH 03755, USA. [5]Department of Physics and Astronomy University of Texas Rio Grande Valley, One West University Blvd, Brownsville, TX 78520, USA. [6]Surfaces, Microstructure and Fracture Group, Cavendish Laboratory, University of Cambridge, Cambridge CB3 0HE, UK. [7]Oden Institute for Computational Engineering & Sciences, The University of Texas at Austin, Austin, TX 78712, USA. [8]Department of Civil, Architectural, and Environmental Engineering, The University of Texas at Austin, Austin, TX 78712, USA. [9]Department of Biomedical Engineering, The University of Texas at Austin, Austin, TX 78712, USA. [10]LaMontagne Center for Infectious Disease, The University of Texas at Austin, Austin, TX 78712, USA. [11]Interdisciplinary Life Sciences Graduate Program, The University of Texas at Austin, Austin, TX 78712, USA. [12]These authors contributed equally: Liyun Wang, Yu-Chern Wong. ✉email: gordon@chaos.utexas.edu

of how bacteria perceive and respond to the mechanics of surfaces where they attach.

The initial accumulation of bacteria on surfaces generally lead to biofilm formation. Passive adhesion of bacteria (and other colloids) will be strongly impacted by the surface energy and how this is reduced by adhesion, to reduce the system's free energy. The hydrophobicity and hydrophilicity of surfaces can be major contributors to surface energy and thereby impact bacterial adhesion[23–27]. The trend of adhesion on hydrophobic and hydrophilic surfaces is different[28]. Electrostatics of the surface and the liquid medium, as well as van der Waals forces between bacteria and the surface, can also impact bacterial adhesion[26,27,29–31]. Living bacteria are not, of course, passive colloids, and may have the biological ability to respond actively to surface properties other than surface energy.

Some research has shown that the accumulation of bacteria varied on surfaces with different mechanics[32–35]. These earlier studies changed surface elasticity by varying characteristics such as cross-linking density or polymer concentration. Sometimes, an inappropriate fabrication may introduce unintended changes to other surface properties, resulting in unintended changes in surface energy, porosity, or the density of adhesion sites, and thereby impact adhesivity (see *Supplementary discussion*), which could act as a confounding factor to obscure the impact of surface elasticity. Perhaps as a result, the literature on the effect of surface mechanics on bacterial accumulation on surfaces does not show consistent trends[32,33,35]. Furthermore, many questions remain about the processes underlying how bacteria modulate their accumulation in response to surface mechanics. These questions are of critical importance because they prevent the design of strategies for controlling early biofilm development by manipulating surface mechanics.

To address these questions, in the present study, we used thin and thick hydrogels coated on glass coverslips to create composite materials with the same gel type, adhesivity and surface chemistry, but with different effective stiffnesses, and monitored *P. aeruginosa* through the early stages of biofilm formation on these surfaces. First, surfaces were exposed to a suspension of bacteria for one hour before quantitative microscopy was used to measure bacterial accumulation. For the immediately-following stages of biofilm formation, characterized by bacteria reproducing on a surface rather than accumulating on the surface from a suspended (planktonic) population, we measured the duration and growth rate of the biofilm lag phase and exponential growth phase, respectively.

For both the accumulation and reproduction stages of biofilm development, we show that bacteria actively recognize and respond to surface mechanics. When bacteria initially attach to a surface, both finite element modeling and experimental measurements of the activity of mechanosensitive ion channels show that attachment to thin composites causes greater changes in the mechanical stress and strain state of the bacterial cell envelopes than does attachment to thick composite. We also find that attachment to thin composites results in higher levels of intracellular c-di-GMP, which leads to greater reduction in motility, a reduced likelihood of detachment, and, as a result, greater accumulation on thin composites. Once the initial accumulation stage has passed, higher levels of cyclic-di-GMP are associated with a longer biofilm lag phase on thin composites. Modulation of c-di-GMP levels in response to surface mechanics is mediated by the cell-surface-exposed protein PilY1, a proposed mechanosensor. In short, this work uses a combination of several imaging modalities, quantitative image analysis, and physical modelling to advance our understanding of the mechanism(s) of mechanical signaling for an important human pathogen.

RESULTS

Adhesion to thin composites leads to greater changes in mechanical stress and strain in the bacterial cell envelope than does adhesion to thick composites

To eliminate effects arising from physicochemical properties of surfaces other than elasticity, such as adhesivity and surface chemistry, we used the same gel composition to fabricate thin and thick hydrogels atop glass coverslips (Fig. 1a and Supplementary Fig. 1a). Thickness measurements, done in triplicate for each hydrogel and thickness combination, found that thin gels were ~5 μm in height and thick gels were ~150 μm in height. We chose this geometry-based approach to modifying substrate mechanics to avoid inadvertently altering material adhesivity/chemistry along with mechanics, which has been observed before (Supplementary discussion) - for instance, poly(dimethylsiloxane) (PDMS) can have different surface adhesivities associated with different stiffnesses, shown by polymer beads found to accumulate more on soft PDMS than on stiff PDMS[36]. Using Fourier-Transform Infrared Spectroscopy, we confirmed that the surface chemistry of thick and thin composites was the same (Fig. 1b and Supplementary Fig. 1b). To confirm that the composite materials had the same surface adhesivity regardless of gel thickness, we incubated both thin and thick hydrogel composites with a suspension of fluorescent polystyrene polymer beads for one hour, and imaged the number of beads attached using confocal microscopy. We verified that the numbers of polystyrene beads that attached did not significantly differ with hydrogel thickness (Fig. 1c and Supplementary Fig. 1c). Thus, we conclude that hydrogel thickness does not impact passive physicochemical adhesion to surfaces.

However, the thickness of the hydrogel coated onto rigid glass coverslips does impact the mechanics of the resulting composite material. Linear elasticity theory was used to derive a closed-form expression for the effective elastic modulus ($E_{effective}$) of hydrogel-coverslip composites (Supplementary Discussion and Supplementary Equation 7). For a hydrogel thickness (t_{gel}) comparable to the 1 micron size of a bacterium, the $E_{effective}$ increases sharply with decreasing t_{gel} (Fig. 1d). According to this model, the composites with thin (~5 μm) hydrogels are approximately 16 times stiffer than those with thick (~150 μm) – effective composite moduli are calculated at ~1 MPa for thin composites and ~50 kPa for thick composites (Fig. 1d and Supplementary Table 1 footnote). We also used a nanoindenter to experimentally impose loads on both types of composites that achieved indentation depth that was 1 μm (comparable to bacterial size) or greater (Fig. 1e). The indentation for a given force and tip geometry was consistently less for the thin gel than for the thick gel, with the maximum indentation depth to maximum load ratio being ~125 nm/μN for thick composites and ~75 nm/μN for thin composites. This experimentally validates that the composite made with thin gel is stiffer than the composite made with thick gel (Supplementary discussion and Fig. 1e).

Cryo-electron microscopy showed no discernible difference between the surface topographies of thick and thin gels (Supplementary Fig. 1d, e). However, atomic force microscopy (AFM) shows slight differences in the topographies, with measured average roughness of 1.25 nm for thin agarose gels and 2.62 nm for thick agarose gels (Fig. 1f, g). This ~1 nm difference in roughness is 3 orders of magnitude smaller than 1 μm bacteria, and this size discrepancy makes it unlikely that differences in surface topography could be sensed by bacteria. Moreover, others have found that the virulence response of *P. aeruginosa* upon adhesion is dependent on the stiffness of the surface but not related to the sizes of surface pores ranging from less than 10 to more than 1000 nms[21]. AFM measures an average roughness of 6.2 nm for thin alginate gels and 9.5 nm for thick alginate gels (Supplementary Fig. 1f, g). This ~3 nm difference in
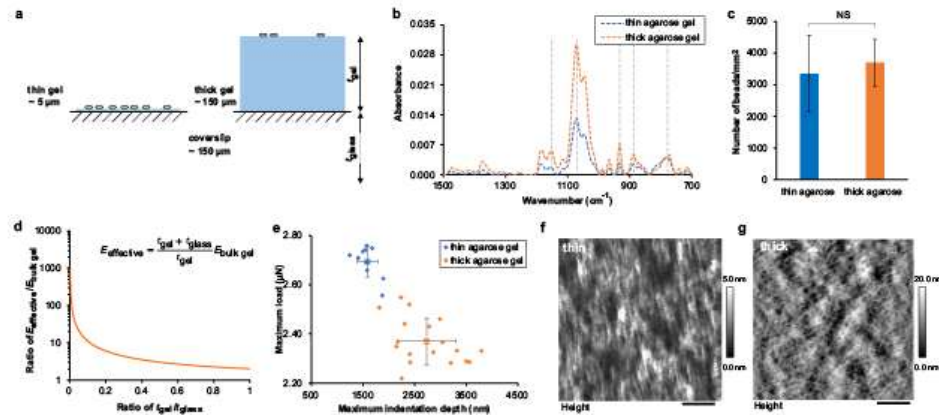
Fig. 1 Fabrication of thin gel and thick gel-coverslip composites with different surface mechanics. a Schematic illustration of composites with different thicknesses of hydrogel, t_{gel}, on top of glass coverslips with constant thickness t_{glass}. **b** FTIR spectra of agarose gel composites with two thicknesses. The dash-dot lines indicate the location of characteristic peaks. $N = 3$. **c** The number of beads attached on agarose gel composites after incubation with bead suspension for 1 h. NS, not significant ($P = 0.15$). ANOVA test. NS indicates that the attachment of beads on thin and on thick gels are not significantly different for agarose gel composites. Data are means ± SD. $N = 2$. **d** The effective Young's modulus of the hydrogel-coverslip composite ($E_{effective}$), where $E_{bulk\ gel}$ is the modulus of bulk hydrogel. The Young's modulus of bulk agarose (3%) gel reported in Kolewe et al. work[32] was 44.8 kPa. The calculated effective composite moduli of thin and thick agarose gel and glass composites are 1388.8 and 89.6 kPa, respectively. The Young's modulus of bulk alginate (2%, 50 mM $CaCl_2$) gel reported in Nunamaker et al. work[89] was 32.0 kPa. The calculated effective composite moduli of thin and thick alginate gel and glass are 992.0 and 64.0 kPa, respectively. **e** Nanoindentation results of agarose gel samples. The relation between maximum load and maximum indentation of indentation curves of gels subjected to large indentation. Individual measurements are shown with solid circles; the means for all measurements per gel type are shown with hollow squares. Error bars are standard deviations. **f, g** AFM images showing the surface topography of thin and thick agarose hydrogels. Scale bar in (f): 800 nm. Scale bar in (g): 1 μm. Greyscale map of height is indicated to the right of each panel.

roughness is similarly far too small for any impact on bacteria to be expected.

Next, we sought to evaluate the degree to which the mechanics of composite substrates impacts bacteria. Upon surface attachment, bacteria are subjected to a mechanical tension in their inner membranes arising from nanoscopic cell envelope deformation due to the adhesion force exerted by the surface[37–39]. If topography had any effect on bacteria, we would expect that the rougher thick composite would exert a greater net adhesion force, due to the increase in surface area consequent to greater roughness. To test whether we could observe a difference in the membrane tension between bacteria adhering to the thin and to the thick composites, we compared the membrane tension in bacteria attached to both composites by measuring the activity of mechanosensitive ion channels. Other researchers have already established much about the mechanical activation of these ion channels – here, our focus is not to understand the ion channels themselves but rather to use their response as a readout to assess whether bacteria experience different degrees of mechanical change when they attach to thin composites than when they attach to thick composites.

These channels are located on the inner, cytoplasmic membrane[40] and act as transducers of membrane tension - closed when the membrane is at low tension and open when the membrane is at high tension, allowing ions to pass through[40,41]. The two major mechanosensitive ion channels are large-conductance- and small-conductance- (MscL- and MscS-, respectively) type channels. When open under increased membrane tension, these channels provide non-selective pores of large and small diameter, respectively, through which sodium ions, Na^+, can pass in very similar ways[41]. We pre-loaded bacteria with a fluorescent indicator for Na^+ and then allowed them to sit for one hour attached to thin and thick agarose gels, in the presence of excess external Na^+, before measuring the indicator brightness distribution as a proxy for internal Na^+ levels.

The brightness distribution for bacteria on the thin composites had a peak at 100–200 arbitrary units (a.u.), whereas brightness distribution for bacteria on thick composites had a peak, representing more than 60% of cells, at 0 to 100 a.u. (Fig. 2a). Both the median (Fig. 2a inset) and the mean fluorescence intensity of bacteria on thin composites were significantly greater than that of cells on thick ones – cells on thin gels had a mean fluorescence intensity of 2840.70 a.u. [2217.75 a.u., 3463.65 a.u.] (95% confidence interval) and cells on thick gels had a mean fluorescence intensity of 677.97 a.u. [478.28 a.u., 877.67 a.u.] (95% confidence interval). These results show that bacteria on thin composites are more permeable to Na^+ than are bacteria on thick composites. Since mechanosensitive ion channels increase permeability upon increased membrane tension, we interpret this finding as indicating that bacteria have higher membrane tension when attached to thin gel surfaces than to the thick. *This is the opposite of what we should expect if the measured differences in surface topography were impacting bacteria.* However, it is entirely congruent with what we should expect if differences in composite mechanics were impacting bacteria, as follows:

Adhesive forces will tend to increase the area of the bacterium in contact with the surface, by deforming the bacterium and the surface. The energy costs for deforming the bacterium and the surface will depend on the elasticity of each. Mechanical equilibrium will be found by minimizing the sum of elastic energy costs (from cell and substrate deformation) and the adhesive energy benefit (from contacting area). Therefore, for constant adhesive area and bacterial elasticity, we expect that the deformation of the bacterial cell envelope will depend on the elasticity of the substrate (i.e., surface mechanics). To validate the trends shown by our experiment results and to elucidate
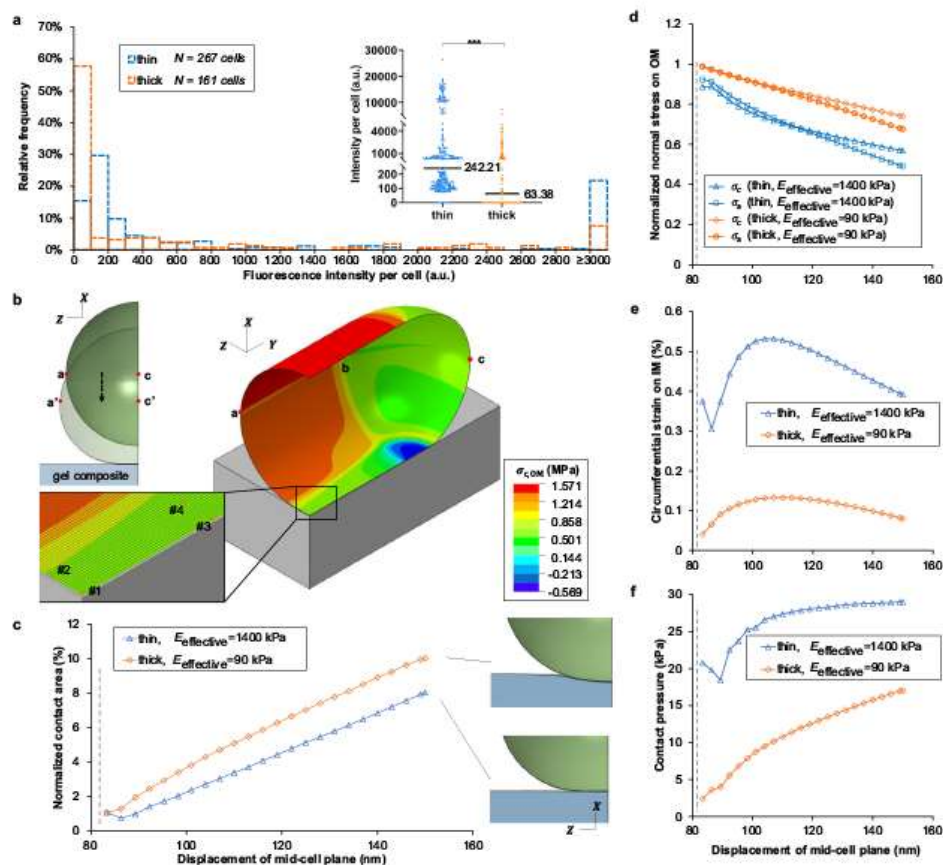
Fig. 2 Adhesion to a thin gel surface leads to greater changes in mechanical stress/strain in the bacterial envelope and increased permeation of the bacterial cell membrane by sodium. a The histogram shows the average intracellular fluorescence intensity per cell of attached WT on thin and thick agarose gel composites after incubating with surfaces for one hour. Inset: Dot plot of the histogram, shown with median values. ***$P < 0.001$; Mann-Whitney u test. This indicates a statistically-significant difference between fluorescence intensity distributions and between median fluorescent intensities for cells on thin and thick gel composites. $N = 3$. The number of cells analyzed for each replicate are 73, 104, and 90 cells in the experiments on thin gels, and 62, 31, and 68 cells in the experiments on thick gels. **b** The finite element model and schematic illustration. Displacement along –X coordinate is applied on curve abc to bring the cell into contact with the surface. The heat map denotes the circumferential stress on OM (outer membrane). Inset: The representative elements analyzed in this study. **c** Contact area with different degree of indentation (displacement along –X coordinate). Contact area is normalized to the cellular surface area in the undeformed configuration. The dash line denotes when the cell first contacts the surface. **d–f** OM stresses become less tensile whereas IM (inner membrane) strain increases at element #1 upon surface adhesion. The degree of changes is greater on thin gels. Contact pressure is greater on thin gels. Subscript c denotes the circumferential direction and subscript a denotes the axial direction. Stresses are normalized to their respective values during the free-floating state and strains are the net change with respect to their respective values during the free-floating state.

further the relationship between surface mechanics and mechanical stresses in adhering bacteria, we developed finite element models (Fig. 2b and Supplementary Fig. 3) to simulate bacterial attachment to gel-coverslip composites. At the molecular level, bacterial surface properties and how they impact attachment to substrates are complex and not well-known[42]. Therefore, we approximated the adhesion process by displacing bacteria into contact with surfaces (Supplementary Discussion, Supplementary Fig. 3c, d). Using our models, we compared the bacterial envelope

mechanics for bacteria interacting with thin and thick gel surfaces for a range of contact-increasing displacements. For any given displacement, the total contact area is greater for bacteria on the thick gel than on the thin one (Fig. 2c), reflecting the fact that the energy cost for deforming a soft material is lower than the cost for deforming a stiff one by the same amount. The initial, free-floating cells were subjected only to a turgor pressure (biologically, this arises from the osmolarity difference between the cytoplasm and the exterior), so that bacteria were in a pre-stressed state. Contact
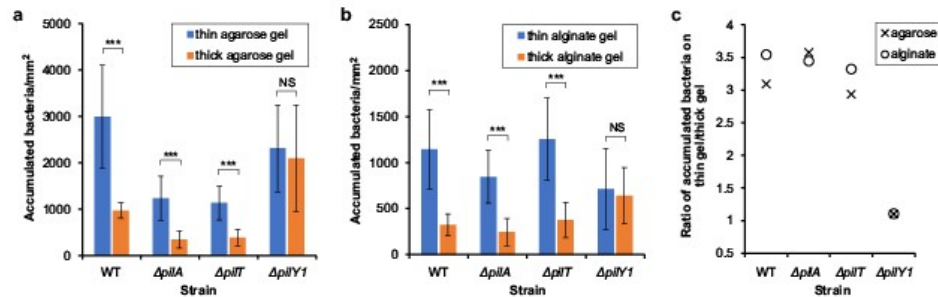
Fig. 3 More bacteria accumulate on thin gel composites during one hour's incubation for initial attachment. a The accumulation of WT, *ΔpilA*, *ΔpilT* and *ΔpilY1* on thin and thick agarose hydrogel composites was determined after incubating with surfaces for one hour. **b** The accumulation of bacteria on thin and thick alginate hydrogel composites. Data are means ± SD. ***$P < 0.001$; NS, not significant ($P = 0.28$ for agarose; $P = 0.29$ for alginate); analysis of variance (ANOVA) test. **c** The ratio of accumulated bacteria on thin to that on thick hydrogel composites. These measurements were done using phase contrast microscopy for $N = 4$ replicates in all cases. Each replicate was imaged with at least 12 randomly-chosen fields of view.

with a surface leads to a decrease in membrane stresses on the outer membrane, an increase in circumferential strain on the inner membrane, and the development of contact pressure (Fig. 2d and Supplementary Fig. 4a–i). These changes are all more pronounced when bacteria attached to thin gel surfaces.

Thus, our modeling results, showing greater strain in the bacterial inner membrane when attached to thin composites than to thick, are consistent with experimental measurements of the activity of mechanosensitive ion channels being greater on thin composites than on thick. This confirms that adhesion to thin gel and glass composites causes greater changes in the mechanical state of the bacterial envelope than does adhesion to thick gel and glass composites, indicating that this effect arises from different composite mechanics. Therefore, the most reasonable expectation is that any difference in bacterial response to the two types of composites should be linked to the difference in effective elasticity of the thick and thin composites.

Early steps in biofilm initiation

The formation of a biofilm on a surface begins when bacteria initially encounter and attach to a surface. Bacteria can either then remain on the surface or detach back into the free-swimming, planktonic phase. The total *accumulation* of bacteria on a surface will depend on both the rate of attachment and the rate of detachment. Subsequent to this initial accumulation (and assuming that the reservoir of planktonic bacteria is removed), the population of bacteria on the surface will experience a phase of little change. This is known as the biofilm *lag phase*, and results from a combination of bacteria replication and detachment from surfaces, such that the population of surface-bound bacteria does not increase[43,44]. The lag phase ends with the onset of *exponential growth* of the population of surface-bound bacteria. Having established in the preceding subsection that adhesion to substrates with different composite elasticities results in different mechanical changes in the bacterial cell envelope, the remainder of our study here focuses primarily on the accumulation of bacteria on surfaces with different composite elasticities, and secondarily on the lag phase and exponential growth of bacteria on surfaces with different composite elasticities.

The pore sizes of the agarose and alginate hydrogels used are far too small to allow the bacterial body to enter the hydrogel; this is confirmed by microscopy observation that all sessile bacteria are attached to the top hydrogel surface, at the gel-fluid interface. This study focuses solely on bacteria attached to the hydrogel

surface, and not on any free-swimming, planktonic bacteria in the fluid phase above. This is appropriate to our goal of better characterizing the role of bacterial mechanosensing in early biofilm development. Since the hydrogel thickness does not notably impinge on surface adhesivity or other surface properties (Fig. 1b, c, f, g and Supplementary Fig. 1b–g), the mechanosensing investigated here is that arising from substrate elasticity. Different adhesion forces[45] and differences in the stiffness of bacterial cell walls[37] could also give rise to different mechanical changes in bacterial envelopes upon adhesion, but these two parameters are not varied in the present study.

PilY1 allows *P. aeruginosa* to differentially accumulate on thick and thin composites

As mentioned above, two categories of sensing pathways may be involved in the mechanosensing by *P. aeruginosa*. Therefore, to assess the impact of surface mechanics on the accumulation of bacteria on surfaces, we incubated the bacterial suspension of wild-type cells (WT), mutants without TFP (*ΔpilA*), mutants without the PilT retraction motor (*ΔpilT*) and mutants without PilY1 (*ΔpilY1*) for one hour with hydrogel-coverslip composites and measured the bacterial accumulation on these surfaces by visualizing the number of bacteria using phase contrast microscopy. Consistent with some previous reports[32–34] but not with others[35], WT accumulated significantly more on thin composites than on thick composites (Fig. 3a, b), as did the *ΔpilA* and *ΔpilT* mutants (Fig. 3a, b). These findings were true across two types of hydrogels, agarose and alginate, supporting the idea that the difference in accumulation is likely to arise from the ~16x contrast in composite elasticity rather than details of surface chemistry.

Accumulation on the thin composites was greater by a factor of ~3.3 for all three strains (Fig. 3c). Thus, while functional TFP can increase the "baseline" accumulation, they have no measurable impact on the greater likelihood of accumulating on thin composites. Similar effects were found for the more starkly-contrasting case of glass versus agarose gel surfaces (Supplementary Discussion and Supplementary Fig. 2a).

In contrast, *ΔpilY1* accumulated equally on thin and thick composites (Fig. 3a, b); this also is true for both agarose and alginate gels. This indicates that *P. aeruginosa* requires the cell-surface-exposed protein PilY1 for distinguishing between, and responding to, different surface mechanics. Again, similar effects were found for the more starkly-contrasting case of glass versus agarose gel surfaces, implying a much more muted response to
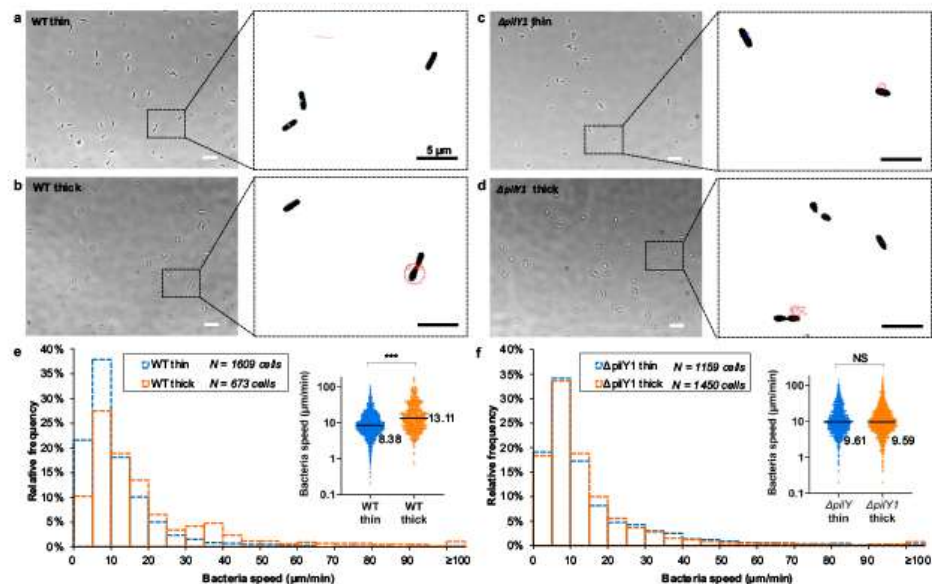
Fig. 4 Adhered bacteria spin during the first hour of accumulation. a–d Phase contrast images of WT and the *ΔpilY1* mutant adhered to thin and thick agarose gel composites. Insets: Tracked trajectories of bacterial centers-of-mass over 62.6 s. Scale bar: 10 μm. **e, f** Histograms showing speed distributions of WT and the *ΔpilY1* mutant on thin and thick gel composites. Insets: Dot plots of the corresponding histogram. The median value is written to the right of each plot. ***P < 0.001; Mann–Whitney u test. *** indicates a statistically-significant difference in the distributions of WT speeds on thin and on thick gel composites and that the median speed of WT adhered to thick gel composites was higher, with statistical significance, than that of WT to thin gel composites. In contrast, NS (not significant) indicates that there is no statistically-significant difference in the distributions of speeds or in the median speeds of the *ΔpilY1* mutant on the two composite types (P = 0.66, Mann–Whitney u test). Biological replicates N = 3 in all cases, with each biological replicate represented by 15 video sequences at randomly-chosen fields of view.

stiffness difference by *ΔpilY1* (Supplementary Discussion and Supplementary Fig. 2a). Adhesion-induced changes can only happen following, not preceding, bacterial contact with surfaces. Since gel thickness does not impact physiochemical surface adhesivity (Fig. 1c and Supplementary Fig. 1c), we expect bacteria to have equal likelihood of encountering and initially sticking to thin and thick composites. Therefore, this finding shows that greater accumulation on thin composites must arise as the result of something that happens after initial surface engagement – i.e., there is an active bacterial response to surface mechanics.

Thus, we hypothesize that WT initially adhered to thick composites will be more likely to detach than cells initially adhered to thin composites and that this difference should require PilY1. We test this hypothesis below.

PilY1 mediates flagellar spinning and detachment rate in response to surface mechanics

Shortly after encountering a surface, many *P. aeruginosa* cells are reversibly tethered by their flagella, which drive spinning about the surface-attached portion of the flagellum (to optical microscopy, the axis of rotation usually appears to go through one end of the cell). Spinning facilitates detachment from surfaces[46,47]. A deficiency in spinning is also associated with decreased probability of detachment[46]. Bacteria can also use TFP to move laterally on surfaces, but, during the first hour after bacteria were introduced to hydrogels (i.e., what we have termed the accumulation stage), we found that the vast majority of surface

motility was in the form of spinning (Supplementary Fig. 5a, b). Therefore, we tracked the center-of-mass speed of surface-adhered bacteria (Fig. 4a–d) as a measure of spinning motility. We expect that a population with faster-spinning bacteria will have a higher rate of detachment[48].

For WT, the distribution of spinning speeds on thick composites was much broader than thin composites (Fig. 4e). Both the median (Fig. 4e inset) and the mean speeds on thick composites were significantly higher than on thin composites - mean speed of 20.06 μm/min [18.43 μm/min, 21.68 μm/min] (95% confidence interval) on thick composites and mean speed of 11.46 μm/min [10.95 μm/min, 11.97 μm/min] (95% confidence interval) on thin composites. In summary, WT are more likely to spin rapidly on thick composites than on thin composites. Upon tracking cells, we indeed found that WT were significantly more likely to detach from thick gels (30 detachment events among 673 tracked cells) than from thin gels (10 detachment events among 1609 tracked cells) (P < 0.001, χ^2 test) (Supplementary Fig. 5c). This is an active bacterial response to surface mechanics.

For the *ΔpilY1* mutant, the peak spinning speed was unchanged from that of WT (Fig. 4e, f), suggesting that loss of PilY1 does not intrinsically disrupt spinning motility. However, for the *ΔpilY1* mutant, neither the distributions of spinning speeds nor the median spinning speeds were significantly different on thin and thick composites (Fig. 4f). The mean speed was 15.08 μm/min [14.16 μm/min, 16.01 μm/min] (95% confidence interval) on thin composites and 14.86 μm/min [13.92 μm/min, 15.81 μm/min] (95% confidence interval) on thick composites.

Furthermore, the Δ*pilY1* mutant was equally likely to detach from thin and thick composites (P = 0.78, χ² test) (Supplementary Fig. 5c). These results are strikingly unlike those for WT and imply that *P. aeruginosa* lacking PilY1 do not adjust their spinning motility, and therefore their likelihood of detachment, in response to surface mechanics. PilY1 is linked to regulating flagellar activity either up or down - increasing spinning speed on thick composites and decreasing spinning speed on thin composites (Supplementary Fig. 5d,e). Notably, we find a linear correlation between spinning speed and the probability of detachment (Supplementary Fig. 5d,e).

These findings raise the question of what provides the causative linkage between PilY1 and changes in flagellar activity. A key regulator of flagellar motility in *P. aeruginosa* and many other microbes is the intracellular second messenger cyclic diguanylate (c-di-GMP)[49,50]. We have shown that, compared with thick composites, thin composites could lead to higher membrane tension in the adhering bacterium. In addition, others have shown that the unfolding and misfolding of inner-membrane and periplasmic proteins associated with surface attachment results in an elevated level of c-di-GMP for *P. aeruginosa*[12].

Therefore, we hypothesized that different surface mechanics arising from thin and thick composites would cause different levels of c-di-GMP production upon surface attachment, and that PilY1 is involved in the c-di-GMP response. We test this hypothesis below.

Composite mechanics impact c-di-GMP signaling in a PilY1-dependent manner during bacterial accumulation

To see whether PilY1 modulates c-di-GMP dynamics in response to composite mechanics, we used a validated reporter plasmid, P_{cdrA}::*gfp*, that produces green fluorescent protein (GFP) in response to increases in c-di-GMP[51]. We previously used this plasmid study c-di-GMP signaling in bacterial mechanosensing of shear[13]. We measure average per-cell GFP intensity, accounting for attenuation by the substrates, as we did in earlier studies[13,52].

For bacteria containing PilY1, we found a sharp rise in c-di-GMP levels during the initial hour of accumulation (−1 to 0 h in Fig. 5a), which is consistent with previous findings that c-di-GMP levels in *P. aeruginosa* increase upon surface attachment[9,13,53]. At the end of the "accumulation" hour (i.e., the beginning of the incubation time), WT on thin composites had significantly higher c-di-GMP levels than did WT on thick composites. This meshes with our finding that WT on thin composites had lower spinning motility than those on thick composites (Fig. 4e), as high levels of c-di-GMP inhibit bacterial motility[49]. These data also suggest that the causative linkage between PilY1 and changes in flagellar activity (which, in turn, modulate the likelihood of detaching from the surface), is likely via PilY1-controlled c-di-GMP signaling.

On both thin and thick composites, the Δ*pilY1* mutant had much lower c-di-GMP levels than did WT (Fig. 5a, b); this finding is consistent with the role of PilY1 in regulating c-di-GMP production[9]. For WT, the mean level of c-di-GMP at the end of the "accumulation" hour was ~2.9 times higher on thin composites than on thick composites, but it was only ~1.4 times higher for the Δ*pilY1* mutant (Fig. 5a, b). This observation is consistent with a loss of the ability to discriminate surface mechanics. This finding is also consistent with the causative connection that PilY1 is required for bacterial mechanoresponse linking surface mechanics to c-di-GMP signaling levels during the initial "accumulation" phase.

This finding also raises the question of how PilY1, and consequent changes in c-di-GMP signaling, impact the growth of the bacterial population on the surface.

PilY1 impacts biofilm growth in the lag phase, in response to composite mechanics, by modulating c-di-GMP signaling

When planktonic bacteria are introduced into new liquid medium, they experience a temporary period of non-replication, termed the "lag phase"[54]. After attachment to a glass surface, *P. aeruginosa* also undergoes a lag phase before exhibiting exponential growth[43,44]. However, unlike the planktonic lag phase, the lag phase of biofilm growth involves a combination of bacteria replication and detachment from surfaces, such that the population of surface-bound bacteria does not increase[43,44].

After allowing bacteria to accumulate on the surfaces of composites for one hour, we replaced the bacterial suspension with fresh, sterile culture medium, so that no more bacteria can attach to the surface from the liquid phase. We designate this timepoint the beginning of the incubation time (0 h in Fig. 5). The duration of the lag phase, from the beginning of the incubation time to the onset of exponential growth, is given by the lag time, τ_{lag}, indicated by hatched color bars in Fig. 5. WT populations had a τ_{lag} of 4 h on thin composites and 1 h on thick composites, but Δ*pilY1* populations had the same τ_{lag} of 1 h on both composite types (Fig. 5d, e). Similar results were found for bacterial growth on bulk gels (soft) and glass slides (stiff) (Supplementary Fig. 2b, c). These results show that composite mechanics can markedly impact the growth of the sessile bacterial population, and that PilY1 is key for this process as well as for the accumulation preceding incubation. When PilY1 was complemented back on an arabinose-inducible plasmid, the Δ*pilY1* mutant populations again had different τ_{lag} on thin and thick composites (Supplementary Discussion and Supplementary Fig. 6c), confirming PilY1's role in surface mechanics sensing. Interestingly, although the early c-di-GMP response of Δ*pilT* was indistinguishable from that of WT, during the subsequent incubation phase the c-di-GMP levels of Δ*pilT* dropped much more quickly than they did for WT (Fig. 5c).

On both thin and thick gels, c-di-GMP levels in WT fell during the lag phase and subsequently oscillated once populations entered the exponential growth phase (Fig. 5a). The high level of c-di-GMP induced by the initial mechanical stimulus of surface contact (0 h in Fig. 5a) allows bacteria to sense the surface and initiate a sessile lifestyle. However, it would be a metabolic burden for cells to maintain such high c-di-GMP levels in the following biofilm development. We speculate that bacteria may have to decrease the c-di-GMP level to allow the beginning of exponential biofilm growth on surfaces; this speculation is consistent with the work of others[55,56]. If so, the longer τ_{lag} for WT on thin composites than on thick composites likely arises from the much higher initial c-di-GMP levels on thin composites and the consequent need for more time to gradually decrease c-di-GMP levels. For Δ*pilY1*, low initial levels of c-di-GMP are associated with a short τ_{lag} on both thin and thick composites (Fig. 5b, e). Interestingly, the lag phase of Δ*pilT* on thin gels was slightly shorter than that of WT, and the Δ*pilT* population's rate of exponential growth is indistinguishable on the two composite types (Fig. 5c, f) – this is unlike the cases for WT and for Δ*pilY1* populations, which have higher exponential growth rates on thick composites (Fig. 5d, e).

We conclude that PilY1 is a required element for controlling *P. aeruginosa*'s initial c-di-GMP response to surface mechanics and consequent lag time in early biofilm growth.

DISCUSSION

Our experimental results show that PilY1 may act as a signal amplifier that mediates c-di-GMP levels and flagellar motility in response to surface mechanics. It is also possible that PilY1 acts as a mechanosensor that transduces mechanical changes upon surface engagement into c-di-GMP signaling. PilY1 is a surface-exposed protein found associated with the TFP tip[9], so PilY1 may be responding to the compressive loading incurred due to surface
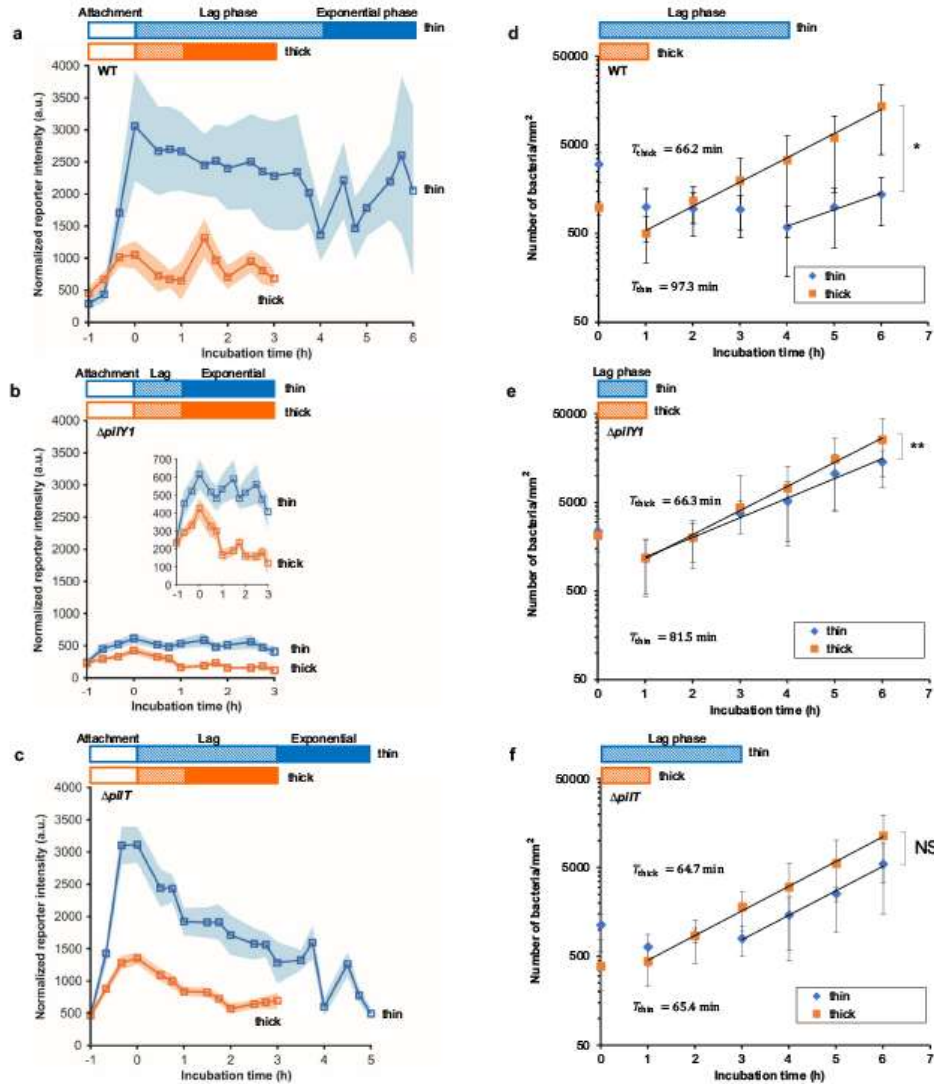
adhesion, a stress state identified in the modeling. A recent study suggested that the conformational changes of PilY1 lead to stimulation of bacterial c-di-GMP production and biofilm formation[57]. The compressive loading may hence engender the required conformational changes on PilY1 for biofilm initiation, while our modeling shows that bacteria adhered to thin composites surfaces will have a greater decrease in the tension in their outer membrane than will bacteria adhered to thick composites.

The differential response of mechanosensitive ion channels to surface mechanics (Fig. 2a) opens the possibility that mechanosensitive ion channels may play a role in the initial development in biofilms on surfaces, although we have not investigated that specifically. At the exponential-growth phase of biofilm formation, our data suggests that the pilus retraction motor PilT may also be involved in responding to surface stiffness in a way that modulates c-di-GMP level and growth rate (Fig. 5c, f)[58], see Supplementary discussion.

The mechanical equilibrium of a system consisting of a bacterium adhering to a surface will be found when the net mechanical energy is minimized. Adhesion energy, which is

225

Fig. 5 On agarose surfaces with different mechanics, PilY1 acts to mediate the duration of the lag phase in biofilm growth and the levels of the intracellular signal c-di-GMP, and PilT is required to mediate the growth rate of the exponential phase of biofilm growth. a–c The average per-cell normalized intensity for fluorescent reporters for changes in intracellular c-di-GMP in WT and the Δ*pilY1* and Δ*pilT* mutants during accumulation, lag phase, and exponential phase. The same vertical scale is used for each plot so that differences between strains are clear. The initial hour of accumulation on a surface is designated by −1 to 0 h, shown by hollow color bars. For each sample, exponential phase was observed for two hours, shown by solid color bars. Squares represent mean levels of c-di-GMP at each time point, linked by lines as a guide to the eye. Shaded regions correspond to 95% confidence intervals. The inset in (b) shows c-di-GMP reporter intensity in the Δ*pilY1* mutant with a smaller y-axis range. N = 3 for all experiments using the reporter plasmid; N = 2 for all experiments using the control plasmid. **d–f** Growth dynamics of attached WT, and the Δ*pilY1* and Δ*pilT* mutants on thin and thick agarose gel composites. Data are means ± SD. The data at 0 time point corresponds to the end of one hour of bacterial accumulation on gel surfaces. The accumulation phase was always one hour long, and was set by the time that a suspension of planktonic bacteria was incubated with the surface. Hatched color bars show the length of the lag phase. The duration of the lag phase was experimentally determined in each case, by measuring the bacterial population on the surface. While that population was roughly constant in time, the system was considered to be in lag phase. The onset of exponential growth phase was determined experimentally in each case, by measuring the bacterial population on the surface. Once the population started to increase as an exponential function of time, the system was considered to be in exponential phase. The doubling time, T, is calculated by the equation $T = \ln 2/a$, where a is the growth rate of bacteria on surfaces (equations of exponential regression, $f(t) = Ae^{at}$, where t is the incubation time). For each bacterial strain, we use T_{thick} to designate the doubling time on the thick gel composite, and T_{thin} to designate the doubling time on the thin gel composite. $^{**}P < 0.01$, $^{*}P < 0.05$; NS, not significant; analysis of covariance (ANCOVA) test. ** and * indicate that the growth rate a_{thin} is significantly different from a_{thick} for WT and for the Δ*pilY1* mutant, while NS means the difference in growth rates on thin and thick gel composites are not significant for Δ*pilT* ($P > 0.1$). Each time point was done for two replicate samples, and at least 12 fields of view were randomly chosen for each replicate. Samples used for measurement at one time point were not used for further incubation or later measurements, i.e., the measurement at each time point was done independently. Thus, for each strain and thickness combination, 14 replicas were measured.

energetically favorable and negative in sign, will increase in magnitude as the adhering area increases. Increasing the adhering area incurs elastic energy costs for deforming the bacterium and the surface; elastic energy costs are energetically disfavorable and positive in sign. More of the elastic energy cost will be borne by the bacterium when the surface is stiff than when it is soft. Therefore, for surfaces that have the same adhesive properties, bacteria adhering to thick composites will deform less than will bacteria adhering to thin composites; this has been confirmed by finite element modeling (Supplementary Fig. 3a, b) and by experiments measuring the activity of mechanosensitive ion channels (Fig. 2a).

For a given adhesion energy, stiffer bacteria would deform less and softer bacteria would deform more. This could alter the mechanosensing response to surface attachment. *P. aeruginosa* maintain tight genomic control of their stiffness[59]. This clearly has benefits for protecting the bacteria against mechanical stress, such as osmotic pressure. This may also benefit bacteria by safeguarding the surface-sensing response, which is essential to this biofilm-former.

The effective modulus of our composites with thin gel was roughly 1 MPa and the effective modulus of composites with thick gel was less than 100 kPa (Supplementary Table 1). These values bracket the stiffnesses reported for *P. aeruginosa* and other Gram-negative bacteria[60–62]. Gram-positive bacterial cells are stiffer[63] than Gram-negative bacterial cells[64–67]. Bacteria themselves are a composite material, comprising the softer cytoplasmic interior and the stiffer envelope. The Young's modulus for the envelope material per se of Gram-negative bacteria is roughly several tens of MPa, and the envelope material of Gram-positive bacteria probably has a similar modulus[64,68]. Our finite element modeling identifies bending as the major envelope deformation modality in the contact zone as bacteria attach to surface. According to the Kirchhoff-Love plate theory[69], the flexural rigidity of a thin plate (effectively the modulus that measures the energy cost for bending a plate) is characterized by $Et^3/12(1−v^2)$ α t^3, where E is the Young's modulus of the plate, v is the Poisson's ratio, and t is the plate thickness. Gram-negative bacteria have a much thinner peptidoglycan cell wall than do Gram-positive bacteria (the cell wall of *P. aeruginosa* (Gram-negative) is ~3 nm thick[70] and that of *B. subtilis* (Gram-positive) is ~30 nm thick[71]). This observation suggests that Gram-positive bacteria will deform less than will Gram-negative bacteria upon adhesion to the same surface, because the energetic cost for deforming Gram-positive bacteria

will be higher. Therefore, we suggest that Gram-positive bacteria may be less well-adapted to using envelope stress and strain to sense and respond to surface stiffness. This inference is in agreement with previous reports that Gram-positive bacteria do not respond to surface stiffness in the same way as Gram-negative bacteria[72,73].

In summary, in this study, we fabricated surfaces with different mechanics using thin and thick hydrogel and coverslip composites. Composite thickness does not change gel composition, surface chemistry (measured by FTIR), or surface adhesivity (measured by passive accumulation of beads). Therefore, these composites are well-suited to elucidating effect of surface mechanics on bacterial accumulation and growth, without many confounding factors arising from other passive physicochemical properties of surfaces[36]. We show that bacterial accumulation on surfaces strongly depends on substrate mechanics: Accumulation of bacteria on a surface is the first step leading toward biofilm development. Consistent with previous findings that misfolding and misregulation of envelope proteins causes elevated level of c-di-GMP for *P. aeruginosa*[12], bacteria adhered to thin composites underwent a greater change in the mechanical strain and stress in the envelope than did bacteria adhered to thick composites. Adhesion to thin composites was also associated with higher c-di-GMP levels than was adhesion to thick composites. Higher c-di-GMP levels were the causative link that led to lower spinning motility, less detachment, and thus greater accumulation than did adhesion to thick composites. Figure 6 graphically summarizes these findings. The cell-surface-associated-protein PilY1 is required for this link between substrate mechanics and bacterial accumulation. Later biofilm growth also shows an impact of surface mechanics, PilY1, and PilT.

METHODS

Strains and plasmids

We used *P. aeruginosa* PA01 WT and Δ*pilA*, Δ*pilT*, Δ*pilY1* mutants[74]. Studies of bacterial accumulation, motility, growth, and c-di-GMP production were done with bacteria that contained the plasmid P$_{CdrA}$::*gfp*. This plasmid is a verified reporter for c-di-GMP; it is a transcriptional fusion between the cyclic di-GMP-responsive *cdrA* promoter and a gene encoding green fluorescent protein (GFP)[51]. Strains containing a promotorless control plasmid pMH487 were used to measure background GFP expression independent of c-di-GMP levels[13]. Confocal laser-scanning microscopy was used for

1. Mechanical input:
Attachment on stiff or soft surfaces

Deformation and stresses in bacterial cell envelope

Low on soft   High on stiff

2. Cyclic-di-GMP signaling:
Low on soft   High on stiff

3. Bacterial responses:
Faster spinning on soft surfaces

More detachment from soft surfaces
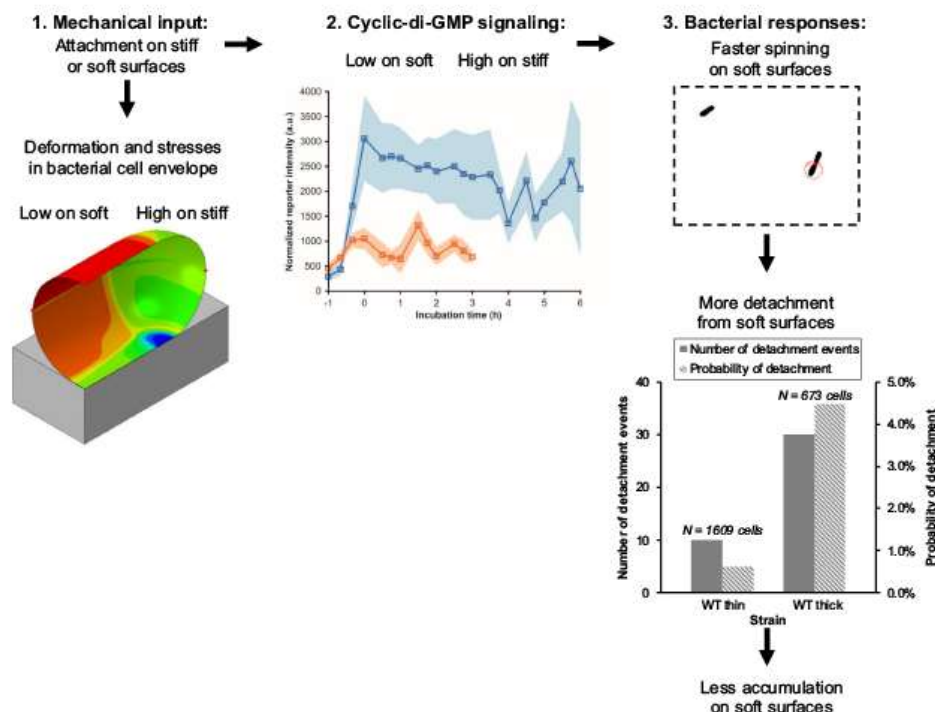
Less accumulation on soft surfaces

Fig. 6 Schematic of the proposed links between surface mechanics and bacterial accumulation. Adhesion to a surface results in changes in mechanical stresses and deformations in the bacterial cell envelope. These changes are greater when the surface is stiff than when it is soft (Fig. 2). Adhesion to a stiff surface results in a greater increase in intracellular levels of c-di-GMP than does adhesion to a soft surface (Fig. 5). Higher levels of c-di-GMP result in faster bacterial spinning (Fig. 4) on soft surfaces and a greater likelihood of detaching from soft surfaces (Supplementary Fig. 5). As a result, more bacteria accumulate on stiff surfaces than on soft (Fig. 3).

measurements of GFP, with calibration for light attenuation by different gel composites[52], and phase contrast microscopy (which imposes a lower light dose on bacteria and therefore reduces potential phototoxicity) was used to measure accumulation, motility, and growth. Strains with the $P_{CdrA}::gfp$ and pMH487 plasmids were grown with 60 μg/mL Gentamycin (Sigma-Aldrich, G1914) for plasmid selection. Fluorescence measurements using the sodium ion indicator were performed using WT that did not contain any plasmid.

Fabrication of thick and thin agarose hydrogel composites

3% (w/w) agarose solution was prepared by dissolving agarose powder (Sigma-Aldrich, A9414) in Millipore water and then autoclaving at 121 ℃ for 15 min.

To form composites of thick agarose gel on glass coverslips, 20 μL of agarose solution was spread (while still liquid) inside an imaging spacer (Grace Bio-Labs, SS1X13, 13 mm diameter × 0.12 mm depth) adhered to a coverslip. This was cooled at 4 ℃ for 2 min in a humid chamber, resulting in gelation.

To form composites of thin agarose gel on glass coverslips, 3 μL of agarose solution (while still liquid) was pipetted onto a glass slide (prior to this, the glass slide had been sonicated in 70% ethanol (Pharmco, 111000200) for 15 min and then dried with nitrogen) and a coverslip was placed on top of the fluid drop. Two

binder clips were used to clamp together the slide and coverslip, spreading the solution between them. After cooling at 4 ℃ for 2 min, the binder clips were removed and the coverslip was detached from the glass slide using a razor blade. This left thin agarose gel coated on the coverslip. The thick and thin agarose gels were then immediately immersed into buffer solutions or bacterial suspension for the following experiments.

Fabrication of thick and thin alginate hydrogel composites

2% (w/w) sodium alginate (SA) solution was prepared by dissolving sodium alginate powder (Sigma-Aldrich, 180947) in Millipore water. After being stirred for 2 h, the SA solution was filter sterilized.

To make thick alginate gel, 20 μL of SA solution was spread into an imaging spacer (Grace Bio-Labs, SS1X13, 13 mm diameter × 0.12 mm depth) adhered to a coverslip that was pretreated with 500 μL of 0.1 mg/mL Poly-L-lysine (Sigma-Aldrich, P9155) for 2 h to facilitate adhesion of the alginate gel to the coverslip surface. The thick alginate gel was formed after the coverslip was immersed in 50 mM Calcium chloride (CaCl₂, Sigma-Aldrich, C3306) solution for 2 h.

To make thin alginate gel, 1 μL of SA solution was pipetted onto a glass slide (the glass slide was sonicated in 70% ethanol for 15 min and then dried with nitrogen before use), and a coverslip

that was pretreated with 500 μL of 0.1 mg/mL Poly-L-lysine for 2 h to facilitate adhesion of the alginate gel to the coverslip was placed on top of the SA solution. Following the spread of SA solution between the glass slide and the coverslip, CaCl$_2$ solution was gently added along the sides of the coverslip and allowed to diffuse in for 2 h. The coverslip was removed from the glass slide using a razor blade, leaving the thin alginate gel coated on the coverslip.

Then both the thin and the thick alginate gel surfaces were immediately washed by Millipore water to remove extra CaCl$_2$ before bacteria or beads were introduced.

Measurement of thicknesses of hydrogels on coverslips

The thicknesses of hydrogels on coverslips were measured using an Olympus IX71 inverted phase contrast microscope with a 60× oil-immersion objective. Hydrogel composites were incubated with bacterial suspension (incubation details can be found in the following section). The microscope stage controller (Applied Scientific Instrumentation MS-2000) displayed the Z-positions of the stage when two locations were in focus (Supplementary Fig. 1a). These locations were a gel-free area at which bacteria were attached directly to the coverslip (Z_1) and the top of the gel to which bacteria were attached (Z_2). Taking the difference between Z_1 and Z_2 gave a measurement of the thickness of the gel on coverslips. Each experiment was repeated three times independently.

The 60x oil objective we used for these measurements has a numerical aperture of NA = 1.25. We have a filter in the microscope so that the illuminating light is green, with wavelength roughly $l = 550$ nm. The immersion oil used with this objective has a refractive index of about $n = 1.5$. Using the following approximation for depth of field[75]

$$d = \frac{l\sqrt{n^2 - (NA)^2}}{(NA^2)} \quad (1)$$

we obtain a depth of field of 291 nm. This is nearly an order of magnitude smaller than a 1-micron bacterial thickness, and more than an order of magnitude smaller than the 5-micron thickness we measure for the thin gel. Therefore, any uncertainties in the measured gel height arising from the depth of field of this microscope objective are negligible.

Characterization of surface mechanical properties of hydrogel composites using nanoindentation

An Optics11 Life Piuma nanoindenter was used to perform surface mechanical measurements on agarose hydrogel composites. Measurements were performed on thick and thin composites (fabricated as described above) glued to the bottom of a petri dish and submerged in DI water at room temperature. A probe with cantilever stiffness of 0.25 N/m and a tip radius of 9.5 μm was used to determine the gel's intrinsic Young's modulus. A probe with cantilever stiffness of 0.23 N/m and a tip radius of 24 μm was used for assessing mechanical differences resulting from the composite structure (Supplementary Discussion). The probe loaded and unloaded samples at a constant piezo-motor displacement rate of 2 μm/s. All specimens were measured at 9 different locations near the center of the gel surface with two replicates for each gel thickness. Indentation profiles where the probe failed to make contact with the surface were excluded, resulting in at least 9 measurements per condition.

To determine the intrinsic Young's modulus of a gel, a loading curve was fit with the Hertzian model[76]:

$$F = \frac{4}{3}\frac{E}{1 - v^2}R^{0.5}\delta^{1.5} \quad (2)$$

where F is the load, E is the Young's modulus, R is the tip radius, δ is the indentation depth, and v is the Poisson's ratio, which we assumed to be 0.5. Data were fit up to an indentation depth equal to 10% of the tip radius. The maximum load and maximum indentation of an indentation curve were recorded and used to examine the composite effect.

Electron microscopy measurement of surface topography

For the purposes of Cryo Electron Microscopy, hydrogel samples were adhered to Electron Microscopy stubs using carbon tape. As suggested by the literature[77] the samples were subsequently plunged into slush nitrogen for ten seconds to vitrify. The samples were immediately, whilst continuously held under vacuum, inserted into a FEI FEG XL30 microscope. For the purposes of the sublimation step, the sample temperature was raised from −170 °C to −90 °C before being lowered back down to −170 °C.

AFM imaging and roughness measurements

AFM measurements were performed on a Bioscope Catalyst AFM (Bruker). AFM tapping mode was selected for these measurements to minimize the damage to the sample topography. Silicon tips with a resonance frequency around 300 kHz, 10 nm in radius, and a spring constant of 40 N were used. Measurements were performed under room temperature in aqueous conditions (Mili-Q water). For each AFM experiment a minimum of three different samples were investigated, and a representative height image of the surface morphology is reported in this article. The NanoScope software (Bruker) was used to analyze AFM images and to evaluate the film surface roughness of a 4×4 μm area from each sample. The mean roughness (R_a) parameter used for these measurements, is the arithmetic average of the deviations from the center plane of the AFM image which is dependents on the sampling size.

Characterization of surface chemistry of hydrogel composites using Fourier transform infrared spectroscopy (FTIR)

Composites of thin and thick agarose or alginate hydrogels on glass were prepared as described, except that this time thick hydrogels were coated on a glass slide instead of a coverslip; thin gels were still made on coverslips, as described above. Before mounting a hydrogel sample on the spectrometer, the imaging spacer that thick hydrogels were spread into was peeled off from a glass slide for firm contact between hydrogels and the ATR crystal of the spectrometer.

Infrared spectra were collected on a Bruker Vertex 70 Fourier transform infrared (FTIR) spectrometer equipped with a liquid nitrogen cooled HgCdTe (MCT) detector and a single reflection attenuated total reflectance (ATR) accessory consisting of a Ge ATR crystal with a 65° angle of incidence. Data were collected over the 400–4000 cm^{-1} range and manually cut to the 700–1500 cm^{-1} or 700–1900 cm^{-1} range for analysis. After hydrogel samples were mounted on the Ge ATR crystal, 500 scans at a resolution of 4 cm^{-1} and 20 kHz scan speed were accumulated to generate the single channel spectra for each sample. A blank spectrum of a clean Ge crystal was subtracted from the sample spectrum to generate the sample absorbance spectrum. A blank spectrum of a glass coverslip (for thin hydrogels) or glass slide (for thick hydrogels) was also subtracted. Finally, baseline tilt in the sample spectrum was corrected using the rubber band correction baseline function in the OPUS Spectroscopic software (OPUS, 6.5.92, Bruker Optik, GmbH, Ettlingen, Germany). Each combination of gel type and gel thickness were characterized in three replicate experiments.

L. Wang et al.

Measurement of bead attachment on surfaces

To compare the passive adhesivity of surfaces, we measured the passive attachment of polymer beads to the surface. For this, fluorescent polystyrene polymer beads (Bangs Laboratories, Inc., Dragon Green, FSDG004, diameter 1 μm) were diluted 1000 times in NaCl buffer (10 mM potassium phosphate composed of 5.4 mM potassium phosphate dibasic (K$_2$HPO$_4$, Sigma-Aldrich, 60353) and 4.6 mM potassium phosphate monobasic (KH$_2$PO$_4$, Sigma-Aldrich, 60218), 135 mM NaCl, pH 7.0).

16 μL of this bead suspension was added into one imaging spacer (Grace Bio-Labs, SS1X13, 13 mm diameter × 0.12 mm depth) adhered to a coverslip, which was then sealed by a hydrogel-coverslip composite (either thick or thin). After 1 h, beads attached on gels were imaged using an Olympus Fluoview1000 confocal microscope with a 60× oil-immersion objective. Fluorescent beads were illuminated with a 488 nm laser using standard GFP filter sets and confocal z-stacks were captured by Fluoview10-ASW version 4.2 software. The confocal z-stacks were processed using the particle analysis function in the Fiji distribution of ImageJ[78] to quantitatively determine the numbers of beads attached on gel composites (i.e., areal density of beads (number of beads/mm²)). Each combination of gel type and gel thickness was tested in two replicate experiments and at least 5 fields of view were randomly chosen for each replicate.

Microscopy measurement of bacterial accumulation on surfaces

Bacteria were streaked from frozen stock onto LB-Miller agar plates (Fisher Scientific, BP1425) and incubated overnight at 37 °C. Single colonies were inoculated into Luria broth (LB, 5 g of yeast extract (Fisher Scientific, BP1422), 10 g of tryptone (Fisher Scientific, BP1421), and 10 g of sodium chloride (NaCl, Sigma-Aldrich, S9888) per L of Millipore water) and grown overnight at 37 °C with shaking at 242 rpm using an orbital shaker (Labnet Orbit 1000). Then, 80 μL of overnight culture was transferred into 20 mL of fresh LB and vortexed. The resulting bacterial suspension was incubated at 37 °C with shaking at 242 rpm for at least 2 h until hydrogel composites were freshly made and ready. Then the bacterial suspension was incubated with hydrogel composites at 37 °C for 1 h.

Surface samples with accumulated bacteria were then gently washed with phosphate buffered saline (PBS, Sigma-Aldrich, P4417) twice, and then visualized using an Olympus IX71 inverted phase contrast microscope with a 60× oil-immersion objective. Images were taken by a QImaging EXi Blue CCD camera controlled by QCapture Pro-6 software and processed using the particle analysis function in Fiji to quantitatively determine the numbers of bacteria on surfaces (i.e., areal density of bacteria (number of bacteria/mm²)). For each combination of bacterial strain and hydrogel type (alginate or agarose), two technical replicates of each type of composite (thin and thick) were tested on each day (for a total of four samples per day). At least 12 fields of view were randomly chosen for each replicate. Each experiment was repeated twice independently on different days (for a total of 4 replicates for each combination of bacterial strain and composite type).

Finite element modeling of the cell-surface interaction

Finite element models (ABAQUS/Standard 2021, Dassault Systems, Providence, RI, USA) were developed to simulate the structural interaction between bacteria and hydrogel substrates upon surface adhesion. A 3D model with geometric nonlinearity was created, and the quarter symmetry was utilized (P. aeruginosa are rod-shaped and substrates are cuboid, Fig. 2b). The simulations were performed on the Frontera Linux cluster of the Texas Advanced Computing Center[79].

As a strain of Gram-negative bacteria, P. aeruginosa feature a thin layer of the bacterial cell envelope (~ 10¹ nm[70], compared to the whole cell ~10³ nm) that encloses the cytoplasm, chromosomes, and other intracellular materials. The bacterial cell envelope is a complicated multilayered structure composed of a rigid layer of cell wall sandwiched between two membranes made of lipid bilayers[80]. The membrane exterior to the cell wall is called the outer membrane (OM) and the membrane interior to the cell wall is the inner (or cytoplasmic) membrane (IM). Both OM and IM harbor a myriad of membrane proteins. The outer membrane is anchored to the cell wall via lipoproteins, and the outer membrane and cell wall together bear most of mechanical loading[62,81,82]. The high osmolarity difference between the internal bacterial cytoplasm and the external environment causes the bacterial cell envelope to be swollen by turgor pressure.

Recognizing these, bacteria were characterized as a thin-walled pressure vessel that consists of a hollow cylindrical trunk with hollow hemispherical caps on both ends with literature-reported properties (Supplementary Table 1). The envelopes were modeled as a two-layered composite material, the outer layer of which is the outer membrane and the inner layer of which is the cell wall. Hydrogel-coverslip composite substrates were assumed to be an isotropic and homogeneous material, with its properties computed from the composite theory (Fig. 1d) and the reported values (Supplementary Table 1).

Due to the thinness of bacterial cell envelopes, we used shell elements (24257 S4R elements with enhanced hourglass control, Supplementary Fig. 3a) to discretize them. The composite shell scheme was used to section cell envelopes into two layers of different materials, with three section points on each layer (at which secondary variables, e.g., stress and strain, were computed). Substrates were discretized by eight-node linear brick elements (436428 C3D8 elements, Supplementary Fig. 3a). Since changes in mechanics, such as stress and strain, primarily occur at locations where the bacterial surface is in contact with the substrate surface, "contact surfaces" were defined by partitioning the lower half of the bacterial surface and the corresponding part of the surface of the substrate into "contact surfaces" (surfaces abcde and fgh, respectively, in Supplementary Fig. 3c); the cellular contact surface is half the entire lower cellular surface and the substrate contact surface is the projection of the cellular contact surface on the substrate. "Contact surfaces" were specifically assigned finer mesh (5 nm mesh size instead of 15 nm in the rest of the model) to allow better resolution of mechanical changes. The contact was formulated as frictionless and 'hard contact' along the normal direction.

A typical simulation comprised two steps. In the first step, an "inflating" turgor pressure was applied to the inner surface of an undeformed and free-floating cell envelope. During "inflation," the cellular mid-plane (curve abc in Supplementary Fig. 2b) was not allowed to move vertically. In the second step, the established turgor pressure was maintained, and the mid-plane was displaced downward by 150 nm to achieve contact between the cell envelope and the substrate. Incremental displacement was applied in ABAQUS and, at every increment at which the bacterium and substrate were in contact, the simulation was analyzed to determine the stresses and strains on bacterial envelopes. Two simulations were performed: one with a stiff substrate and one with a soft substrate (Supplementary Table 1).

We investigated the stress and strain state of four representative shell elements (in the bacterium) that are within the contact surface (inset of Fig. 2b). Stresses were normalized to the respective values at the end of the first step; strains were computed as the net logarithmic strain change between the first and second step. We interpreted the strain state on the innermost section point of a shell element (i.e., on the interior of cell wall) as that experienced by the inner membrane, based on the assumption that the inner membrane is constantly pressed

against the cell wall by turgor pressure. The CAREA output variable in ABAQUS was requested at every increment to keep track of the total area in contact as displacement grew. The cell volume enclosed by cell envelopes was calculated using the BOUNDARY syntax in MATLAB (MATLAB 2020 (R2020b), The MathWorks Inc., Natick, MA, USA).

To analyze convergence, the mesh size within the contact surfaces was varied from 30, 25, 20, 15, 10, 7.5, 5, to 2.5 nm (Supplementary Fig. 4j). The circumferential stress on the outer membrane at element #1 (inset of Fig. 2b) was compared at different mesh sizes, and it was found that the mesh size we adopted in our modeling is within the convergence range.

To model surface adhesion by assigning boundary conditions in the form of forces (i.e., the adhesion force scheme), the first step was simply applying turgor pressure to a stress-free cell envelope, the same as the first, "inflation", step in the displacement scheme described above. In the second step, the mid-plane of the cell envelope was displaced toward the substrate by 90 nm to achieve initial contact and hence easier convergence in the following step. In the last step, vertical, attractive surface tractions with a magnitude of 110 kPa were applied over the contact surfaces of cell envelopes and substrates, resulting in further contact between the two (Supplementary Fig. 3c).

Levels of intracellular sodium ions in surface-adhered bacteria

In the presence of excess external Na^+, sodium enters cells through mechanosensitive ion channels that are activated by mechanical tension in the membrane. The assay measuring the intracellular sodium level was done using procedures reported previously[83] with some modifications. Bacteria were cultured in Tryptone broth (T-broth, 1% tryptone and 0.5% NaCl) at 37 °C with shaking. Two mL of day culture were centrifuged using an Eppendorf Centrifuge 5810 R at 2000×g for 2 min, and the supernatant was discarded. Pelleted bacteria were resuspended in 2 mL potassium chloride (KCl) buffer (10 mM potassium phosphate composed of 5.4 mM K_2HPO_4 and 4.6 mM KH_2PO_4, 135 mM KCl (Sigma-Aldrich, P9333), pH 7.0) and mixed using a Fisherbrand analog vortex mixer (02215365). The suspension of bacteria in the KCl buffer was then centrifuged (2000×g for 2 min) to pellet bacteria; then, pelleted bacteria were resuspended and mixed in fresh KCl buffer again, as described above. This washing procedure was repeated three times in total. Bacteria were then resuspended and mixed by vortex in 2 mL ethylenediaminetetraacetic acid (EDTA) buffer (the KCl buffer plus 10 mM EDTA (Sigma-Aldrich, EDS)) and left for 10 min at room temperature. The suspension of bacteria in the ETDA buffer was centrifuged at 2000×g for 6 min, and the supernatant was discarded. The resulting pellet of bacteria was resuspended in 2 mL KCl buffer and mixed by vortexing. The resulting bacteria suspension in KCl buffer was centrifuged (2000×g for 5 min), and pelleted bacteria were resuspended and mixed in fresh KCl buffer again. This washing procedure was repeated three times in total. Then, bacteria were resuspended in 750 µL of loading buffer, consisting of 40 µM Sodium Green (sodium ion fluorescence indicator, ThermoFisher Scientific, S6901) in KCl buffer, and left for 30 min in the dark at room temperature. The stock solution of Sodium Green (1 mM) was freshly prepared at each experiment by dissolving Sodium Green in dimethyl sulfoxide (DMSO, Sigma-Aldrich, W387520). The suspension of bacteria in the loading buffer was centrifuged at 2000×g for 5 min, and the supernatant was discarded. The resulting pellet of bacteria was resuspended in 750 µL NaCl buffer (10 mM potassium phosphate composed of 5.4 mM K_2HPO_4 and 4.6 mM KH_2PO_4, 135 mM NaCl, pH 7.0) and mixed by vortexing. The resulting bacterial suspension in NaCl buffer was centrifuged (2000×g for 5 min), and pelleted bacteria were resuspended and mixed in fresh NaCl buffer again. This washing procedure was repeated three times in total. Bacteria

loaded with Sodium Green were resuspended in 400 µL NaCl buffer, and 16 µL of this bacterial suspension was added into one imaging spacer (Grace Bio-Labs, SS1X13, 13 mm diameter × 0.12 mm depth) adhered to a coverslip, which was then sealed by an agarose-coverslip composite (either thick or thin). Bacteria were allowed to attach to the gel composite for 1 h.

Then, bacteria attached on thin or thick agarose composites were imaged using an Olympus FV1000 confocal microscope with a 60× oil-immersion objective. The Sodium Green fluorescence indicator was illuminated with a 488 nm laser using standard GFP filter sets and confocal z-stacks were captured by FV10-ASW version 4.2 software. At least 15 stacks were taken at different fields of view for each sample. Each experiment was repeated three times independently. The fluorescence intensity of each bacterium was measured using Fiji. Spinning bacteria were excluded from the analysis. The section below describes the calibration done to account for different attenuations of light by gels of different thicknesses.

Calibrating for light attenuation by gels of different thicknesses for intracellular sodium ion measurements

Fluorescent polystyrene polymer beads (Bangs Laboratories, Inc., Dragon Green, FSDG004, diameter 1 µm) were used to assess the effect of attenuation of exciting and emitted light passing through gels of different thicknesses. Beads were diluted 1000 times in NaCl buffer (10 mM potassium phosphate composed of 5.4 mM K_2HPO_4 and 4.6 mM KH_2PO_4, 135 mM NaCl, pH 7.0). 16 µL of this bead suspension was added into one imaging spacer (Grace Bio-Labs, SS1X13, 13 mm diameter × 0.12 mm depth) adhered to a coverslip, which was then sealed by an agarose-coverslip composite (either thick or thin). Beads attached on agarose gel composites were imaged using an Olympus FV1000 confocal microscope with a 60× oil-immersion objective. Fluorescent beads were illuminated with a 488 nm laser using standard GFP filter sets and confocal z-stacks were captured by FV10-ASW version 4.2 software. Supplementary Fig. 6a shows the average fluorescence intensity of beads attached on thick and thin agarose gel composites. Each data point was measured using one photomultiplier tube (PMT) voltage, and by changing the PMT voltage, we obtained an exponential fitted curve to the dataset. Each voltage has 5 different fields of view for one gel sample, and each field of view has about 60-70 beads.

To calibrate the measured intensity of bacterial fluorescence for attenuation by hydrogels, the exponential fitted curve (Supplementary Fig. 6a) was used to convert the fluorescence intensity of each bacterium attached on the thin gel into the equivalent intensity on the thick gel. To do this, the fluorescence intensity of a bacterium was substituted in for the variable x in the fitted equation (Supplementary Fig. 6a), and the y-value, corresponding to intensity on the thick gel, calculated. The resulting converted (or calibrated) fluorescence intensities of bacteria on thin gels were compared with the measured intensities of bacteria on the thick gel.

Speeds of surface-adhered bacteria during bacterial accumulation

An adhesive imaging chamber (Grace Bio-Labs, PCI-A-2.5, 20 mm diameter × 2.6 mm depth) was filled with 650 µL of bacterial suspension in LB medium and then sealed by a coverslip coated with an agarose gel (either thick or thin). For the next hour, surface-attached bacteria on gel surfaces was observed using an Olympus IX71 inverted phase contrast microscope with a 60× oil-immersion objective. The microscope stage was enclosed within an incubator chamber heated to 37 °C.

Fifteen time-lapse sequences taken at different fields of view for each sample were captured by a Hamamatsu digital camera C11440 controlled by MetaMorph Advanced version

7.7.6.0 software. The acquisition rate was one frame per 0.42 s, and each sequence had 150 frames (total recording time for each sequence was 62.6 s). Each experiment was repeated three times independently.

Trajectories of bacterial centers-of-mass were tracked and the bacteria speed during each interval (0.42 s) was measured using the TrackMate plugin in Fiji[84,85]. The average speed of each tracked bacterium over the tracking period was collected for data analysis. Near-surface swimming bacteria, which displayed a much higher instantaneous speed and a much shorter tracking period (less than 5 s) than surface-attached bacteria, were also tracked by the software. We excluded these swimming bacteria from data analysis.

Measurement of fractions of surface motility during bacterial accumulation
Among the total tracked surface-attached bacteria, some bacteria remained stationary on surfaces, and the others were motile showing spinning or twitching surface motility. The time-lapse sequences taken to track bacterial trajectories were projected into single-frame images using the ZProjection function (with minimum intensity projections) in Fiji. Projections of stationary bacteria showed the same bacterial cell size as seen in a single time slice-slice. Projections of spinning bacteria reflected motion in a circle, with bacteria appearing as the petals of a "daisy". Projections of twitching bacteria showed an irregular shape. Using these projections, the number of stationary, spinning and twitching bacteria was counted and recorded. The number of motile bacteria was the sum of the number of spinning bacteria and that of twitching bacteria.

Measurement of detachment events during bacterial accumulation
The tracks of some surface-attached bacteria had shorter durations than the total recording time (62.6 s). The positions of such short tracks were given by the TrackMate plugin of Fiji. We manually observed bacteria at these locations to determine whether the abbreviated length of the track arose from a bacterium detaching from the surface or from a bacterium newly attaching during the recording period. The number of detachment events was recorded.

Microscopy measurement of growth of bacteria on surfaces
Bacterial growth curves on surfaces were measured on agarose gel composites. After allowing bacteria suspended in LB medium to accumulate on a gel surface at 37 °C for an hour, surfaces were gently rinsed twice with fresh LB medium and incubated with fresh LB medium at 37 °C. Rinsing and incubation with fresh LB medium was repeated hourly.

After 1, 2, 3, 4, 5, and 6 h of incubation, sample surfaces were gently washed with PBS twice, and then visualized an Olympus IX71 inverted phase contrast microscope with a 60× oil-immersion objective. Images were taken by a QImaging EXi Blue CCD camera controlled by QCapture Pro-6 software and processed using the particle analysis function (for counting single bacteria) and the multi-point function (for counting bacteria in micro-colonies and in clusters) in Fiji, to quantitatively determine the numbers of bacteria on surfaces (i.e., areal density of bacteria (number of bacteria/mm²)). Each time point was done for two replicate samples, and at least 12 fields of view were randomly chosen for each replicate. Samples used for measurement at one time point were not used for further incubation or later measurements, i.e., the measurement at each time point was done independently.

Construction of complemented mutant strains and plasmids
Strains and plasmids used to construct complemented mutant strains and primers used for plasmid construction are listed in Supplementary Table 2. Multicopy plasmids pMQ72 and pMQ70[86] were used for expression of PilT and PilY1, respectively. Plasmids were designed by homologous recombination using the yeast machinery[86] or by Gibson assembly[87] using NEBuilder HiFi DNA Assembly™ (NEB, Boston, MA), as previously described. All inserts were sequenced to confirm the integration of the correct sequence. Plasmids were then isolated from *E. coli* S17-λ-pir overnight-grown strains and then electroporated into *P. aeruginosa* PAO1 and grown on the appropriate antibiotic selection plates, as reported previously[86].

Microscopy measurement of growth of complemented strains on surfaces
For plasmid maintenance in complemented strains, LB agar and LB liquid medium were supplemented with 60 µg/mL gentamycin for Δ*pilT* pBAD::*pilT* and with 150 µg/mL carbenicillin for Δ*pilY1* pBAD::*pilY1*. Bacterial growth curves on surfaces were measured on thick and thin agarose gel composites. The LB medium used for rinsing and incubating gel composites with accumulated bacteria was supplemented with 0.025% arabinose for plasmid induction. The overnight culture was first diluted by 1:100 in the LB medium supplemented with arabinose and then grown at 37 °C with shaking until the diluted suspension reached an optical density (OD_{600}) of 0.7 for proper plasmid induction before growth curves were measured. With this exception, growth was measured experimentally as also done for the microscopy growth assays described above for *P. aeruginosa* PAO1 WT and the Δ*pilT* and Δ*pilY1* mutants. Each time point was done for one replicate sample, and at least 15 fields of view were randomly chosen for each replicate. Samples used for measurement at one time point were not used for further incubation or later measurements.

Statistical analysis of exponential growth rate
The exponential regression ($f(t) = Ae^{at}$) for exponential phase datasets was transformed into the linear equation $\ln(f(t)) = \ln(A) + at$, using Microsoft Excel. Statistical significance of slopes of the linear equation, i.e., bacterial growth rate a on gels was determined by ANCOVA testing using the R programming language.

Measurement of c-di-GMP signaling during bacterial accumulation and growth on surfaces
A suspension of bacterium in LB medium was prepared as described in the section above on assaying bacterial accumulation.

Both the liner cover of the adhesive side and the polycarbonate cover of the non-adhesive side of an imaging chamber (Grace Bio-Labs, PCI-A-2.5, 20 mm diameter × 2.6 mm depth) were peeled off by a tweezer. The adhesive side of the chamber was adhered to a coverslip coated with an agarose gel (either thick or thin). The chamber was then filled with 650 µL of bacterial suspension in LB medium and a coverslip was placed on top of the chamber.

As bacteria accumulated on the gel surface for the next hour, bacteria containing either the reporter plasmid pCdrA::*gfp* or the control plasmid pMH487 were imaged using an Olympus FV1000 confocal microscope with a 60× oil-immersion objective. Bacteria were illuminated with a 488 nm laser using standard GFP filter sets and confocal z-stacks were captured by FV10-ASW version 4.2 software. The microscope stage was enclosed within an incubator chamber heated to 37 °C.

After one hour of bacterial accumulation, the coverslip on top of the imaging chamber was removed, the bacterial suspension in the imaging chamber was gently removed and replaced by 650 µL

of fresh LB medium using a pipette, and a new coverslip was placed on top of the imaging chamber. The fresh LB medium was stored at 37 °C before each use. For the following hour of bacterial growth on gel surfaces, bacteria were imaged using confocal microscope as described above. At hourly intervals, the LB medium in the imaging chamber was removed and replaced by fresh LB medium. The experiment was carried on until the end of two hours after the onset of exponential growth indicated in Fig. 5d–f. Each experiment of bacteria containing the reporter plasmid pCdrA::gfp was repeated three times independently. Each experiment of bacteria containing the control plasmid pMH487 was repeated twice independently.

The sets of images collected within each 15 min time interval were analyzed separately. Images taken during the first 15 min interval after each replacement of medium were excluded from analysis to avoid including any effects of temperature fluctuation on c-di-GMP signaling. For the second, third, and fourth 15 min interval in each hour, the fluorescent intensity of each bacterium was measured using Fiji, and calibrated using the following bead calibration for light attenuation by gels of different thicknesses. Then the intensity of each bacterium containing the reporter plasmid pCdrA::gfp was normalized by subtracting the average per-cell intensity of an ensemble of cells carrying a control plasmid for producing GFP that lacks the cdrA promoter (pMH874)[13].

Calibrating for light attenuation by gels of different thicknesses for c-di-GMP measurements

We used an approach very similar to the one we developed previously[52]. Fluorescent polystyrene polymer beads (Bangs Laboratories, Inc., Dragon Green, FSDG004, diameter 1 μm) were diluted 1000 times in LB medium. Both the liner cover of the adhesive side and the polycarbonate cover of the non-adhesive side of an imaging chamber (Grace Bio-Labs, PCI-A-2.5, 20 mm diameter × 2.6 mm depth) were peeled off by a tweezer. The adhesive side of the chamber was adhered to a coverslip coated with an agarose gel (either thick or thin). The chamber was then filled with 650 μL of the bead suspension in LB medium and a coverslip was placed on top of the chamber.

Beads attached on agarose gel composites were imaged using confocal microscopy, as described in the bead calibration for measurements of intracellular sodium ions. The microscope stage was enclosed within an incubator chamber heated to 37 °C. Supplementary Fig. 6b shows the average fluorescence intensity of beads attached on thick and thin agarose gel composites. Each data point was measured under one PMT voltage, and by changing the PMT voltage, we obtained an exponential fitted curve to the dataset. Each voltage has 5 different fields of view for one gel sample.

To calibrate the measured fluorescence intensity of GFP for attenuation by hydrogels, the exponential fitted curve (Supplementary Fig. 6b) was used to convert the fluorescence intensity of GFP in each bacterium on the thin gel into the equivalent intensity on the thick gel. To do this, the fluorescence intensity of GFP in a bacterium was substituted in for the variable x in the fitted equation (Supplementary Fig. 6b), and the y-value, corresponding to intensity on the thick gel, calculated. The resulting converted (or calibrated) fluorescence intensities of GFP in bacteria on thin gels were compared with the measured intensities of GFP in bacteria on the thick gel.

Bacterial accumulation and growth on glass and bulk agarose gel surfaces

Bacterial accumulation and growth on glass and bulk agarose gel surfaces were done with WT and mutants that did not contain any plasmid. A suspension of bacteria in LB medium was prepared as

described in Method in the manuscript on assaying bacterial accumulation on thin and thick gel composites.

Glass slides were sonicated in 70% ethanol for 15 min and then dried with nitrogen before use. Both the liner cover of the adhesive side and the polycarbonate cover of the non-adhesive side of an imaging chamber (Grace Bio-Labs, PCI-A-2.5, 20 mm diameter × 2.6 mm depth) were peeled off using tweezers. The adhesive side of the chamber was adhered to a glass slide. The chamber was then filled with 750 μL of bacterial suspension.

3% (w/w) agarose solution was autoclaved, and 500 μL of agarose solution was pipetted into each well of a 24-well plate (15.6 mm diameter of well). The plate was cooled at 4 °C for 2 min, resulting in gelation. Each well was filled with 456 μL of bacterial suspension on top of the bulk gel surface. The height of the bacterial suspension above the glass slide and the bulk gel surface was the same.

To measure the initial accumulation of bacteria after one hour at 37 °C, the bacterial suspension was removed and the glass and bulk gel surfaces were then gently washed with PBS three times. The imaging chamber on the glass surface was removed and the bulk gel was gently removed from the well. Each sample surface was sonicated in 15 mL PBS for 20 min to detach accumulated bacteria. The bacterial concentrations in the 15 mL PBS were measured using a conventional serial dilution method, with the dilutions spread onto the surfaces of agar plates[88]. The agar plates were cultivated at 37 °C for 18 h; the numbers of colonies cultured from the serial dilutions were then counted and the measured counts converted to colony-forming unit (CFU) per mL after multiplication with the dilution factor. Sample surface area was ~314 mm² for glass and ~191 mm² for bulk gel. This was used to determine areal density of bacteria (CFU/mm²) on the sample surface.

To measure bacterial growth after the initial one-hour accumulation, the bacterial suspension was removed from the sample surface and replaced by fresh LB medium, which was stored at 37 °C before each use. At hourly intervals thereafter, the numbers of bacteria on surfaces were determined using the plate-counting method described above. Also, at hourly intervals, the LB medium was removed and replaced by fresh LB medium. Each sample has two replicates and each experiment was repeated twice independently.

Reporting summary

Further information on research design is available in the Nature Research Reporting Summary linked to this article.

REFERENCES

1. Cheng, B. et al. Cellular mechanosensing of the biophysical microenvironment: a review of mathematical models of biophysical regulation of cell responses. *Phys. Life Rev.* **22**, 88–119 (2017).
2. Iskratsch, T., Wolfenson, H. & Sheetz, M. P. Appreciating force and shape—the rise of mechanotransduction in cell biology. *Nat. Rev. Mol. Cell Biol.* **15**, 825–833 (2014).

3. Persat, A. Bacterial mechanotransduction. *Curr. Opin. Microbiol.* **36**, 1–6 (2017).

4. Gordon, V. D. & Wang, L. Bacterial mechanosensing: the force will be with you, always. *J. Cell Sci.* **132**, jcs227694 (2019).

5. Dufrêne, Y. F. & Persat, A. Mechanomicrobiology: how bacteria sense and respond to forces. *Nat. Rev. Microbiol.* **18**, 1–14 (2020).

6. Ellison, C. K. et al. Obstruction of pilus retraction stimulates bacterial surface sensing. *Science* **358**, 535–538 (2017).

7. Hug, I., Deshpande, S., Sprecher, K. S., Pfohl, T. & Jenal, U. Second messenger-mediated tactile response by a bacterial rotary motor. *Science* **358**, 531–534 (2017).

8. Persat, A., Inclan, Y. F., Engel, J. N., Stone, H. A. & Gitai, Z. Type IV pili mechanochemically regulate virulence factors in *Pseudomonas aeruginosa. Proc. Natl Acad. Sci. USA* **112**, 7563–7568 (2015).

9. Luo, Y. et al. A hierarchical cascade of second messengers regulates *Pseudomonas aeruginosa* surface behaviors. *mBio* **6**, e02456–02414 (2015).

10. Siryaporn, A., Kuchma, S. L., O'Toole, G. A. & Gitai, Z. Surface attachment induces *Pseudomonas aeruginosa* virulence. *Proc. Natl Acad. Sci. USA* **111**, 16860–16865 (2014).

11. Talà, L., Fineberg, A., Kukura, P. & Persat, A. *Pseudomonas aeruginosa* orchestrates twitching motility by sequential control of type IV pili movements. *Nat. Microbiol.* **4**, 774–780 (2019).

12. O'Neal, L. et al. The Wsp system of *Pseudomonas aeruginosa* links surface sensing and cell envelope stress. *Proc. Natl Acad. Sci. USA* **119**, e2117633119 (2022).

13. Rodesney, C. A. et al. Mechanosensing of shear by *Pseudomonas aeruginosa* leads to increased levels of the cyclic-di-GMP signal initiating biofilm development. *Proc. Natl Acad. Sci. USA* **114**, 5906–5911 (2017).

14. Sanfilippo, J. E. et al. Microfluidic-based transcriptomics reveal force-independent bacterial rheosensing. *Nat. Microbiol.* **4**, 1274–1281 (2019).

15. Nguyen, Y. et al. *Pseudomonas aeruginosa* minor pilins prime type IVa pilus assembly and promote surface display of the PilY1 adhesin. *J. Biol. Chem.* **290**, 601–611 (2015).

16. Guimaraes, C. F., Gasperini, L., Marques, A. P. & Reis, R. L. The stiffness of living tissues and its implications for tissue engineering. *Nat. Rev. Mater.* 1–20 (2020).

17. Wang, Y. et al. Interactions of *Staphylococcus aureus* with ultrasoft hydrogel biomaterials. *Biomaterials* **95**, 74–85 (2016).

18. Campoccia, D., Montanaro, L. & Arciola, C. R. The significance of infection related to orthopedic devices and issues of antibiotic resistance. *Biomaterials* **27**, 2331–2339 (2006).

19. Funt, D. & Pavicic, T. Dermal fillers in aesthetics: an overview of adverse events and treatment approaches. *Clin. Cosmet. Investig. Dermatol.* **6**, 295 (2013).

20. Wald, H. L. & Kramer, A. M. Nonpayment for harms resulting from medical care: catheter-associated urinary tract infections. *Jama* **298**, 2782–2784 (2007).

21. Koch, M. D., Black, M. E., Han, E., Shaevitz, J. W. & Gitai, Z. *Pseudomonas aeruginosa* distinguishes surfaces by stiffness using retraction of type IV pili. *Proc. Natl Acad. Sci. USA* **119**, e2119434119 (2022).

22. Cont, A., Vermeil, J. & Persat, A. Material Substrate Physical Properties Control *Pseudomonas aeruginosa* Biofilm Architecture. *mBio* **14**, e03518–e03522 (2023).

23. Bayoudh, S. et al. Quantification of the adhesion free energy between bacteria and hydrophobic and hydrophilic substrata. *Mater. Sci. Eng. C* **26**, 300–305 (2006).

24. Bruinsma, G., Van der Mei, H. & Busscher, H. Bacterial adhesion to surface hydrophilic and hydrophobic contact lenses. *Biomaterials* **22**, 3217–3224 (2001).

25. Yang, K. et al. Bacterial anti-adhesion surface design: Surface patterning, roughness and wettability: A review. *J. Mater. Sci. Technol.* **99**, 82–100 (2022).

26. Yuan, Y., Hays, M. P., Hardwidge, P. R. & Kim, J. Surface characteristics influencing bacterial adhesion to polymeric substrates. *RSC Adv.* **7**, 14254–14261 (2017).

27. Wang, Y., Lee, S. M. & Dykes, G. The physicochemical process of bacterial attachment to abiotic surfaces: Challenges for mechanistic studies, predictability and the development of control strategies. *Crit. Rev. Microbiol.* **41**, 452–464 (2015).

28. Cheng, Y., Feng, G. & Moraru, C. I. Micro-and nanotopography sensitive bacterial attachment mechanisms: a review. *Front. Microbiol.* **10**, 191 (2019).

29. Vadillo-Rodriguez, V., Busscher, H. J., van der Mei, H. C., de Vries, J. & Norde, W. Role of *lactobacillus* cell surface hydrophobicity as probed by AFM in adhesion to surfaces at low and high ionic strength. *Colloids Surf. B: Biointerf.* **41**, 33–41 (2005).

30. Zhang, X. et al. Interpretation of adhesion behaviors between bacteria and modified basalt fiber by surface thermodynamics and extended DLVO theory. *Colloids Surf. B: Biointerf.* **177**, 454–461 (2019).

31. Carniello, V., Peterson, B. W., van der Mei, H. C. & Busscher, H. J. Physico-chemistry from initial bacterial adhesion to surface-programmed biofilm growth. *Adv. Colloid Interf. Sci.* **261**, 1–14 (2018).

32. Kolewe, K. W., Peyton, S. R. & Schiffman, J. D. Fewer bacteria adhere to softer hydrogels. *ACS Appl. Mater. Interf.* **7**, 19562–19569 (2015).

33. Peng, Q. et al. Three-dimensional bacterial motions near a surface investigated by digital holographic microscopy: effect of surface stiffness. *Langmuir* **35**, 12257–12263 (2019).

34. Kolewe, K. W., Zhu, J., Mako, N. R., Nonnenmann, S. S. & Schiffman, J. D. Bacterial adhesion is affected by the thickness and stiffness of poly (ethylene glycol) hydrogels. *ACS Appl. Mater. Interf.* **10**, 2275–2281 (2018).

35. Song, F. et al. How bacteria respond to material stiffness during attachment: a role of *Escherichia coli* flagellar motility. *ACS Appl. Mater. Interf.* **9**, 22176–22184 (2017).

36. Straub, H. et al. Bacterial Adhesion on Soft Materials: Passive Physicochemical Interactions or Active Bacterial Mechanosensing? *Adv. Healthc. Mater.* **8**, 1801323 (2019).

37. Carniello, V., Peterson, B. W., Sjollema, J., Busscher, H. J. & van der Mei, H. C. Surface enhanced fluorescence and nanoscopic cell wall deformation in adhering *Staphylococcus aureus* upon exposure to cell wall active and non-active antibiotics. *Nanoscale* **10**, 11123–11133 (2018).

38. Otto, K. & Silhavy, T. J. Surface sensing and adhesion of *Escherichia coli* controlled by the Cpx-signaling pathway. *Proc. Natl Acad. Sci. USA* **99**, 2287–2292 (2002).

39. Shimizu, T., Ichimura, K. & Noda, M. The surface sensor NlpE of enterohemorrhagic *Escherichia coli* contributes to regulation of the type III secretion system and flagella by the Cpx response to adhesion. *Infect. Immun.* **84**, 537–549 (2016).

40. Booth, I. R. Bacterial mechanosensitive channels: progress towards an understanding of their roles in cell physiology. *Curr. Opin. Microbiol.* **18**, 16–22 (2014).

41. Booth, I. R., Edwards, M. D., Black, S., Schumann, U. & Miller, S. Mechanosensitive channels in bacteria: signs of closure? *Nat. Rev. Microbiol.* **5**, 431 (2007).

42. Laventie, B.-J. & Jenal, U. Surface sensing and adaptation in bacteria. *Annu. Rev. Microbiol.* **74**, 735–760 (2020).

43. Lee, C. K. et al. Multigenerational memory and adaptive adhesion in early bacterial biofilm communities. *Proc. Natl Acad. Sci. USA* **115**, 4471–4476 (2018).

44. Lee, C. K. et al. Social cooperativity of bacteria during reversible surface attachment in young biofilms: a quantitative comparison of *Pseudomonas aeruginosa* PA14 and PAO1. *mBio* **11**, e02644–19 (2020).

45. Wang, C., Hou, J., van der Mei, H. C., Busscher, H. J. & Ren, Y. Emergent properties in *Streptococcus mutans* biofilms are controlled through adhesion force sensing by initial colonizers. *mBio* **10**, 01908–01919 (2019).

46. Conrad, J. C. et al. Flagella and pili-mediated near-surface single-cell motility mechanisms in *P. aeruginosa. Biophys. J.* **100**, 1608–1616 (2011).

47. Gibiansky, M. L. et al. Bacteria use type IV pili to walk upright and detach from surfaces. *Science* **330**, 197–197 (2010).

48. Bennett, R. R. et al. Species-dependent hydrodynamics of flagellum-tethered bacteria in early biofilm development. *J. R. Soc. Interf.* **13**, 20150966 (2016).

49. Jenal, U., Reinders, A. & Lori, C. Cyclic di-GMP: second messenger extraordinaire. *Nat. Rev. Microbiol.* **15**, 271 (2017).

50. Hengge, R. Principles of c-di-GMP signalling in bacteria. *Nat. Rev. Microbiol.* **7**, 263–273 (2009).

51. Rybtke, M. T. et al. Fluorescence-based reporter for gauging cyclic di-GMP levels in *Pseudomonas aeruginosa. Appl. Environ. Microbiol.* **78**, 5060–5069 (2012).

52. Blacutt, J., Lan, Z., Cosgriff-Hernandez, E. M. & Gordon, V. D. Quantitative confocal microscopy and calibration for measuring differences in cyclic-di-GMP signalling by bacteria on biomedical hydrogels. *R. Soc. Open Sci.* **8**, 201453 (2021).

53. Laventie, B.-J. et al. A surface-induced asymmetric program promotes tissue colonization by *Pseudomonas aeruginosa. Cell Host Microbe* **25**, 140–152.e146 (2019).

54. Bertrand, R. L. Lag phase is a dynamic, organized, adaptive, and evolvable period that prepares bacteria for cell division. *J. Bacteriol.* **201**, e00697–00618 (2019).

55. Park, S. & Sauer, K. Controlling Biofilm Development Through Cyclic di-GMP Signaling. *Pseudomonas aeruginosa: Biol. Pathogen. Control Strategies*, **1386**; 69–94 (2022).

56. Lichtenberg, M. et al. Cyclic-di-GMP signaling controls metabolic activity in *Pseudomonas aeruginosa. Cell Rep.* **41**, 111515 (2022).

57. Webster, S. S. et al. Force-induced changes of PilY1 drive surface sensing by *Pseudomonas aeruginosa. mBio* **13**, e03754–03721 (2022).

58. Geiger, C. J. & O'Toole, G. A. Evidence for the Type IV Pilus Retraction Motor PilT as a Component of the Surface Sensing System in Pseudomonas aeruginosa. *J. Bacteriol.* **205**, e00179–00123 (2023).

59. Trivedi, R. R. et al. Mechanical genomic studies reveal the role of D-alanine metabolism in *Pseudomonas aeruginosa* cell stiffness. *mBio* **9**; e01340–18 (2018).

60. Formosa, C., Grare, M., Duval, R. E. & Dague, E. Nanoscale effects of antibiotics on. *P. aeruginosa. Nanomed.: NBM* **8**, 12–16 (2012).

61. Mathelié-Guinlet, M. et al. Detrimental impact of silica nanoparticles on the nanomechanical properties of *Escherichia coli*, studied by AFM. *J. Colloid Interf. Sci.* **529**, 53–64 (2018).

62. Rojas, E. R. et al. The outer membrane is an essential load-bearing element in Gram-negative bacteria. *Nature* **559**, 617–621 (2018).

233

63. Auer, G. K. & Weibel, D. B. Bacterial cell mechanics. *Biochemistry* **56**, 3710–3724 (2017).
64. Tuson, H. H. et al. Measuring the stiffness of bacterial cells from growth rates in hydrogels of tunable elasticity. *Mol. Microbiol.* **84**, 874–891 (2012).
65. Vadillo-Rodriguez, V., Schooling, S. R. & Dutcher, J. R. In situ characterization of differences in the viscoelastic response of individual gram-negative and gram-positive bacterial cells. *J. Bacteriol.* **191**, 5518–5525 (2009).
66. Kumar, U., Vivekanand, K. & Poddar, P. Real-time nanomechanical and topographical mapping on live bacterial cells-*Brevibacterium casei* under stress due to their exposure to Co²⁺ ions during microbial synthesis of Co₃O₄ nanoparticles. *J. Phys. Chem. B* **113**, 7927–7933 (2009).
67. Francius, G., Domenech, O., Mingeot-Leclercq, M. P. & Dufrêne, Y. F. Direct observation of *Staphylococcus aureus* cell wall digestion by lysostaphin. *J. Bacteriol.* **190**, 7904–7909 (2008).
68. Thwaites, J. J. & Mendelson, N. H. Mechanical behaviour of bacterial cell walls. *Adv. Microb. Physiol.* **32**, 173–222 (1991).
69. Timoshenko, S. P. & Woinowsky-Krieger, S. *Theory of plates and shells.* (McGraw-hill, 1959).
70. Matias, V. R., Al-Amoudi, A., Dubochet, J. & Beveridge, T. J. Cryo-transmission electron microscopy of frozen-hydrated sections of *Escherichia coli* and *Pseudomonas aeruginosa.* *J. Bacteriol.* **185**, 6112–6118 (2003).
71. Hayhurst, E. J., Kailas, L., Hobbs, J. K. & Foster, S. J. Cell wall peptidoglycan architecture in *Bacillus subtilis. Proc. Natl Acad. Sci. USA* **105**, 14603–14608 (2008).
72. Saha, N., Monge, C., Dulong, V., Picart, C. & Glinel, K. Influence of Polyelectrolyte Film Stiffness on Bacterial Growth. *Biomacromolecules* **14**, 520–528 (2013).
73. Guégan, C. et al. Alteration of bacterial adhesion induced by the substrate stiffness. *Colloids Surf. B Biointerf.* **114**, 193–200 (2014).
74. Jacobs, M. A. et al. Comprehensive transposon mutant library of *Pseudomonas aeruginosa. Proc. Natl Acad. Sci. USA* **100**, 14339–14344 (2003).
75. Shillaber, C. P. *Photomicrography in theory and practice.* (Wiley, 1944).
76. Krieg, M. et al. Atomic force microscopy-based mechanobiology. *Nat. Rev. Phys.* **1**, 41–57 (2019).
77. Tivol, W. F., Briegel, A. & Jensen, G. J. An improved cryogen for plunge freezing. *Microsc. Microanal.* **14**, 375–379 (2008).
78. Schindelin, J. et al. Fiji: an open-source platform for biological-image analysis. *Nat. Methods* **9**, 676–682 (2012).
79. Stanzione, D. et al. in *Practice and Experience in Advanced Research Computing* 106-111 (2020).
80. Silhavy, T. J., Kahne, D. & Walker, S. The bacterial cell envelope. *Cold Spring Harb. Perspect. Biol.* **2**, a000414 (2010).
81. Morris, D. M. & Jensen, G. J. Toward a biomechanical understanding of whole bacterial cells. *Annu. Rev. Biochem.* **77**, 583–613 (2008).
82. Shaevitz, J. W. Microbiology: peeling back the layers of bacterial envelope mechanics. *Curr. Biol.* **28**, R1210–R1211 (2018).
83. Lo, C.-J., Leake, M. C. & Berry, R. M. Fluorescence measurement of intracellular sodium concentration in single *Escherichia coli* cells. *Biophys. J.* **90**, 357–365 (2006).
84. Ipiña, E. P., Otte, S., Pontier-Bres, R., Czerucka, D. & Peruani, F. Bacteria display optimal transport near surfaces. *Nat. Phys.* **15**, 610 (2019).
85. Tinevez, J.-Y. et al. TrackMate: An open and extensible platform for single-particle tracking. *Methods* **115**, 80–90 (2017).
86. Shanks, R. M., Caiazza, N. C., Hinsa, S. M., Toutain, C. M. & O'Toole, G. A. *Saccharomyces cerevisiae*-based molecular tool kit for manipulation of genes from gram-negative bacteria. *Appl. Environ. Microbiol.* **72**, 5027–5036 (2006).
87. Rudenko, O. & Barnes, A. C. Gibson Assembly facilitates bacterial allelic exchange mutagenesis. *J. Microbiol. Methods* **144**, 157–163 (2018).
88. Ben-David, A. & Davidson, C. E. Estimation method for serial dilution experiments. *J. Microbiol. Methods* **107**, 214–221 (2014).
89. Nunamaker, E. A., Otto, K. J. & Kipke, D. R. Investigation of the material properties of alginate for the development of hydrogel repair of dura mater. *J. Mech. Behav. Biomed.* **4**, 16–33 (2011).

AUTHOR CONTRIBUTIONS

L.W., Y.-C.W., G.O, K.B., B.D., L.W., E.C.-H., and V.D.G. designed research; L.W., Y.-C.W., B.B., J.C., M.W., R.L. and A.T. did experiments; C.G., S.W., and G.O. made bacterial strains and plasmids, L.W., Y.-C.W. and A.T. analyzed data; Y.-C.W. conducted modeling; and L.W., Y.-C.W., and V.D.G. wrote the paper. L.W. and Y.-C.W. contributed equally to this work and should be considered co-first author.

COMPETING INTERESTS

The authors declare no competing interests.

ADDITIONAL INFORMATION

Supplementary information The online version contains supplementary material available at https://doi.org/10.1038/s41522-023-00436-x.

Correspondence and requests for materials should be addressed to Vernita D. Gordon.

Reprints and permission information is available at http://www.nature.com/reprints

Publisher's note Springer Nature remains neutral with regard to jurisdictional claims in published maps and institutional affiliations.

MASTER REFERNCE LIST

1. O'Toole GA, Wong GC. 2016. Sensational biofilms: surface sensing in bacteria. Current Opinion in Microbiology 30:139-146.

2. Flemming H-C, Wuertz S. 2019. Bacteria and archaea on Earth and their abundance in biofilms. Nature Reviews Microbiology 17:247-260.

3. Maier B, Wong GCL. 2015. How Bacteria Use Type IV Pili Machinery on Surfaces. Trends Microbiol 23:775-788.

4. Shanice S. Webster, Gerard C. L. Wong, O'Toole GA. 2022. The Power of Touch: Type 4 Pili, the von Willebrand A Domain, and Surface Sensing by Pseudomonas aeruginosa. J Bacteriol 204.

5. Ha D-G, O'Toole GA. 2015. c-di-GMP and its Effects on Biofilm Formation and Dispersion: a <i>Pseudomonas Aeruginosa</i> Review. Microbiology Spectrum 3.

6. Bodey GP, Ricardo B, Fainstein V, Jadeja L. 1983. Infections Caused by Pseudomonas aeru. 5.

7. Burrows LL. 2012. Pseudomonas aeruginosa Twitching Motility: Type IV Pili in Action. Annual Review of Microbiology 66:493-520.

8. Köhler T, Curty LK, Barja F, Delden Cv, Pechère J-C. 2000. Swarming of *Pseudomonas aeruginosa* is dependent on cell-to-cell signaling and requires Ffagella and pili. Journal of Bacteriology 182:5990-5996.

9. Ha D-G, Kuchma SL, O'Toole GA. 2014. Plate-Based Assay for Swimming Motility in Pseudomonas aeruginosa, p 59-65 doi:10.1007/978-1-4939-0473-0_7. Springer New York.

10.	Toutain CM, Caizza NC, Zegans ME, O'Toole GA. 2007. Roles for flagellar stators in biofilm formation by Pseudomonas aeruginosa. Res Microbiol 158:471-7.

11.	Toutain CM, Zegans ME, O'Toole GA. 2005. Evidence for Two Flagellar Stators and Their Role in the Motility of *Pseudomonas aeruginosa*. Journal of Bacteriology 187:771-777.

12.	Baker AE, Webster SS, Diepold A, Kuchma SL, Bordeleau E, Armitage JP, O'Toole GA. 2019. Flagellar Stators Stimulate c-di-GMP Production by Pseudomonas aeruginosa. Journal of Bacteriology 201.

13.	Skerker JM, Berg HC. 2001. Direct observation of extension and retraction of type IV pili. Proceedings of the National Academy of Sciences 98:6901-6904.

14.	Talà L, Fineberg A, Kukura P, Persat A. 2019. Pseudomonas aeruginosa orchestrates twitching motility by sequential control of type IV pili movements. Nature Microbiology 4:774-780.

15.	Chiang P, Sampaleanu LM, Ayers M, Pahuta M, Howell PL, Burrows LL. 2008. Functional role of conserved residues in the characteristic secretion NTPase motifs of the Pseudomonas aeruginosa type IV pilus motor proteins PilB, PilT and PilU. Microbiology 154:114-126.

16.	Thomsen ND, Berger JM. 2008. Structural frameworks for considering microbial protein- and nucleic acid-dependent motor ATPases. Mol Microbiol 69:1071-90.

17.	McCallum M, Benlekbir S, Nguyen S, Tammam S, Rubinstein JL, Burrows LL, Howell PL. 2019. Multiple conformations facilitate PilT function in the type IV pilus. Nat Commun 10:5198.

18.	McCallum M, Tammam S, Khan A, Burrows LL, Howell PL. 2017. The molecular mechanism of the type IVa pilus motors. Nat Commun 8:15091.

19.   Craig L, Forest KT, Maier B. 2019. Type IV pili: dynamics, biophysics and functional consequences. Nat Rev Microbiol 17:429-440.

20.   Armbruster CR, Lee CK, Parker-Gilham J, De Anda J, Xia A, Zhao K, Murakami K, Tseng BS, Hoffman LR, Jin F, Harwood CS, Wong GC, Parsek MR. 2019. Heterogeneity in surface sensing suggests a division of labor in Pseudomonas aeruginosa populations. eLife 8.

21.   Lee CK, Vachier J, De Anda J, Zhao K, Baker AE, Bennett RR, Armbruster CR, Lewis KA, Tarnopol RL, Lomba CJ, Hogan DA, Parsek MR, O'Toole GA, Golestanian R, Wong GCL. 2020. Social Cooperativity of Bacteria during Reversible Surface Attachment in Young Biofilms: a Quantitative Comparison of Pseudomonas aeruginosa PA14 and PAO1. mBio 11.

22.   Kasetty S, Katharios-Lanwermeyer S, O'Toole GA, Nadell CD. 2021. Differential Surface Competition and Biofilm Invasion Strategies of Pseudomonas aeruginosa PA14 and PAO1. J Bacteriol 203:e0026521.

23.   Lee CK, De Anda J, Baker AE, Bennett RR, Luo Y, Lee EY, Keefe JA, Helali JS, Ma J, Zhao K, Golestanian R, O'Toole GA, Wong GCL. 2018. Multigenerational memory and adaptive adhesion in early bacterial biofilm communities. Proceedings of the National Academy of Sciences 115:4471-4476.

24.   Luo Y, Zhao K, Baker AE, Kuchma SL, Coggan KA, Wolfgang MC, Wong GC, O'Toole GA. 2015. A hierarchical cascade of second messengers regulates *Pseudomonas aeruginosa* surface behaviors. MBio 6.

25.   Comolli JC, Hauser AR, Waite L, Whitchurch CB, Mattick JS, Engel JN. 1999. *Pseudomonas aeruginosa* Gene Products PilT and PilU Are Required for Cytotoxicity In Vitro and Virulence in a Mouse Model of Acute Pneumonia. Infection and Immunity 67:3625-3630.

26.   Fuchs EL, Brutinel ED, Klem ER, Fehr AR, Yahr TL, Wolfgang MC. 2010. In Vitro and In Vivo Characterization of the Pseudomonas aeruginosa Cyclic AMP (cAMP)

Phosphodiesterase CpdA, Required for cAMP Homeostasis and Virulence Factor
Regulation. Journal of Bacteriology 192:2779-2790.

27.   Siryaporn A, Kuchma SL, O'Toole GA, Gitai Z. 2014. Surface attachment induces
        Pseudomonas aeruginosa virulence. Proceedings of the National Academy of
        Sciences 111:16860-16865.

28.   Bertrand JJ, West JT, Engel JN. 2010. Genetic Analysis of the Regulation of Type IV
        Pilus Function by the Chp Chemosensory System of *Pseudomonas
        aeruginosa*. Journal of Bacteriology 192:994-1010.

29.   Whitchurch CB, Leech AJ, Young MD, Kennedy D, Sargent JL, Bertrand JJ, Semmler
        ABT, Mellick AS, Martin PR, Alm RA, Hobbs M, Beatson SA, Huang B, Nguyen L,
        Commolli JC, Engel JN, Darzins A, Mattick JS. 2004. Characterization of a complex
        chemosensory signal transduction system which controls twitching motility in
        Pseudomonas aeruginosa. Molecular Microbiology 52:873-893.

30.   Katharios-Lanwermeyer S, O'Toole GA. 2022. Biofilm Maintenance as an Active
        Process: Evidence that Biofilms Work Hard to Stay Put. J Bacteriol 204.

31.   Katharios-Lanwermeyer S, Whitfield GB, Howell PL, O'Toole GA. 2021.
        Pseudomonas aeruginosa Uses c-di-GMP Phosphodiesterases RmcA and MorA To
        Regulate Biofilm Maintenance. mBio 12.

32.   Stefan Katharios-Lanwermeyer a, Sophia A. Koval aaKEB, a George A. O'Toolea.
        2022. The Diguanylate Cyclase YfiNof Pseudomonas aeruginosa Regulates Biofilm
        Maintenance in Response to Peroxide. J Bacteriol 204.

33.   Kim S-K, Lee J-H. 2016. Biofilm dispersion in Pseudomonas aeruginosa. Journal of
        Microbiology 54:71-85.

34.   Rumbaugh KP, Sauer K. 2020. Biofilm dispersion. Nature Reviews Microbiology
        18:571-586.

35. Fuchs EL, Brutinel ED, Jones AK, Fulcher NB, Urbanowski ML, Yahr TL, Wolfgang MC. 2010. The Pseudomonas aeruginosa Vfr Regulator Controls Global Virulence Factor Expression through Cyclic AMP-Dependent and -Independent Mechanisms. Journal of Bacteriology 192:3553-3564.

36. Inclan YF, Persat A, Greninger A, Von Dollen J, Johnson J, Krogan N, Gitai Z, Engel JN. 2016. A scaffold protein connects type IV pili with the Chp chemosensory system to mediate activation of virulence signaling in *Pseudomonas aeruginosa*. Molecular Microbiology 101:590-605.

37. Wolfgang MC, Lee VT, Gilmore ME, Lory S. 2003. Coordinate Regulation of Bacterial Virulence Genes by a Novel Adenylate Cyclase-Dependent Signaling Pathway. Developmental Cell 4:253-263.

38. Beatson SA, Whitchurch CB, Sargent JL, Levesque RC, Mattick JS. 2002. Differential Regulation of Twitching Motility and Elastase Production by Vfr in Pseudomonas aeruginosa. Journal of Bacteriology 184:3605-3613.

39. Chawla R, Gupta R, Lele TP, Lele PP. 2020. A skeptic's guide to bacterial mechanosensing. J Mol Biol 432:523-533.

40. Dufrêne YF, Persat A. 2020. Mechanomicrobiology: how bacteria sense and respond to forces. Nature Reviews Microbiology 18:227-240.

41. Purcell EM. 1977. Life at Low Reynolds Number. American Journal of Physics 45:3-11.

42. De Anda J, Lee EY, Lee CK, Bennett RR, Ji X, Soltani S, Harrison MC, Baker AE, Luo Y, Chou T, O'Toole GA, Armani AM, Golestanian R, Wong GCL. 2017. High-Speed "4D" Computational Microscopy of Bacterial Surface Motility. ACS Nano 11:9340-9351.

43. Lele PP, Hosu BG, Berg HC. 2013. Dynamics of mechanosensing in the bacterial flagellar motor. Proceedings of the National Academy of Sciences 110:11839-11844.

44.   Tipping MJ, Delalez NJ, Lim R, Berry RM, Armitage JP. 2013. Load-dependent assembly of the bacterial flagellar motor. mBio 4.

45.   Castillo DJ, Nakamura S, Morimoto YV, Che Y-S, Kami-Ike N, Kudo S, Minamino T, Namba K. 2013. The C-terminal periplasmic domain of MotB is responsible for load-dependent control of the number of stators of the bacterial flagellar motor. BIOPHYSICS 9:173-181.

46.   Che YS, Nakamura S, Morimoto YV, Kami-Ike N, Namba K, Minamino T. 2014. Load-sensitive coupling of proton translocation and torque generation in the bacterial flagellar motor. Molecular Microbiology 91:175-184.

47.   Chawla R, Ford KM, Lele PP. 2017. Torque, but not FliL, regulates mechanosensitive flagellar motor-function. Scientific Reports 7.

48.   Block SM, Berg HC. 1984. Successive incorporation of force-generating units in the bacterial rotary motor. Nature 309:470-472.

49.   Beeby M, Ribardo DA, Brennan CA, Ruby EG, Jensen GJ, Hendrixson DR. 2016. Diverse high-torque bacterial flagellar motors assemble wider stator rings using a conserved protein scaffold. Proceedings of the National Academy of Sciences 113:E1917-E1926.

50.   Blair DF, Berg HC. 1988. Restoration of torque in defective flagellar motors. Science.

51.   Leake MC, Chandler JH, Wadhams GH, Bai F, Berry RM, Armitage JP. 2006. Stoichiometry and turnover in single, functioning membrane protein complexes. Nature 443:355-358.

52.   Nord AL, Gachon E, Perez-Carrasco R, Nirody JA, Barducci A, Berry RM, Pedaci F. 2017. Catch bond drives stator mechanosensitivity in the bacterial flagellar motor. Proceedings of the National Academy of Sciences 114:12952-12957.

53.   De Anda J, Kuchma SL, Webster SS, Boromand A, Lewis KA, Lee CK, Contreras M, Pereira VFM, Hogan DA, O'Hern CS, O'Toole GA, Wong GCL. 2023. How individual *P. aeruginosa* cells with diverse stator distributions collectively form a heterogeneous macroscopic swarming population doi:10.1101/2023.04.10.536285. Cold Spring Harbor Laboratory.

54.   Kuchma SL, Ballok AE, Merritt JH, Hammond JH, Lu W, Rabinowitz JD, O'Toole GA. 2010. Cyclic-di-GMP-Mediated Repression of Swarming Motility by *Pseudomonas aeruginosa*: the *pilY1* Gene and Its Impact on Surface-Associated Behaviors. Journal of Bacteriology 192:2950-2964.

55.   O'Toole GA, Kolter R. 1998. Flagellar and twitching motility are necessary for *Pseudomonas aeruginosa* biofilm development. Molecular Microbiology 30:295-304.

56.   Hug I, Deshpande S, Sprecher KS, Pfohl T, Jenal U. 2017. Second messenger–mediated tactile response by a bacterial rotary motor. Science 358:531-534.

57.   Wu DC, Zamorano-Sánchez D, Pagliai FA, Park JH, Floyd KA, Lee CK, Kitts G, Rose CB, Bilotta EM, Wong GCL, Yildiz FH. 2020. Reciprocal c-di-GMP signaling: Incomplete flagellum biogenesis triggers c-di-GMP signaling pathways that promote biofilm formation. PLOS Genetics 16:e1008703.

58.   Guttenplan SB, Kearns DB. 2013. Regulation of flagellar motility during biofilm formation. FEMS Microbiology Reviews 37:849-871.

59.   Koch MD, Fei C, Wingreen NS, Shaevitz JW, Gitai Z. 2021. Competitive binding of independent extension and retraction motors explains the quantitative dynamics of type IV pili. Proceedings of the National Academy of Sciences 118:e2014926118.

60.   Gibiansky ML, Conrad JC, Jin F, Gordon VD, Motto DA, Mathewson MA, Stopka WG, Zelasko DC, Shrout JD, Wong GCL. 2010. Bacteria Use Type IV Pili to Walk Upright and Detach from Surfaces. Science 330:197-197.

61.   Maxsim L. Gibiansky JCC, 2* Fan Jin,1 Vernita D. Gordon,1 Dominick A. Motto,4 Margie A. Mathewson,3 Wiktor G. Stopka,3 Daria C. Zelasko,3 Joshua D. Shrout,4 Gerard C. L. Wong1,3†. 2010. Bacteria use type IV pili to walk upright and detach from surfaces. Science.

62.   Conrad JC. 2012. Physics of bacterial near-surface motility using flagella and type IV pili: implications for biofilm formation. Res Microbiol 163:619-29.

63.   Jacinta, Maxsim, Jin F, Vernita, Dominick, Margie, Wiktor, Daria, Joshua, Gerard. 2011. Flagella and Pili-Mediated Near-Surface Single-Cell Motility Mechanisms in P. aeruginosa. Biophysical Journal 100:1608-1616.

64.   Maier B, Potter L, So M, Seifert HS, Sheetz MP. 2002. Single pilus motor forces exceed 100 pN. Proceedings of the National Academy of Sciences 99:16012-16017.

65.   Biais N, Ladoux B, Higashi D, So M, Sheetz M. 2008. Cooperative Retraction of Bundled Type IV Pili Enables Nanonewton Force Generation. PLoS Biology 6:e87.

66.   Ribbe J, Baker AE, Euler S, O'Toole GA, Maier B. 2017. Role of Cyclic Di-GMP and Exopolysaccharide in Type IV Pilus Dynamics. Journal of Bacteriology 199:JB.00859-16.

67.   Beaussart A, Baker AE, Kuchma SL, El-Kirat-Chatel S, O'Toole GA, Dufrêne YF. 2014. Nanoscale Adhesion Forces of <i>Pseudomonas aeruginosa</i> Type IV Pili. ACS Nano 8:10723-10733.

68.   Jin F, Conrad JC, Gibiansky ML, Wong GCL. 2011. Bacteria use type-IV pili to slingshot on surfaces. Proceedings of the National Academy of Sciences 108:12617-12622.

69.   Biais N, Higashi DL, Brujić J, So M, Sheetz MP. 2010. Force-dependent polymorphism in type IV pili reveals hidden epitopes. Proceedings of the National Academy of Sciences 107:11358-11363.

70.   Chlebek JL, Hughes HQ, Ratkiewicz AS, Rayyan R, Wang JC, Herrin BE, Dalia TN, Biais N, Dalia AB. 2019. PilT and PilU are homohexameric ATPases that coordinate to retract type IVa pili. PLoS Genet 15:e1008448.

71.   Evan Couser JLC, Ankur B. Daliaa. 2022. Retraction ATPase Motors from Three Orthologous Type IVa Pilus Systems Support Promiscuous Retraction of the Vibrio cholerae Competence Pilus. Journal of Bacteriology.

72.   Adams DW, Pereira JM, Stoudmann C, Stutzmann S, Blokesch M. 2019. The type IV pilus protein PilU functions as a PilT-dependent retraction ATPase. PLOS Genetics 15:e1008393.

73.   Whitchurch CB, Mattick JS. 1994. Characterization of a gene, pilU, required for twitching motility but not phage sensitivity in Pseudomonas aeruginosa. Molecular Microbiology 13:1079-1091.

74.   Zöllner R, Cronenberg T, Maier B. 2019. Motor Properties of PilT-Independent Type 4 Pilus Retraction in Gonococci. Journal of Bacteriology 201.

75.   Chlebek JL, Denise R, Craig L, Dalia AB. 2021. Motor-independent retraction of type IV pili is governed by an inherent property of the pilus filament. Proceedings of the National Academy of Sciences 118:e2102780118.

76.   Persat A, Inclan YF, Engel JN, Stone HA, Gitai Z. 2015. Type IV pili mechanochemically regulate virulence factors in Pseudomonas aeruginosa. Proc Natl Acad Sci U S A 112:7563-8.

77.   Ellison CK, Kan J, Dillard RS, Kysela DT, Ducret A, Berne C, Hampton CM, Ke Z, Wright ER, Biais N, Dalia AB, Brun YV. 2017. Obstruction of pilus retraction stimulates bacterial surface sensing. Science 358:535-538.

78.   Kuchma SL, O'Toole GA. 2022. Surface-Induced cAMP Signaling Requires Multiple Features of the Pseudomonas aeruginosa Type IV Pili. Journal of Bacteriology.

79.   Cooley RB, Smith TJ, Leung W, Tierney V, Borlee BR, O'Toole GA, Sondermann H. 2016. Cyclic Di-GMP-Regulated Periplasmic Proteolysis of a Pseudomonas aeruginosa Type Vb Secretion System Substrate. Journal of Bacteriology 198:66-76.

80.   Courtney Reichhardt, Holly M. Jacobs aMM, a Cynthis Wong,a Daniel J. Wozniak, Parsek MR. 2020. The Versatile Pseudomonas aeruginosa Biofilm Matrix Protein CdrA Promotes Aggregation through Different Extracellular Exopolysaccharide Interactions. J Bacteriol 202.

81.   Bru J-L, Kasallis SJ, Zhuo Q, Høyland-Kroghsbo NM, Siryaporn A. 2023. Swarming of <i>P. aeruginosa</i>: Through the lens of biophysics. Biophysics Reviews 4.

82.   Laventie B-J, Sangermani M, Estermann F, Manfredi P, Planes R, Hug I, Jaeger T, Meunier E, Broz P, Jenal U. 2019. A Surface-Induced Asymmetric Program Promotes Tissue Colonization by Pseudomonas aeruginosa. Cell Host & Microbe 25:140-152.e6.

83.   Vrabioiu AM, Berg HC. 2022. Signaling events that occur when cells of <i>Escherichia coli</i> encounter a glass surface. Proceedings of the National Academy of Sciences 119:e2116830119.

84.   Fulcher NB, Holliday PM, Klem E, Cann MJ, Wolfgang MC. 2010. The Pseudomonas aeruginosa Chp chemosensory system regulates intracellular cAMP levels by modulating adenylate cyclase activity. Molecular Microbiology 76:889-904.

85.   Treuner-Lange A, Chang Y-W, Glatter T, Herfurth M, Lindow S, Chreifi G, Jensen GJ, Søgaard-Andersen L. 2020. PilY1 and minor pilins form a complex priming the type IVa pilus in Myxococcus xanthus. Nature Communications 11.

86.   Ng D, Harn T, Altindal T, Kolappan S, Marles JM, Lala R, Spielman I, Gao Y, Hauke CA, Kovacikova G, Verjee Z, Taylor RK, Biais N, Craig L. 2016. The Vibrio cholerae Minor Pilin TcpB Initiates Assembly and Retraction of the Toxin-Coregulated Pilus. PLOS Pathogens 12:e1006109.

87.   Webster SS, Lee CK, Schmidt WC, Wong GCL, O'Toole GA. 2021. Interaction between the type 4 pili machinery and a diguanylate cyclase fine-tune c-di-GMP levels during early biofilm formation. Proceedings of the National Academy of Sciences 118:e2105566118.

88.   Shanice S. Webster aWCS, d,e,f, Marion Mathelié-Guinlet bGCLW, d,e,f, Andreia F. Verissimo cYFD, b, Daniel Schultz aAV, b George A. O'Toole. 2022. Force-Induced Changes of PilY1 Drive Surface Sensing by Pseudomonas aeruginosa. mBio 13.

89.   McCallum M, Tammam S, Rubinstein JL, Burrows LL, Howell PL. 2021. CryoEM map of Pseudomonas aeruginosa PilQ enables structural characterization of TsaP. Structure 29:457-466.e4.

90.   Lee CK, Schmidt WC, Webster SS, Chen JW, O'Toole GA, Wong GCL. 2022. Broadcasting of amplitude- and frequency-modulated c-di-GMP signals facilitates cooperative surface commitment in bacterial lineages. Proceedings of the National Academy of Sciences 119:e2112226119.

91.   Moscoso JA, Jaeger T, Valentini M, Hui K, Jenal U, Filloux A. 2014. The Diguanylate Cyclase SadC Is a Central Player in Gac/Rsm-Mediated Biofilm Formation in Pseudomonas aeruginosa. Journal of Bacteriology 196:4081-4088.

92.   Yahr TL, Vallis AJ, Hancock MK, Barbieri JT, Frank DW. 1998. ExoY, an adenylate cyclase secreted by the*Pseudomonas aeruginosa*type III system. Proceedings of the National Academy of Sciences 95:13899-13904.

93.   Inclan YF, Huseby MJ, Engel JN. 2011. FimL Regulates cAMP Synthesis in Pseudomonas aeruginosa. PLoS ONE 6:e15867.

94.   Topal H, Fulcher NB, Bitterman J, Salazar E, Buck J, Levin LR, Cann MJ, Wolfgang MC, Steegborn C. 2012. Crystal Structure and Regulation Mechanisms of the CyaB Adenylyl Cyclase from the Human Pathogen Pseudomonas aeruginosa. Journal of Molecular Biology 416:271-286.

95.   Endoh T, Engel JN. 2009. CbpA: a Polarly Localized Novel Cyclic AMP-Binding Protein in Pseudomonas aeruginosa. Journal of Bacteriology 191:7193-7205.

96.   Buensuceso RNC, Nguyen Y, Zhang K, Daniel-Ivad M, Sugiman-Marangos SN, Fleetwood AD, Zhulin IB, Junop MS, Howell PL, Burrows LL. 2016. The Conserved Tetratricopeptide Repeat-Containing C-Terminal Domain of Pseudomonas aeruginosa FimV Is Required for Its Cyclic AMP-Dependent and -Independent Functions. Journal of Bacteriology 198:2263-2274.

97.   Carter T, Buensuceso RN, Tammam S, Lamers RP, Harvey H, Howell PL, Burrows LL. 2017. The Type IVa Pilus Machinery Is Recruited to Sites of Future Cell Division. mBio 8.

98.   Bernhardt TG, De Boer PAJ. 2003. The Escherichia coli amidase AmiC is a periplasmic septal ring component exported via the twin-arginine transport pathway. Molecular Microbiology 48:1171-1182.

99.   Heidrich C, Templin MF, Ursinus A, Merdanovic M, Berger J, Schwarz H, De Pedro MA, Höltje J-V. 2001. Involvement of N-acetylmuramyl-l-alanine amidases in cell separation and antibiotic-induced autolysis of Escherichia coli. Molecular Microbiology 41:167-178.

100.   Peters NT, Dinh T, Bernhardt TG. 2011. A Fail-Safe Mechanism in the Septal Ring Assembly Pathway Generated by the Sequential Recruitment of Cell Separation Amidases and Their Activators. Journal of Bacteriology 193:4973-4983.

101.   Buensuceso RNC, Daniel-Ivad M, Kilmury SLN, Leighton TL, Harvey H, Howell PL, Burrows LL. 2017. Cyclic AMP-Independent Control of Twitching Motility in Pseudomonas aeruginosa. Journal of Bacteriology 199.

102.   Schniederberend M, Williams JF, Shine E, Shen C, Jain R, Emonet T, Kazmierczak BI. 2019. Modulation of flagellar rotation in surface-attached bacteria: A pathway for rapid surface-sensing after flagellar attachment. PLOS Pathogens 15:e1008149.

103. Darzins A. 1994. Characterization of a Pseudomonas aeruginosa gene cluster involved in pilus biosynthesis and twitching motility: sequence similarity to the chemotaxis proteins of enterics and the gliding bacterium Myxococcus xanthus. Molecular Microbiology 11:137-153.

104. Darzins A. 1993. The pilG gene product, required for Pseudomonas aeruginosa pilus production and twitching motility, is homologous to the enteric, single-domain response regulator CheY. Journal of Bacteriology 175:5934-5944.

105. Kearns DB, Robinson J, Shimkets LJ. 2001. *Pseudomonas aeruginosa* Exhibits Directed Twitching Motility Up Phosphatidylethanolamine Gradients. Journal of Bacteriology 183:763-767.

106. Limoli DH, Warren EA, Yarrington KD, Donegan NP, Cheung AL, O'Toole GA. 2019. Interspecies interactions induce exploratory motility in Pseudomonas aeruginosa. Elife 8.

107. Yarrington KD, Shendruk TN, Limoli DH. 2022. Twitching cells use a chemoreceptor to detect bacterial competitors doi:10.1101/2022.11.28.518211. Cold Spring Harbor Laboratory.

108. Nolan LM, McCaughey LC, Merjane J, Turnbull L, Whitchurch CB. 2020. ChpC controls twitching motility-mediated expansion of Pseudomonas aeruginosa biofilms in response to serum albumin, mucin and oligopeptides. Microbiology 166:669-678.

109. Jansari VH, Potharla VY, Riddell GT, Bardy SL. 2016. Twitching motility and cAMP levels: signal transduction through a single methyl-accepting chemotaxis protein. FEMS Microbiol Lett 363.

110. Kühn MJ, Macmillan H, Talà L, Inclan Y, Patino R, Pierrat X, Al-Mayyah Z, Engel JN, Persat A. 2023. Two antagonistic response regulators control *Pseudomonas aeruginosa* polarization during mechanotaxis. The EMBO Journal doi:10.15252/embj.2022112165.

111. Kühn MJ, Talà L, Inclan YF, Patino R, Pierrat X, Vos I, Al-Mayyah Z, Macmillan H, Negrete J, Engel JN, Persat A. 2021. Mechanotaxis directs <i>Pseudomonas aeruginosa</i> twitching motility. Proceedings of the National Academy of Sciences 118:e2101759118.

112. Koch MD, Black ME, Han E, Shaevitz JW, Gitai Z. 2022. Pseudomonas aeruginosa distinguishes surfaces by stiffness using retraction of type IV pili. Proc Natl Acad Sci U S A 119:e2119434119.

113. Geiger CJ, O'Toole GA. 2023. Evidence for the Type IV Pilus Retraction Motor PilT as a Component of the Surface Sensing System in Pseudomonas aeruginos. J Bacteriol 205.

114. McCallum M, Tammam S, Little DJ, Robinson H, Koo J, Shah M, Calmettes C, Moraes TF, Burrows LL, Howell PL. 2016. PilN Binding Modulates the Structure and Binding Partners of the Pseudomonas aeruginosa Type IVa Pilus Protein PilM. Journal of Biological Chemistry 291:11003-11015.

115. Chang YW, Rettberg LA, Treuner-Lange A, Iwasa J, Sogaard-Andersen L, Jensen GJ. 2016. Architecture of the type IVa pilus machine. Science 351:aad2001.

116. Denise R, Abby SS, Rocha EPC. 2019. Diversification of the type IV filament superfamily into machines for adhesion, protein secretion, DNA uptake, and motility. PLOS Biology 17:e3000390.

117. Aukema KG, Kron EM, Herdendorf TJ, Forest KT. 2005. Functional Dissection of a Conserved Motif within the Pilus Retraction Protein PilT. Journal of Bacteriology 187:611-618.

118. Misic AM, Satyshur KA, Forest KT. 2010. P. aeruginosa PilT Structures with and without Nucleotide Reveal a Dynamic Type IV Pilus Retraction Motor. Journal of Molecular Biology 400:1011-1021.

119. Satyshur KA, Worzalla GA, Meyer LS, Heiniger EK, Aukema KG, Misic AM, Forest KT. 2007. Crystal Structures of the Pilus Retraction Motor PilT Suggest Large Domain Movements and Subunit Cooperation Drive Motility. Structure 15:363-376.

120. Cowles KN, Gitai Z. 2010. Surface association and the MreB cytoskeleton regulate pilus production, localization and function in Pseudomonas aeruginosa. Molecular Microbiology 76:1411-1426.

121. Jain R, Sliusarenko O, Kazmierczak BI. 2017. Interaction of the cyclic-di-GMP binding protein FimX and the Type 4 pilus assembly ATPase promotes pilus assembly. PLOS Pathogens 13:e1006594.

122. Sievers F, Higgins DG. 2018. Clustal Omega for making accurate alignments of many protein sequences. Protein Science 27:135-145.

123. Varadi M, Anyango S, Deshpande M, Nair S, Natassia C, Yordanova G, Yuan D, Stroe O, Wood G, Laydon A, Zidek A, Green T, Tunyasuvunakool K, Petersen S, Jumper J, Clancy E, Green R, Vora A, Lutfi M, Figurnov M, Cowie A, Hobbs N, Kohli P, Kleywegt G, Birney E, Hassabis D, Velankar S. 2022. AlphaFold Protein Structure Database: massively expanding the structural coverage of protein-sequence space with high-accuracy models. Nucleic Acids Res 50:D439-D444.

124. Evans R, O'Neill M, Pritzel A, Antropova N, Senior A, Green T, Žídek A, Bates R, Blackwell S, Yim J, Ronneberger O, Bodenstein S, Zielinski M, Bridgland A, Potapenko A, Cowie A, Tunyasuvunakool K, Jain R, Clancy E, Kohli P, Jumper J, Hassabis D. 2021. Protein complex prediction with AlphaFold-Multimer doi:10.1101/2021.10.04.463034. Cold Spring Harbor Laboratory.

125. Jumper J, Evans R, Pritzel A, Green T, Figurnov M, Ronneberger O, Tunyasuvunakool K, Bates R, Žídek A, Potapenko A, Bridgland A, Meyer C, Kohl SAA, Ballard AJ, Cowie A, Romera-Paredes B, Nikolov S, Jain R, Adler J, Back T, Petersen S, Reiman D, Clancy E, Zielinski M, Steinegger M, Pacholska M, Berghammer T, Bodenstein S, Silver D, Vinyals O, Senior AW, Kavukcuoglu K, Kohli P, Hassabis D. 2021. Highly accurate protein structure prediction with AlphaFold. Nature 596:583-589.

126. Ben Chorin A, Masrati G, Kessel A, Narunsky A, Sprinzak J, Lahav S, Ashkenazy H, Ben-Tal N. 2020. ConSurf-DB: An accessible repository for the evolutionary conservation patterns of the majority of PDB proteins. Protein Science 29:258-267.

127. Ashkenazy H, Abadi S, Martz E, Chay O, Mayrose I, Pupko T, Ben-Tal N. 2016. ConSurf 2016: an improved methodology to estimate and visualize evolutionary conservation in macromolecules. Nucleic Acids Res 44:W344-50.

128. Bradley D. 1980. a function of *Pseudomonas aeruginosa* PAO polar pili: twitching motility. Canadian Journal of Microbiology 26:146-154.

129. Speers AM, Schindler BD, Hwang J, Genc A, Reguera G. 2016. Genetic Identification of a PilT Motor in Geobacter sulfurreducens Reveals a Role for Pilus Retraction in Extracellular Electron Transfer. Front Microbiol 7:1578.

130. Black WP, Wang L, Jing X, Saldaña RC, Li F, Scharf BE, Schubot FD, Yang Z. 2017. The type IV pilus assembly ATPase PilB functions as a signaling protein to regulate exopolysaccharide production in Myxococcus xanthus. Scientific Reports 7.

131. Dye KJ, Yang Z. 2020. Cyclic-di-GMP and ADP bind to separate domains of PilB as mutual allosteric effectors. Biochem J 477:213-226.

132. Keane J. Dye, Safoura Salar UA, 1 Wraylyn Smith,1, Yang Z. 2023. Myxococcus xanthus PilB interacts with c-di-GMP and modulates motility and biofilm formation. J Bacteriol 205.

133. Welker A, Cronenberg T, Zöllner R, Meel C, Siewering K, Bender N, Hennes M, Oldewurtel ER, Maier B. 2018. Molecular Motors Govern Liquidlike Ordering and Fusion Dynamics of Bacterial Colonies. Physical Review Letters 121.

134. Berne C, Ellison CK, Ducret A, Brun YV. 2018. Bacterial adhesion at the single-cell level. Nature Reviews Microbiology 16:616-627.

135. Kreve S, Reis ACD. 2021. Bacterial adhesion to biomaterials: What regulates this attachment? A review. Jpn Dent Sci Rev 57:85-96.

136. Lee SW, Phillips KS, Gu H, Kazemzadeh-Narbat M, Ren D. 2021. How microbes read the map: Effects of implant topography on bacterial adhesion and biofilm formation. Biomaterials 268:120595.

137. Shah M, Taylor VL, Bona D, Tsao Y, Stanley SY, Pimentel-Elardo SM, McCallum M, Bondy-Denomy J, Howell PL, Nodwell JR, Davidson AR, Moraes TF, Maxwell KL. 2021. A phage-encoded anti-activator inhibits quorum sensing in Pseudomonas aeruginosa. Molecular Cell 81:571-583.e6.

138. Amelia K. Schmidt aADF, b Patrick R. Secora Caleb M. Schwartzkopf,a Dominick R. Faith,a Laura K. Jennings,a, Devin J. Hunt aLAM, a Aviv Hargil,c QingquanChen,c Paul L. Bollyky,c David W.Dorward,d Karen L. Maxwell,b, a. 2022. A Filamentous Bacteriophage Protein Inhibits Type IV Pili To Prevent Superinfection of Pseudomonas aeruginosa. mBio 13.

139. Chung I-Y, Jang H-J, Bae H-W, Cho Y-H. 2014. A phage protein that inhibits the bacterial ATPase required for type IV pilus assembly. Proceedings of the National Academy of Sciences 111:11503-11508.

140. Jean-Pierre F, Hampton TH, Schultz D, Hogan DA, Groleau M-C, Déziel E, O'Toole GA. 2023. Community composition shapes microbial-specific phenotypes in a cystic fibrosis polymicrobial model system. eLife 12.

141. Utada AS, Bennett RR, Fong JCN, Gibiansky ML, Yildiz FH, Golestanian R, Wong GCL. 2014. Vibrio cholerae use pili and flagella synergistically to effect motility switching and conditional surface attachment. Nature Communications 5:4913.

142. L. McCarter, M. Hilmen, Silverman M. 1988. Flagellar dynamometer controls swarmer cell defferentiation of V. parahaemolyticus. Cell 54:345-351.

143. McCarter L, Silverman M. 1990. Surface-induced swarmer cell differentiation of Vibrio parahaemoiyticus. Molecular Microbiology 4:1057-1062.

144. Jenal U, Reinders A, Lori C. 2017. Cyclic di-GMP: second messenger extraordinaire. Nature Reviews Microbiology 15:271-284.

145. Silversmith RE, Wang B, Fulcher NB, Wolfgang MC, Bourret RB. 2016. Phosphoryl Group Flow within the Pseudomonas aeruginosa Pil-Chp Chemosensory System. Journal of Biological Chemistry 291:17677-17691.

146. Budzik JM, Rosche WA, Rietsch A, O'Toole GA. 2004. Isolation and Characterization of a Generalized Transducing Phage for *Pseudomonas aeruginosa* Strains PAO1 and PA14. Journal of Bacteriology 186:3270-3273.

147. Hoang TT, Kutchma AJ, Becher A, Schweizer HP. 2000. Integration-proficient plasmids for Pseudomonas aeruginosa: site-specific integration and use for engineering of reporter and expression strains. Plasmid 43:59-72.

148. Bradley D. 1972. Evidence for the retraction of *Pseudomonas aeruginosa* RNA phage pili. Biochemical and Biophysical Research Communications 47:142-149.

149. Choi K-H, Schweizer HP. 2006. mini-Tn7 insertion in bacteria with single attTn7 sites: example Pseudomonas aeruginosa. Nature Protocols 1:153-161.

150. Choi K-H, Gaynor JB, White KG, Lopez C, Bosio CM, Karkhoff-Schweizer RR, Schweizer HP. 2005. A Tn7-based broad-range bacterial cloning and expression system. Nature Methods 2:443-448.

151. Karimova G, Pidoux J, Ullmann A, Ladant D. 1998. A bacterial two-hybrid system based on a reconstituted signal transduction pathway. Proceedings of the National Academy of Sciences 95:5752-5756.

152.   Kuchma SL, Griffin EF, O'Toole GA. 2012. Minor Pilins of the Type IV Pilus System Participate in the Negative Regulation of Swarming Motility. Journal of Bacteriology 194:5388-5403.

153.   Simon R, Priefer U, Pühler A. 1983. A Broad Host Range Mobilization System for In Vivo Genetic Engineering: Transposon Mutagenesis in Gram Negative Bacteria. Bio/Technology 1:784-791.

154.   Rahme LG, Stevens EJ, Wolfort SF, Shao J, Tompkins RG, Ausubel FM. 1995. Common Virulence Factors for Bacterial Pathogenicity in Plants and Animals. Science 268:1899-1902.

155.   Shanks RMQ, Caiazza NC, Hinsa SM, Toutain CM, O'Toole GA. 2006. <i>Saccharomyces cerevisiae</i>-Based Molecular Tool Kit for Manipulation of Genes from Gram-Negative Bacteria. Applied and Environmental Microbiology 72:5027-5036.

156.   Hoang TT, Karkhoff-Schweizer RR, Kutchma AJ, Schweizer HP. 1998. A broad-host-range Flp-FRT recombination system for site-specific

excision of chromosomally-located DNA sequences: application for

isolation of unmarked Pseudomonas aeruginosa mutants. Gene 212:77-86.

157.   De Lorenzo V, Eltis L, Kessler B, Timmis KN. 1993. Analysis of Pseudomonas gene products using lacP/Ptrp-lac plasmids and

transposons that confer conditional phenotypes. Gene 123.

158.   Beaussart A, Baker AE, Kuchma SL, El-Kirat-Chatel S, O'Toole GA, Dufrene YF. 2014. Nanoscale adhesion forces of *Pseudomonas aeruginosa* type IV Pili. ACS Nano 8:10723-33.

159.   Palmer GC, Whiteley M. 2015. Metabolism and pathogenicity of *Pseudomonas aeruginosa* infections in the lungs of individuals with Cystic Fibrosis. Microbiol Spectr 3.

160. Bergan T. 1981. Pathogenetic factors of Pseudomonas aeruginosa. Scand J Infect Dis Suppl 29:7-12.

161. Costerton JW, Stewart PS, Greenberg EP. 1999. Bacterial biofilms: a common cause of persistent infections. Science 284:1318-22.

162. Giamarellou H, Kanellakopoulou K. 2008. Current therapies for *Pseudomonas aeruginosa*. Crit Care Clin 24:261-78, viii.

163. Govan JR, Deretic V. 1996. Microbial pathogenesis in cystic fibrosis: mucoid Pseudomonas aeruginosa and Burkholderia cepacia. Microbiol Rev 60:539-74.

164. O'Toole GA, Kolter R. 1998. Flagellar and twitching motility are necessary for Pseudomonas aeruginosa biofilm development. Molecular microbiology 30:295-304.

165. Burrows LL. 2012. *Pseudomonas aeruginosa* twitching motility: type IV pili in action. Annu Rev Microbiol 66:493-520.

166. Leighton TL, Buensuceso RN, Howell PL, Burrows LL. 2015. Biogenesis of Pseudomonas aeruginosa type IV pili and regulation of their function. Environ Microbiol 17:4148-63.

167. Matsukawa M, Greenberg EP. 2004. Putative exopolysaccharide synthesis genes influence *Pseudomonas aeruginosa* biofilm development. J Bacteriol 186:4449-4456.

168. Friedman L, Kolter R. 2004. Genes involved in matrix formation in *Pseudomonas aeruginosa* PA14 biofilms. Mol Microbiol 51:675-690.

169. Friedman L, Kolter R. 2004. Two genetic loci produce distinct carbohydrate-rich structural components of the *Pseudomonas aeruginosa* biofilm matrix. J Bacteriol 186:4457-4465.

170.	Moreau-Marquis S, Bomberger JM, Anderson GG, Swiatecka-Urban A, Ye S, O'Toole GA, Stanton BA. 2008. The DeltaF508-CFTR mutation results in increased biofilm formation by Pseudomonas aeruginosa by increasing iron availability. American journal of physiology Lung cellular and molecular physiology 295:L25-37.

171.	El-Kirat-Chatel S, Beaussart A, Boyd CD, O'Toole GA, Dufrene YF. 2014. Single-cell and single-molecule analysis deciphers the localization, adhesion, and mechanics of the biofilm adhesin LapA. ACS Chem Biol 9:485-94.

172.	El-Kirat-Chatel S, Boyd CD, O'Toole GA, Dufrene YF. 2014. Single-molecule analysis of *Pseudomonas fluorescens* footprints. ACS Nano 8:1690-8.

173.	Boyd CD, Smith TJ, El-Kirat-Chatel S, Newell PD, Dufrene YF, O'Toole GA. 2014. Structural features of the *Pseudomonas fluorescens* biofilm adhesin LapA required for LapG-dependent cleavage, biofilm formation, and cell surface localization. J Bacteriol 196:2775-88.

174.	Ciesluk M, Deptula P, Piktel E, Fiedoruk K, Suprewicz L, Paprocka P, Kot P, Pogoda K, Bucki R. 2020. Physics comes to the aid of medicine-clinically-relevant microorganisms through the eyes of atomic force microscope. Pathogens 9.

175.	Viljoen A, Mignolet J, Viela F, Mathelie-Guinlet M, Dufrene YF. 2020. How microbes use force to control adhesion. J Bacteriol 202.

176.	Dufrene YF. 2015. Sticky microbes: forces in microbial cell adhesion. Trends Microbiol 23:376-82.

177.	Dufrene YF, Ando T, Garcia R, Alsteens D, Martinez-Martin D, Engel A, Gerber C, Muller DJ. 2017. Imaging modes of atomic force microscopy for application in molecular and cell biology. Nat Nanotechnol 12:295-307.

178.	Puchner EM, Gaub HE. 2009. Force and function: probing proteins with AFM-based force spectroscopy. Curr Opin Struct Biol 19:605-14.

179. Touhami A, Jericho MH, Boyd JM, Beveridge TJ. 2006. Nanoscale characterization and determination of adhesion forces of Pseudomonas aeruginosa pili by using atomic force microscopy. J Bacteriol 188:370-7.

180. Ivanov IE, Boyd CD, Newell PD, Schwartz ME, Turnbull L, Johnson MS, Whitchurch CB, O'Toole GA, Camesano TA. 2012. Atomic force and super-resolution microscopy support a role for LapA as a cell-surface biofilm adhesin of *Pseudomonas fluorescens*. Res Microbiol 163:685-91.

181. Maier B, Wong GC. 2015. How bacteria use Type IV pili machinery on surfaces. Trends Microbiol 23:775-88.

182. O'Toole GA, Wong GC. 2016. Sensational biofilms: surface sensing in bacteria. Curr Opin Microbiol 30:139-46.

183. Colvin KM, Gordon VD, Murakami K, Borlee BR, Wozniak DJ, Wong GC, Parsek MR. 2011. The Pel polysaccharide can serve a structural and protective role in the biofilm matrix of *Pseudomonas aeruginosa*. PLoS Pathog 7:e1001264.

184. Hug I, Deshpande S, Sprecher KS, Pfohl T, Jenal U. 2017. Second messenger-mediated tactile response by a bacterial rotary motor. Science 358:531-534.

185. Ribbe J, Baker AE, Euler S, O'Toole GA, Maier B. 2017. The role of cyclic di-GMP and exopolysaccharide in type IV pilus dynamics. J Bacteriol doi:10.1128/JB.00859-16.

186. Monds RD, O'Toole GA. 2009. The developmental model of microbial biofilms: ten years of a paradigm up for review. Trends in microbiology 17:73-87.

187. Lee CK, de Anda J, Baker AE, Bennett RR, Luo Y, Lee EY, Keefe JA, Helali JS, Ma J, Zhao K, Golestanian R, O'Toole GA, Wong GCL. 2018. Multigenerational memory and adaptive adhesion in early bacterial biofilm communities. Proc Natl Acad Sci U S A 115:4471-4476.

188.   Lee CK, Vachier J, de Anda J, Zhao K, Baker AE, Bennett RR, Armbruster CR, Lewis KA, Tarnopol RL, Lomba CJ, Hogan DA, Parsek MR, O'Toole GA, Golestanian R, Wong GCL. 2020. Social cooperativity of bacteria during reversible surface attachment in young biofilms: a quantitative comparison of *Pseudomonas aeruginosa* PA14 and PAO1. mBio 11.

189.   Zhao K, Tseng BS, Beckerman B, Jin F, Gibiansky ML, Harrison JJ, Luijten E, Parsek MR, Wong GCL. 2013. Psl trails guide exploration and microcolony formation in *Pseudomonas aeruginosa* biofilms. Nature 497:388-391.

190.   Doyle TB, Hawkins AC, McCarter LL. 2004. The complex flagellar torque generator of P*seudomonas aeruginosa*. J Bacteriol 186:6341-50.

191.   Toutain CM, Zegans ME, O'Toole GA. 2005. Evidence for two flagellar stators and their role in the motility of *Pseudomonas aeruginosa*. J Bacteriol 187:771-7.

192.   Ha DG, Kuchma SL, O'Toole GA. 2014. Plate-based assay for swarming motility in *Pseudomonas aeruginosa*. Methods Mol Biol 1149:67-72.

193.   Morris JD, Hewitt JL, Wolfe LG, Kamatkar NG, Chapman SM, Diener JM, Courtney AJ, Leevy WM, Shrout JD. 2011. Imaging and analysis of *Pseudomonas aeruginosa* swarming and rhamnolipid production. Appl Environ Microbiol 77:8310-7.

194.   Siryaporn A, Kuchma SL, O'Toole GA, Gitai Z. 2014. Surface attachment induces Pseudomonas aeruginosa virulence. Proc Natl Acad Sci U S A 111:16860-5.

195.   Webster SS, Wong GCL, O'Toole GA. 2022. The power of touch: Type 4 Pili, the von Willebrand A domain, and surface sensing by *Pseudomonas aeruginosa*. J Bacteriol 204:e0008422.

196.   Merritt JH, Brothers KM, Kuchma SL, O'Toole GA. 2007. SadC reciprocally influences biofilm formation and swarming motility via modulation of exopolysaccharide production and flagellar function. J Bacteriol 189:8154-64.

197. Ha DG, Kuchma SL, O'Toole GA. 2014. Plate-based assay for swimming motility in *Pseudomonas aeruginosa*. Methods Mol Biol 1149:59-65.

198. Caiazza NC, O'Toole GA. 2004. SadB is required for the transition from reversible to irreversible attachment during biofilm formation by *Pseudomonas aeruginosa* PA14. J Bacteriol 186:4476-85.

199. O'Toole GA. 2011. Microtiter Dish Biofilm Formation Assay. Journal of Visualized Experiments doi:10.3791/2437.

200. Cady KC, Bondy-Denomy J, Heussler GE, Davidson AR, O'Toole GA. 2012. The CRISPR/Cas adaptive immune system of *Pseudomonas aeruginosa* mediates resistance to naturally occurring and engineered phages. J Bacteriol 194:5728-38.

201. Henrici AT. 1933. Studies of Freshwater Bacteria. Journal of Bacteriology 25:277-287.

202. Zobell CE, Allen EC. 1935. The Significance of Marine Bacteria in the Fouling of Submerged Surfaces. Journal of Bacteriology 29:239-251.

203. Hershey DM. 2021. Integrated control of surface adaptation by the bacterial flagellum. Curr Opin Microbiol 61:1-7.

204. Hershey DM, Fiebig A, Crosson S. 2021. Flagellar Perturbations Activate Adhesion through Two Distinct Pathways in Caulobacter crescentus. mBio 12.

205. Harrison JJ, Almblad H, Irie Y, Wolter DJ, Eggleston HC, Randall TE, Kitzman JO, Stackhouse B, Emerson JC, McNamara S, Larsen TJ, Shendure J, Hoffman LR, Wozniak DJ, Parsek MR. 2020. Elevated exopolysaccharide levels in Pseudomonas aeruginosa flagellar mutants have implications for biofilm growth and chronic infections. PLoS Genet 16:e1008848.

206. Hershey DM, Fiebig A, Crosson S. 2019. A Genome-Wide Analysis of Adhesion in Caulobacter crescentus Identifies New Regulatory and Biosynthetic Components for Holdfast Assembly. mBio 10.

207. Yukihiro Hiramatsu1* TN, Dendi Krisna Nugraha1, Mayuko Osada-Oka2, Daisuke Nakane3, Katsumi Imada4, Yasuhiko Horiguchi1,. 2022. Interference of flagellar rotation up-regulates the expression of small RNA contributing to Bordetella pertussis infection. Science.

208. Lewis K, Vermilyea, D. M., Webster, S. S., Geiger, C. J., de Anda, J., Wong, G. C. L., O'Toole, G. A., Hogan, D. 2022. Nonmotile Subpopulations of Pseudomonas aeruginosa Repress Flagellar Motility in Motile Cells through a Type IV Pilus- and Pel-Dependent Mechanism. Journal of Bacteriology.

209. Ellison CK, Rusch DB, Brun YV. 2019. Flagellar Mutants Have Reduced Pilus Synthesis in Caulobacter crescentus. Journal of Bacteriology 201.

210. Floyd KA, Lee CK, Xian W, Nametalla M, Valentine A, Crair B, Zhu S, Hughes HQ, Chlebek JL, Wu DC, Hwan Park J, Farhat AM, Lomba CJ, Ellison CK, Brun YV, Campos-Gomez J, Dalia AB, Liu J, Biais N, Wong GCL, Yildiz FH. 2020. c-di-GMP modulates type IV MSHA pilus retraction and surface attachment in Vibrio cholerae. Nat Commun 11:1549.

211. Courtney K. Ellison1*† JK, 3, Jennifer L. Chlebek1, Katherine R. Hummels1, Gaël Panis4, Patrick H. Viollier4, Nicolas Biais2,3, Ankur B. Dalia1, Yves V. Brun1,5*. 2019. A bifunctional ATPase drives tad pilus extension and retraction. Science.

212. Sangermani M, Hug I, Sauter N, Pfohl T, Jenal U. 2019. Tad Pili Play a Dynamic Role in Caulobacter crescentus Surface Colonization. mBio 10.

213. Ha D-G, Kuchma SL, O'Toole GA. 2014. Plate-Based Assay for Swarming Motility in Pseudomonas aeruginosa, p 67-72 doi:10.1007/978-1-4939-0473-0_8. Springer New York.

214.   Chattopadhyay I, J RB, Usman TMM, Varjani S. 2022. Exploring the role of microbial biofilm for industrial effluents treatment. Bioengineered 13:6420-6440.

215.   Sharma S, Mohler J, Mahajan SD, Schwartz SA, Bruggemann L, Aalinkeel R. 2023. Microbial Biofilm: A Review on Formation, Infection, Antibiotic Resistance, Control Measures, and Innovative Treatment. Microorganisms 11:1614.

216.   Aldridge P, Hughes K. 2002. Regulation of flagellar assembly. Cell regulation.

217.   Homma M, Kojima S. 2022. The Periplasmic Domain of the Ion-Conducting Stator of Bacterial Flagella Regulates Force Generation. Front Microbiol 13:869187.

218.   Guo S, Liu J. 2022. The Bacterial Flagellar Motor: Insights Into Torque Generation, Rotational Switching, and Mechanosensing. Front Microbiol 13:911114.

219.   Deme JC, Johnson S, Vickery O, Aron A, Monkhouse H, Griffiths T, James RH, Berks BC, Coulton JW, Stansfeld PJ, Lea SM. 2020. Structures of the stator complex that drives rotation of the bacterial flagellum. Nature Microbiology 5:1553-1564.

220.   Wadhwa N, Phillips R, Berg HC. 2019. Torque-dependent remodeling of the bacterial flagellar motor. Proceedings of the National Academy of Sciences 116:11764-11769.

221.   Zhu S, Takao M, Li N, Sakuma M, Nishino Y, Homma M, Kojima S, Imada K. 2014. Conformational change in the periplamic region of the flagellar stator coupled with the assembly around the rotor. Proceedings of the National Academy of Sciences 111:13523-13528.

222.   Morimoto YV, Nakamura S, Hiraoka KD, Namba K, Minamino T. 2013. Distinct Roles of Highly Conserved Charged Residues at the MotA-FliG Interface in Bacterial Flagellar Motor Rotation. Journal of Bacteriology 195:474-481.

223.   Hook AL, Flewellen JL, Dubern JF, Carabelli AM, Zaid IM, Berry RM, Wildman RD, Russell N, Williams P, Alexander MR. 2019. Simultaneous Tracking of Pseudomonas

aeruginosa Motility in Liquid and at the Solid-Liquid Interface Reveals Differential Roles for the Flagellar Stators. mSystems 4.

224. Zhengyu Wu aaMT, a Rongjing Zhang,a Junhua Yuana. 2021. Dynamics of the Two Stator Systems in the Flagellar Motor of Pseudomonas aeruginosa Studied by a Bead Assay. Applied and Environmental Microbiology 87.

225. Gibson DG, Young L, Chuang R-Y, Venter JC, Hutchison CA, Smith HO. 2009. Enzymatic assembly of DNA molecules up to several hundred kilobases. Nature Methods 6:343-345.

226. Wong SM, Mekalanos JJ. 2000. Genetic footprinting with <i>mariner</i> -based transposition in <i>Pseudomonas</i> <i>aeruginosa</i>. Proceedings of the National Academy of Sciences 97:10191-10196.

227. Kulasekara HD, Ventre I, Kulasekara BR, Lazdunski A, Filloux A, Lory S. 2005. A novel two-component system controls the expression of <i>Pseudomonas aeruginosa</i> fimbrial <i>cup</i> genes. Molecular Microbiology 55:368-380.

228. Pastora A, O'Toole GA. 2023. The regulator FleQ both transcriptionally and posttranscriptionally regulates the level of RTX adhesins of Pseudomonas fluorescens. Journal of Bacteriology 205.

229. O'Toole GA, Pratt LA, Watnick PI, Newman DK, Weaver VB, Kolter R. 1999. Genetic Approaches To Study of Biofilms, p 91-109, Methods in Enzymology, vol 310.

230. Spiers AJ, Bohannon J, Gehrig SM, Rainey PB. 2003. Biofilm formation at the air–liquid interface by the <i>Pseudomonas fluorescens</i> SBW25 wrinkly spreader requires an acetylated form of cellulose. Molecular Microbiology 50:15-27.

231. Ghafoor A, Hay ID, Rehm BHA. 2011. Role of Exopolysaccharides in Pseudomonas aeruginosa Biofilm Formation and Architecture. Applied and Environmental Microbiology 77:5238-5246.